Universitat Politècnica de València
Departamento de Máquinas y Motores Térmicos

Doctoral Thesis

Study of the gasoline direct injection process under novel operating conditions

Presented by:
Abián Bautista Rodríguez

Supervised by:
Dr. Raúl Payri Marín

in fulfillment of the requirements for the degree of
Doctor of Philosophy

Valencia, April 2021

Ph.D. Thesis

Study of the gasoline direct injection process under novel operating conditions

Written by: Mr. Abián Bautista Rodríguez
Supervised by: Dr. Raúl Payri Marín

Examination committee:

Chairman: Dr. Pablo Cesar Olmeda González
Secretary: Dr. Ángel Ramos Diezma
Member: Dr. Noureddine Guerrassi

Reviewing board:

Dr. Noureddine Guerrassi
Dr. Andrea Cavicchi
Dr. Juan José Hernández Adrover

Valencia, April 2021

Abstract

Fuel injection is among the engine research topics one of the critical pieces to obtain an efficient engine. The role is even more significant when a direct injection strategy is pursued. The internal geometry and pintle movement determine the injector flow behavior, which is known to hugely affect the external spray development and, ultimately, the combustion performance inside the chamber. Climate change and pollutants awareness has been growing, pushing forward the effort on cleaner engines. In this regard, gasoline engines have a wider margin to improve than diesel engines. The evolution from old Port Fuel Injectors to modern direct injection strategies, which are used in new generation engines, demonstrates this trend. GDI systems have the potential to comply with stringent emissions and increase fuel economy, however, it still faces many challenges. This work involves the use of two injectors, one is a modern research GDI nozzle appointed by the Engine Combustion Network (ECN), and the other is a production injector unit (PIU) with the same technology and slightly different geometry. Both hardware's undergo a complete characterization (internal and external flow) covering the state-of-the-art techniques in various experimental facilities. Furthermore, a new facility is designed and built to perform experiments under flash boiling conditions (when the fuel injected's vapor pressure is higher than the pressure in the discharge volume).

The developed facility is designed to simulate a discharge ambient at certain engine conditions in which flash boiling phenomena could occur. Thus, due to typical gasoline fuel properties, it was a requirement to operate from chamber pressures from 0.2 bar to 15 bar. Also, the ambient temperature was controlled by implementing a resistor that can heat the ambient gas. The facility operates in an open loop, being able to renovate the gas volume between injections. Finally, three wide optical accesses were built to accommodate many optical diagnostic techniques such as DBI, MIE, shadowgraphy, or PDA, among others.

For the internal flow description, it was determined the nozzles geometry and holes orientation, the pintle movement, and finally, the characterization of the rate of momentum (ROM) and rate of injection (ROI) of both nozzles. The nozzles geometry and needle lift were measured using advanced optical x-ray techniques at Argonne National Laboratory (ANL). The ROI and ROM measurements were performed using CMT-Motores Térmicos facilities following the know-how applied in diesel injectors and adapting it to GDI nozzles. The ROI allowed us to compare the nozzles, whose orifices number and geometry were different, although they deliver approximately the same amount of

fuel. It was tested their response to typical boundary conditions such as rail pressure, discharge pressure, fuel temperature, etc. For the research nozzle "Spray G", it was developed a 0-D model of the rate of injection allowing to obtain the signal for different injection duration and conditions, which is useful in engine calibration and CFD validation. Furthermore, for the ROM characterization, the plastic deformation technique methodology was developed to obtain spray cone orientation and adequately guide the fuel jets for measuring ROM. The hydraulic analysis combined the data to study the low discharge coefficient and area coefficient values, which could result from low needle lift combined with novel hole designs in both nozzles that promote cavitation and air interaction from inside the orifice.

In the external flow characterization, it was used the new developed vessel to study the external spray covering flash boiling conditions. It was employed four surrogate fuels to simulate different volatility properties of gasoline compounds and ultimately reproduce more extreme flashing conditions. It was used lateral visualization using DBI and Schlieren in addition to frontal MIE visualization. Some of the most extreme flashing conditions produced the spray collapse phenomena due to the jet expansion and interaction, in which the fuel concentrates in the injector axis. The two nozzles employed collapsed at different conditions because of different spray cone angles. Moreover, two spray structures were observed, one for transitional and the other for fully collapse sprays. The phenomena completely modify the expected trends in the behavior of the jets. Finally, it was explored the use of advanced x-rays diagnostics to study spray wall interaction. It was tested two configurations using different impact angles. Two rail pressure and discharge pressure were studied, including one flash boiling condition. The results were coherent, finding that the fuel accumulation and spray spreading velocity changed because of injection pressure or impact angle. After impact, the spreading speed for the flash boiling conditions increased compared to the non-flash boiling cases.

Resumen

La inyección de combustible es, entre los temas de investigación de motores, una de las piezas críticas para obtener un motor eficiente. El papel es aún más significativo cuando se persigue una estrategia de inyección directa. La geometría interna y el movimiento de la aguja determinan el comportamiento del flujo del inyector, que se sabe que afecta enormemente al desarrollo externo del spray y, en última instancia, al rendimiento de la combustión dentro de la cámara. La conciencia sobre el cambio climático y los contaminantes ha ido creciendo, impulsando el esfuerzo en motores más limpios. En este sentido, los motores de gasolina tienen un margen más amplio para mejorar que los motores diesel. La evolución de los antiguos PFI a las modernas estrategias de inyección directa, que se utilizan en los motores de nueva generación, demuestra esta tendencia. Los sistemas GDI tienen el potencial de cumplir con las estrictas emisiones y aumentar el ahorro de combustible, sin embargo, todavía se enfrenta a muchos desafíos. Este trabajo implica el uso de dos inyectores, uno es una moderna tobera de GDI de investigación designada por el Engine Combustion Network (ECN), y el otro es una unidad de inyección de producción (PIU) con la misma tecnología y una geometría ligeramente diferente. Ambos equipos se someten a una completa caracterización (flujo interno y externo) que abarca las técnicas más avanzadas en diversas instalaciones experimentales. Además, se diseña y construye una nueva instalación para realizar experimentos en condiciones de evaporación instantánea (cuando la presión de vapor del combustible inyectado es superior a la presión del volumen de descarga).

La instalación construida está diseñada para simular un ambiente de descarga en ciertas condiciones del motor en las que podrían producirse fenómenos de flash boiling. Así, debido a las propiedades típicas del combustible de gasolina, era un requisito operar con presiones de cámara de 0,2 a 15 bares. Además, la temperatura ambiente se controlaba mediante la implementación de una resistencia que puede calentar el gas ambiente. La instalación funciona en un bucle abierto, pudiendo renovar el volumen de gas entre las inyecciones. Por último, se construyeron tres amplios accesos ópticos para acomodar muchas técnicas de diagnóstico óptico como DBI, MIE, shadowgraphy o PDA, entre otros.

Para la evaluación del flujo interno se determinó la geometría de las toberas y la orientación de los agujeros, el movimiento de la aguja y, por último, la caracterización del ratio de inyección (ROM) y el momento de inyección (ROI) de ambas toberas. La geometría de las toberas y la elevación de la aguja se midieron mediante técnicas avanzadas de rayos X en el Laboratorio Nacional

de Argonne (ANL). Las mediciones de ROI y ROM se realizaron utilizando las instalaciones de CMT-Motores Térmicos siguiendo los conocimientos técnicos aplicados en los inyectores de gasóleo y adaptándolos a las toberas de GDI. El ROI nos permitió comparar las boquillas, cuyo número de orificios y geometría eran diferentes, aunque entregan aproximadamente la misma cantidad de combustible. Se ensayó la respuesta a condiciones típicas de motor como variaciones en la presión del rail, la presión de descarga, la temperatura del combustible, etc. Para el inyector de investigación "Spray G", se desarrolló un modelo 0-D de la velocidad de inyección que permite obtener la señal para diferentes condiciones y duración de la inyección, lo cual es útil para la calibración del motor y la validación del CFD. Además, para la caracterización de la ROM, se desarrolló la metodología de la técnica de deformación plástica para obtener la orientación del cono del spray y orientar adecuadamente los chorros de combustible para la medición de ROM. En el análisis hidráulico se combinaron los datos para estudiar los bajos valores del coeficiente de descarga y del coeficiente de área, que podrían resultar de la baja elevación de la aguja combinada con novedosos diseños de orificios en ambas toberas que promueven la cavitación y la interacción del aire desde el interior del orificio.

En la caracterización del flujo externo, se utilizó la nueva maqueta desarrollada para estudiar la atomización externa, cubriendo las condiciones de flash boiling. Se utilizaron cuatro combustibles sustitutivos para simular diferentes propiedades de volatilidad de los compuestos de la gasolina y, en última instancia, reproducir las condiciones de flash boiling más extremas. Se utilizó la visualización lateral utilizando DBI y Schlieren además de la visualización frontal MIE. Algunas de las condiciones de flash boiling más extremas produjeron el fenómeno de colapso del cono del spray debido a la expansión e interacción de los chorros individuales, en los que el combustible se concentra en el eje del inyector. Los dos inyectores empleados colapsaron en diferentes condiciones debido a los diferentes ángulos del cono del spray. Además, se observaron dos estructuras de los jets, una de transición y otra de colapso total. Este fenómeno modifica completamente las tendencias esperadas en el comportamiento de los chorros. Finalmente, se exploró el uso de diagnósticos avanzados de rayos X para estudiar la interacción chorro-pared. Se probaron dos configuraciones usando diferentes ángulos de impacto. Además, se estudiaron dos presiones de rail y de descarga, incluyendo una condición de flash boiling. Los resultados fueron coherentes, encontrando que la acumulación de combustible y la velocidad de propagación del spray eran función de la presión de inyección o el ángulo de impacto. Después del impacto, la velocidad de propagación para las condiciones de flash boiling aumentó en comparación con los casos en los que no había.

Resum

La injecció de combustible és, entre els temes d'investigació de motors, una de les peces crítiques per a obtindre un motor eficient. El paper és encara més significatiu quan es persegueix una estratègia d'injecció directa. La geometria interna i el moviment de l'agulla determinen el comportament del flux de l'injector, que se sap que afecta enormement el desenvolupament extern de l'esprai i, en última instància, al rendiment de la combustió dins de la cambra. La consciència sobre el canvi climàtic i els contaminants ha anat creixent, impulsant l'esforç en motors més nets. En aquest sentit, els motors de gasolina tenen un marge més ampli per a millorar que els motors dièsel. L'evolució dels antics PFI a les modernes estratègies d'injecció directa, que s'utilitzen en els motors de nova generació, demostra aquesta tendència. Els sistemes GDI tenen el potencial de complir amb les estrictes emissions i augmentar l'estalvi de combustible, no obstant això, encara s'enfronta a molts desafiaments. Aquest treball implica l'ús de dos injectors, un és una moderna tovera de GDI d'investigació designada pel Engine Combustion Network (ECN), i l'altre és una unitat d'injecció de producció (PIU) amb la mateixa tecnologia i una geometria lleugerament diferent. Tots dos equips se sotmeten a una completa caracterització (flux intern i extern) que abasta les tècniques més avançades en diverses instal·lacions experimentals. A més, es dissenya i construeix una nova instal·lació per a realitzar experiments en condicions d'evaporació instantània (quan la pressió de vapor del combustible injectat és superior a la pressió del volum de descàrrega).

La instal·lació construïda està dissenyada per a simular un ambient de descàrrega en certes condicions del motor en les quals podrien produir-se fenòmens de flash boiling. Així, a causa de les propietats típiques del combustible de gasolina, era un requisit operar amb pressions de cambra de 0,2 a 15 bars. A més, la temperatura ambient es controlava mitjançant la implementació d'una resistència que pot calfar el gas ambiente. La instal·lació funciona en un bucle obert, podent renovar el volum de gas entre les injeccions. Finalment, es van construir tres amplis accessos òptics per a acomodar moltes tècniques de diagnòstic òptic com DBI, MIE, shadowgraphy o PDA, entre altres.

Per a l'avaluació del flux intern es va determinar la geometria de les toveres i l'orientació dels forats, el moviment de l'agulla i, finalment, la caracterització del ràtio d'injecció (ROM) i el moment d'injecció (ROI) de totes dues toveres. La geometria de les toveres i l'elevació de l'agulla es van mesurar mitjançant tècniques avançades de raigs X en el Laboratori Nacional de Argonne (ANL). Els mesuraments de ROI i ROM es van realitzar utilitzant les instal·lacions de CMT-Motores Térmicos seguint els coneixements tècnics aplicats en els

injectors de gasoil i adaptant-los a les toveres de GDI. El ROI ens va permetre comparar els filtres, el nombre d'orificis dels quals i geometria eren diferents, encara que entreguen aproximadament la mateixa quantitat de combustible. Es va assajar la resposta a condicions típiques de motor com a variacions en la pressió del rail, la pressió de descàrrega, la temperatura del combustible, etc. Per a l'injector d'investigació "Esprai G", es va desenvolupar un model 0-D de la velocitat d'injecció que permet obtindre el senyal per a diferents condicions i duració de la injecció, la qual cosa és útil per al calibratge del motor i la validació del CFD. A més, per a la caracterització de la ROM, es va desenvolupar la metodologia de la tècnica de deformació plàstica per a obtindre l'orientació del con de l'esprai i orientar adequadament els dolls de combustible per al mesurament de ROM. En l'anàlisi hidràulica es van combinar les dades per a estudiar els baixos valors del coeficient de descàrrega i del coeficient d'àrea, que podrien resultar de la baixa elevació de l'agulla combinada amb nous dissenys d'orificis en totes dues toveres que promouen la cavitació i la interacció de l'aire des de l'interior de l'orifici.

En la caracterització del flux extern, es va utilitzar la nova maqueta desenvolupada per a estudiar l'atomització externa, cobrint les condicions de flash boiling. Es van utilitzar quatre combustibles substitutius per a simular diferents propietats de volatilitat dels compostos de la gasolina i, en última instància, reproduir les condicions de flash boiling més extremes. Es va utilitzar la visualització lateral utilitzant DBI i Schlieren a més de la visualització frontal MIE. Algunes de les condicions de flash boiling més extremes van produir el fenomen de col·lapse del con de l'esprai degut a l'expansió i interacció dels dolls individuals, en els quals el combustible es concentra en l'eix de l'injector. Els dos injectors emprats van col·lapsar en diferents condicions a causa dels diferents angles del con de l'esprai. A més, es van observar dues estructures dels jets, una de transició i una altra de col·lapse total. Aquest fenomen modifica completament les tendències esperades en el comportament dels dolls. Finalment, es va explorar l'ús de diagnòstics avançats de raigs X per a estudiar la interacció doll-paret. Es van provar dues configuracions usant diferents angles d'impacte. A més, es van estudiar dues pressions de rail i de descàrrega, incloent una condició de flash boiling. Els resultats van ser coherents, trobant que l'acumulació de combustible i la velocitat de propagació de l'esprai eren funció de la pressió d'injecció o l'angle d'impacte. Després de l'impacte, la velocitat de propagació per a les condicions de flash boiling va augmentar en comparació amb els casos en els quals no hi havia.

"Somewhere, something incredible is waiting to be known."
Carl Sagan

A mi familia, amigos y pareja
Especialmente a mi tío Julio

Agradecimientos

Quisiera aprovechar esta oportunidad para agradecer a todas aquellas personas que han contribuido de alguna manera en la elaboración de este trabajo. Durante todo este tiempo he tenido la suerte de coincidir con maravillosas personas de las que he podido aprender y crecer, además de forjar buenas amistades.

En primer lugar, me gustaría agradecer a mi director de tesis Raúl Payri por su incansable guía y consejo a lo largo del desarrollo de la tesis. Siempre orientando en la dirección adecuada de una manera practica y buscando nuevos retos, sin duda es un extraordinario team leader para el grupo de inyección. También quiero agradecer al Instituto CMT por permitirme la oportunidad de formar parte del prestigioso grupo de investigación, por proporcionarme los medios y recursos para llevar a cabo la tesis. Además, agradezco el trato personal de secretaría y de informática por ayudarme en todos los procedimientos burocráticos.

Asimismo, tengo que dar un especial agradecimiento a Christopher Powell por darme la oportunidad de realizar la estancia de investigación en Argonne National Laboratory y acogerme como un miembro más de su equipo. También agradecer al equipo de fuel sprays: Brandon Sforzo y Aniket tekawade por su acogimiento, buenos momentos y enseñanzas durante mi estancia. Agradecer también a todos lo que hicieron que mi estancia fuera más amena Alan kastengren, Roberto Torelli, Gina M. Magnotti, Jorge, Johannes, Fran, Ale, y algunos más que me dejo, gracias. Finalmente, a Mario Medina por acogerme en su familia. Tanto en Valencia como en Chicago fue un gran amigo.

Tengo que mostrar mi gratitud a todo el equipo de inyección del CMT. Especialmente a Jaime Jimeno, Gabriela Bracho y Alberto Viera, por dedicarme su tiempo y ayuda resolviendo mis preguntas. Al despacho por compartir muchos momentos juntos y con los cuales fue un placer trabajar, primero Daniel, Alberto y Tomás, y en mi último año con Rami y Victor. A María y a Vincenzo por los viajes increíbles y momentos para desconectar. A Armando y Mario por acompañarme y guiarme en todos los retos e ir acompasados durante el doctorado, por ayudarme en todos los procedimientos. A Jesús y Marco por la música para calmar y desahogarse. También quiero agradecer al resto del equipo, profesores y doctorandos por su amistad y compañerismo por todo este tiempo: Marcos, Pedro, Javi, Santi, Cesar, Mary, Lucas, Kike, David, Carlos, etc. Asimismo, a todos los proyectandos que me ayudaron con el trabajo experimental: Sai, Luca, Alejandro, Eduardo, Carlos, Daniele Arduino, Alejandro Ortega, y Pedro. También a otros doctorandos del CMT, Vishnu, Jorge, Leo

y Dani entre otros, y especialmente a Guille, María, Natalia y Mario por acompañarme tantos años en la UPV.

De igual forma agradezco a los técnicos de laboratorio José Enrique y Omar por toda su ayuda y aprendizaje, sin ellos hubiera sido imposible realizar los experimentos y construir la maqueta. Además de todos los buenos momentos y risas en el laboratorio que hacían que las mediciones fueran mucho más amenas. Tampoco puede faltar agradecer a Jose Torner, por su capacidad de arreglar todos los desastres con las piezas y sacar una sonrisa con sus bromas.

Por último, me gustaría agradecer a mi familia por su interminable apoyo en los momentos más difíciles y en las decisiones que he tomado a lo largo de mi vida, además de creer en mi en todo momento. A Nayarit por acompañarme y darme su apoyo incesante en esta última etapa del camino. Por inspirarme a ser mejor persona e ilusionarme con su actitud positiva y trabajadora ante la vida. Especialmente agradezco a mi tío Julio, que, aunque ya no esté, me enseño desde pequeño la importancia de la lectura y los estudios, me apoyó incondicionalmente durante toda mi vida, siendo como un segundo padre para mí atento en todos los momentos importantes.

A todos ustedes, gracias.

Contents

List of Figures

List of Tables

Nomenclature

Acronyms

ANL	Argonne National Laboratory.
APD	Avalanche photo-diode.
APS	Advanced Photon Source.
CAD	Crank Angle Degree.
CFD	Computational Fluid Dynamics.
CIDI	Compression-Ignition Direct-Injection.
CI	Compression Ignition.
CN	Cavitation Number.
CO	Carbon monoxide.
CV	Control volume.
DBI	Diffuse back-illumination.
DBI	Diffused back-illumination.
DI	Direct Injection.
DOI	Duration of injection.
DP	Double-pass.
ECN	Engine Combustion Network.
ECU	Electronic Control Unit.
ECU	Engine Control Unit.
EGR	Exhaust Gas Cecirculation.
EOI	End of injection.
ET	Energizing Time.

FTP	Federal Test Procedure.
GDI	Gasoline Direct Injection.
HC	Hydro Carbon.
HPHT	High pressure high temperature.
ICE	Internal combustion Engines.
IRDCI	Injection Rate Discharge Curve Indicator.
L-wall	Lateral wall.
LED	Light-emitting diode.
LES	Large-Eddy Simulation.
MIE	Mie-scattering.
MPFI	Multi-point Fuel Injection.
NOx	Nitrogen oxides.
OEM	Original Equipment Manufacturer.
P-wall	Perpendicular wall.
PDA	Phase Doppler Anemometry.
PFI	Port Fuel Injection.
PID	Proportional-Integral-Derivative.
ROI	Rate of injection.
ROM	Rate of momentum.
RSD	Relative standard deviation.
SEM	Scanning Electron Microscope.
SF	Safety Factor.
SG	Spray Guided.
SI	Spark Ignition.
SOE	Start of energizing.
SOI	Start of injection.
SP	Single-pass.
SWI	Spray-wall interaction.
TDC	Top Dead Center.
TIM	Tranverse Integrated Mass.
UHC	Unbunred hydrocarbon.
UV	Ultra violet.
VCO	Production Injector Unit.
VOF	Volume of Fluid.

Greek symbols

ΔP	Pressure difference throughout the nozzle.
Δp	Pressure difference (general).
Δu_f	Variation of fuel flow velocity.
λ	Air-fuel equivalence ratio.
μ	Phase change pontential.
ρ	Density (general).
ρ_f	Density of the fuel.
σ	Surface tension.
τ	Optical thickness.
Θ	Fuel-air equivalence ratio.
θ	Spray spreading angle.
ε	Angular deflection of a ray.
ϖ	Surface of the control volume.

Latin symbols

$\dot{m_{teo}}$	Theoretical mass flow rate.
$\dot{M}$	Momentum flux.
$\dot{m}$	Mass flow rate.
a_f	Speed of sound in the fuel.
A_o	Outlet area of the nozzle.
A_t	Tube cross-sectional area.
A_{eff}	Effective area.
C_a	Area coefficient.
C_d	Discharge coefficient.
C_M	Momentum coefficient.
C_v	Velocity coefficient.
d_i	Distance for spreading angle calculations.
D_o	Nozzle outlet diameter.
F	Force (general).
I	Pixel-wise intensity distribution of the current image.
I_0	Pixel-wise intensity distribution of the reference image.
J	Rate of nucleation.
$k - factor$	Orifice conicity factor.
k_{GD}	Gladstone-Dale coefficient.

k_{adjust}	Mass scaling factor.
L	Optical path length.
L_n	Nozzle length.
m_{int}	Mass integrated from the signal.
m_{scale}	Mass measured by the scale.
n	Refractive index (general).
n_0	Refractive index of the surroundings.
p	Pressure (general).
p_0	Reference pressure.
P_b	Discharge pressure.
P_r	Rail pressure.
S	Spray penetration.
T	Temperature (general).
t	Time (general).
T_0	Reference temperature.
T_f	Fuel temperature.
u	Velocity (general).
u_t	Theoretical discharge velocity.
u_{eff}	Effective velocity.

Chapter 1

Introduction

This chapter presents the motivations for studying the gasoline direct injection (GDI) process as well as the effect of flash boiling in typical and some extreme conditions of GDI engines. First, the context of this study in the research community is introduced. Next, it is presented the objectives it aims to fulfill and the methodology followed. Finally, it is described a summary of the subsequents chapters discussed in the thesis.

1.1 General context

Internal Combustion Engines (ICEs) are one of the most notable inventions of the last century and have greatly impacted on society. They are the foundation of many technological advancements, and it has definitely revolutionized transportation and mobility. For example, uses of this type of engine had spread over a variety of fields besides automotive, like agriculture, naval propulsion, power generator, etc. It uses the chemical energy stored in fuels to produce mechanical power, by means of a controlled combustion reaction. Its undoubted success in powering transportation systems is supported by a high power-to-weight ratio, the high energy density of the fuels available and cost-effectiveness.

From the mass use of ICE, it was realized that the harmful pollutants and emissions produced by the combustion of the fuel are not neglectable. Nitrogen oxides (NOx), greenhouse gas like CO_2, soot and unburned fuels are the primary emissions that in large quantities could jeopardize nature and

human life. Thus, government agencies in the EU, US and Asia have presented directions to limit them to obtain breathable air in the cities and to mitigate the effect of climate change. The frequents regulations are being tightened over the years, which are pushing the automotive industry to keep researching for new technologies that allow lowering emissions and improve fuel economy.

Lately, the global automotive industry has suffered a profound transformation process from the use of conventional internal combustion engines towards electrified ones either hybridized or full electrical powertrains. However, there is still a significant part for combustion engines, and it is foreseen a market share of 85% for 2030 [1]. The electrical powertrains do not produce emissions directly and facilitate the application of renewable energy in the transportation field. Nevertheless, the use of this type of propulsion could harm as well the environment if the source of energy is not clean. Unless the power production is composed mostly by renewable sources, the well to wheels analysis may not be better than ICEs. In addition, the life cycle of lithium batteries employed in current electric cars is a big problem since the waste treatment of these are toxic to the environment.

For the past 50 years in Europe, the diesel engines have been the predominant type for light-duty systems and an extensive part of personal vehicles. The two main reasons have been higher efficiency compared to gasoline engines and higher energy density for diesel fuel. In the past years because of the scandal of Dieselgate (where some OEMs cheated the emission test for diesel engines), the appreciation of diesel engines as highly polluting cars has spread which made the manufactures to present and sell more gasoline engines. In addition, the difficulty to meet with the regulations particularly with NOx emissions (typical emission from this engine), have forced to the development of expensive after-treatment systems which increase the final price of the product. The scenario presented leads the manufacturers to lean towards gasoline engines, which are of much simpler and cheaper systems. The current advancements in gasoline engines include downsizing and turbocharging to improve fuel economy. Also, due to their simplicity, it is the preferred engine for hybrid vehicles. All these reasons have led in Europe to a higher portion of gasoline engines.

The fuel injection technology is one of the key factors for engine improvement, whose importance has received a great deal of attention over the last 20 years [2]. By understanding the phenomenons involved in the injection, which are evaporation, mixing, and combustion, it is possible to design new generation injectors to reduce the emissions. The gasoline direct injection systems are the state of the art for gasoline engines. Although diesel systems

have used fuel directly injected into the combustion chamber since the first successful prototype in 1894, the first application of this technology in gasoline engine was in aviation during First World War in Junkers aeroplanes. Later, GDI was implemented in some German cars in the 1950s; however it presented many difficulties and inflexibility so did not succeed. The mass use of GDI in vehicles was not until 1996 when Mitsubishi launched an electronic GDI system. From that moment GDI experienced a rapid implantation among OEMs, and for example in the US increased from 2.3% in models from 2008 to close to 50% for models of 2016 [3]. The primary advantage of GDI over the previous port fuel injection (PFI) systems is that the injection occurs directly in the cylinder, which avoids the wall wetting of the intake port and valves. Moreover, the evaporation of the fuel in the cylinder cools the air and the compression ratio of the engine can be higher, thus, it facilitates the implementations of turbocharging and downsizing without the risk of knocking [4–6]. Furthermore, it provides advantages in specific engine conditions of part loads or cold start [7]. Also, they permit the development of advance combustion strategies like the Gasoline Compression Ignition which blurs the line which separates the definition between Otto and Diesel engines.

Historically, Diesel injectors have been the focus of research because of the direct implication in the mixture formation and combustion, which ultimately affects fuel economy and production of pollutants. Nonetheless, in PFI gasoline engines, the injectors were not as critical. It was not until the introduction of the GDI system that efforts were dedicated to understanding deeply these injectors. The delivery of the fuel in GDI engines is not yet completely understood, and it confronts challenges in term of fuel consumption and emissions. Thus, big efforts are being made by industry and research institutions to develop their potential. The GDI injectors are accountable for delivering the right amount of fuel at the desired location in the cylinder, in addition to provide the right atomization, evaporation and mixing with the air in the desired time. The first GDI engines took advantage of the flexibility of the injections to work at stratified charge at part loads, and homogeneous at high loads. However, that strategy is not used anymore today. It permits slightly higher compression ratios without knock, a leaner air-fuel ratio but the drawback is the increased NOx formation because of the presence of exceedingly lean zones, and to comply with regulations, NOx after-treatment could be a requirement.

Flash boiling is a complex phenomenon that could appear at certain operating conditions in GDI engines. It occurs when heated fuel (from heat transfer from the engine block) is injected into a setting where the ambient pressure is lower than the saturation vapor pressure of the fuel. During GDI

operation, it could occur, for example, when injecting in the admission stroke. In that circumstance the chamber pressure is sub-atmospheric because of vacuum. The flash boiling affects fuel air mixing process because it modifies spray characteristics of cone angle, penetration and droplet size. It could promote the atomization, so it could be beneficial for the air-fuel mixing. However, in some cases for multi-hole injector it could provoke spray collapse, in which the typical models employed for optimization or fuel location prediction may not be appropriate.

Two injectors have been analyzed during this thesis:

1. The Spray G from the Engine Combustion Network (ECN), which is a group composed by research institutions, academia and industry with the objective to join the efforts in investigating atomization and combustion phenomena. It emphasizes in providing a meticulous methodology to obtain high quality data. The established approach allows an easy comparison between research institutions and reliable dataset to develop computational fluid dynamics (CFD) models. The Spray G is a Delphi multi-hole solenoid GDI injector.

2. A GDI Denso injector, used by a car manufacturer in their gasoline engines. For later references will be called Production Injector Unit (PIU).

Although the Spray G is a research injector and the PIU one is dedicated to mass production, both injectors present similar construction and technology, being solenoid activated. However, the biggest differences are the shape and number of holes and their distribution on the injector tip. This will take an important role in the different behaviors presented.

This work has been developed in the research institute CMT-Motores Térmicos which belongs to the Polytechnic University of Valencia (Spain). The institute has built up an important reputation worldwide in the field of combustion engines since it was founded more than 40 years ago. Its strong point has been the study of diesel engines but its work includes combustion, air management, noise, after-treatments, fuel/urea/water injection, simulations etc. The institution has published over the years more than 180 books, 500 journal articles, and completed over 165 doctoral thesis. In recent years, because of growing interest in GDI, the department has decided to invest and specialize in this technology given its potential future. The current thesis is the second in the department oriented to GDI investigation.

1.2 Objectives and methodology

The present work comes from the need to get a more in-depth insight into the phenomenon of flash boiling, which could frequently appear on GDI engines and its consequences are not entirely understood. The Injection research group of the CMT-Motores Térmicos, which has typically work with Diesel injectors, has done little investigation on GDI and this is the second thesis in gasoline injection related topic [8]. However, it was possible to transfer some know-how available in the group from Diesel injectors into GDI. To perform the necessary experiments, it was required to develop a dedicated vessel to study the phenomenon. Thus, the two main objectives of the present thesis could be presented as follow:

1. To develop the necessary test equipment and be able to replicate the conditions of flash boiling in a controlled environment. The new test rig should allow the utilization of different optical techniques for the diagnostic and analysis of the flash boiling phenomena, through the measurement of several characteristics spray variables.

2. To contribute to the understanding of flash boiling during the injection event, by means of an experimental approach comparing two injectors with different holes distributions. Also, evaluate the effects of the phenomena in the air-fuel mixing.

To imply relations in flash boiling conditions, a complete characterization of the injector has been carried out. The experiments could be separated into hydraulic characterization and external visualization. The experimental facilities available in the CMT laboratories can be summarized using this groups:

- Hydraulic characterization
  - Rate of injection
  - Plastic deformation technique
  - Momentum Flux test rig
- Spray Visualization
  - GDI visualization test rig
  - X-ray visualization

As stated before, for the visualization part a new test rig was developed to broad the operation range which was not possible to operate with High Pressure High Temperature (HPHT) test rig already available at CMT-Motores Térmicos. For the experiments two same technology but different nozzle injectors and four fuels were used. In a first instance the conditions used were the ones in the guidelines of the ECN [9], and variations around it. It was tested real engine conditions as well as not as typical due to research more extreme conditions of flash boiling, always within the capabilities of the available facilities.

1.3 Thesis outline

The document is organized in seven chapters to make this thesis structured and easy to understand. It starts with a general introduction (**chapter 1**) which provides the reader with a general context and motivations for the thesis.

Chapter 2 gives fundamental concepts of combustion engines. The evolution of combustion engines is discussed as well as its basic working principles. Then, more specific GDI theory and concepts are introduced, which are more related to the actual theme of this work. Lastly, the most recent works related to this topic are discussed to set the ground to this research.

In **chapter 3** is explained the methodology followed during the thesis, besides, it is described the experimental facilities and pieces of equipment used to obtain the experimental data. The injector's hardware employed is presented as well as the explanation of the selected operating conditions. Then, internal hydraulic characterization facilities are explained such as rate of injection, rate of momentum test rigs, as well as a description of the plastic deformation technique. In addition, visualization experimental equipment are described, including visualization test rigs and the x-rays techniques employed during the research stay at Argonne National Laboratory (ANL). Finally, it is discussed various optical arrangements utilized and the data (image) processing methodology employed to obtain the final results.

Chapter 4 illustrates the process of conceptualizing, designing and built the test rig employed to study gasoline sprays, specifically in controlled conditions that allow to investigate the flash boiling phenomena. It discuss the requirements necessary to operate at flash boiling conditions and how the available facilities at CMT-Motores Térmicos could not meet the requirements. The reasoning behind selecting materials, instrumentation, and op-

eration mode is presented along with simulations and tests that validate the design and the safe operation.

The fifth chapter (**chapter 5**) is the first one including results, in which the hydraulic characterization outcomes are presented and discussed. This section reports from rate of injection, plastic deformation technique and rate of momentum measurements. Each of the sections motivates and introduced the test conditions selected for the experiments. Although every results is discussed in its section, there are several examples of combining results from different sections to obtain a global overview and support in arriving to conclusions.

In **chapter 6** is exposed the visualization results obtained from the injector external flow. It is divided in two main sections. The first section is about the biggest experimental campaign of this thesis involving four fuels, wide range of experimental conditions, and the use of the dedicated test rig to study flash boiling effects in sprays, which was extensively explained in chapter 4. The different volatility of the fuels allows to investigate various levels of flash boiling in the flow within the test vessel range of conditions. Also, the two injectors permit to infer different behavior depending on the nozzle geometry and holes distribution.

In the second part of this chapter is presented the results obtained in the experimental campaign performed during the research stay at ANL. It was studied the wall impingement of the gasoline spray using the ECN hardware. It was researched two wall configurations, two x-rays techniques, in which one condition on flash boiling was tested (G2 conditions from ECN [9]).

Finally, the seventh and last chapter (**chapter 7**) provides a summary and overview of the principal results of this thesis, emphasizing the most important conclusions of the previous chapters presented. At last, it is suggested future works and directions that could be taken to advance the research on this topic.

References

[1] Gomot, Dipl Baudouin and Hülser, Holger. "Delphi Technologies Next Generation GDi-System, improved Emissions and Efficiency with higher Pressure". In: *Internationales Wiener Motorensymposium* (2019), pp. 1–21.

[2] Kuo, Kenneth K. and Zarchan, Paul. *Recent Advances in Spray Combustion: Spray Atomization and Drop Burning Phenomena*. 1996. DOI: 10.2514/4.866418.

[3] EPA. "Light-Duty Automotive Technology, Carbon Dioxide Emissions, and Fuel Economy Trends: 1975 Through 2016 - Executive Summary (EPA-420-S-16-001, November 2016)". In: November (2016), pp. 1–11.

[4] Zimmerman, Naomi, Wang, Jonathan M, Jeong, Cheol Heon, Wallace, James S, and Evans, Greg J. "Assessing the Climate Trade-Offs of Gasoline Direct Injection Engines". In: *Environmental Science and Technology* (2016). DOI: 10.1021/acs.est.6b01800.

[5] Fontanesi, Stefano, D'Adamo, Alessandro, and Rutland, Christopher J. "Large-Eddy simulation analysis of spark configuration effect on cycle-to-cycle variability of combustion and knock". In: *International Journal of Engine Research* (2015). DOI: 10.1177/1468087414566253.

[6] Saliba, Georges et al. "Comparison of Gasoline Direct-Injection (GDI) and Port Fuel Injection (PFI) Vehicle Emissions: Emission Certification Standards, Cold-Start, Secondary Organic Aerosol Formation Potential, and Potential Climate Impacts". In: *Environmental Science and Technology* (2017). DOI: 10.1021/acs.est.6b06509.

[7] Johnson, Timothy. "Vehicular Emissions in Review". In: *SAE International Journal of Engines* 7.3 (2014), pp. 2014–01–1491. DOI: 10.4271/2014-01-1491.

[8] Vaquerizo, Daniel. "Study on Advanced Spray-Guided Gasoline Direct Injection Systems". PhD thesis. Universitat Politècnica de València, 2017.

[9] "Engine Combustion Network". In: *https://ecn.sandia.gov/gasoline-spray-combustion/* (2020).

Chapter 2

Fundamentals of fuel injection

2.1 Introduction

If there is something that has characterized technology throughout its existence, it is a tool at the service of humanity. This allows society to evolve, being the improvement of people's living conditions their main objective. The pace of technological evolution is accentuated over the years, having exploded with the birth of the industrial revolution and driven by modern capitalist society, in which the need for technological innovation becomes an essential parameter for industrial competitiveness.

Since the appearance of the first vehicle propelled by an internal combustion engine in 1860 until today, the automobile industry has been involved in constant changes. This has had to adapt successively to the needs demanded by society, which has led to an industry, although young, highly developed. In recent years, especially since the signing of the Kyoto protocol, the car industry has been strongly marked by climate change. A new era that implies the need to reduce pollutants produced by limiting harmful NOx exhaust gases, as well as the search for alternative propulsion models to those using fossil fuels.

This path to sustainability is what the future holds. The automobile industry must continue the adaptation process that has characterized it since its inception, which entails a modernization process through an evolution of the propellant plants, and begins with guaranteeing maximum emissions of 95

g/km by 2020, as the European Comission. From here, these emissions should gradually decrease until they disappear, scheduled for 2050.

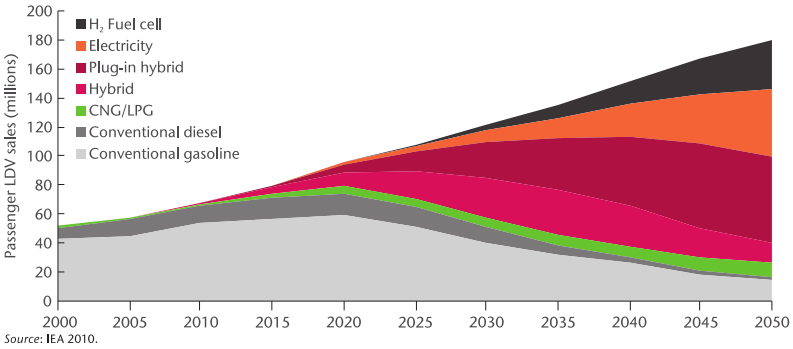

Figure 2.1: Extrapolation of annual sales of light vehicles by type of technology [1].

According to Figure 2.1 the road that guarantees sustainability leads to the appearance of different propulsion models such as the electric car or hydrogen fuel. However, until these technologies are able to completely replace diesel and gasoline engines, what is intended is to reduce the emissions of the latter with the aim of extending their period of use and thus take advantage of all the technology developed. To meet this objective, GDI (direct fuel injection) engines appear, which focus on reducing fuel consumption and translates into a reduction in pollutant emissions per kilometer.

In the particular case we have today with Covid-19, CO_2 emissions due to fuel consumption has been affected by the country's economic conditions as depicted in Figure 2.2. There is a large increase in emissions linked to fuel energy consumption over the years. It can be observed that the emissions have decrease in each crisis, emphasizing on the actual one. However, it is most probable that there would be a recuperation to the previous levels that, although being not desirable in terms of emission, would mean the activation of the economy.

Probably because of the pandemic the objective of drastically reduce the emissions from passenger car using alternative propulsion would have to wait longer and the trend would be to improve hybrid and non-hybrid GDI engines. The current government directives toward reducing pollulants have caused that most manufacturers are already equipping their gasoline models with direct injection engines. The pioneer was the Japanese brand Mitsubishi with the GDI engines. Renault is now followed by IDE engines, the PSA group with HPi engines, and Volkswagen with FSi engines.

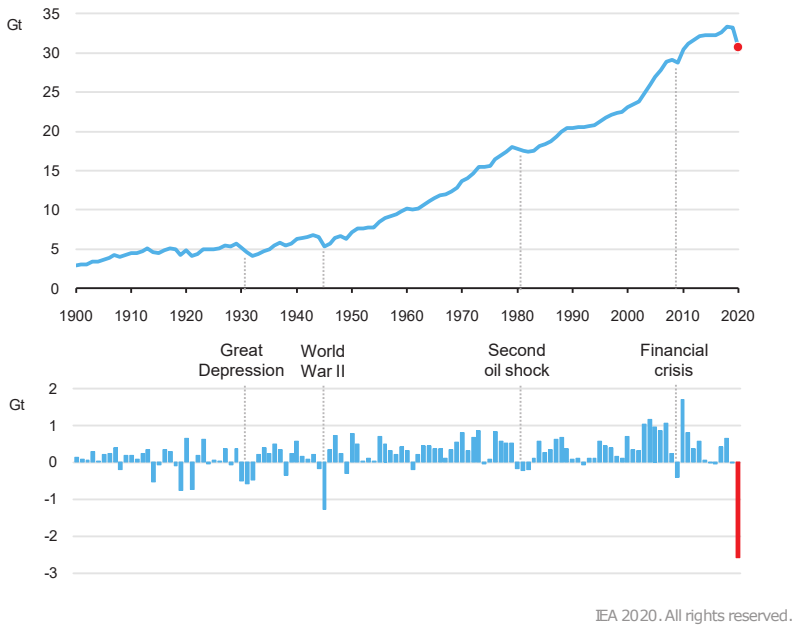

Figure 2.2: Global energy-related CO2 emissions and annual change, 1900-2020 [2].

2.2 Description and types of ICEs

The internal combustion engines (ICE) are heat machines that turn most of the energy released by the combustion chemical reaction of fuels into useful mechanical work. The "internal" term refers to the location where the reaction occurs, which in this case takes place inside the machine.

There are various common classifications of ICEs according to the thermodynamic cycle, and depending on how many steps take to perform it (2 strokes or 4 strokes). In two-stroke engines, the crankshaft achieves one revolution during one cycle when the piston has moved two times. For four-stroke engines, the piston inside the engines moves four times, and there are two revolutions of the crankshaft in once cycle. The first one is simpler and cheaper, so for propulsion is typically used in light vehicles or motorbikes, or when the application requires a small engine. The four-stroke engine allows for higher fuel economy and is more popular in passenger vehicles.

Other classification could be made depending on different thermodynamic cycles. The two most popular cycles of ICE engines are Otto and Diesel, named after their creators. Each one presents a particular difference in the way that the fuel is ignited. For Diesel engines, the fuel is ignited by achieving the necessary temperature and pressure conditions in the cylinder, that is why

they are denominated compression ignition (CI) engines. The four-step cycle of this type of engines can be synthesized as follows:

- Intake: the piston begins at the top dead center (TDC) and ends at the bottom dead center (BDC). With the intake valve open, the air is dragged into the cylinder, due to the vacuum pressure generated as the piston is moving downwards.
- Compression: the intake valves are closed, and the piston starts to rise, compressing the air trapped in the cylinder.
- Combustion: when the piston is arriving back to the initial position, fuel is injected in the chamber. At this moment, the conditions of pressure and temperature in the cylinder are sufficient to auto-ignite the mixture. The energy released by the oxidation reaction increases the pressure and temperature, making the piston to go down.
- Exhaust: the exhaust valve is opened, and the products of the combustion are sweep away by the piston moving upwards. At the TDC the crankshaft would have rotated two revolutions and cycle is completed.

As has been described, only air is introduced in the cylinder. The combustion is controlled by the injection of the fuel when the piston is near the TDC. At that moment, the ignition conditions are achieved as the fuel is injected and evaporation and mixing occur. As consequence, a diffusion flame is created in the borders of the spray. It is intrinsically a heterogeneous combustion since it only befalls in areas where the air-fuel mixture is adequately rich. Therefore, the injector plays a critical role since the characteristics of the fuel jet and air movement inside the cylinder control the combustion.

In the other hand, the Otto cycle runs using constant volume combustion, which is started by a spark that gives the necessary energy to begin the combustion. They are also known as spark ignition (SI) engines. Recent investigations are trying to have further control of the ignition by substituting the spark for plasma or laser ignition [3–7]. However, these technologies are not ready for production at the moment, and actually Denso (a car component manufacturer) suspended the development of a type of plasma ignition system due to its unfeasibility [8]. The four steps of the Otto cycle are described next:

- Intake: through the open intakes valves, a mixture of fuel and air is dragged as the piston moves downwards.

- Compression: the intake valves are closed. The piston starts to rise until it arrives at the TDC, compressing and increasing the temperature of the air-fuel mixture trapped in the cylinder.
- Combustion: the spark plug ignites the mixtures. The pressure increase generated by the gases resulting from combustion pushes the piston downward.
- Exhaust: in this last step, the exhaust valve is opened, and the piston scavenges the combustion products away.

As stated, the combustion in gasoline engines starts by adding energy by an electric arc in the spark plug. The timing of the combustion can be precisely controlled to obtain the most efficient combustion at that engine condition. The Otto cycle example was described for a homogeneous charge, at the stoichiometric air-fuel ratio. This is true for conventional gasoline engines working with carburettor or port fuel injectors (indirect injection), where the amount of air-fuel mixture is controlled by a throttle valve located upstream the intake valves. For instance, at a higher power demand, the throttle opens to its maximum, and since the amount of fuel is proportional to the air to achieve stoichiometrically, more mixture enters the cylinder accomplishing higher in-cylinder pressure and power. However, it will be later explained that GDI engines permit to operate at both homogeneous and stratified charge since there is a direct injection inside the cylinder so that the operating mode depends on the timing of the injection event.

As seen, the two principal differences between both cycles are first, how the mixture is formed. And secondly, how the combustion starts and develops. The characteristics and operating conditions capable of each engine depend essentially on that.[9]

2.3 Fuel injection process

2.3.1 Gasoline injection systems

As mentioned previously, the injectors for gasoline engines were not a critical component since the mixture is performed in the admission duct. However, for the well functioning of the cycle, the mixture should be able to ignite when required by the spark plug (within the flammability limits). The air-fuel quantities must be determined by the engine regime, and are normally handled using two main definitions. First, the Lambda (λ) or air-fuel equivalence ratio,

which expresses the ratio of actual mixture to stoichiometric. The ratio is described in Equation 2.1 and the value gives information of the mixture: $\lambda = 1.0$ represents stoichiometry conditions, whereas $\lambda < 1.0$ for rich mixtures and $\lambda > 1.0$ for lean mixtures.

$$\lambda = \frac{\text{Mass of air}}{\text{Stoichiometric mass of air}} \tag{2.1}$$

Another frequently used definition is the fuel-air equivalence ratio (ϕ) and similarly is determined as the ratio of fuel-to-oxidizer to the stoichiometric fuel-to-oxidizer as depicted in Equation 2.2. This definition is equal to the inverse of the λ value.

$$\phi = \frac{m_{fuel}/m_{ox}}{(m_{fuel}/m_{ox})_{st}} = \frac{1}{\lambda} \tag{2.2}$$

These ratios are of great importance since they describe the flammability limits of the mixture, thus possible functioning points. The limits are more restrictive in SI engines than CI engines due to the nature of the combustion. For SI, the limits for stable combustion are for ϕ values between 0.6 and 1.6. However, if the engine is aiming for maximum fuel efficiency, it would go for slightly lean mixtures ($\phi < 1$), conversely, for maximum power, the values are around $\phi \approx 1.15$ corresponding to moderately rich mixtures. In the end, the exact values would depend on the temperature and pressure of the cylinder, besides the throttle valve angle, among other factors [9]. Besides, if a three-way catalyst is used to reduce the harmful emissions, a strict operation at an equivalent ratio of approximately one must be used through all engine conditions for the proper functioning of reducing oxides of nitrogen (NO_x).

In contrast to CI engines, whose injector controls the air-fuel mixture, in SI the fuel is injected in the intake valve, allowing more time for mixing thus functioning in homogeneous mode. The carburetors first, and then the Port fuel injection are the systems which have been typically used for gasoline engines injection. The amounts of air and fuel are precisely controlled to achieve the optimum mixture. However, to control the load, a throttle valve is used to limit the amount of air through the intake by creating a pressure loss which decreases the volumetric efficiency. This undesirable loss, together with avoidance of wall-wetting are some of the reasons for pursuing direct injection systems [10, 11], which will be discussed in section 2.4.

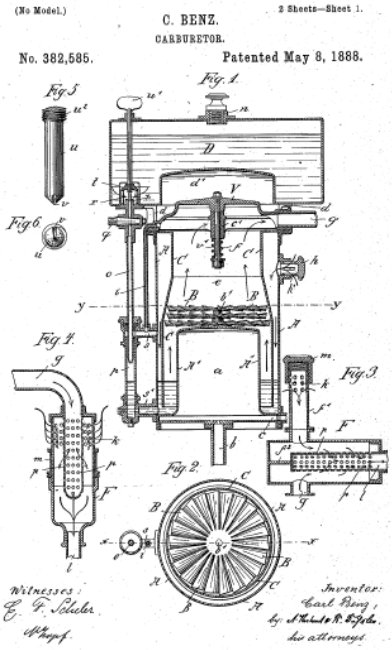

Figure 2.3: Sketch of a cut-section of the carburetor patent of C. Benz [12].

Carburetors

The carburetor was among the initial patents by Karl Benz (1885 Germany, 1888 US) as he improved internal combustion engines and their components (See Figure 2.3). It performs a mixture of air and fuel before entering the cylinder. The first models of carburetors were surface type, in which the mixture is performed by passing the air around a wet surface with gasoline. It works using the concept of a Venturi tube and Bernoulli's equations. The carburetor depends on the throttle of the engine, which controls the airflow that is pushed in. The speed and pressure of the airflow when passing through the carburetor determines the amount of fuel drawn into the airstream. The carburetor was improved over the years and used as the first fuel delivery systems in passenger cars.

It was not until 1937 that aircrafts engines needed the fuel to be pressurized, then the gasoline injectors were introduced substituting the carburetors for these applications. The fuel injection was developed in parallel with the carburetors. In the seventies, they were hard to improve, and the catalytic converters needed a more precise control over the air-fuel mixture, which led to the implementation of the gasoline injectors. EU legislation concerning

emission required all vehicles sold and produced after 1992 to have a catalytic converter. Hence, the use of a closed-loop system that used an oxygen sensor provided better accuracy for the fuel injection to operate at an adequate ϕ. The carburetors for passenger cars were gradually phased out by the 90s in favor of the fuel injection, which was already common for expensive cars.

The gasoline injection that it is referred to this moment is gasoline indirect injection, in which the mixture is realized before the intake valve. Thus, the injection system could be classified into indirect or direct injection, whether the injection is done outside or inside the combustion chamber.

Gasoline Indirect injection

Indirect fuel injection is the technology that has replaced the carburetors, and it is still present in many gasoline engines. The fuel is delivered upstream of the intake valves in a single or multi-point configuration using one or several injectors.

The most popular indirect injection schemes are:

- Single-point injection: it uses a single injector at the throttle body, in the same location as the carburetors. It was used in the 1940s in large aircrafts engines and in the 80s in the automotive world. The justification of the single point injection is because it was a low cost/better performance substitute for the carburetors.
- Continuous injection: the fuel flows from the injectors at all times but at a variable flow rate, in contrast to most fuel injection systems which work delivering fuel in short pulses. It was mostly used for luxury-high performance cars.
- Multipoint fuel injection (MPI) or port fuel injection (PFI): In this case, the fuel is injected just before the cylinder inlet valve for each engine cylinder. Typical fuel pressure for these injectors is between 2 to 5 bars. They are normally timed to inject while the intake stroke occurs. Figure 2.4 shows a schematic of the MPI in an engine.

In the port fuel injection, the spray is injected in the intake duct and valve, which cools down the valve and starts to vaporize. The fuel demand is such for some engine loads and speeds that the injector is continuously injecting even when the valve is closed. The manifold heat promotes the vaporization, and thus a better mixing with the air is achieved when the

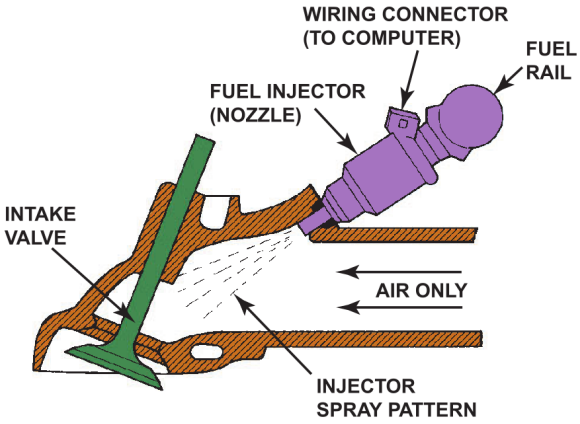

Figure 2.4: Sketch of a typical port fuel-injection system squirting fuel into the low pressure (vacuum) of the intake manifold, about 70 to 100 mm from the intake valve [13].

spark plug activates. In opposition to Single point injection, in which the fuel has to travel a longer distance to enter the cylinder suffering higher wall wetting, the PFI produces less wall wetting and so generally fewer emissions and higher volumetric efficiency [9, 14, 15]. In addition, the inlet manifold for this system is designed in a way that enhances the airstream when entering the cylinder. However, PFI has to overcome the short injection time during idle conditions with controlled and precise fuel delivery. Also, PFI has the risk of producing rich mixtures due to the short travel distance and time to blend with the air.

The first indirect injector was mechanically operated, and its application was on gasoline-fueled aviation by Leon Levavasseur in 1902. It was not until the 50s that the technology was introduced in high-end cars, coliving with the carburetors. Mechanical injectors had limited adjustments to deliver the right amount of fuel for each condition that the engine needs to operate, such as a variety of speeds and loads, starting regime, different atmospheric pressure, and temperatures induced by a change of altitude, etc. The electronic fuel injection (EFI) relied upon many sensors and controls which avoid the lack of management of the fuel. When working together, sensors provide inputs to the system to compute based on an "engine map" the optimum amount of fuel for the condition and thus better engine performance for the given requirements.

In 1957, Bendix corporation presented the first electronic injection systems [16], which was the first movement towards better control and timing of the fuel, however as the first version presented many problems, so it was imple-

mented in very few cars. Later, Bosh bought the patent and developed the first mass-production electronic injection systems called "D-Jetronic" controlled by intake pressure. It was superseded by the "L-Jetronic" and "K-Jetronic". The latest incorporated the first close-loop control using the lambda oxygen sensor. Later the "L-Jetronic" was combined with engine management technology to include a programmed engine map control of the ignition. These architectures were designed for multi-port fuel injection. However, the "Mono-Jetronic" was developed in 1987 which was a lower-cost solution that helped wide-spreading the fuel injection and its accessibility to the masses. It consisted of a single port injector (SPI) that was placed in the main throttle body, which was a perfect solution for mid to small vehicles. From that point on, the carburetors were not used anymore; fuel injection was needed for the proper functioning of the three-way catalyst and the necessary close-loop with the lambda sensor. Besides, fuel injection provided lower fuel consumption and exhaust emissions, increased output, torque, and volumetric efficiency, better driveability and response, and finally, less noise than the carburetors [14]. The most common architecture in actual cars uses a combination of Motronic injection with a multipoint injection to comply with fuel economy and emissions requirements [17]. PFI must satisfy various performance requirements, among which are fast opening and closing, resistance to deposits, a small deviation between pulses, a broad range of mass flows, correct atomization, etc. These reasons makes them complicated pieces of the engine still under research and development for future engines, including hybrid type [15, 17–25].

2.4 Gasoline direct injection

2.4.1 Introduction to GDI

Gasoline engines have been the predominant thanks to the simpler architecture, low cost, excellent driveability, and high specific power. However, increasingly stringent emissions regulations have led to the development of gasoline engines with the aim of reducing emissions. In Europe, the use of diesel engines has been the predominant means of reducing CO_2 emissions, occupying a share of more than half of the car market. However, diesel engines have more complex fuel injection and gas after-treatment systems, as well as needing more robust engine blocks, so they tend to be more expensive. The strategy followed in the current developments tries to make gasoline engines compete with diesel engines in terms of pollutants and fuel consumption. To this end, the development of new technologies such as gasoline direct injection (GDI) are proposed as potential solutions to achieve this, as they are a

solution that does not deviates away from conventional IC engine technology. GDI engines expect to overcome current problems with gasoline systems, such as improving fuel economy by being able to prevent knocking at high loads [26, 27], reduce pollutants of HC and NOx and decrease the pumping losses at part load conditions [28]. Since injection occurs directly in the cylinder, evaporation of the fuel helps to cool the mixture and reduce its temperature. This directly affects a decrease in NOx during combustion as well as minimizing knocking. HC reduction is mainly achieved during cold start: wall wetting on intake valves is reduced by means of a split injection strategy. Regarding the reduction of pumping losses, it is achieved virtually through the use of stratified combustion, where there is a rich mixture around the spark plug but the overall mixture in the cylinder remains stoichiometric. However, although stratified mode presents benefits in relation to fuel consumption, its direct use is not evident since it also presents important limitations that have prevented its expansion. The implementation of GDI also allows the use of new approaches to reduce emissions, such as the implementation of downsizing, increasing the compression ratio, turbocharging or a combination of these. The use of GDI has also physically enabled the development and exploration of new combustion models previously impossible to implement such as HCCI (Homogeneous Charge Compression Ignition), GDCI (Gasoline Direct Compression Ignition), RCCI (Reactivity Controlled Compression Ignition), homogeneous lean spark ignition, water injection for knocking resistance [14, 28, 29].

The earliest prototype for GDI engine was built in 1916 in Germany for a Junkers airplane running gasoline on diesel engines, direct injection was employed to avoid missfires. Nevertheless, the first application in passenger cars in 1952 when Bosch developed a mechanical GDI system powering two-stroke engine in the Goliath GP700 and Gutbrod Superior. Later, in 1955 it was presented the Mercedes-Benz 300SL, which was powered by the first four-stroke engine to use GDI technology [9]. Figure 2.5 depicts an sketch of the technology at this early stage. During this first vehicle applications, besides fuel economic the main reason to use GDI was to increase the performance of the powertrain. Throughout the 70's, companies like American Motor Company (AMC) and Ford tried to implement mechanical prototypes of GDI, however, none of them came to market. The standardization of electronic injection in the 1990s, along with the development of common rail in diesel engines, brought together the technology needed to successfully implement the GDI engine. In fact, in 1996 the Mitsubishi Galant was introduced to the Japanese market, the first car produced on a large scale to be equipped with a GDI engine. Which arrived in Europe a year later under the model

"Carisma" [30]. Almost simultaneously, Toyota also presented its GDI engine model to the European and Japanese markets [31]. From this point on, car manufacturers began releasing their gasoline direct injection engine variants, while maintaining and improving PFI units.

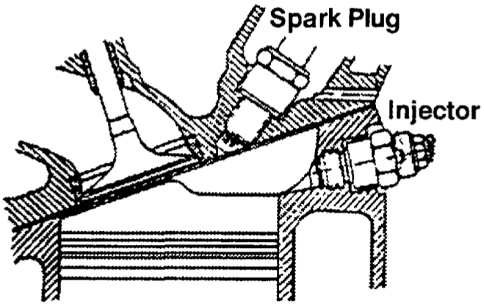

Figure 2.5: Sketch of GDI combustion system of Benz 300SL (1954) adapted from [30].

Figure 2.6 illustrates the main components that constitute a gasoline DI engine. The injector is installed inside the cylinder, which is supplied by high pressure fuel. The fuel is delivered and blend with the air that comes through the electronic throttle valve and the intake valve. In this example there are two lambda sensor at each side of the after-treatment device. They work in a closed-loop linked to the ECU, which decides the adequate amount of fuel for each operation point [32, 33].

Nonetheless, at this time the fuel efficiency in real-world driving conditions in DI gasoline engines was less than claimed. The reason is that the tighter emission regulation commanded the use of an expensive and less efficient lean-burn NOx after-treatment for stratified lean-combustion operation since the three-way catalytic system could only work for stoichiometric conditions [32]. In addition, gasoline engines working under stratified combustion modes experienced more soot generation because of the liquid fuel films in the piston surface, HC emissions due to incomplete combustion and flame quenching [34]. Subsequently, GDI engines after 2001 have been designed to operate at homogeneous charge mode. They are configured and marketed for their greater performance. Actually, at high rpm the GDI system might not have time to provide all of the fuel needed. Thus, some car manufacturer combined the system with an PFI structure to achieve maximum power and fluid operation at part load conditions using stoichiometric charge.

Besides GDI targeting the high performance engines, in the mid 2000's the new trend of downsizing and turbocharging represented a new era for DI

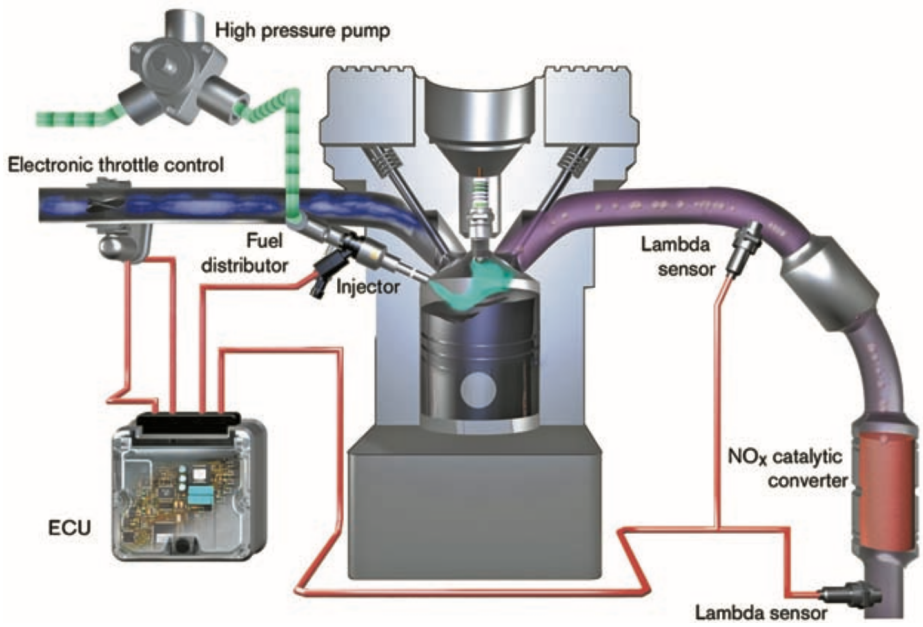

Figure 2.6: The component schematic of a GDI system. Adapted from [33].

gasoline engines [35–37]. Audi and VW group have been the most advanced leading the production of the popular TSI 1.4 liter DI gasoline combining a mechanical supercharger and turbocharger and producing remarkable 90 kW/liter power density [32]. This approach can substantially increase engine efficiency since the load could be controlled with the boost degree instead of the throttle valve.

Despite the difficulties in making an efficient and emission-compliant GDI engine, these engines have continued to be developed and researched because of their potential for improvement [21–24, 35–40].

2.4.2 Stratified charge combustion

Traditionally petrol engines have operated with stoichiometric mixtures, in which the load is determined by the throttle valve. This valve is the cause of the loss of volumetric efficiency when the engine is running at part-load conditions. Reducing this loss of air intake would potentially improve fuel consumption to some extend. The objective of stratified charge mode is to reduce this loss by eliminating or restraining the use of the throttle valve to control the engine load. In order to keep a globally stoichiometric ratio, a rich and ignitable mixture (within flammability limits) is provided in the

surroundings of the spark plug while maintaining a lean one in the remaining combustion chamber. Therefore, this strategy accomplishes a reduction of part-load pumping losses compared to throttle configuration, reduction of gas temperatures in the cylinder and thus reduction of thermal losses and NOx production, and finally, increases the work extracted by increasing the ratio of specific heats [34].

The time at which the injection event occurs is the substantial difference between stratified and homogeneous charge modes. The injection during the stratified charge mode happens during the compression stroke at around 60-70 crank angles degrees (CAD) before top dead center (BTDC), whereas at homogeneous charge mode, the fuel is delivered at the intake stroke (much earlier) at 270-300 CAD BTDC [15]. A representation of the two different combustion modes is shown in Figure 2.7. For the stratified mode (right) the fuel does not have time to mix well with the air contained in the chamber by the time that the spark plug activates, nevertheless, for the homogeneous mode the injection is performed much earlier during the intake. The airstream turbulence and the longer time make possible a sufficient homogeneous mixture. The ideal operation is to actuate in stratified charge mode at part-load to avoid the volume efficiency loss (throttle valve halfway close), while at full load operate in homogeneous charge mode with the throttle valve fully open [11, 32].

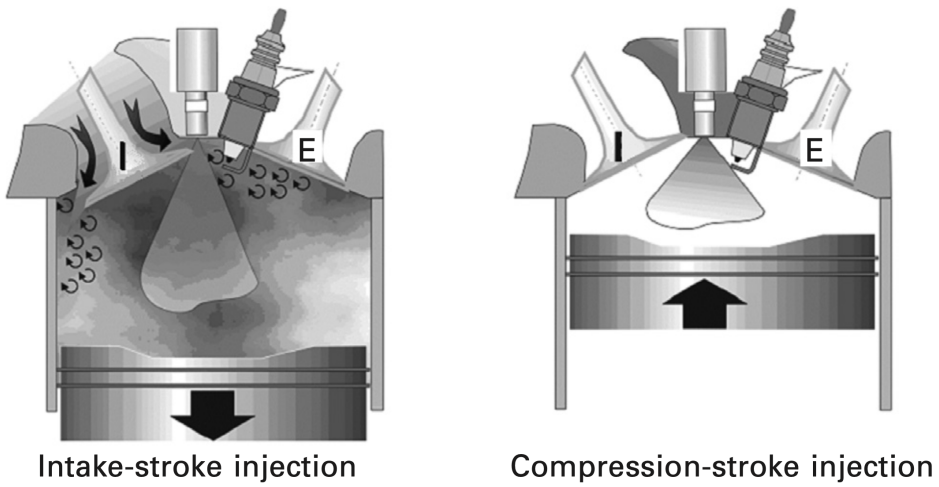

Figure 2.7: Operating combustion modes for GDI. Homogeneous operation (left) and Stratified charge (right). Adapted from [32].

In stratified mode, the fuel delivery process is not an easy task as there is very little time to get a proper mix around the spark plug. The success

for a good fuel convection and mixture depends on many variables, but also the approach taken. There are three different strategies to form a ignitable mixture near the spark plug, which are wall-guided, air-guided and spray-guided, represented in Figure 2.8.

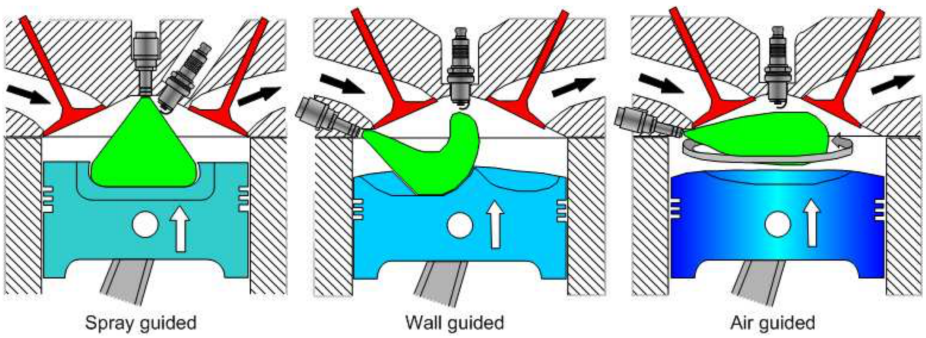

Figure 2.8: Configurations overview of DI gasoline engine concepts. Adapted from [41].

First DI engines used the wall-guided system, which employed a special shape in the piston surface to transport the fuel to the spark plug [42]. The use of this system alone is not efficient. The fuel injected in the piston surface cannot completely evaporate which created many HC and CO emissions, and fuel consumption is not optimal. On the other hand, in air-guided approach the fuel is injected in the airstream which transports it to the spark plug surroundings. The desired airflow is achieved by a special design of the intake ports. This strategy does not wet the piston or cylinder, and uses a combination of swirl and tumble air movement, usually combined with special surfaced piston to move the compact fuel cloud to the sought location. In these two strategies the injector is located far from the spark plug.

VW was one of the first to introduce DI combustion system in the early 2000s using a combination of wall-guided and air-guided strategies, which showed advantages in stratified as well as homogeneous charge modes. Figure 2.9 shows a schematic of this system. The injector is mounted next to the intake port and the piston head has two bowls: one on the intake side between the intake valves and another in the exhaust side. The bowl near to the injector nozzle guided the fuel towards the spark plug, whereas the other bowl creates an air motion that transported the remaining fuel to the ignition area [43]. The correct functioning of these strategies depends strongly on air movement inside the cylinder as well as on inconvenient piston head shapes, both of them contributing to a decrease in engine performance and thermal

efficiency due to heat loss. In addition, due to their design these strategies tend to intrinsically originate wall wetting on the piston head and therefore generate too many HC and soot emissions.

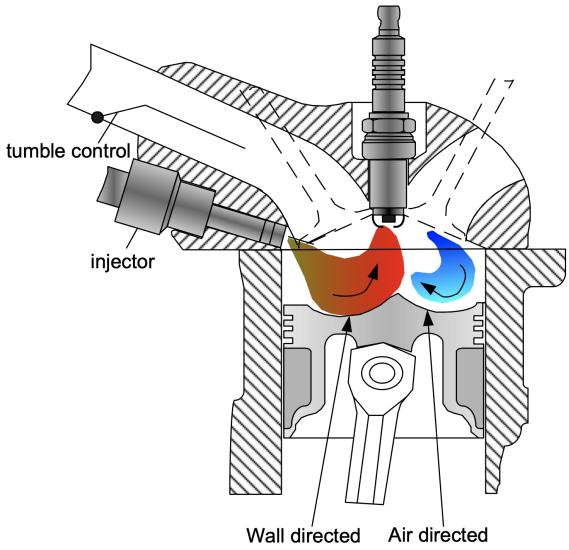

Figure 2.9: Volkswagen (VW) FSI engine air-wall guided engine design. Adapted from [14].

The last engine concept is the spray-guided direct injection (SGDI) system, which is the most modern configuration. Mercedes and BMW introduced this system in 2006 what could be considered the second generation of DI gasoline engines with wider operational range [15]. The injector is principally responsible for delivering the fuel close to the spark plug, where it also evaporates. It has to provide repeatable spray pattern for all flow and pressure conditions in the chamber. This approach presents the highest theoretical efficiency and it is still researched today for new combustion concepts [42, 44–49]. It has some advantages respect to the previous systems: wider stratified operation region, less sensitive to in cylinder flow variation, decreased wall wetting, and reduced HC emissions. However, there are particular problems or new challenges to solve in SGDI systems. SG injectors could develop coking at the injector nozzle tip principally due to low combustion temperatures, which can be addressed by meticulously design holes or counterbores [46, 50]. The spark plug reliability is also compromised because of fouling. Finally, this system has poor robustness since it is tremendously sensitive to injection and ignition timing. When operating in stratified mode, there is limited time for mixture formation which could result in too rich zones that cause HC emissions,

misfires and unstable combustion. At the introduction of stratified gasoline engines, Europe has responded with Euro VI as an attempt to regulate the maximum PM emitted by gasoline engines. New combustion strategies are being researched such as Homogeneous Stratified combustion, which uses a split injection during the intake to form a lean homogeneous charge and a second injection during the compression stroke to provide a rich mixture around the spark plug [42]. This concept and some other have the potential to overcome shortcomings of the stratified charge, and although important efforts have been done, the GDI operating under stratified charge is still a challenge being researched [51–56].

2.4.3 New combustion concepts and GDI technology

Besides the stratified mode, the DI gasoline engines are very resourceful since they also have permitted the use of other technologies and combustion strategies. Turbocharging is a technology that has traditionally serve to increase performance keeping the same engine architecture, however, more recently combined with engine downsizing have presented a manner to increase resistance to knocking, and thanks to variable camshaft phasing devices, increase the manifold pressure and operate at much greater BMEP [32]. Downsizing pursuits to reduce pumping losses by fitting an smaller swept volume engine than is common for a given power output. Then, for full load performance, it recover the loss by using a pressure charging system. The result is that for any given load the throttle valve is wider open which reduces the irreversible losses in during the aistream entrance. Since the industry is predisposed to continue using the 4-stroke engine, the great advantage of this approach to minimizing losses comes from the fact that it is not affected by the fuel specifications or the requirements for emissions compliance. The shift of the compressor map is possible by increasing the scavenging, which is achieved by delaying the fuel injection until the exhaust valve has closed. This practice results in improved system driveability (by a turbo lag reduction), solving one of the characteristics costumers give more value: engine response, which is more notable in big displacement engines.

The main approach for increase engine thermal efficiency is to increment compression ratio either by piston displacement design or supercharging. However, is significantly limited by knocking. Cooled Engine Gas Recirculation (EGR) and air excess are promising approaches to minimize knocking, although the use of DI itself provides great control over fuel self-ignition. The use of alcohols could increase the heat of vaporization of the fuels, so it is also an approach to reduce knocking.

There are other combustion concepts like gasoline direct compression ignition (GDCI), which uses a stratified mixture formed from multiple late injections allowing reduced fuel consumption, PM emissions and NOx. This novel concept could overcome the drawbacks of stratified combustion discussed in subsection 2.4.2. This system can be the trigger for a new generation of engines that take advantage of both SI and CI approaches. It would use fuels with low cetane numbers, which would have a longer ignition delay and therefore allow more time to achieve a better mixture ultimately reducing soot and HC [15].

The lean boost combustion is a concept that exemplifies the combined use of downsizing with direct injection, in addition to pressure charging during lean operation. An important factor for the proper functioning of supercharging in an engine is the octane rating of the fuel. Normally, it is necessary to reduce the geometric compression ratio of the engine to accommodate the boost and thus avoid knocking (negatively affecting thermal efficiency). However, if it is used homogeneous lean operation and DI, the octane requirement is reduced and a higher compression ratio can be assumed. The operating limits are enclosed between the risk of knocking on the rich side, and spark initiation and flame propagation on the lean side. By adding the boost to the equation, the operating range is shifted to higher λ values. The change to lean side causes the engine output to decrease, so eventually to operate you need to increase the boost to a higher level than the naturally aspirated one that allows downsizing but with lean conditions. To minimize air demand, it will be used the richest mixture that provides stable operation. Therefore, the reduction of the octane requirement is achieved thanks to DI and the knocking suppressant action of the excess air [55–59].

To conclude with the charging and combustion strategies, it should be noted that in direct injection the injector is the main component since it is responsible for providing the appropriate spray for each situation. Therefore, much attention is paid to the development of injectors. As the requirements for new combustion strategies increase and narrow, the same will apply to both GDI and PFI injectors. They must not only provide the proper amount of fuel, but also obtain the degree of atomization and location of fuel required in each engine operating scenario. The following section presents the different types of GDI injectors developed so far, with emphasis on SG systems being the main players along this work.

2.5 GDI fuel injectors

2.5.1 Evolution and types of gasoline injectors

Considerable technology and know-how has been transferred from the design and manufacture of diesel injectors to gasoline DI. Both types of injectors have common features that are mutually beneficial. Fuel injection is a very important process in DI engines. The injector must meet requirements to provide fuel at high pressure and low pressure depending on the operating condition and strategy to be followed in a precise and consistent manner. The injectors have to be able to provide a well atomized mixture distributed along the cylinder as needed to operate under homogeneous load conditions, as well as in case of operating in stratified mode be able to provide a fuel rich zone around the spark plug. To achieve the degree of atomization and the amount of fuel required in such a short time, the injectors operate at high pressures, usually working at pressures between 50 and 250 bar [17, 26, 32, 60–63]. However, thanks to the advance of new materials and designs, it is studied that the use of higher pressures would bring several benefits. Johansson et al. [64] employed an injector capable of operating up to 350 bar as an attempt to decrease particle emissions although he found that the use of high pressure directly affected soot production. Hoffmann et al. [65] from Delphi technologies studied the viability of pressure increase not only in the injector performance but in the fuel pump and other components. In fact, Delphi claimed in 2016 the introduction of the first commercial GDI injector that operates at 350 bar [66]. Furthermore Granqvist [67], president of Denso Sweden, stated in 2017 that there was not mass production GDI injector and pump durable above 35 MPa so far. Husted et al. [68] used a 400 bar injector to research to what extent the rail pressure affects the fuel consumption. They conclude that increasing the fuel pressure results in a small increment of fuel economy despite of higher energy demand of the fuel pump. Currently, several manufacturers of injectors such as Bosch, Delphi, Magneti Marelli, Continental, are investigating new GDI concepts using injection pressures from 400 bar up to 800 bar which have the potential of reducing fuel consumption and decrease emissions [65, 69, 70]. In Figure 2.10 is depicted the 800 bar prototype of injector and fuel pump from Magneti Marelli.

As mentioned in the previous subsection 2.4.2, the first generations of GDI were installed in a wall-guided system, which operated between 50 and 100 bar. The design of this first injectors was swirl-type, which had a single hole and a pintle that moved inward to let the fuel pass through. The principle

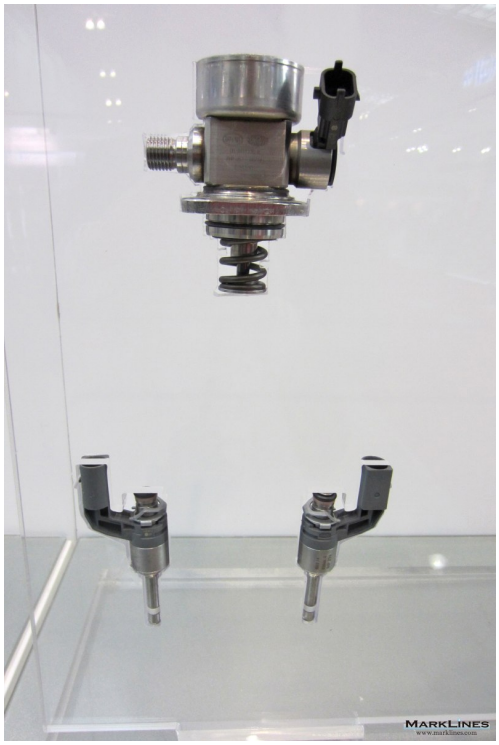

Figure 2.10: High-pressure pump and injectors for gasoline direct injection system prototypes under development from Magneti Marelli. Exhibit in SAE China 2015 [69].

of operation of these injectors was to apply a rotational motion to the fuel at the outlet nozzle by means of tangential holes or slots, which succeeded in imposing a swirl movement on the liquid. The principal characteristic of this type of injection is that the swirl movement produced a hollow-cone spray [11]. This design had some disadvantages, however the most important was that the cone angle produced varied considerably with different engine operating points and ambient conditions so calibration and determining the correct design was very difficult. In addition, the use of a camera for swirl production resulted in a loss of volumetric efficiency, which led to the development of slit-type injectors [71]. The next generation of GDI injectors were SG type, which were necessary to improve the stratified load systems at full load conditions, in addition to extending their operation range. To meet the requirements of these systems, piezo-electrically actuated and solenoid-actuated multi-hole injectors were developed and used [32]. Piezoelectric injectors take advantage of the phenomenon of mechanical deformation suffered by some ceramics after

being excited by a electric charge. The geometrical change in a piezoelectric material is very small, so to obtain sufficient displacement, the injectors are equipped with a crystal stack, commonly referred to as a piezo-stack [72]. Figure 2.11 illustrates a descriptive scheme of a GDI piezoelectric injector.

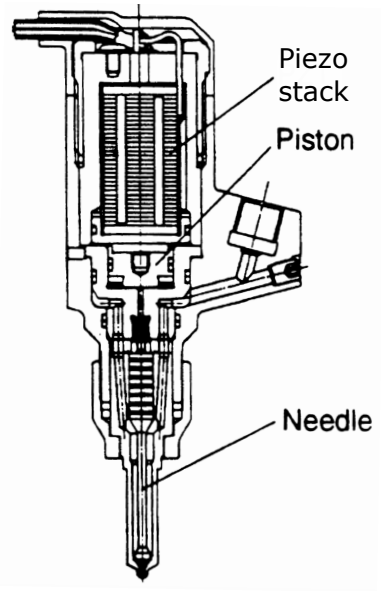

Figure 2.11: Descriptive diagram of a GDI piezoelectric injector. Adapted from [11].

The piezo injectors open outwards, which means that the needle comes out of the injector to let the fuel through. They leave a small radial opening, which forms a hollow-cone thin spray. The outward opening of these nozzles is advantageous since it prevents the formation of deposits that could interfere with the flow, thus avoiding the undesirable cocking that normally forms in other types of nozzles such as multi-orifice. One of the most notable capabilities of this type of injector is its rapid response, and ability to provide precisely small amounts of fuel in a consistent manner, making it the most suitable injector for multi-injection strategies. Solenoid multi-hole injectors are more popular than piezo injectors because they are more economical by sacrificing the repeatability and precision [34, 73]. Dahlander et al. [74] investigated and compared the injection rate of piezoelectric and solenoid driven injectors. They concluded that for short energizing times, piezo injectors provide fuel more consistently than solenoid injectors. While the piezo could deliver precise small quantities lower than 1 mg @ 15 bar, the solenoid was only capable of providing robust doses from 1.8 mg. Even so, for the new generation of

GDI solenoids, these disadvantages can be solved by employing the ballistic regime, which requires a combination of precise fuel metering in the injector's side, and electronic system management that adjusts the injection signals and duration in real time [34, 70].

One of the most important parameters of the injectors in GDI engines is the penetration speed, which is a critical parameter that defines the mixing process. High spray penetration speeds can improve the mixture, however they also present a danger of moistening the cylinder walls, which could result in higher soot and unburned HCs. The use of piezo injectors to increase atomization (improving mixture) and decrease penetration was advocated by Mercedes' BlueDirect technology [75], although the application was for luxury car engines. Figure 2.12 shows the fuel spray from a standard piezo driven outwardly opening nozzle, a multi-hole and a pressure swirl injectors.

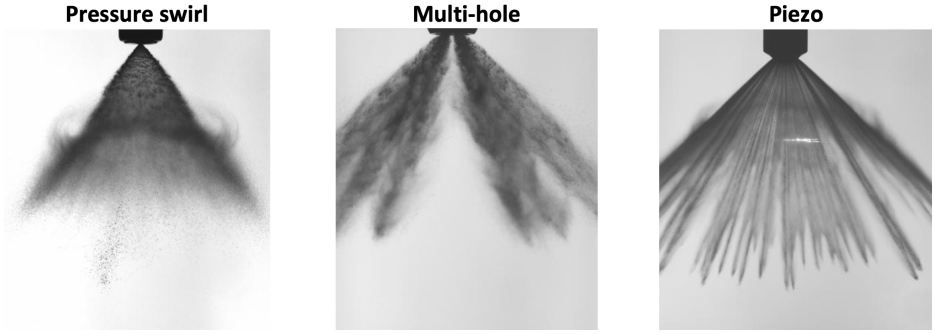

Figure 2.12: Spray from different types of GDI injectors [72, 76].

The combination of fast response, accurate fuel metering, deposit resistance and preferable penetration make the piezo injectors very suitable for operating GDI engines in stratified charge mode as well as homogeneous mode [42, 77, 78]. However, despite their evident benefits, they are not always preferable for real engine testing. Besides, the injector temperature affects greatly in the performance and different voltages are needed to operated the piezo-stack [79]. Smith et al. [80] investigated and compared the performance between one SG multi-hole solenoid driven and outward-opening piezo injector under steady state warm up conditions. Over a simulated Federal Test Procedure (FTP) cycle, the multi-hole system had 15% lower hydrocarbon and 18% lower carbon monoxide emissions, and more significantly a 3% benefit over fuel consumption. Solenoid driven multi-hole injectors have been used more extensively than piezo ones, due mostly to lower cost. Nevertheless, these have another outstanding advantage which is that its multi-orifice design allows

the maximum combination of possibilities to distribute the fuel spray to the desired location, therefore an adequate distribution can be achieved so as not to impact walls or get closer to the spark plug depending on the combustion chamber [81]. Due to its versatility and being cost-effective, the use of this type of injectors is very common in GDI engines, so the amount of studies and scientific effort has been notably higher in these injectors [32, 34, 82, 83].

Due to the above reasons, the ECN group (explained in chapter 1) has preferred to use this hardware for gasoline spray research, referring to it as "Spray G" [84].

2.5.2 Test injectors: Multi-hole solenoid driven type

GDI injectors have been developed with transferred diesel injector technology, as an existing evolution of older PFI injectors, still, redesigned to operate at significantly higher pressures [34]. The normal range of operation of these injectors is from 50 to 200 bar [17, 61, 62], however there are already several designs on the market capable of operating at 350 bar [64, 70], 400 bar [85], and the feasibility of operating with pressures of 500 to 800 bar is currently being analyzed [65, 69, 86].

A cross-section drawing of a typical GDI solenoid-driven multi-hole injector from Bosh can be observed in Figure 2.13, although similar structure and technology is used by other manufacturers as well. The fuel enters through the inlet (1), which is connected with the valve seat (the fuel has the same pressure). While not actuating, the nozzle orifices are covered by the ball at the end of the needle. To inject, the coil is excited by a current coming from the electrical connector, which creates a magnetic field that forces the needle upwards. Finally, a spring is employed to return the needle to its initial position closing the valve.

The injectors used for this work are valve covered orifice (VCO). One is the Spray G from the ECN and the other is a comercial GDI injector which from this point on is referred as Production Injector Unit (PIU). Figure 2.14 depicts a close up picture of both nozzles. The left image shows the Spray G nozzle, which has eight straight orifices configured with a stepped geometry also known as "counterbore". The orifices are equally distributed around the injector axis and are drilled on a bump with a hemispherical shape which provides the space and proper angle for the holes. On the right is the PIU nozzle, which has six straight orifices, however, in this case they are not equally distributed and the centroid of them is deviated from the injector axis (what is normally called skew angle). One of the most notable differences between

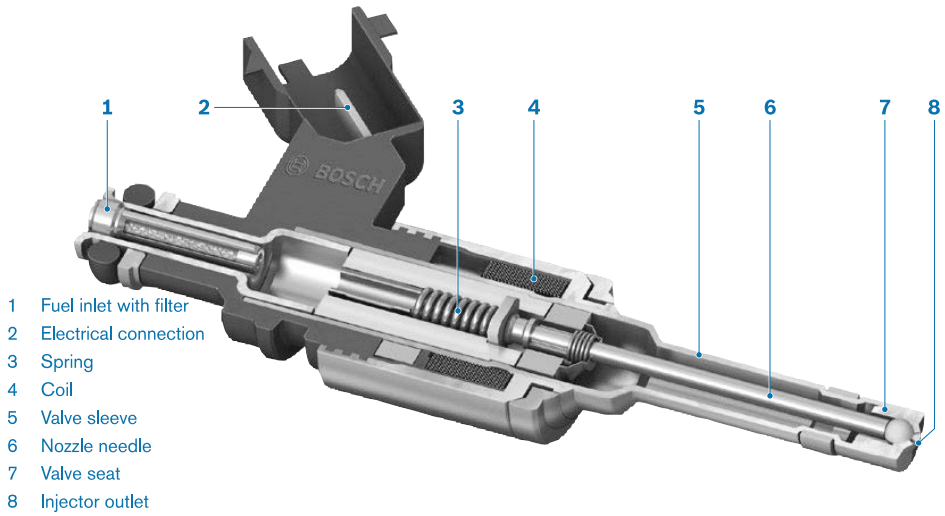

Figure 2.13: Design of a Bosch HDEV5 high-pressure injector. Adapted from [17].

these injectors and a typical diesel injector is that the holes are much closer together. This is due to larger hole diameters, and the desired angle between the holes and the injector axis is smaller.

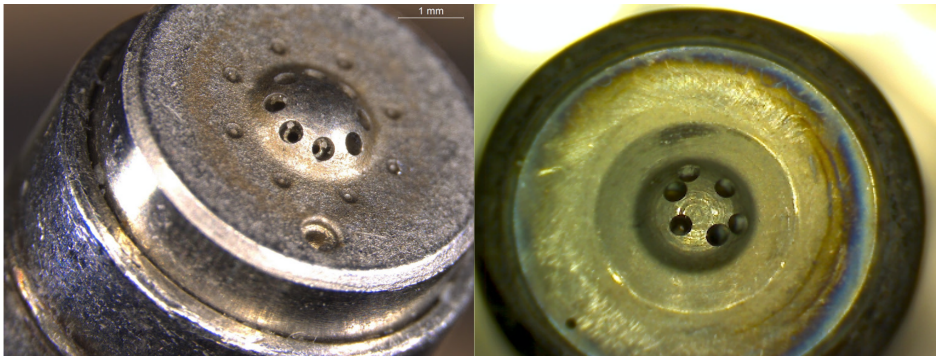

Figure 2.14: Close up picture of the injector nozzles used in this work. Spray G from ECN [26] (left), and PIU (right).

These two injectors are a sample of the possible combinations and versatility that are available in the multi-orifice solenoid driven. The advantage of freely arrange the orifices allows, once located the injector in the combustion chamber, configuring the nozzle to avoid impingement on the wall or valves and optimize the mixture. The SG injectors can be mounted centrally at the top of the cylinder or at the side (normally at the intake port side). The researched injectors are a example of each type of combination, being the Spray

G designed as a centrally mounted injector, while the PIU configured for a side mount, whose nozzle presents a clear deviation (skew angle) from the injector axis to avoid wall wetting. Other possible variable to control de fuel jet is through different diameter orifices, as shown in Figure 2.15, the optimization of individual spray hole size enhances fuel distribution and reduce soot emissions (prevent wall wetting). However, this is not the case for the injectors in this work, which have same diameter orifices.

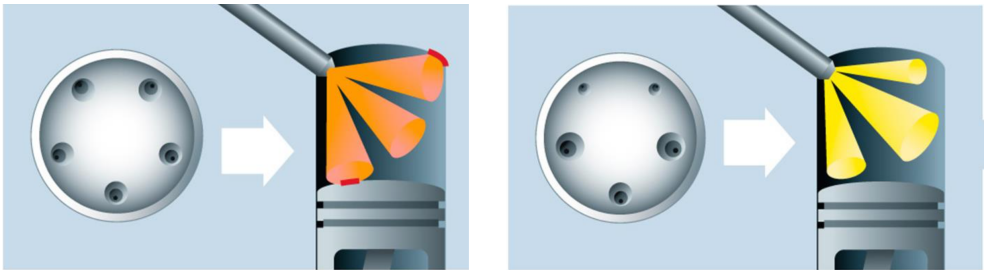

Figure 2.15: Representation of wall wetting control through diameter and drill angle change. Source Bosch.

Rivera et al. [82] and Yi et al. [83] used CFD simulations and optimization tools to select the most favorable hole arrangement and spray pattern to enhance mixing and avert wall wetting. Injectors configured with small numbers of holes are typically used for research purposes, since the effect of pressure, fuel or geometry could be isolated and studied more easily (experimentally or computationally) [85, 87, 88]. Nevertheless, for real applications, injectors usually have six or more holes so that they can deliver the necessary amount of fuel in a limited time and distribute the fuel optimally throughout the combustion chamber.

Moon et al. [89] applied ultra-fast x-ray to study the effects of nozzle hole length and number on the spray formation in multi-holes GDI injectors with configuration two and ten orifices. They concluded that when the number of holes increases the radial and axial flow velocity decreases, which reduces flow break-up and atomization. The needle lift plays an important role since for these injectors it has a displacement of tenths of a micrometer, which is much smaller than the size of the orifices. The small needle lift accelerates and limits the flow of fuel upstream the sac. This influences the output of fuel through the holes causing instabilities and turbulence in the fuel jet. On the one hand, the turbulence induced by the needle lift can help the atomization of the fuel, but on the other hand, the pressure drop produced in the bag when there are several holes makes the speed of the spray jet and brake up

slow down. Therefore, there is a balance between the number of holes needed in the nozzle and the displacement of the needle, which requires a great effort for its optimization due to the complexity of the internal flow.

To represent these distribution of holes and needle heads, a tomographic pictures of the nozzles used in this research can be seen in Figure 2.16. The Spray G nozzle (up) depicts a slice through two opposing holes and is easier to look at since the holes are symmetrical with respect to the injector axis. It can be noted the needle head-ball resting in the needle seat in addition to the two holes and their counterbores. In the other hand, the PIU injector does not have counterbore and it is not axisymmetric. Figure 2.16 (bottom) shows a projection of the tomography of the PIU nozzle, where it can be observed that the needle head is not spherical having rather sharp edges. However, the PIU nozzle has a plane of symmetry that is shown in right side of Figure 2.14.

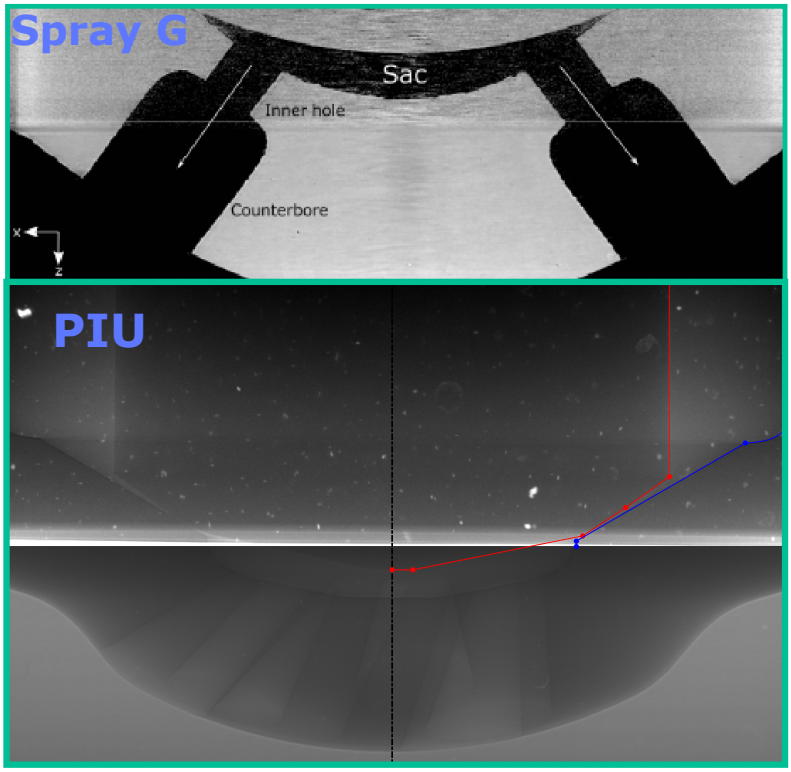

Figure 2.16: Symmetry plane slice from the tomographic reconstruction of the Spray G nozzle (up) and tomographic projection of the PIU nozzle (bottom). The needle shape is shown in both figures (For the PIU nozzle the red line follows the needle profile).

One important parameter to consider when designing the orifices is the length (L) and the diameter (D), which are normally studied through the L/D ratio. A small L/D is normally desirable because it increases the spray angle and jet velocity, atomize to smaller droplets and reduce the brake up length [90]. Befrui et al. [91] used a single hole nozzle geometry to compute Volume of Fluid Large-Eddy Simulation (VOF-LES), and exposed that flow characteristics in GDI holes are significantly different to Diesel injector holes, mainly due to the short L/D ratio (close to 1 versus values from 5-7 in diesel nozzles). Results from this work reported complete detachment of the flow caused by flow separation at the nozzle entrance. In addition, nozzles with L/D ratio from 0.8 to 1.5 experienced hydraulic flip, which is a phenomena associated with cavitation that occurs when the cavitation bubbles continue beyond the nozzle domain and blend with the ambient. The ambient condition, which is normally at a higher pressure than the vapor saturation pressure of the fuel, causes the suction of ambient air to the nozzle domain between the liquid core and orifice's wall. Thus the liquid-wall interaction is greatly diminished and the instabilities between the interface liquid-air increased are improved [92]. Shost et al. [93] simulated the flow of two nozzles with L/D ratios of 0.5 and 1.1 and identified that the shorter holes presented greater plume cone angles. Shost [94] also assessed the effect of L/D ratio between nozzles L/D=3 and L/D=1.1. The comparison was made by LES simulation, which yielded a important difference in the discharge coefficient from a value of 0.8 for the long nozzle compared to 0.6 for the short one. Moon et al. [89] researched the effect of orifices lengths in various multi-holes GDI nozzles observing that shorter holes caused the increment of axial and radial flow velocity at the nozzle exit, besides they reveal higher void fraction inside those holes. These higher velocities led to shorter break up length, stronger turbulence and diminished spray penetration in the direction of the plume axis. Results that are consistent with the conclusions of LES simulation comparing nozzle lengths from Befrui et al. [91].

Injector manufacturers have different approaches to injectors holes. Some of them, like Delphi in the Spray G, present to what is called counterbore or step-hole. This is a enlargement of the orifice diameter in the outside part of the nozzle. This geometry can be hardly appreciated in Figure 2.14 (left) where the external diameter belongs to the counterbore, albeit is easier to observe in the x-ray of Figure 2.16 (up). Counterbores are a designing result when pursuing nozzles with low L/D ratios. The GDI nozzles have to withstand high injection working pressures, so if the number and size of the holes is maintained, the implementation of a geometry of L/D=1 would not withstand the mechanical stresses in the nozzle (using L as wall thickness).

The solution is the step-hole, which provides the desired L/D ratio while keeping the injector integrity. In addition to maintaining thickness for structural safety, the counterbore is also essential because it includes additional protection from the combustion chamber's high temperatures at the exit of the inner holes. However, one drawback of this type of geometry is the ease with which deposits can be built up at the nozzle exit. Therefore, it must be taken into account in the careful hole design because otherwise, it would affect the spray morphology. Thus combustion and emissions performance [94].

The effect of counterbore has been researched by Shost [94] through VOF-LES simulations. In the study, two similar single hole nozzles were used, one with counterbore and another without it keeping the same diameter and length (L/D). The internal nozzle flow and the plume angle were found similar in both nozzles. Conversely, in the counterbore domain, it was observed a spread of vorticity of the fuel jet into the neighboring air, which is probably due to a combination of pressure disturbances and jet-induced air movement. Additional visualization experiments and VOF-LES simulations using a different three hole nozzle showed an apparent reduction of spray cone angle own to the influence of the counterbore [85]. Payri et al. [95] studied step-hole effect experimentally in diesel injectors, reporting that cone angle is increased and spray penetration speed reduced with the counterbores, which was coherent with GDI results. As stated previously, courterbore design must be performed meticulously to avoid deposits but also it could be source of liquid droplets in the nozzle tip, which could harm the emissions performance [70]. In the case of the "Spray G" study injector, the present step-holes are relatively small to accommodate all the orifices. Thus, strong interaction between the flow and step-holes walls was found in internal nozzle flow simulations [96].

Other important geometrical characteristic of the nozzle holes is the conicity. The nozzle orifices could be straight (cylindrical) or conical (tapered). It has been extensively studied in diesel injectors, which showed that straight nozzles are prone to cavitate because of flow separation at the inner edges, to finally present lower discharge coefficients. Nevertheless, cavitation can be helpful for cleaning possible deposits in the orifices in addition to promote atomization [97]. On the other hand, GDI nozzle holes are generally straight as this benefits the spray break up. Befrui et al. [91] and Shost [94] analyzed the influence of conicity on GDI nozzles performance, comparing a straight orifice with a tapered one. It was confirmed the similar trend that was already investigated in diesel nozzles (tapered holes decreased the cavitation and flow separation). For the GDI nozzles it was observed that tapered nozzle presented discharge coefficient significantly higher than straight nozzles ($C_d \approx 0.9$, compared with $C_d \approx 0.6$ for the straight one). Nevertheless,

the almost nonexistent flow separation produced less instabilities in the flow, resulting in an undesirable longer break up length.

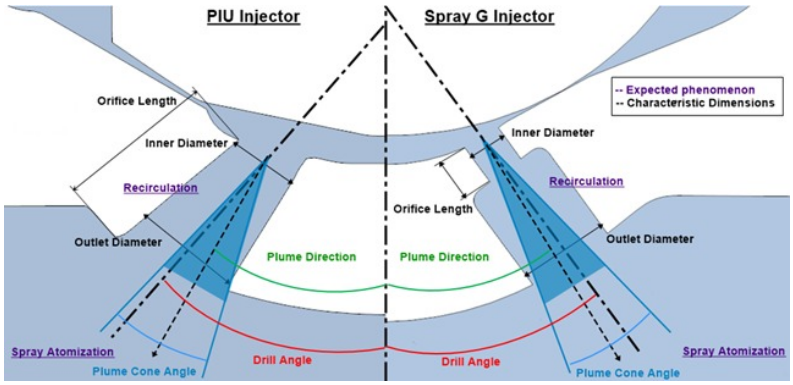

Figure 2.17: Slide comparing both injector orifices [98].

As we have seen so far, the nozzle geometry strongly influences the development and behavior of the fuel flow inside and outside of the injector. Therefore, for a proper investigation of the nozzle performance, is necessary to have reliable information of the final nozzle shape, especially for the CFD analysis. There are several approaches to measure nozzle geometry. Optical microscope could be used to take measurements of the orifices from outside, like counterbore and inner hole diameter, albeit it is very challenging to measure the diameter and not its projection. Other approach exposed by Macian et al. [99] is to use silicone mold to make a negative of the orifices, which is later gold coated to be seen by the Scanning Electron Microscope (SEM). This methodology was applied in the Spray G nozzles to successfully obtain the detailed geometry [60]. Nevertheless, this approach is difficult to asses in injectors whose nozzle can not be removed, then only cutting the injector would provide the nozzle to proceed. Moreover, the final silicon mold is often hard to homogeneously coat, which could result in imperfections and errors in the later SEM pictures.

A third approach to measure nozzle geometry is by x-rays tomography. Manin et al. [100] employed a commercial x-ray source to obtain nozzle geometry from same Spray G injector. It was reported acceptable resolution in the areas of the counterbore where the metal was not thick (the x-rays have to go through less metal), though the contrast was weaker in the nozzle seat and inner holes(more metal to go through). Matusik et al. [101] used x-rays, however, it was a stronger and continuous beam in the installations of the Advance Photon Source at Argonne National Laboratory. This greater

energy x-rays allowed a high-resolution tomography of the same injector, resulting in a stronger contrast images and increased pixel resolution even in the inside nozzle regions like the needle seat. The nozzle model was easier to obtain due to the increased differentiation between metal and air and a pixel resolution of 1.17 μm, which even showed the surface imperfections as shown in Figure 2.18. Strek et al. [102] used the same beam source to measure the density projections of near nozzle flow and compared them with Eulerian internal simulations. Matusik et al. [103] also applied the same methodology to eight Spray G nozzles to assess the effect of small geometrical variability in key nozzle dimensions and correlate those with time-resolved projected density of the injectors.

Shahangian et al. [98] used the same methodology on the PIU injector, However, they performed a surface smoothing because of many artifacts in the geometry. Figure 2.19 show the final geometry employed for their simulations.

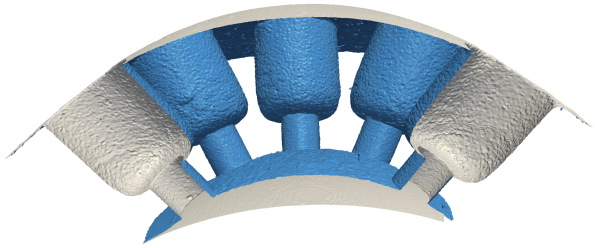

Figure 2.18: Iso-surface, showing Surface finish and internal geometry of one of the Spray G nozzles [101].

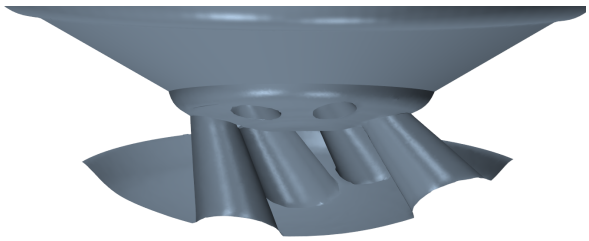

Figure 2.19: Iso-surface of the PIU nozzle. Light weight Geometry after applying surface smoothing [98].

2.6 Cavitation and Flash Boiling

Cavitation is a phenomenon in which there is a formation of small vapor-filled cavities due to sudden changes of pressure in a liquid. It plays an important role in GDI nozzles due to several factors, such as the geometry of the orifices (straight and short or inversely tapered [98]), low needle lift and finally because they atomize low vapor pressure fuels (gasoline, ethanol, and various mono-component fuels used for research purposes like iso-octane, n-heptane, n-hexane or pentane among others). The cavitation number (CN) is introduced to describe the potential initiation and development of cavitation in a flow, stated in Equation 2.3 [104]. Where P_{inj} is the injection fuel pressure, P_b is the pressure in the discharge chamber and P_v is the vapor pressure of the liquid fuel.

$$CN = \frac{P_{inj} - P_b}{P_b - P_v} \tag{2.3}$$

The cavitation number have been first thoroughly studied in Diesel nozzles [97, 105–108], and the ratio represent the forces supporting to the ones opposing cavitation. Bode et al. [109] employed diesel injectors to expose the limit between cavitating and non-cavitating flow through a critical CN, which was found to be around 5. Nonetheless in later study, Arcoumanis et al. [105] determined that the onset of cavitation was around 2 in diesel injectors. For GDI injectors, however, CN values are located around another much lower range. Gilles-Birth et al. [110] studied two GDI nozzles, finding noticeable lower cavitation numbers and that critical CN is dependent of the holes drill angle. It was found a critical CN of 0.81 for the nozzle with 50° (N50) and 0.64 for the one with 45° (N45), whose values are compared with two diesel injectors (from several authors) in Figure 2.20. The image depicts low critical CN values in the GDI nozzles in the whole domain, which the authors indicate is due to the fact that they are continuously in cavitation regime, and only the type of phenomena (string cavitation, bubbles, and super-cavitation) changes depending on the condition. One important conclusion from this work is that cavitation in this type of nozzles is highly dependent on the drill angle, being more severe for lower drill angle nozzle.

Other phenomenon that can appear during gasoline engine operation is flash boiling. It occurs when a liquid (in this case fuel) is injected into a volume, where the discharge pressure is lower than the saturation vapor pressure of the liquid (at that temperature). Flash boiling is a growing topic in gasoline direct injection research, and it takes place when injecting at the

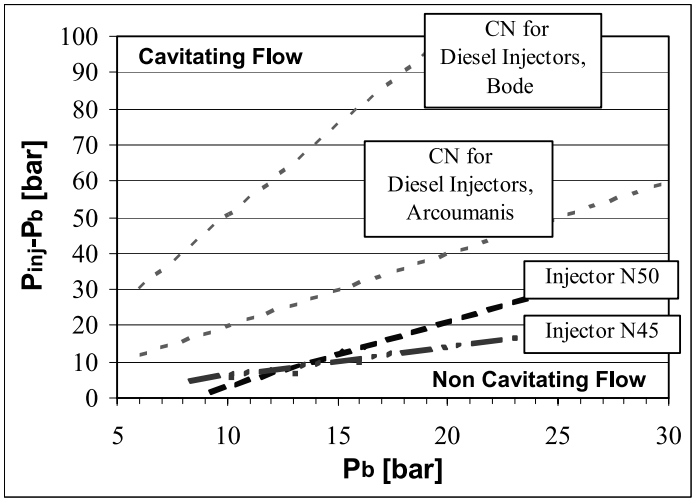

Figure 2.20: Comparison of the critical cavitation number for diesel injectors and two GDI nozzles with drill angles of 50° and 45° . Adapted from [110].

intake-stroke which creates vacuum (sub-atmospheric pressures) inside the cylinder. That sudden pressure change below its corresponded vapor pressure makes a super-heated liquid. For a regular (non-flashing) injection, the discharge chamber conditions are such that the fuel does not go through phase change but experienced primary and secondary atomization while exiting the nozzle. Figure 2.21 illustrates in a pressure-enthalpy diagram the states for the flash boiling injection. The initial compressed liquid fuel (1) experiences an adiabatic expansion process while going through the nozzle orifice. When the liquid accelerates and enter the meta-stable region (2-3), vapor nuclei form and grow, peaking on the liquid spinodal curve (3). At that point the liquid can be superheated without evaporation [111]. Beyond that point the liquid phase becomes unstable, and the phase change into gas develops promptly. Finally, the spray atomization completes the flashing phenomena. In conclusion, flash boiling is identified as a rapid phase change process which can be favorable to fast atomization and evaporation of the fuel spray in the cylinder.

There is a substantial amount of research in flash-boiling conditions in gasoline engines, and mostly in the last decade due to the development of GDI [87, 114–125]. Moulai et al. [117] employed a long distance microscope lens to look at the near nozzle flow and asses the interaction between step-hole wall and the liquid flow. It was noticed the plumes expansion was greater at flashing conditions, increasing their angle and interaction with other plumes besides nozzle wall and tip. Saha et al. [118] and Baldwin et al. [115] researched

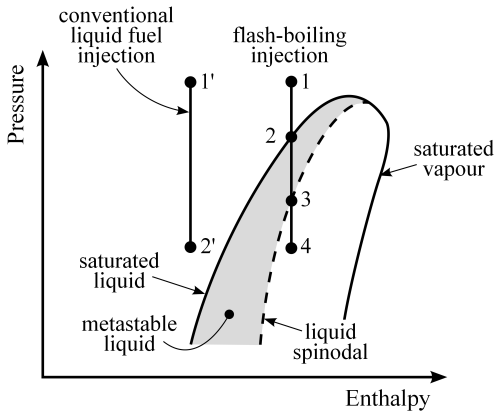

Figure 2.21: Representation of a conventional injection and one under Flash Boiling conditions in a pressure-enthalpy diagram. Adapted from [112, 113].

the vapor generation because of cavitation and flash boiling in internal flow through LES simulations. They found that the plumes angles and the droplets velocity increased when at flash boiling operation. Guo et al. [120, 125] also observed wide spray plumes in flashing conditions when visualizing the external spray through MIE scattering technique. The strong plume interaction can led to the collapse of the sprays into a big single one, as observed in other studies [119, 126]. Spray collapse could occur as well at high ambient density condition, though the trigger and development mechanism are different [100, 120].

One parameter to measure the degree of superheated fuel is the relation between the ambient pressure over the saturation pressure at that fuel temperature, showed in Equation 2.4 [122].

$$R_p = \frac{P_{sat}(f(T_f))}{P_{amb}} \tag{2.4}$$

Essentially, two flashing regimes has been identified according to the location of the radial expansion, which are called internal and external flashing [113]. It has been reported that external flashing occurs at relatively low R_p while internal flashing occurs at relatively high R_p [127, 128].

However, it does not always describe well the fuel jet, as reported by Guo et al. [123]. They found that for sub-cooled and transitional regions where $R_p < 3.3$ there is good relation between R_p and spray width, which represent the radial expansion. However, for $R_p > 3.3$ the jet width is different for similar R_p. The radial expansion is a parameter that tries to explain the

spray collapse [125]. At high super-heated levels, the interaction between under-expanded flashing jets make them deflect towards each other, which ends up merging into one jet moving along the central axis resulting in spray collapse. It is ascribed to the pressure drop in the central area between the jets. Li et al. [129] demonstrated that the collapse of multi jet flash boiling sprays was induced by vapor condensation at the nozzle exit. It stated that nozzle configuration plays a major role in the possibilities of developing spray collapse or not. Guo et al. [120] observed two spray collapses types due to different spray conditions and both related with radial expansion. At elevated ambient pressure the spray collapse occurred in the near field whereas under flash boiling conditions the collapse occurred in the far field. It was reported that the near field collapse at elevated ambient pressure occurred due to the low pressure zones of the surrounding high speed jets. The collapse at flash boiling conditions was attributed to the low pressure zone caused by the temperature drop and vapor condensation.

Since the flash boiling is related to the bubble formation and evaporation in the jet. Through the nucleation rate it could be explained the radial expansion [122]. In the classical nucleation theory, the rate of nucleation (J) could be expressed as:

$$J \propto \sqrt{\frac{2\sigma}{\pi m}} exp\left(-\frac{\Delta G^*}{k_B T_{fuel}}\right) \tag{2.5}$$

where m is the liquid molecular mass, σ is the surface tension, ΔG^* is the free energy barrier and k_B is the Boltzmann constant. For this case, the free energy barrier for homogeneous nucleation can be described as:

$$G^* = \frac{16\pi v_m^2 \sigma^3}{3\Delta\mu^2} \tag{2.6}$$

where $\Delta\mu = k_B T_{fuel} ln(R_p)$ is the chemical potential difference between the liquid and vapor phases, then $v_m = m/(\rho_l N_A)$ is the specific volume of liquid state, in which ρ_l is the liquid density and N_A is the Avogadro constant.

Guo et al. [122] found that there was a relation between the spray width and the exponent of Equation 2.5 (which they called X), since it mostly determines the nucleation rate. They reported two different stages, the first one where the spray width increases with $X^{-0.5}$ and the second where it becomes less sensitive. The second stage level is much related to the fuel temperature as it can be observed in Figure 2.22. They state that in the

first stage the radial expansion is governed by the nucleation rate while in the second by the thermal energy for vaporization.

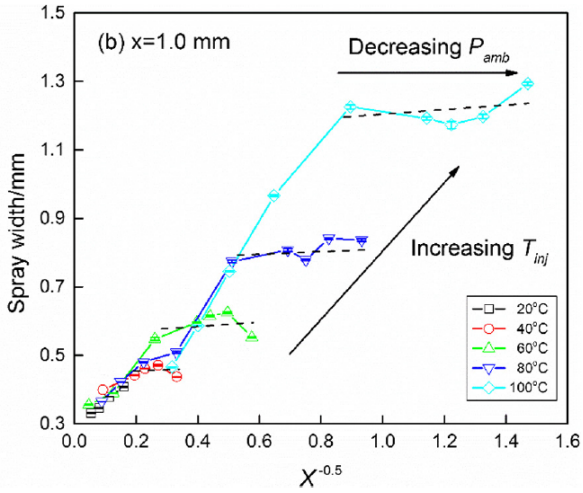

Figure 2.22: Spray width versus $X^{-0.5}$ at 1 mm from the nozzle exit [122].

These studies are reviewed further in chapter 6 while introducing the results from this work reporting the characterization of the external spray of both nozzles.

References

[1] IEA. *A technology roadmap: Electric and plug-in hybrid electric vehicles*. Tech. rep. June. International Energy Agency, 2011, pp. 3471–3473.

[2] IEA. "Global Energy Review 2020". In: *Global Energy Review 2020* (2020). DOI: 10.1787/a60abbf2-en.

[3] Starikovskiy, Andrey and Aleksandrov, Nickolay. "Plasma-assisted ignition and combustion". In: *Progress in Energy and Combustion Science* 39.1 (2013), pp. 61–110. DOI: 10.1016/j.pecs.2012.05.003.

[4] Olusegun, Atanda et al. "We are IntechOpen , the world ' s leading publisher of Open Access books Built by scientists , for scientists TOP 1 %". In: *Intech* i.tourism (2012), p. 38. DOI: 10.1016/j.colsurfa.2011.12.014.

[5] Wang, Zhongli et al. "Experimental Study of Influence on Microwave Plasma Ignition Combustion Performance of Pulse Microwave Signals". In: *IEEE Access* 7 (2019), pp. 23951–23958. DOI: 10.1109/ACCESS.2019.2899911.

[6] Pavel, Nicolaie et al. "Laser ignition - Spark plug development and application in reciprocating engines". In: *Progress in Quantum Electronics* 58.April (2018), pp. 1–32. DOI: 10.1016/j.pquantelec.2018.04.001.

[7] Chehroudi, Bruce. "Laser Ignition For Combustion Engines". In: *Engineering* October (2004), pp. 1–5. DOI: 10.13140/2.1.1845.1206.

[8] Okahara, Akio. "Problems of Plasma Ignition System". In: 1 (2016), pp. 64–72.

[9] Payri, Francisco and Desantes, Jose Maria. *Motores de combustion interna alternativos*. Editorial Universitat Politecnica de Valencia, 2011.

[10] Spicher, U., Reissing, J., Kech, J. M., and Gindele, J. "Gasoline Direct Injection (GDI) Engines - Development Potentialities". In: *SAE Technical Papers*. 724. 1999. DOI: 10.4271/1999-01-2938.

[11] Zhao, F., Lai, M.-C, and Harrington, D.L. "Automotive spark-ignited direct-injection gasoline engines". In: *Progress in Energy and Combustion Science* 25.5 (1999), pp. 437–562. DOI: 10.1016/S0360-1285(99)00004-0.

[12] Benz, Carlz. *No. 382,585*. 1888.

[13] Halderman, James D. *Automotive Fuel and Emissions control systems*. 2012.

[14] Bahattin, Mustafa and Ozdaly, Bulent. "Gasoline Direct Injection". In: *Fuel Injection*. Sciyo, 2010. DOI: 10.5772/9693.

[15] Pham, P.X., Vo, D.Q., and Jazar, R.N. "Development of fuel metering techniques for spark ignition engines". In: *Fuel* 206 (2017), pp. 701–715. DOI: 10.1016/j.fuel.2017.06.043.

[16] Ingraham, Joseph C. *Automobiles: Races; Everybody Manages to Win Something At the Daytona Beach Contests*. 1957.

[17] Konrad Reif, ed. *Gasoline Engine Management*. Wiesbaden: Springer Fachmedien Wiesbaden, 2015. DOI: 10.1007/978-3-658-03964-6.

[18] Saliba, Georges et al. "Comparison of Gasoline Direct-Injection (GDI) and Port Fuel Injection (PFI) Vehicle Emissions: Emission Certification Standards, Cold-Start, Secondary Organic Aerosol Formation Potential, and Potential Climate Impacts". In: *Environmental Science and Technology* (2017). DOI: 10.1021/acs.est.6b06509.

[19] He, Lv, Jingyuan, Li, Xiumin, Yu, Mengliang, Li, and Tian, Yang. "Numerical study on combustion and emission characteristics of a PFI gasoline engine with hydrogen direct-injection". In: *Energy Procedia* 158 (2019), pp. 1449–1454. DOI: 10.1016/j.egypro.2019.01.348.

[20] Ma, Dong Shuo and Sun, Z. Y. "Progress on the studies about NOx emission in PFI-H2ICE". In: *International Journal of Hydrogen Energy* 45.17 (2020), pp. 10580–10591. DOI: 10.1016/j.ijhydene.2019.11.065.

[21] McCaffery, Cavan, Durbin, Thomas D., Johnson, Kent C., and Karavalakis, Georgios. "The effect of ethanol and iso-butanol blends on polycyclic aromatic hydrocarbon (PAH) emissions from PFI and GDI vehicles". In: *Atmospheric Pollution Research* August (2020), pp. 0–1. DOI: 10.1016/j.apr.2020.08.024.

[22] Chen, Longfei, Liang, Zhirong, Zhang, Xin, and Shuai, Shijin. "Characterizing particulate matter emissions from GDI and PFI vehicles under transient and cold start conditions". In: *Fuel* 189 (2017), pp. 131–140. DOI: 10.1016/j.fuel.2016.10.055.

[23] Zhu, Rencheng et al. "Tailpipe emissions from gasoline direct injection (GDI) and port fuel injection (PFI) vehicles at both low and high ambient temperatures". In: *Environmental Pollution* 216 (2016), pp. 223–234. DOI: 10.1016/j.envpol.2016.05.066.

[24] Yang, Zhengjun et al. "Real driving particle number (PN) emissions from China-6 compliant PFI and GDI hybrid electrical vehicles". In: *Atmospheric Environment* 199.September 2018 (2019), pp. 70–79. DOI: 10.1016/j.atmosenv.2018.11.037.

[25] Li, Yaoting et al. "A comprehensive experimental investigation on the PFI spray impingement: Effect of impingement geometry, cross-flow and wall temperature". In: *Applied Thermal Engineering* 159.May (2019), p. 113848. DOI: 10.1016/j.applthermaleng.2019.113848.

[26] Vaquerizo, Daniel. "Study on Advanced Spray-Guided Gasoline Direct Injection Systems". PhD thesis. Universitat Politècnica de València, 2017.

[27] Chincholkar, S.P. and Suryawanshi, J.G. "Gasoline Direct Injection: An Efficient Technology". In: *Energy Procedia* 90.December 2015 (2016), pp. 666–672. DOI: 10.1016/j.egypro.2016.11.235.

[28] Shuai, Shijin, Ma, Xiao, Li, Yanfei, Qi, Yunliang, and Xu, Hongming. "Recent Progress in Automotive Gasoline Direct Injection Engine Technology". In: *Automotive Innovation* 1.2 (2018), pp. 95–113. DOI: 10.1007/s42154-018-0020-1.

[29] Van Basshuysen, Richard and Spicher, Ulrich. *Gasoline engine with direct injection : processes, systems, development, potential*. eng. Ed. by Richard Van Basshuysen and Ulrich Spicher. Wiesbaden, 2009.

[30] Iwamoto, Y., Noma, K., Nakayama, O., Yamauchi, T., and Ando, H. "Development of Gasoline Direct Injection Engine". In: *SAE Technical Papers*. 412. 1997. DOI: 10.4271/970541.

[31] Harada, Jun, Tomita, Tsutomu, Mizuno, Hiroyuki, Mashiki, Zenichiro, and Ito, Yasushi. "Development of direct injection gasoline engine". In: *SAE Technical Papers* 412 (1997). DOI: 10.4271/970540.

[32] Zhao, Hua. *Advanced direct injection combustion engine technologies and development*. Woodhead Publishing Limited, 2010. DOI: 10.1533/9781845697327.

[33] Erjavec, Jack. *Automotive Technology : A systems approach*. 5th. Cengage Learning, Inc, 2009, p. 1665.

[34] Fansler, Todd D. and Parrish, Scott E. "Spray measurement technology: a review". In: *Measurement Science and Technology* 26.1 (2015), p. 012002. DOI: 10.1088/0957-0233/26/1/012002.

[35] Zhuang, Yuan et al. "Investigation of water injection benefits on downsized boosted direct injection spark ignition engine". In: *Fuel* 264.October 2019 (2020). DOI: 10.1016/j.fuel.2019.116765.

[36] Berni, Fabio, Breda, Sebastiano, Lugli, Mattia, and Cantore, Giuseppe. "A numerical investigation on the potentials of water injection to increase knock resistance and reduce fuel consumption in highly downsized GDI engines". In: *Energy Procedia* 81 (2015), pp. 826–835. DOI: 10.1016/j.egypro.2015.12.091.

[37] Cho, Jaeho, Kim, Kangjin, Baek, Sungha, Myung, Cha Lee, and Park, Simsoo. "Abatement potential analysis on CO2 and size-resolved particle emissions from a downsized LPG direct injection engine for passenger car". In: *Atmospheric Pollution Research* 10.6 (2019), pp. 1711–1722. DOI: 10.1016/j.apr.2019.07.002.

[38] Cavicchi, Andrea, Postrioti, Lucio, and Scarponi, Edoardo. "Hydraulic analysis of a GDI injector operation with close multi-injection strategies". In: *Fuel* 235.July 2017 (2019), pp. 1114–1122. DOI: 10.1016/j.fuel.2018.08.089.

[39] Cavicchi, Andrea and Postrioti, Lucio. "Simultaneous needle lift and injection rate measurement for GDI fuel injectors by laser Doppler vibrometry and Zeuch method". In: *Fuel* 285.August 2020 (2021), p. 119021. DOI: 10.1016/j.fuel.2020.119021.

[40] Cavicchi, Andrea, Postrioti, Lucio, Berni, Fabio, Fontanesi, Stefano, and Di Gioia, Rita. "Evaluation of hole-specific injection rate based on momentum flux measurement in GDI systems". In: *Fuel* 263.June 2019 (2020). DOI: 10.1016/j.fuel.2019.116657.

[41] Hentschel, Werner. "Optical Diagnostics Combustion Process Development DI Gasoline Engines". In: 28 (2000), pp. 1119–1135.

[42] Costa, M. et al. "Split injection in a homogeneous stratified gasoline direct injection engine for high combustion efficiency and low pollutants emission". In: *Energy* 117.2016 (2016), pp. 405–415. DOI: 10.1016/j.energy.2016.03.065.

[43] Hentschel, W. et al. "Optical Diagnostics and CFD-Simulations to Support the Combustion Process Development of the Volkswagen FSI® Direct-Injection Gasoline Engine". In: *SAE Technical Papers*. 724. 2001. DOI: 10.4271/2001-01-3648.

[44] Zeng, Wei, Sjöberg, Magnus, Reuss, David L., and Hu, Zongjie. "The role of spray-enhanced swirl flow for combustion stabilization in a stratified-charge DISI engine". In: *Combustion and Flame* 168.x (2016), pp. 166–185. DOI: 10.1016/j.combustflame.2016.03.015.

[45] Zeng, Wei and Sjöberg, Magnus. "Utilizing boost and double injections for enhanced stratified-charge direct-injection spark-ignition engine operation with gasoline and E30 fuels". In: *International Journal of Engine Research* 18.1-2 (2017), pp. 131–142. DOI: 10.1177/1468087416685512.

[46] Moon, Seoksu, Huang, Weidi, and Wang, Jin. "Spray formation mechanism of diverging-tapered-hole GDI injector and its potentials for GDI engine applications". In: *Fuel* 270.March (2020), p. 117519. DOI: 10.1016/j.fuel.2020.117519.

[47] Lee, Ziyoung, Kim, Taehoon, Park, Sungwook, and Park, Suhan. "Review on spray, combustion, and emission characteristics of recent developed direct-injection spark ignition (DISI) engine system with multi-hole type injector". In: *Fuel* 259.July 2019 (2020), p. 116209. DOI: 10.1016/j.fuel.2019.116209.

[48] Duan, Xiongbo et al. "Quantitative investigation the influences of the injection timing under single and double injection strategies on performance, combustion and emissions characteristics of a GDI SI engine fueled with gasoline/ethanol blend". In: *Fuel* 260.August 2019 (2020), p. 116363. DOI: 10.1016/j.fuel.2019.116363.

[49] Cho, Jungkeun and Song, Soonho. "Prediction of hydrogen-added combustion process in T-GDI engine using artificial neural network". In: *Applied Thermal Engineering* 181.May (2020), p. 115974. DOI: 10.1016/j.applthermaleng.2020.115974.

[50] Zhou, Jianwei et al. "Characteristics of near-nozzle spray development from a fouled GDI injector". In: *Fuel* 219.92 (2018), pp. 17–29. DOI: 10.1016/j.fuel.2018.01.070.

[51] Banerjee, R. and Kumar, Santhosh. "Numerical investigation of stratified air/fuel preparation in a GDI engine". In: *Applied Thermal Engineering* 104 (2016), pp. 414–428. DOI: 10.1016/j.applthermaleng.2016.05.050.

[52] Su, Yu Hsuan and Kuo, Ting Fu. "CFD-assisted analysis of the characteristics of stratified-charge combustion inside a wall-guided gasoline direct injection engine". In: *Energy* 175.x (2019), pp. 151–164. DOI: 10.1016/j.energy.2019.03.031.

[53] Zheng, Zhaolei, Tian, Xuefeng, and Zhang, Xiaoyu. "Effects of split injection proportion and the second injection time on the mixture formation in a GDI engine under catalyst heating mode using stratified charge strategy". In: *Applied Thermal Engineering* 84 (2015), pp. 237–245. DOI: 10.1016/j.applthermaleng.2015.03.041.

[54] Feng, Shuang et al. "Influence of stratified charge organized by double injection strategy on combustion and emissions on an EGR diluted GDI engine". In: *Applied Thermal Engineering* 158.May (2019), p. 113803. DOI: 10.1016/j.applthermaleng.2019.113803.

[55] Gong, Changming, Yi, Lin, Zhang, Zilei, Sun, Jingzhen, and Liu, Fenghua. "Assessment of ultra-lean burn characteristics for a stratified-charge direct-injection spark-ignition methanol engine under different high compression ratios". In: *Applied Energy* 261.January (2020), p. 114478. DOI: 10.1016/j.apenergy.2019.114478.

[56] Jeon, J., Bock, N., and Northrop, W. F. "In-cylinder flame luminosity measured from a stratified lean gasoline direct injection engine". In: *Results in Engineering* 1.January (2019), p. 100005. DOI: 10.1016/j.rineng.2019.100005.

[57] Costa, M., Catapano, F., Sementa, P., Sorge, U., and Vaglieco, B. M. "Mixture preparation and combustion in a GDI engine under stoichiometric or lean charge: an experimental and numerical study on an optically accessible engine". In: *Applied Energy* 180 (2016), pp. 86–103. DOI: 10.1016/j.apenergy.2016.07.089.

[58] Jeon, Joonho. "Spatiotemporal flame propagations, combustion and solid particle emissions from lean and stoichiometric gasoline direct injection engine operation". In: *Energy* 210 (2020), p. 118652. DOI: 10.1016/j.energy.2020.118652.

[59] Yu, Xiumin et al. "Investigation of combustion and emissions of an SI engine with ethanol port injection and gasoline direct injection under lean burn conditions". In: *Energy* 189 (2019), p. 116231. DOI: 10.1016/j.energy.2019.116231.

[60] Payri, Raul, Gimeno, Jaime, Marti-Aldaravi, Pedro, and Vaquerizo, Daniel. "Momentum Flux Measurements on an ECN GDi Injector". In: *SAE Technical Paper 2015-01-1893*. 2015. DOI: 10.4271/2015-01-1893.

[61] Payri, Raul, Gimeno, Jaime, Martí-Aldaraví, Pedro, and Vaquerizo, Daniel. "Internal flow characterization on an ECN GDi injector". In: *Atomization and Sprays* 26.9 (2016), pp. 889–919. DOI: 10.1615/AtomizSpr.2015013930.

[62] Payri, Raul, Bracho, Gabriela, Gimeno, Jaime, and Bautista, Abian. "Rate of injection modelling for gasoline direct injectors". In: *Energy Conversion and Management* 166 (2018), pp. 424–432. DOI: 10.1016/j.enconman.2018.04.041.

[63] Parotto, Marco, Sgatti, Stefano, and Sensi, Fabio. "Advanced GDI Injector Control with Extended Dynamic Range". In: *SAE Technical Papers*. Vol. 2. 2013. DOI: 10.4271/2013-01-0258.

[64] Johansson, Anders N., Hemdal, Stina, and Dahlander, Petter. "Reduction of Soot Formation in an Optical Single-Cylinder Gasoline Direct-Injected Engine Operated in Stratified Mode Using 350 Bar Fuel Injection Pressure, Dual-Coil and High-Frequency Ignition Systems". In: *SAE International Journal of Engines* 10.3 (2017), pp. 2017–01–9278. DOI: 10.4271/2017-01-9278.

[65] Hoffmann, Guy, Befrui, Bizhan, Berndorfer, Axel, Piock, Walter F., and Varble, Daniel L. "Fuel System Pressure Increase for Enhanced Performance of GDi Multi-Hole Injection Systems". In: *SAE International Journal of Engines* 7.1 (2014), pp. 2014–01–1209. DOI: 10.4271/2014-01-1209.

[66] Gomot, Dipl Baudouin and Hülser, Holger. "Delphi Technologies Next Generation GDi-System, improved Emissions and Efficiency with higher Pressure". In: *Internationales Wiener Motorensymposium* (2019), pp. 1–21.

[67] Granqvist, Peter. "High efficient SI-engine with ultra high injection pressure [Research @ Chalmers University]". In: October. Gothenburg, Sweden: Energirelaterad forskning 2017, 2017.

[68] Husted, Harry, Spegar, Timothy D., and Spakowski, Joseph. "The Effects of GDi Fuel Pressure on Fuel Economy". In: *SAE Technical Papers*. Vol. 1. 2014. DOI: 10.4271/2014-01-1438.

[69] Magneti Marelli. "Gasoline Direct Injection Technology advancements". In: *2015 SAE-China Congress & Exhibition*. Shanghai, China: Society of Automotive Engineers, 2015.

[70] Pauer, Thomas, Yilmaz, Hakan, Zumbrägel, Joachim, and Schünemann, Erik. "New Generation Bosch Gasoline Direct-injection Systems". In: *MTZ worldwide* 78.7-8 (2017), pp. 16–23. DOI: 10.1007/s38313-017-0053-6.

[71] Kanda, Mutsumi et al. "Application of a New Combustion Concept to Direct Injection Gasoline Engine". In: *SAE Technical Papers*. Vol. 2000. 724. 2000. DOI: 10.4271/2000-01-0531.

[72] Wood, Andrew. "Optical investigations of the sprays generated by gasoline multi-hole injectors under novel operating conditions". PhD thesis. Loughborough University, 2014.

[73] Wu, Zengyang, Wang, Libing, Badra, Jihad A., Roberts, William L., and Fang, Tiegang. "GDI fuel sprays of light naphtha, PRF95 and gasoline using a piezoelectric injector under different ambient pressures". In: *Fuel* 223.December 2017 (2018), pp. 294–311. DOI: 10.1016/j.fuel.2018.03.009.

[74] Dahlander, Petter, Iemmolo, Daniele, and Tong, Yifei. "Measurements of Time-Resolved Mass Injection Rates for a Multi-Hole and an Outward Opening Piezo GDI Injector". In: *SAE Technical Papers*. Vol. 2015-April. April. 2015. DOI: 10.4271/2015-01-0929.

[75] Vent, Guido and Enderle, Christian. "The new 2.0 l turbo engine from the Mercedes-Benz 4-cylinder engine family". In: *2nd Aachen Colloquium China* (2012).

[76] Wigley, G., Pitcher, G., Nuglisch, H., Helie, J., and Ladommatos, N. "Fuel Spray Formation and Gasoline Direct Injection". In: *8th AVL international symposium on combustion diagnostics*. 2008.

[77] Marchi, A., Nouri, J., Yan, Y., and Arcoumanis, C. "Spray stability of outwards opening pintle injectors for stratified direct injection spark ignition engine operation". In: *International Journal of Engine Research* 11.6 (2010). Ed. by Dinos Arcoumanis, pp. 413–437. DOI: 10.1243/14680874JER605.

[78] Zigan, L., Schmitz, I., Flügel, A., Wensing, M., and Leipertz, A. "Structure of evaporating single- and multicomponent fuel sprays for 2nd generation gasoline direct injection". In: *Fuel* 90.1 (2011), pp. 348–363. DOI: 10.1016/j.fuel.2010.08.001.

[79] Payri, Raul, Gimeno, Jaime, Mata, Carmen, and Viera, Alberto. "Rate of injection measurements of a direct-acting piezoelectric injector for different operating temperatures". In: *Energy Conversion and Management* 154.October (2017), pp. 387–393. DOI: 10.1016/j.enconman.2017.11.029.

[80] Smith, James, Szekely Jr, Gerald, Solomon, Arun, and Parrish, Scott. "A Comparison of Spray-Guided Stratified-Charge Combustion Performance with Outwardly-Opening Piezo and Multi-Hole Solenoid Injectors". In: *SAE International Journal of Engines* 4.1 (2011), pp. 2011–01–1217. DOI: 10.4271/2011-01-1217.

[81] Kwak, H.C. et al. "The New V6 3.5L Turbo GDI Engine from Hyundai-Kia". In: *27th Aachen Colloquium Automobile and Engine Technology*. Aachen, 2018.

[82] Rivera, Edwin A., Mastro, Noreen, Zizelman, James, Kirwan, John, and Ooyama, Robert. "Development of Injector for the Direct Injection Homogeneous Market using Design for Six Sigma". In: *SAE Technical Papers*. 2010. DOI: 10.4271/2010-01-0594.

[83] Yi, Jianwen et al. "Development and Optimization of the Ford 3.5L V6 EcoBoost Combustion System". In: *SAE International Journal of Engines* 2.1 (2009), pp. 2009–01–1494. DOI: 10.4271/2009-01-1494.

[84] "Engine Combustion Network". In: *https://ecn.sandia.gov/gasoline-spray-combustion/* (2020).

[85] Befrui, Bizhan, Hoffmann, Guy, Kirwan, John, Piock, Walter, and Schilling, Sebastian. "Analytical Optimization of Delphi GDi Fuel Injection Systems". In: *15th Conference "The Working Process of the Internal Combustion Engine"* September 2015 (2015).

[86] Delphi Technologies. "New 500+ bar GDi system cuts particulates by up to 50% without engine changes". In: *News release* (2019).

[87] Postrioti, Lucio et al. "Momentum Flux Measurement on Single-Hole GDI Injector under Flash-Boiling Condition". In: *SAE Technical Papers*. Vol. 24. 2480. 2015. DOI: 10.4271/2015-24-2480.

[88] Cavicchi, Andrea et al. "Numerical and experimental analysis of the spray momentum flux measuring on a GDI injector". In: *Fuel* 206 (2017), pp. 614–627. DOI: 10.1016/j.fuel.2017.06.054.

[89] Moon, Seoksu et al. "Ultrafast X-ray study of multi-hole GDI injector sprays: Effects of nozzle hole length and number on initial spray formation". In: *Experimental Thermal and Fluid Science* 68 (2015), pp. 68–81. DOI: 10.1016/j.expthermflusci.2015.03.027.

[90] Tu, Po-Wen et al. "Numerical Investigation of GDI Injector Nozzle Geometry on Spray Characteristics". In: *SAE Technical Papers*. Vol. 2015-Septe. September. 2015. DOI: 10.4271/2015-01-1906.

[91] Befrui, Bizhan, Corbinelli, Giovanni, Spiekermann, Peter, Shost, Mark, and Lai, Ming-Chia. "Large Eddy Simulation of GDI Single-Hole Flow and Near-Field Spray". In: *SAE International Journal of Fuels and Lubricants* 5.2 (2012), pp. 2012–01–0392. DOI: 10.4271/2012-01-0392.

[92] Befrui, B., Corbinelli, G., Hoffmann, G., Andrews, R. J., and Sankhalpara, S. R. "Cavitation and Hydraulic Flip in the Outward-Opening GDi Injector Valve-Group". In: *SAE Technical Papers*. 2009. DOI: 10.4271/2009-01-1483.

[93] Shost, Mark A., Lai, Ming-Chia, Befrui, Bizhan, Spiekermann, Peter, and Varble, Daniel L. "GDi Nozzle Parameter Studies Using LES and Spray Imaging Methods". In: *SAE Technical Papers*. Vol. 1. 2014. DOI: 10.4271/2014-01-1434.

[94] Shost, Mark Anthony. "Evaluation of nozzle geometry on high pressure Gasoline Direct Injection spray atomization". PhD thesis. Wayne State University, 2014, p. 295.

[95] Payri, Raul, Hardy, Gilles, Gimeno, Jaime, and Bautista, Abian. "Analysis of counterbore effect in five diesel common rail injectors". In: *Experimental Thermal and Fluid Science* 107 (2019), pp. 69–78. DOI: 10.1016/j.expthermflusci.2019.05.008.

[96] Befrui, Bizhan et al. "ECN GDi Spray G : Coupled LES Jet Primary Breakup - Lagrangian Spray Simulation and Comparison with Data". In: *ILASS Americas 28th* June (2016).

[97] Payri, F., Payri, Raul, Salvador, F.J., and Martínez-López, Jorge. "A contribution to the understanding of cavitation effects in Diesel injector nozzles through a combined experimental and computational investigation". In: *Computers & Fluids* 58 (2012), pp. 88–101. DOI: 10.1016/j.compfluid.2012.01.005.

[98] Shahangian, Navid et al. "Transient nozzle flow simulations of gasoline direct fuel injectors". In: *Applied Thermal Engineering* 175.January (2020). DOI: 10.1016/j.applthermaleng.2020.115356.

[99] Macian, Vicente, Bermudez, V., Payri, Raul, and Gimeno, Jaime. "New technique for determination of internal geometry of a diesel nozzle with the use of silicone methodology". In: *Experimental Techniques* 27.2 (2003), pp. 39–43. DOI: 10.1111/j.1747-1567.2003.tb00107.x.

[100] Manin, Julien et al. "Experimental Characterization of DI Gasoline Injection Processes". In: 2015. DOI: 10.4271/2015-01-1894.

[101] Matusik, Katarzyna E, Duke, Daniel J, Swantek, Andrew B, Powell, Christopher F, and Kastengren, Alan L. "High Resolution X-Ray Tomography of Injection Nozzles". In: *ILASS Americas 28th Annual Conference on Liquid Atomization and Spray Systems, Dearborn, MI, May 2016*. May. 2016.

[102] Strek, Piotr et al. "X-Ray Radiography and CFD Studies of the Spray G Injector". In: *SAE Technical Papers* 2016-April.April (2016). DOI: 10.4271/2016-01-0858.

[103] Matusik, Katarzyna E et al. "A study on the relationship between internal nozzle geometry and injected mass distribution of eight ECN Spray G nozzles." In: *Proceedings ILASS,ÄìEurope 2017. 28th Conference on Liquid Atomization and Spray Systems*. September. Valencia: Universitat Politècnica València, 2017, pp. 6–8. DOI: 10.4995/ILASS2017.2017.4766.

[104] Bergwerk, W. "Flow Pattern in Diesel Nozzle Spray Holes". In: *Proceedings of the Institution of Mechanical Engineers* 173.1 (1959), pp. 655–660. DOI: 10.1243/PIME_PROC_1959_173_054_02.

[105] Arcoumanis, C., Flora, H., Gavaises, M., and Badami, M. "Cavitation in Real-Size Multi-Hole Diesel Injector Nozzles". In: *SAE Technical Papers*. 724. 2000. DOI: 10.4271/2000-01-1249.

[106] Desantes, Jose Maria, Payri, Raul, Salvador, Francisco Javier, and Gimeno, Jaime. "Measurements of Spray Momentum for the Study of Cavitation in Diesel Injection Nozzles". In: *SAE Technical Paper 2003-01-0703*. Society of Automotive Engineers, Inc., Warrendale, Pennsylvania, USA, 2003. DOI: 10.4271/2003-01-0703.

[107] Desantes, Jose Maria, Payri, Raul, Salvador, Francisco Javier, and Morena., J. de la. "Cavitation effects on spray characteristics in the near-nozzle field". In: *SAE Technical Paper 09ICE-0151*. 2009. DOI: 10.4271/2009-24-0037.

[108] Payri, Francisco, Arrègle, Jean, Lopez, Jose Javier, and Hermens, Sjoerd. "Effect of Cavitation on the Nozzle Outlet Flow, Spray and Flame Formation in a Diesel Engine." In: *SAE Paper 2006-01-1391* (2006).

[109] Bode, J et al. "Fuel spray in Diesel engines. Part I: Spray formation". In: *ATA 92A065* (1992).

[110] Gilles-Birth, Isabell, Bernhardt, Sören, Spicher, Ulrich, and Rechs, Manfred. "A Study of the In-Nozzle Flow Characteristic of Valve Covered Orifice Nozzles for Gasoline Direct Injection". In: *SAE Technical Papers*. 724. 2005. DOI: 10.4271/2005-01-3684.

[111] Sher, Eran, Bar-Kohany, Tali, and Rashkovan, Alexander. "Flash-boiling atomization". In: *Progress in Energy and Combustion Science* 34.4 (2008), pp. 417–439. DOI: 10.1016/j.pecs.2007.05.001.

[112] Poursadegh, Farzad. "An experimental and theoretical investigation of direct fuel injection". PhD thesis. The University Of Melbourne, 2017, p. 205.

[113] Oza, Rajshekhar D. and Sinnamon, James F. "An Experimental and Analytical Study of Flash-Boiling Fuel Injection". In: *SAE Technical Papers*. 1983. DOI: 10.4271/830590.

[114] Serras-Pereira, J et al. "Cavitation, primary break-up and flash boiling of gasoline, iso-octane and n-pentane with a real-size optical direct-injection nozzle". In: *Fuel* (2010). DOI: 10.1016/j.fuel.2010.03.030.

[115] Baldwin, E.T. et al. "String flash-boiling in gasoline direct injection simulations with transient needle motion". In: *International Journal of Multiphase Flow* 87 (2016), pp. 90–101. DOI: 10.1016/j.ijmultiphaseflow.2016.09.004.

[116] Chan, Qing N., Bao, Yongming, and Kook, Sanghoon. "Effects of injection pressure on the structural transformation of flash-boiling sprays of gasoline and ethanol in a spark-ignition direct-injection (SIDI) engine". In: *Fuel* 130 (2014), pp. 228–240. DOI: 10.1016/j.fuel.2014.04.015.

[117] Moulai, Maryam, Grover, Ronald, Parrish, Scott, and Schmidt, David. "Internal and Near-Nozzle Flow in a Multi-Hole Gasoline Injector Under Flashing and Non-Flashing Conditions". In: *SAE Technical Papers*. Vol. 2015-April. April. 2015. DOI: 10.4271/2015-01-0944.

[118] Saha, Kaushik et al. "Numerical Investigation of Two-Phase Flow Evolution of In- and Near-Nozzle Regions of a Gasoline Direct Injection Engine During Needle Transients". In: *SAE International Journal of Engines* 9.2 (2016), pp. 2016–01–0870. DOI: 10.4271/2016-01-0870.

[119] Montanaro, Alessandro and Allocca, Luigi. "Flash Boiling Evidences of a Multi-Hole GDI Spray under Engine Conditions by Mie-Scattering Measurements". In: *SAE Technical Paper 2015-01-1945* (2015).

[120] Guo, Hengjie et al. "Comparison of spray collapses at elevated ambient pressure and flash boiling conditions using multi-hole gasoline direct injector". In: *Fuel* 199 (2017), pp. 125–134. DOI: 10.1016/j.fuel.2017.02.071.

[121] Guo, Hengjie et al. "Effect of flash boiling on microscopic and macroscopic spray characteristics in optical GDI engine". In: *Fuel* 190 (2017), pp. 79–89. DOI: 10.1016/j.fuel.2016.11.043.

[122] Guo, Hengjie, Wang, Bo, Li, Yanfei, Xu, Hongming, and Wu, Zhijun. "Characterizing external flashing jet from single-hole GDI injector". In: *International Journal of Heat and Mass Transfer* 121 (2018), pp. 924–932. DOI: 10.1016/j.ijheatmasstransfer.2018.01.042.

[123] Guo, Hengjie et al. "Radial expansion of flash boiling jet and its relationship with spray collapse in gasoline direct injection engine". In: *Applied Thermal Engineering* 146.October 2018 (2019), pp. 515–525. DOI: 10.1016/j.applthermaleng.2018.10.031.

[124] Guo, Hengjie, Li, Yanfei, Wang, Bo, Zhang, Huiqiang, and Xu, Hongming. "Numerical investigation on flashing jet behaviors of single-hole GDI injector". In: *International Journal of Heat and Mass Transfer* 130 (2019), pp. 50–59. DOI: 10.1016/j.ijheatmasstransfer.2018.10.088.

[125] Guo, Hengjie, Li, Yanfei, Xu, Hongming, Shuai, Shijin, and Zhang, Huiqiang. "Interaction between under-expanded flashing jets: A numerical study". In: *International Journal of Heat and Mass Transfer* 137 (2019), pp. 990–1000. DOI: 10.1016/j.ijheatmasstransfer.2019.04.010.

[126] Payri, Raul, Salvador, Francisco Javier, Martí-Aldaraví, Pedro, and Vaquerizo, Daniel. "ECN Spray G external spray visualization and spray collapse description through penetration and morphology analysis". In: *Applied Thermal Engineering* 112 (2017), pp. 304–316. DOI: 10.1016/j.applthermaleng.2016.10.023.

[127] Lin, Tien Chu, Shen, Yi Jun, and Wang, Muh Rong. "Effects of superheat on characteristics of flashing spray and snow particles produced by expanding liquid carbon dioxide". In: *Journal of Aerosol Science* 61 (2013), pp. 27–35. DOI: 10.1016/j.jaerosci.2013.03.005.

[128] Cleary, Vincent, Bowen, Phil, and Witlox, Henk. "Flashing liquid jets and two-phase droplet dispersion. I. Experiments for derivation of droplet atomisation correlations". In: *Journal of Hazardous Materials* 142.3 (2007), pp. 786–796. DOI: 10.1016/j.jhazmat.2006.06.125.

[129] Li, Yanfei et al. "An exploration on collapse mechanism of multi-jet flash-boiling sprays". In: *Applied Thermal Engineering* 134.May 2017 (2018), pp. 20–28. DOI: 10.1016/j.applthermaleng.2018.01.102.

Chapter 3

Experimental tools and methodologies

3.1 Introduction

Throughout this chapter, the experimental tools and methodology followed in the work are reviewed. It presents the experimental equipment used, as well as the methodology followed during the measurements and data analysis reported in the results (Chapters 5 and 6). The first sections are dedicated to introduce the injector and injection systems, whereas the rest of sections describe the laboratory facilities employed. Also, the experimental configuration taken in each facility as well as the instructions for raw data processing is described here. Most of the measurements have been preformed in the CMT-Motores Térmicos installations. However, the x-rays measurements were performed at Argonne National Laboratory (ANL), using the synchrotron situated at the Advanced Photon Source (APS).

3.2 Injection system

Fuel at high-pressure is required by the injector for proper delivery in the test chambers. Its conditions must be controlled and stable for a wide operation range necessary for the research. The injection system consists of injector, common rail, high pressure unit and fuel supply source, all of them commercially available components adapted for research and laboratory use.

3.2.1 Injectors: Spray G and Denso commercial injector

There are two Gasoline DI injectors employed in this research work. The first is the Spray G injector (serial AV67-026), one of the injectors and drives donated by Delphi to the ECN for research purposes [1]. The other, PIU, is a commercial GDI injector manufactured by Denso. A picture of the injectors is depicted in Figure 2.14.

Both injectors are solenoid-driven multi-holes especially designed for DI spark ignition configurations. The Spray G is configured to be situated at the top of the chamber next to the spark plug, however, the PIU is designed to be located next to the intake valve. Both injectors are designed to operate at similar regimes, therefore, further in this work they will be compared under same conditions of injection pressure, temperature and duration. The design characteristics of both injectors are shown in table Table 3.1.

Table 3.1: Geometrical characteristics of the researched injectors.

Parameter	Spray G	PIU
Cone bend angle	0°	$\sim$ 26°
# Holes	8	6
Orifice	circular	circular
Hole	straight	diverging
Nozzle	step hole	conical hole
L/D ratio	1.4	2.4
Orifice diamter	165 μm	195 μm
Orifice length	160-180 μm*	465 μm
Step/Outlet diameter	388 μm	360 μm
Orifice drill angle	0°	variable
Spray umbrella angle	80°	37°

*Lengths of inner and outer diameters

3.2.2 Injector's control unit

The commanded electrical signal for the injectors are different for each injector. The current required to activate the solenoid is specified by each manufacturer and assures the correct functioning of the injector hardware.

The driver for the Spray G injector was provided by Delphi, which consist of a simplified Engine Control Unit (ECU) depicted in Figure 3.1a. It is capable of creating the current needed to operate the injector solenoid upon receiving a trigger to determine the start and duration of the signal. For the

PIU, it was used a commercial injector driver, which permits to configure the signal profile needed in the injector. There are two main parameters to define the signal; one is the peak current, which is the intensity needed to initially break the forces to lift the needle and determines the start of the injection. The second parameter is the maintained signal required to keep the injector open so it is the one that determines the duration. Figure 3.1 shows both injector drivers.

(a) Delphi injector driver (Spray G).

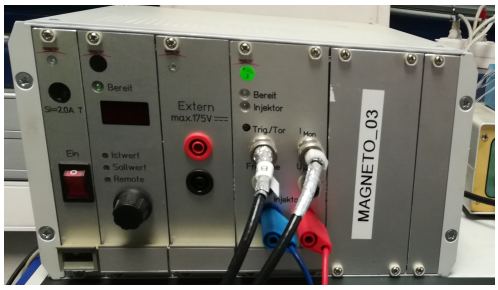

(b) Commercial injector driver (PIU injector).

Figure 3.1: Injector drivers for each hardware.

3.2.3 High pressure system

The systems providing high-pressure fuel has been described previously in several publications [2–6], which is similar to the one used for diesel injectors. The system is composed by a high-pressure pump, which suctions fuel from the tank and compresses it to a first rail used to regulate the injection pressure. Then, the desired pressurized fuel arrives at a second rail, used mostly to damper the pressure oscillations from the pump. In the second rail, there is installed a Kistler pressure sensor to measure injection pressure accurately. Since the pump can pressurize beyond 200 MPa, a safety valve installed in the second rail, which assures fuel pressure under 30 MPa to keep the injectors integrity. The pump and the fuel diverted back to the tank are cooled by a heat exchange that uses glycol at 5°C. Figure 3.2 presents a schematic diagram and picture of the high-pressure system.

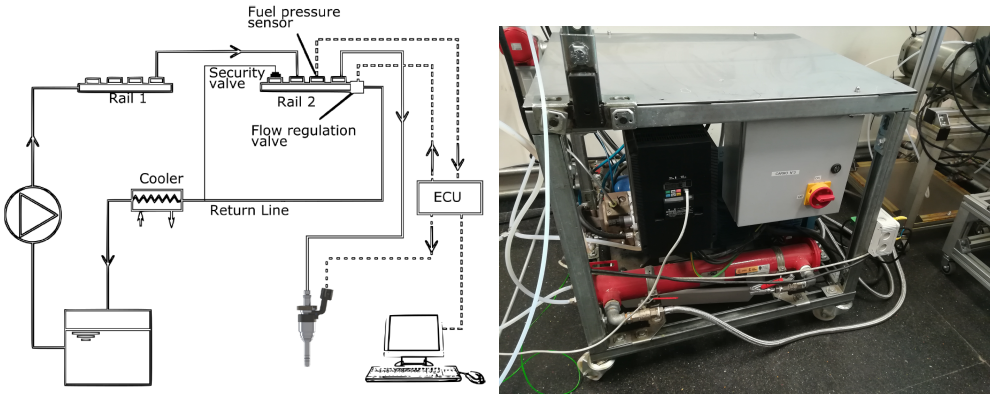

(a) Diagram of the high pressure system circuit. Adapted from [2].

(b) Picture of the high pressure system block.

Figure 3.2: High pressure system circuit (Diagram and picture).

3.3 Rate of injection technique

3.3.1 Background

The injection rate, also called rate of injection (ROI), is one of the most important characteristic of an injection system. It evaluates and determines the rate and quantity at which the fuel is delivered. Precision in rate of injection was not as vital in old PFI gasoline engines, however, critical accuracy in ROI measurements is needed in advanced GDI engines [7].

This methodology was first developed for diesel injectors and it has been described in several previous works for diesel [3, 4, 8–10] and gasoline injectors [5, 11]. The mass flow rate was performed using a Injection Rate Discharge Curve Indicator (IRDCI) from IAV. It is based on the Bosch long-tube method [12], whose principle resides in the theory of pressure wave propagation in a liquid tube. A diagram of the IRDCI is illustrated in Figure 3.3.

Fuel is injected in the inlet, generating a pressure wave that travels inside the long tube, previously filled with fuel. The wave travels at the speed of sound the known distance, until arrives to the release volume where it is dampened. The pressure inside the instrument can be adjusted by nitrogen at desired discharge pressure, which acts on the equalizing piston. Once the piston is in equilibrium, and fuel have enter the piston cavity through the particle filter, other new injection creates a pressure increase and adds additional mass. Thus, the piston would move and unseal the outlet, which lets a small mass equivalent to the one injected out the IRDCI.

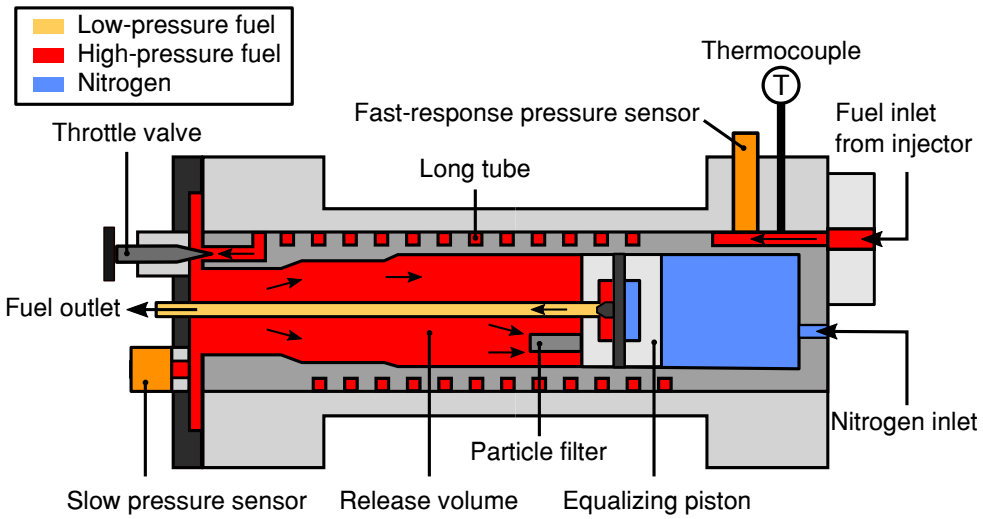

Figure 3.3: Schematic diagram of the Injection Rate Discharge Curve Indicator [3].

The fast-response pressure sensor records the pressure change due to an injection event. From its electrical signal is possible to determine the mass flow rate. Given a cylindrical control volume where the pressure wave travels, with a cross section area A_c. The equation of momentum conservation, if the gravity is neglected, results in:

$$(p_v + \Delta p)\, A_c - p_v \cdot A_c = \rho_f \cdot A_c \cdot a_f \cdot \Delta u_f \tag{3.1}$$

where p_v is the pressure in the volume, Δp represents the pressure difference produced by the wave (injection event), ρ_f is the fuel density, a_f is the fuel speed of sound in the medium and Δu_f is the fuel flow velocity variation in the discharge section. As it may be noticed, the equation 3.1 can be simplified as follows:

$$\Delta p = \rho_f \cdot a_f \cdot \Delta u_f \tag{3.2}$$

The pressure increase due to the injection event is captured by a piezoelectric sensor that is sufficiently close to the injector tip to avoid the attenuation of the signal due to friction losses. When the pressure wave enters the release volume, it realizes of a section change on the tube, which creates a reflection wave that travels upstream. To avoid this interfering on the measurement, the IRDCI implements two solutions: first, the long tube provides

a temporal difference between the two signals. Secondly, the throttle valve at the tube end can change the cross-sectional flow area so the reflected wave can be tuned to some extend. Finally, the pressure difference induced by the wave is related to the mass flow rate using the continuity equation shown in Eq.3.3:

$$\dot{m}(t) = \rho_f \cdot A_c \cdot \Delta u_f \tag{3.3}$$

Then, solving Equation 3.2 and Equation 3.3 for Δu_f, the mass flow rate is defined by:

$$\dot{m}(t) = \frac{A_c \Delta p}{a_f} \tag{3.4}$$

3.3.2 Measurement setup and methodology

An injector holder made of steel is designed to install the injectors on the IRDCI fuel inlet (see Figure 3.3). Each injector has its specific adaptation piece due to slightly differences in the geometry and needs to accurately seal on the o-rings. Figure 3.4 illustrates a render of the injector inside its holder. It has a cooling circuit to help maintain the required temperature of operation. Moreover, it is also depicted the real piece mounted in the facility while in operation (3.4b).

The IRDCI has a termocouple installed in the fuel side to measure fuel temperature and a pressure sensor in the nitrogen side to know the fuel pressure. These two parameters are crucial to adequately calculate the speed of sound in the fuel. Figure 3.5 presents an schematic of the measurement set up. First, fuel is supplied to the high pressure pump, which delivers pressurized fuel to the common-rail. Then, the rail is connected by a high-pressure rigid line to the injector, both lines and rails are chosen to comply with ECN standards [1]. At the IRDCI exit, there is a gavimetric scale continuously measuring the exiting fuel weight. This is performed to minimize the uncertainties that are generated because of the calculation of the speed of sound in the fuel used. It highly depends on the fuel composition as well as the pressure and temperature of the system. In addition, speed of sound data for iso-octane (2,2,4 - Trimethylpentane) was not available in the literature, so instead it was used octane data published in the NIST web-book [13]. It was determined an injection frequency of 10 Hz for the measurements and once the injected quantity value at the balance is stabilized, data acquisition starts recording 50 injections using a digital oscilloscope. The information about

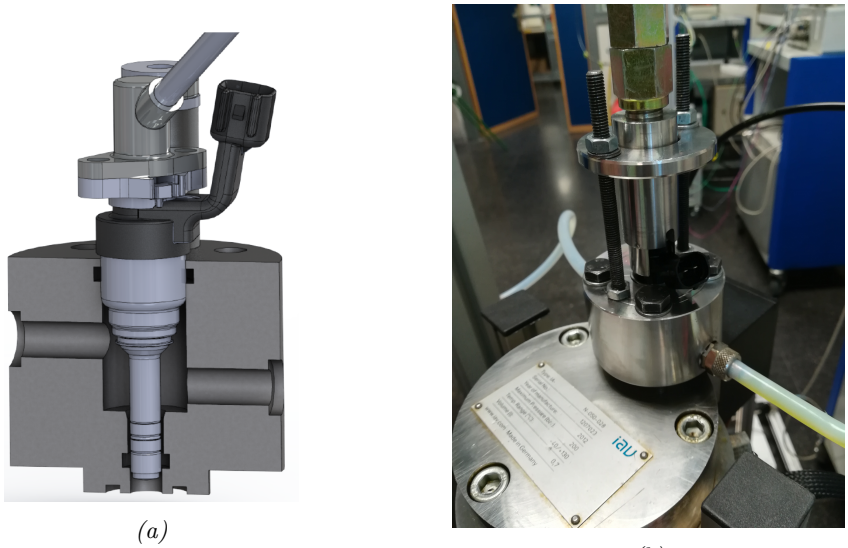

(a) *(b)*

Figure 3.4: ROI adaptor Render (a) and picture of the piece while operation (b).

ROI, rail pressure and drive signal are collected and stored the lab computer. Finally, it is obtained a ROI signal from IRDCI whose integrating average value may differ with the one measured in the balance. Thus, a K value is calculated as the ration between them to finally scale the ROI signal to make its integral equal to the injected mass measured in the balance, as shown in Equation 3.5.

$$K_{adjust} = \frac{M_{balance}}{M_{int}} \tag{3.5}$$

Where $M_{balance}$ is the mass measured by the balance upon reaching stabilization and M_{int} is the integral value of the ROI signal average of the 50 repetitions. Lastly, K_{adjust} is the scaling factor, which is the ratio between the previous values and normally ranges among 1.05 and 0.95.

A final aspect to consider when obtaining the final ROI signal is the accumulation phenomena that occurs when measuring with IRDCI and is extensively discussed by Payri et al. [14]. It happens during the injection event, the added fuel increases as the measurement is performed creating an artifact of continuous signal increase which must be corrected. The solution in the published work is implemented to correct the raw signal [14].

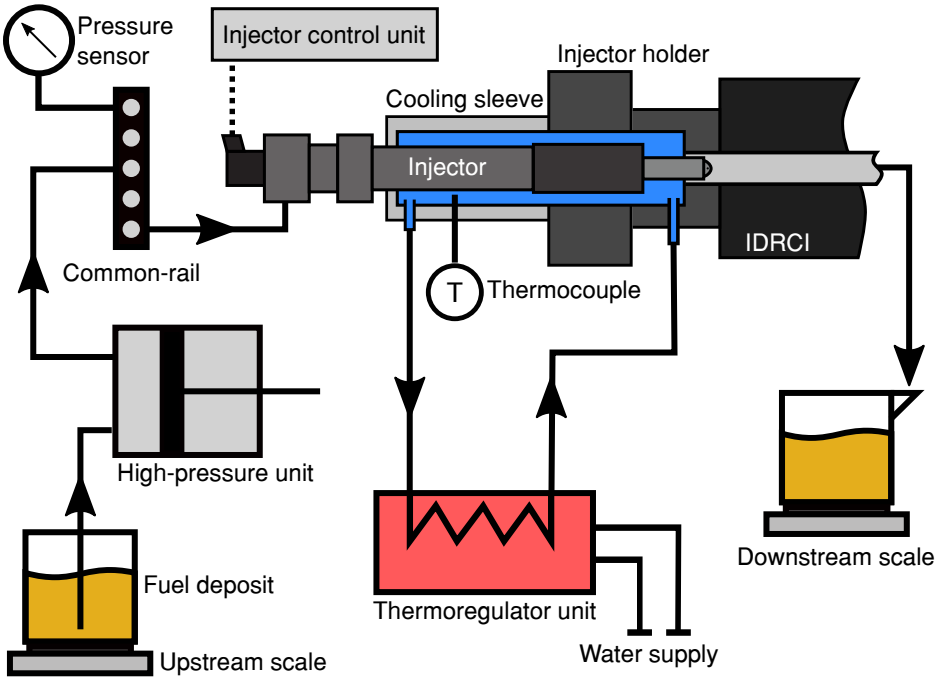

Figure 3.5: Set-up employed in rate of injection (ROI) measurements.

3.3.3 Methodology for rate of injection Modelling

In this work, a simplified 0D model that imitates the ROI signal has been developed. The model, based on mathematical expressions and correlations, is able to reproduce the mass flow rate obtained by the experiments using the Bosch tube method. It has to be noted that most injectors have a trapezoidal injection rate profile, thus in certain conditions and after some tuning, the model could be used for other injectors. It is focused on the injected mass and the shape, providing some typical parameters such as ET, injection pressure, back pressure, etc. The two primary objectives of the model are to operate at the lowest computational cost and to produce a realistic injected mass quantity. The potential advantages of the model are that simulation results can be obtained rapidly and easily for any operating points. Moreover, it can be used in engine test bench for mass estimations as a real-time model when doing experiments or calibration activities.

The steps followed to create the model are:

(1) To complete the mass flow rate measurements, a wide-enough test matrix established before. It should cover the operational range of the injection

system (rail pressure, ET) and the pretended engine conditions that want to be reproduced by means of back pressure.

(2) A signal decomposition is done, separating the elements that can construct the injection rate signal and at the same time selecting the most appropriate mathematical expressions that could fit such curves. Various alternatives could be considered, for instance: straight slopes, first and second order system response, polynomial, exponential and Bezier curves.

(3) The available measured dataset is used to adjust the model expressions. For example, the coefficients are determined using the best fitting with all the measured conditions. Each equation coefficient is modelled as a function of the input parameters. This last step is an iterative process, since not always a good correlation is found at first. Depending on the ROI shape, several trials and errors are necessary, until the form of the equations and the coefficients obtained satisfies the requirements or are representative enough for all the conditions.

At the latter step, sometimes there is not a simple representative expression for all the conditions thus separations among rail pressures or distinction between long and short injections are necessary to find a fit of the coefficients good enough for all the conditions.

3.4 Plastic deformation technique

3.4.1 Background

The plastic deformation technique is a method which allows for the calculation of spray orientation in a gasoline direct injector. It is well known that not always the drill angles (geometrical angles) on the injector nozzles correspond to the exit sprays due to internal or in-orifices flow iterations that deviates the core direction of the plume. It is very important to know the real orientation of the plumes before any further measurement or study on the injector because precise positioning is needed to minimized any possible error [15]. For example, the spray orientation is vital for Rate of Momentum (ROM) measurements (explained in section 3.5).

The new generation nozzles of spray guided gasoline direct injectors, are normally positioned at the top of the combustion chamber or right under the intake valves. The first is normally designed with equally distributed orifices around the injector axis, however the latest always present atypical

holes distributions due to the positioning of the injector and requirements in delivering fuel into specific zones in the chamber. Alternatives to this method is the use of x-rays to look at sprays and through fuel concentrations determine the jet orientation, nevertheless, it is a costly experiment and accessing the equipment is difficult [16].

The working principle behind this technique is to assess the footprint of the spray at a controlled known distance from the injector tip. The formation of the footprint is due to repeated injections that deform the material, which is carefully selected to avoid reaction with the fuel and adequately deform a magnitude related with the fuel plume momentum. Applying trigonometry with information of the footprint and the position of the nozzle tip the orientation angle of each orifice can be calculated.

3.4.2 Measurement setup and methodology

On the experimental set up, the injector was situated at a distance of 14 mm from the material, which is found to be an adequate separation. The injector was held using a cylinder which helped align the nozzle and cylinder axis, in addition to add support to the installation. It was performed up to 20 injections to achieve sufficient deformation on the material surface so there was enough contrast to differentiate the footprint. Then, the footprint is digitized to apply a post processing algorithm that reveal the spray plumes impact coordinates. This is achieved by fitting the cylinder footprint to a circumference to find the center axis, and then, relate that reference to discover the impact locations. Figure 3.6 shows the raw injector spray footprint on the material surface. Finally, the spray jet orientation angles are found by trigonometry, using the information of orientation and position of the nozzle tip and impact coordinates.

3.5 Momentum flux technique

3.5.1 Background

The rate of momentum (ROM) is a useful measurement to characterize the injector nozzle. Data from ROM is typically combined with ROI to obtain even deeper detailed information about the fuel flow at the nozzle outlet. Payri et al. [17] defined the ROM as the rate of injection multiplied by the velocity. Given a mass flow rate $\dot{m}$, with a momentum rate of $\dot{M}$, with density

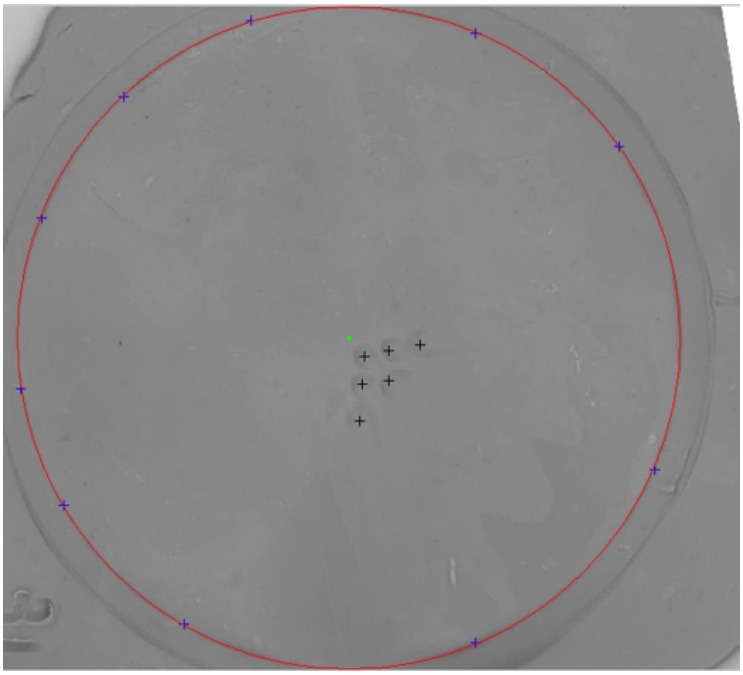

Figure 3.6: Digitized spray plumes footprint, displaying location of the impacts.

ρ, moving through an area A_0 at a velocity u, ROI and ROM can be described as in Equation 3.6 and 3.7:

$$\dot{m} = \int_{A_0} u\rho dA \tag{3.6}$$

$$\dot{M} = \int_{A_0} u^2\rho dA \tag{3.7}$$

Useful information is found when hydraulic injector measurements (ROI and ROM) are combined, which is used to analyze the flow in more detail. Given the cross-section area of A_0 used for the previous definitions, the flow can be described as in Figure 3.7 (a) with possible cavitation or unknown information about its composition. However, it can be simplified conserving mass and momentum flux by introducing flow coefficients such as the effective area A_{eff} (Eq. 3.8) and effective velocity u_{eff} (Eq. 3.9), which describe the outlet flow with reduced complexity as in Figure 3.7 (b).

$$A_{\text{eff}} = \frac{\dot{m}_f^2}{\rho_f M_f} \tag{3.8}$$

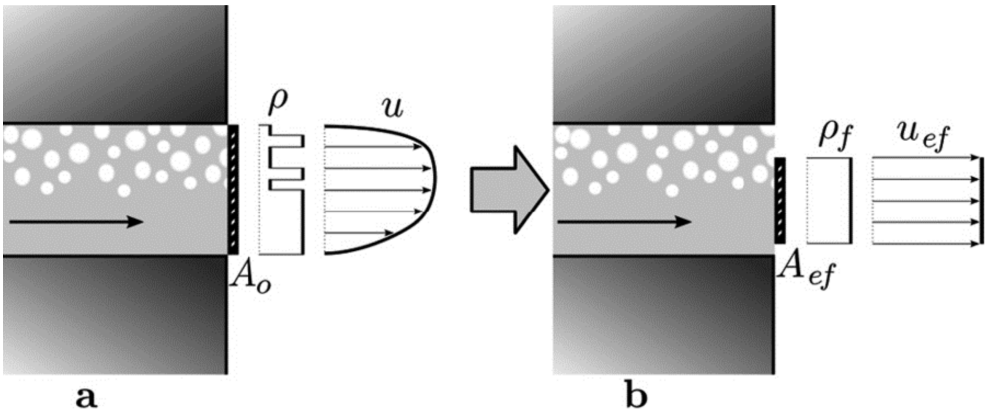

Figure 3.7: Schematic representation of the flow exiting the nozzle orifice. In (a) is represented the real parameter and in (b) the effective parameters [18].

$$u_{\text{eff}} = \frac{\dot{M}_f}{\dot{m}_f} \tag{3.9}$$

$\dot{M}_f$ and $\dot{m}_f$ are the rate of momentum (ROM) and rate of injection (ROI), and ρ_f represents the fuel density. Then, applying Bernoulli's equation to the studied geometry, it can be obtained a theoretical velocity (u_{th}) Equation 3.10:

$$u_{\text{th}} = \sqrt{\frac{2\Delta P}{\rho_f}} \tag{3.10}$$

where ΔP represents the pressure difference between inlet and outlet of the injector nozzle. Then, combining the definition of mass flow rate of Equation 3.6 and substituting for the u_{th} (Eq. 3.10), it can be defined the discharge coefficient (3.11) as the ratio of the measured ROI to the theoretical ROI:

$$C_d = \frac{\dot{m}}{u_{\text{th}}\rho_f A_0} \tag{3.11}$$

Similarly, Equation 3.12 shows the momentum coefficient (C_M), which can be defined as the ratio of the measured momentum to the theoretical momentum from combining Equation 3.7 and 3.10.

$$C_M = \frac{\dot{M}}{u_{\text{th}}^2 \rho_f A_0} = \frac{\dot{M}}{2A_0\Delta P} \tag{3.12}$$

Payri et al. [17] also defined two additional coefficients to describe the losses in area and velocity. Those are the effective area and effective velocity, which are shown in Equation 3.13 and 3.14.

$$C_a = \frac{A_{\text{eff}}}{A_0} = \frac{D_{\text{eff}}^2}{D_0^2} \tag{3.13}$$

$$C_{\text{v}} = \frac{u_{\text{eff}}}{u_{\text{th}}} \tag{3.14}$$

Finally, Equation 3.15 relates the different coefficients into one equation.

$$C_M = C_d C_{\text{v}} = C_{\text{v}}^2 C_a \tag{3.15}$$

3.5.2 Measurement setup and methodology

The test rig used for ROM measurements was developed and conceived at the CMT-Motores Térmicos, as one of the objectives of Gimeno [18] PhD thesis. The device is composed by a constant volume vessel, that can simulate in-engine pressure conditions up to 10 MPa. Although it was thought for measuring diesel injectors, it was possible to use it for GDI ones by manufacturing several adaptation parts. Its basic principle consists in measuring the instantaneous impact force (F) of the spray plume into a calibrated piezo-electric sensor, as illustrated in Figure 3.8.

Given a cylindrical control volume which encloses the domain between the nozzle orifice and the sensor, as shown in the figure 3.8, several assumptions are made for rate of momentum measurements [17, 18]:

- There is uniform pressure within the volume.
- Gravity force is neglected.
- The fuel spray axis is perpendicular to the sensor surface.
- The air entering the control volume and the fuel exiting it after the impact are both perpendicular to the spray axis. Accordingly, the axial components of momentum flux and viscous stress are null.

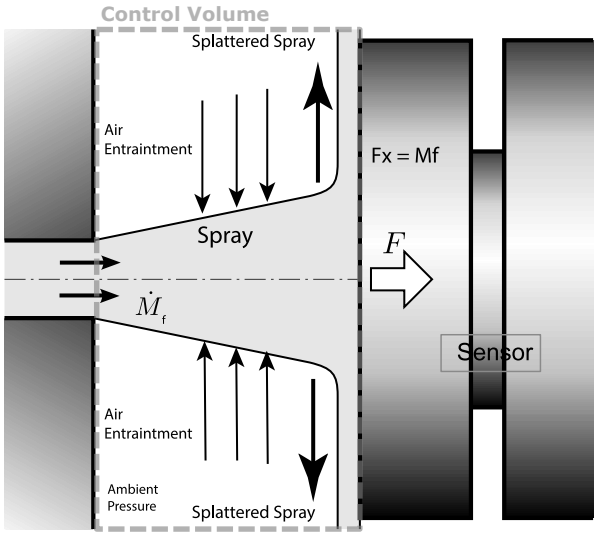

Figure 3.8: Principle and assumptions of rate of momentum [17].

Considering the previous assumptions and simplifying on the momentum conservation equation, the force produced by the spray into the sensor can be expressed as in Equation 3.16:

$$F = \frac{\partial}{\partial t} \int_{\mathrm{CV}} \rho u d\varpi + \dot{M} \tag{3.16}$$

Therefore, the force is defined as two terms. The first one represents the instantaneous variation of momentum flux of the mixture inside the control volume, where ρ and u are density and velocity of the mixture through the CV, and ϖ is the surface contour of the CV. The second term, $\dot{M}$, represents the momentum flux at the orifice outlet. At steady state conditions, however, the Equation 3.16 can be reduced to:

$$F = \dot{M} \tag{3.17}$$

Thus, the sensor directly captures the ROM signal, provided the sensor surface is perpendicular to the spray axis, the impact area is smaller than the sensor target, and the fuel after the impingement is deflected perpendicularly.

3.5.3 GDI considerations

This facility was designed for diesel injectors, particularly, was configured for measuring a mono-orifice injector (using a frontal configuration as depicted

in fig Figure 3.9), or diesel multi-orifice injectors (using a lateral configuration). Nevertheless, the sensor surface must be perpendicular to the spray axis. To this end, the sensor can be situated at the vessel bottom for frontal configuration or on a side for lateral configuration.

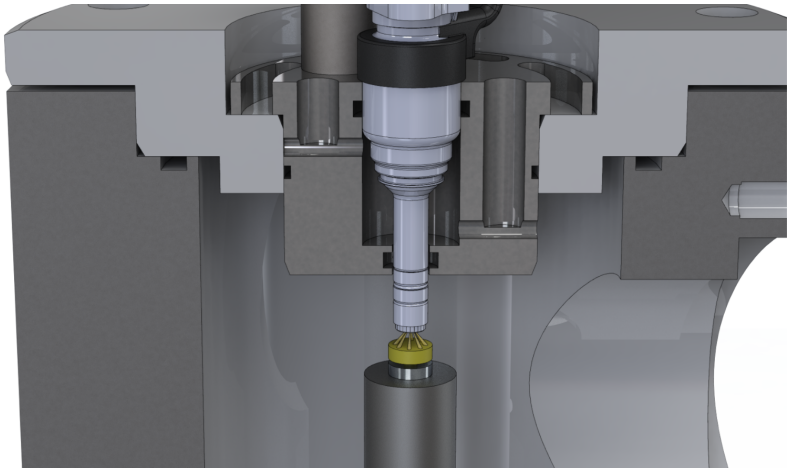

Figure 3.9: Rate of momentum set up displaying frontal impact configuration. Adapted from [19].

Apparently, the method is totally compatible with GDI injectors, however, because of the different nozzle geometry, the measurements are more difficult in the researched nozzles. The injectors of study present much narrower spray cones for spray interaction and flame propagation [20, 21], as well as the pressures in which they operate makes it difficult to measure.

In particular, there is a problem with spray separation, which is more difficult with GDI injectors because they have holes that are much closer together than diesel injectors. On the other hand, the pressures at which GDIs operate are an order of magnitude lower than diesel. Therefore, measuring a single orifice would generate a lot of measurement uncertainty for the sensor range. This impediment along with the fact that it is very difficult to separate the orifices has resulted in measurements of the entire spray cone. Payri et al. [19] investigated the two configurations on the Spray G, as shown in Figure 3.9 and 3.10. They claimed the frontal configuration produced more consistent values in the measurements.

On rate of momentum measurement, the injector nozzle have to be situated at certain distance from the sensor, as a trade off balance between close enough so all the jet impinges in the sensor target but far so there is not interaction

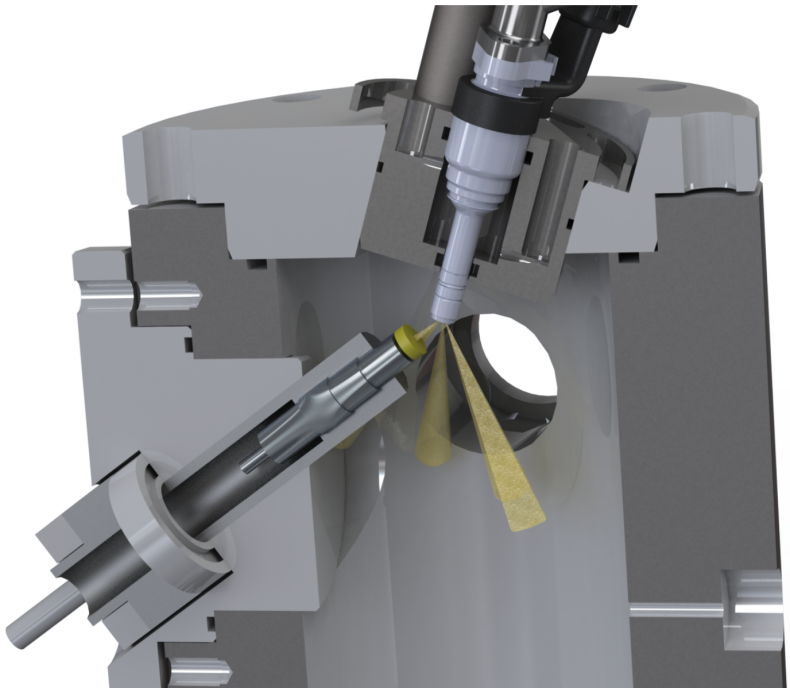

Figure 3.10: Rate of momentum set up displaying lateral impact configuration (Capturing only one spray plume). Adapted from [19].

with adjacent sprays. Also, when the distance is too far and the control volume surface exceed the sensor target surface, aerodynamic effects may take place slowing down the spray as they involve more air from the surroundings and transferring momentum so the final momentum measured could artificially diminish.

The set-up used to measure the injector's ROM of this work was the frontal configuration. As it is stated previously in section 3.5.2, one of the assumptions taken for ROM measurements is that the spray axis is perpendicular to the sensor surface, which cannot be true if all the fuel jets are captured at the same time. Although this implies more complicated aerodynamic interactions than the simplified problem in Figure 3.8, a coherent measurement can be taken if the signal captured is corrected with the spray angles. To this end, spray angles were obtained by applying the plastic deformation technique (section 3.4). Shahangian et al. [15] used a method to correct the ROM measurements of a commercial multi-orifice GDI injector successfully. The

momentum correction M_c is executed by using Equation 3.18:

$$M_c = \sum_{i=1}^{n} \frac{M_m/n}{\cos \alpha_i} \tag{3.18}$$

Where M_m is the total momentum measured, n is the number of orifices that are impacting the sensor and α_i is the angle of each the core fuel jet with respect to the sensor surface.

Likewise rate of injection methodology, it was recorded 50 injections for each test condition. A digital oscilloscope is used to record ROM signal as well as pressure signal from the rail and the electrical driving signal from the ECU. The results reported from these measurements are always the averages of the 50 repetitions similarly to ROI.

3.6 X-rays measurements

3.6.1 Background

X-rays is a growing versatile technique, that even it is difficult to access (due to hugely expensive equipment), it is worth the effort because of the amount of information that it could reveal. Its use is mostly in investigating the internal flow, which greatly influences the performance of the injector during rate of injection, rate of momentum as well as near-nozzle flow atomization and mixing [2, 4, 16, 20, 22–26]. Characteristic injector parameters such as internal geometry, pintle motion, cavitation or near-nozzle flow field could be investigated through this technique which could reveal small changes with accuracy [27–29]. One of the main advantages of the x-rays is that they can penetrate through metal, which permits to visualize geometry or phenomena inside the nozzle. In addition, when calibrating absorption coefficients of fuel and air while using monochromatic beam, it is possible to determine mass concentrations in the regions of interest (only once the fuel is outside the nozzle).

The measurements of x-rays reported in this work were performed at Argonne National Laboratory (ANL). Spray G has been investigated thoroughly in many previous occasions and the data is available to be used through the ECN network, however, there has never been a direct comparison with another GDI similar injector like the one of this work. The principal objective of these measurements is to investigate how the individual features of each injector affect the internal and near-nozzle flow.

The facility employed for the measurements was the Advance Photon Source (APS) at ANL, which is founded by the Department of Energy of the United States of America and controlled through by U. Chicago Argonne LLC. The APS is a synchrotron-radiation light source, which uses electrons emitted from a cathode heated to approximately 1000°C, and then accelerated by high-voltage alternating electric fields in a linear accelerator to 450 MeV. Next, they are injected into the booster synchrotron, a ring of electromagnets which accelerated them from 450 MeV to 7 GeV in two seconds. At that stated, they are traveling at relativistic velocities (>99.999999% of the speed of light). Then, the high-energy electrons are injected into the storage ring, a 1104 m circumference, composed of more tan 1000 electromagnets and located in a radiation-proof concrete enclosure [30]. Figure 3.11 shows an aerial view of the APS facility. Surrounding the storage ring is situated the experiment hall, which is composed by 35 sectors with access to the beamlines. The measurements from this investigation were performed at sectors 7-BM (Bending Magnet) and 32-ID (Insertion Device) of APS, which are the ones specialized in fuel injection using x-ray diagnostics.

Figure 3.11: Aerial view of the APS facility, showing the characteristic circular shape ring building.

3.6.2 Pintle motion by x-ray imaging

Measurements of pintle motion were executed at 32-ID beam-line of the APS [31]. Its was performed following the methodology by Viera et al. [32]. The high pressure fuel is achieved by a pressurized cylindrical container, whose pressure is controlled by an adjacent nitrogen volume which transfer the force trough a piston. Injection pressure is controlled by a valve in the common rail, in a similar fashion to the one explained in (section 3.2). The vessel where the injection occurs, is pressurized with N_2 to simulate engine pressure and it is equipped with Kapton optical accesses due to its advantageous property of low x-ray absorption. The installation did not have temperature control capabilities, thus, all the measurements were performed at room temperature. However, from previous studies [5, 8, 11] it is known that rate of injection shows to be very little sensitivity to fuel temperature change. Thus it can be assumed similar conclusion for needle lift.

Figure 3.12 shows a schematics of the experimental set up. The electrons go through the ondulator, which force them to follow a wave-like path that produces a broadband high-energy x-ray beam. It works under full spectrum radiation (white-beam mode), since it needs to penetrate thick metal such as the injector nozzle with sufficient temporal resolution. Downstream, the mechanical slits and shutter release some of the heat load of the windows and injector, and shape the beam to optimal imaging in the region of interest.

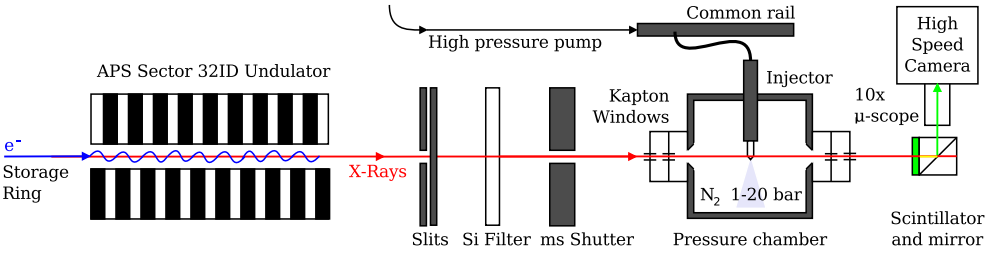

Figure 3.12: Schematic diagram of x-ray phase-contrast imaging experiment at the 32-ID beamline of the Advanced Photon Source at Argonne National Laboratory to obtain pintle motion (not to scale). Adapted from [32].

Once the beam reaches the nozzle, some of the energy is absorbed by the metal. After passing through it, the energy available in the beam is proportional to that absorbed by the metal. Then, a scintillator converts the x-ray radiation to visible light, which is later redirectioned, using a 45° angle mirror, to a high-speed camera. The camera used was a Photron SA-Z, featuring a 10X long distance microscope lens to optimal imaging. The

image's signal-to-noise ratio is not good for just one injection due to the fast imaging required. Therefore, 90 repetitions were performed and averages for each test condition. The image acquisition speed featured 87500 fps and a exposition time of 10 μs. Figure 3.13 illustrate the two states of the Spray G injector, (upper part) shows the closed injector, where the needle is resting in the needle seat, and (bottom part) shows the maximum needle lift (stationary regime) when injecting. It was achieved a pixel resolution of approximately 3.9 μm/pixel, which was measured using a gold Xradia resolution pattern [33].

When tracking the pintle motion of the injector, not only the vertical movement (z) is researched, but movements in x and y axis are of interest because it can influence and transfer instabilities to the flow. It can explain some variability observed in rate of injection or rate of momentum results [5, 11]. To obtain movement of the x and y axis, two views at 90° separation were performed in the facility using a rotatory stage.

To process the pintle motion imaging data, the first step is to average the 90 repetitions to enhance the signal-to-noise ratio. Then, a developed python algorithm specially dedicated to process the images and extract the pintle movement is employed. The routine uses the template matching principle, which consist in select a template (or region of interest) and search along the next image where that template is. The algorithm goes through all the images (time steps) trying to find the location of the template, which is achieved by two-dimensional normalized cross-correlation [34–36]. The cross-correlation is evaluated by multiplying the template pixel matrix by the small region of the full image (where is intended to find the template). This operation is repeated in all the possible position, and since it is a normalized cross-correlation, the position that results in higher correlation coefficient is the most likely location that the template is situated in the image. The routine is applied in all the images resulting in a time dependent coordinate of the template, that in this case tracks the needle motion. Not always the region of interest selected is appropriate for needle motion tracking, therefore, three working regions are selected to minimize the random errors and obtain quantitative deviation of the measurement. As an example, Figure 3.13 depicts the initial template selected on the Spray G, and the template tracked at a different time when the needle is fully open.

3.6.3 X-ray tomography: internal nozzle geometry

One important difference between this technique and other x-rays methods are the time independence and that there is no need for injection so the high-pressure fuel system and driver are not required, which simplifies the installa-

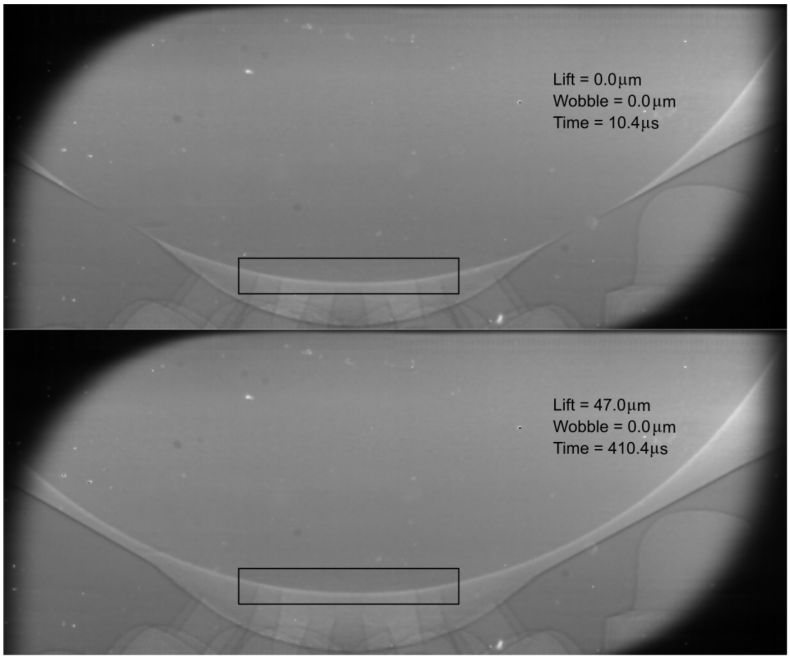

Figure 3.13: Template matching example on Spray G injector. The black rectangle in the top image represent the region of interest (template) that will be tracked. On the bottom is shown the region of interest when the needle is at maximum lift [2].

tion. The methodology followed for geometry determination is similar to the pintle motion one and was performed at the section 7-BM using white-beam mode [37]. Figure 3.14 illustrates an sketch of the set up. The poly-chromatic or white-beam travels through two filters that remove the unwanted radiation before encounter a rotating gate that acts as shutter which shapes the beam and reduces some of the heat load from the nozzle. Similarly to pintle motion method, part of the energy is absorbed by the injector nozzle, so the beam after the nozzle carries information about the geometry (proportional to the absorbed energy). Finally, the x-rays are converted into visible light thanks to the scintillator, and recorded by a CMOS camera sensor, featuring a 5X microscope lens.

For the case of the Spray G, 8 injectors were imaged presenting 1.17 μm/pixel. It was recorded 5 images for each angle position of the nozzle, from 0° to 180° using a step of 0.1°, which makes a total of 1800 angle steps. The five images taken at each position were used to eliminate high intensity pixel, also called "zingers", that are generated by the ionizing radiation impacting in the sensor and occurs at random locations. The saturated pixels

are removed and replaced with the same non-saturated of other images. Upon zingers removal, the five images are averaged to increase the signal-to-noise ratio. Figure 3.15 shows an example of one of the averaged images.

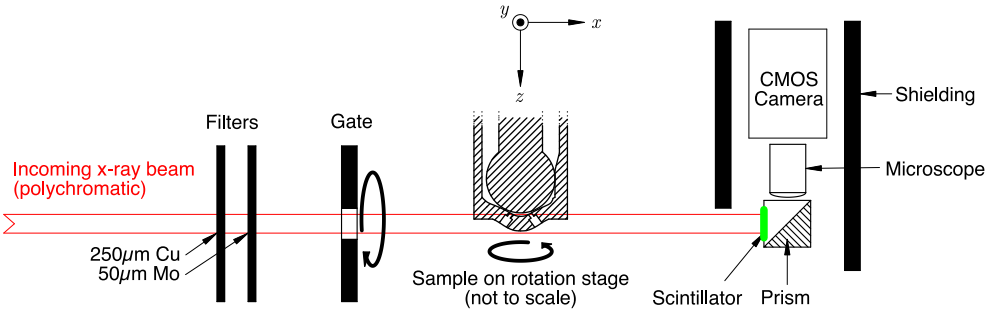

Figure 3.14: Sketch illustrating the elements employed in injector geometry measurements [38].

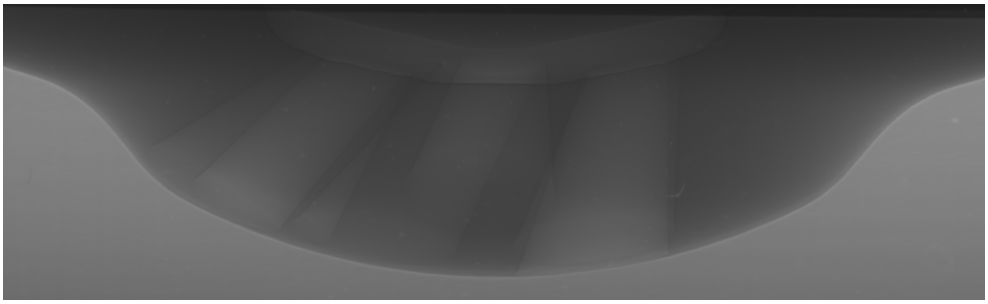

Figure 3.15: Average of 5 images of the PIU injector, at one angle for tomographic reconstruction.

The image acquisition is only the first step. Then, the set is processed for geometry reconstruction using a python open-source software called TomoPy [39], which was developed at ANL. Figure 3.16 shows an example of the data after reconstruction of the Spray G. The left image shows a slice in the longitudinal plane through two holes, whereas the right-side image depicts a slice in the transverse plane at a certain height. Each slice is enhanced by removing background and increasing the contrast. From the nozzle reconstructed geometry it is possible to measure features such as the exact length and diameters of the orifices, manufacture imperfections and one of the main advantages is the use of the geometry for internal flow CFD simulations.

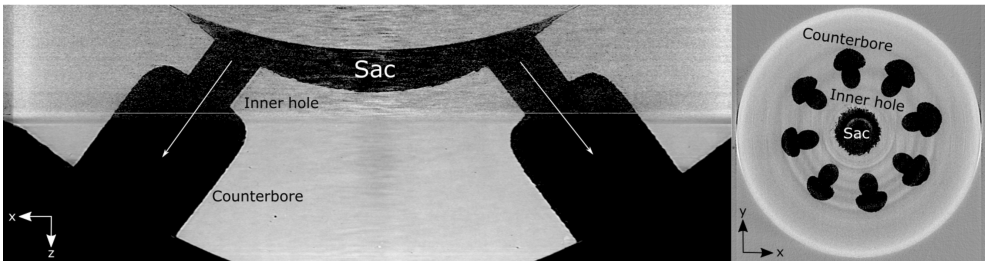

Figure 3.16: Spray G reconstructed geometry. Slice through two opposite orifices at the longitudinal plane (left) and transverse plane at a certain height (right).

3.6.4 X-ray radiography in the near nozzle field

The interest of using x-rays diagnostics is not only limited to internal flow, but in the near nozzle region as well. It could reveal important information of the flow even in dense regions of sprays, while other optical techniques cannot access. The x-ray radiography technique allows to measure the time dependent density distribution in the near region of the spray (0.1 mm - 20 mm) where the spray has enough density concentration for x-ray absorption.

The observations were performed at the 7-BM beamline in the Advanced Photron Source (APS). Many previous works detail the principles of x-ray radiography and ANL experimental facilities [16, 37, 38]. However, in brief, the monochromatic beam produced by the synchrotron is guided through a double-multilayer monochromator to end up with a beam of 8keV per photon of monochromatic x-rays. The ray is shaped to a 1.3 x 1.3 mm square cross-section by beam defining slits. Also, a diamond monitor is located downstream to measure the incident beam intensity (I_0). The beam was focused by a pair of KB mirrors to a section of 6.45 μm by 3.87 μm (H x V) at the level of the tip of the injector, which was confirmed by the Prosilica camera.

The injection occurs in a dedicated spray chamber where the beam goes through the special x-rays transparent windows installed in the vessel. Once the beam is transmitted through the spray region of interest, it is collected by a time accurate x-ray detector, which in this case was an avalanche photodiode (APD). Since the beam is fixed at one position, the spray chamber travels (thanks to a translation stage) through the beam to obtain a time-resolved distribution map of the spray. The signal of the APD is synchronized with the injector command and time-averaged over the orbit period of the synchrotron storage ring of 3.68 μs, which determines the temporal resolution of the measurements. The signal to noise ratio of the data was improved by recording and averaging in each location 32 injection events.

Each test point is taken along the line of sight of the beam at that particular location. Therefore the measurements of projected mass (M) is taken in just a small volume of the spray. A grid of coordinate points over the perpendicular plane of the spray is created to obtain spacial information. In this case, an example of the distribution is depicted in Figure 3.17, where it can be observed a grid refinement next to the wall aiming to obtain a better resolution in the region of interest. The experiments are performed at a view angle of 0° determined by the fuel tube inlet. The uncertainty of the data acquired was found to be up to 5%, in coherence with [28].

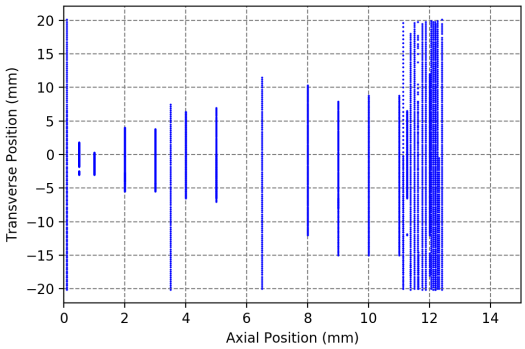

Figure 3.17: Grid shape by measuring points.

The projected mass (M) along the line of sight of the beam is calculated from the recorded intensity (I), under the Lambert-Beer law:

$$M(\mu g/mm^2) = \frac{-1}{\mu} log \frac{I}{I_0} = \int \rho_{fuel} dz \tag{3.19}$$

Where μ is the relative absorption coefficient of the liquid fuel and I_0 is a reference intensity. The calibration of the absorption coefficient is performed against air and water in a cuvette and is adjusted to allow for displacement of the ambient gas in the chamber. A Yokogawa digital oscilloscope was used to record the signal from the APD sensor every 1 ns to 2 ms. Moreover, the validation of the signal was performed by monitoring nonintrusively the beam intensity with an ionization chamber. The Figure 3.18 depicts the schematic of the experimental setup.

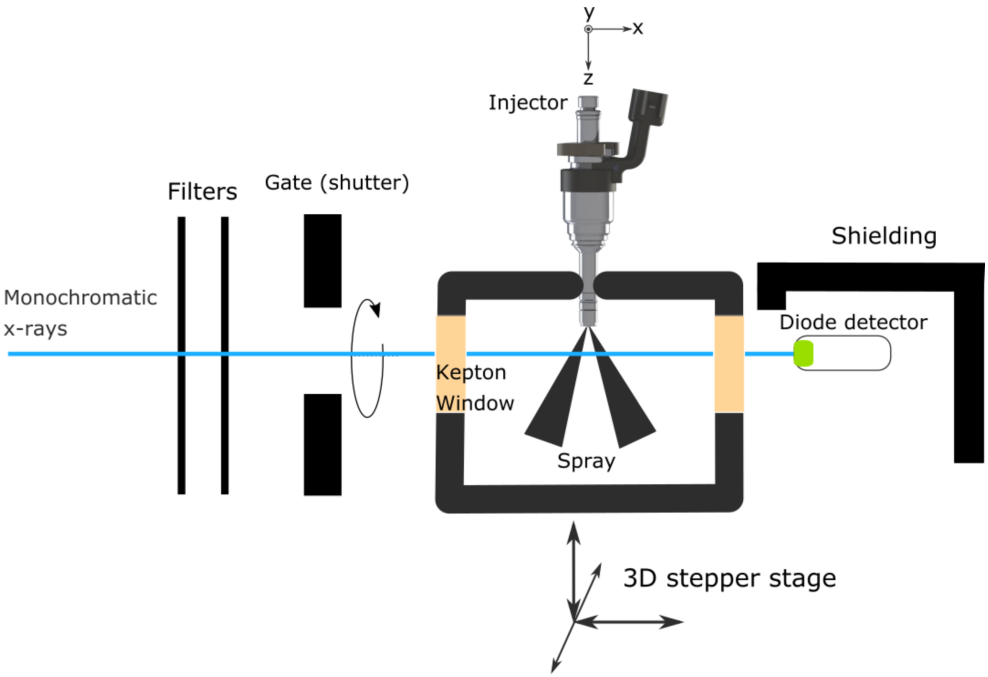

Figure 3.18: Sketch of the experimental set up for x-ray radiography measurements. The X-rays travel from left to right. (not to scale)

3.6.5 X-ray tomography radiography in the near nozzle field

The technique allows to study the plume-to-plume variation, reveal information inside the injector sprays cone, or in this particular case report about the spray impingement at a very close distance to the wall by measuring te fuel mass distribution. It consists in performing similar measurement to the previous explained (subsection 3.6.4), the only difference is how the data is processed afterwards. To reconstruct a flow field tomography, horizontal scans must be executed at a selected distance from the nozzle, however in difference with Figure 3.18, the injector and vessel installation is located on a rotation stage that allows turning the injector the 180° needed to perform the tomographic reconstruction. However, it is only valid if the injector is rotated in the centroid axis of the sprays.

It was measured from 0° to 180° in steps of 1° . Moreover, the tomography was performed at 0.005 mm from the perpendicular wall. The time-resolved tomographic reconstruction was performed employing a penalized maximum likelihood algorithm, which was extensively explained in previous works [38–40].

3.6.6 Researched Wall configurations

During my research stay at ANL I was able to explore the viability of researching spray wall impingement through x-rays techniques, which it has never been done before. As mentioned in chapter 2, the study of wall impingement is of great importance when implementing GDI injectors. Therefore, two different wall configurations were proposed for this study. Since spray impact angles can vary greatly depending on the distribution of nozzle holes and between nozzles, it was decided, for simplicity, to use two fundamental wall configurations. The first is a flat wall located perpendicular to the axis of the nozzle at a distance of 12.30 mm forming a 90° angle, this configuration is illustrated in Figure 3.19. The second configuration is a wall located parallel to the axis of the injector at a distance of 7.33 mm, which is shown in Figure 3.20.

The hardware used for this study was the ECN Spray G. Its spray plumes have 40° angle to the injector axis. Thus, the impact angles with the wall were 60° for the perpendicular configuration and 40° for the lateral configuration.

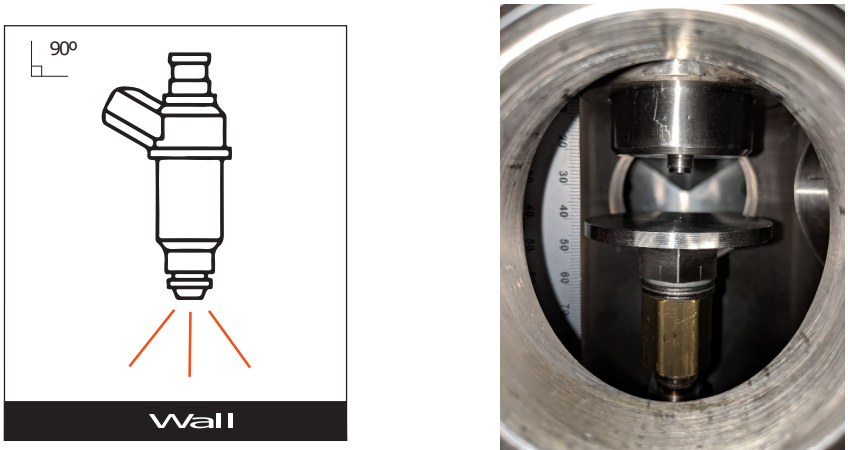

(a) *(b)*

Figure 3.19: Perpendicular wall configuration sketch (a) and picture of the final set up (b).

3.7 Optical techniques for spray visualization

3.7.1 Background

Optical techniques normally allow for a non-intrusive study of the flow. The first techniques date back from the 1800s, when shawdography and Schlieren

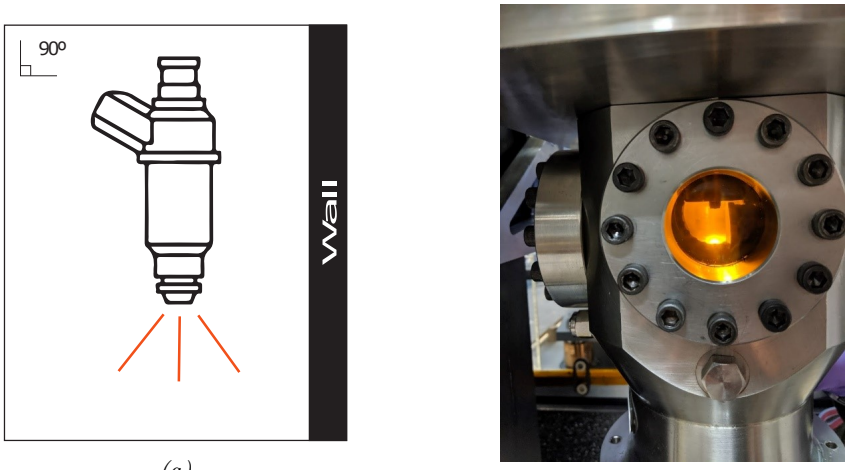

(a) (b)

Figure 3.20: Parallel wall configuration sketch (a) and picture of the final set up (b).

revealed flow structures [41]. Latest technologies advancements in fast-cameras, optics, illumination lasers and x-rays have permitted to research the flow phenomena and injector's spray in a detail that have never seen before. This section aims to explain the optical techniques principles using visible light during the spray visualization campaigns in this research.

3.7.2 Diffuse back-illumination

Diffuse back-illumination (DBI) is an optical setup for quantitative, line-of-sight extinction imaging that is capable of working in harsh optical environments with high temporal resolution.

One of the most common spray characteristic researched through the technique is liquid penetration, often used to study the mixing processes in gasoline and diesel sprays [6, 8, 21]. The technique can be included in the category that use visible-wavelength light as source of illumination which uses light scattered set ups. MIE scattering (section 3.7.3) is another example of this kind of techniques.

In DBI, the light is extincted because of the optical depth (τ) of the spray core and droplets. The extinction is calculated each instant using the Beer-Lambert law described in Equation 3.20:

$$\frac{I}{I_0} = e^{-\tau} \tag{3.20}$$

Where I is the intensity of the frame taken into account attenuated by the spray and I_0 is the reference image from the source without attenuation. In the recent years, the implementation of fast light-emitting diode (LED) in the set up, has allowed to enhance the nature of the images acquired. LED combined with modern circuit permit very short light pulses with the order of nanoseconds. Therefore, the exposure is limited by pulse duration and not by the camera shutter speed. The result is much sharper images than if a continuous light source had been used [2, 6, 21, 38, 42].

The DBI optical improved set up used in the experiments was first introduced by Ghandhi and Heim [43] and is shown schematically in Figure 3.21. It is composed (from right to left) by a LED light source, diffuser, field (Fresnel) lens and a high-speed camera at the other side of the test chamber. The blue LED unit used was composed by the control circuit, heat sink, and a parabolic reflector in order to reduce the LED light aperture from 120° to 25° so concentrating and reducing light loss. Then, a 100mm diameter engineered diffuser with 20.5° of divergence angle is used to homogenize the light. Next, a Fresnel lens with a focal length of 67mm was employed to replicate the diffused light source at the optical plane of interest of the spray. A blue LED was used since combined with a blue filter before the camera lens allows to reduce the light interference from other optical set up measuring at the same time, resulting in a much clearer captured image.

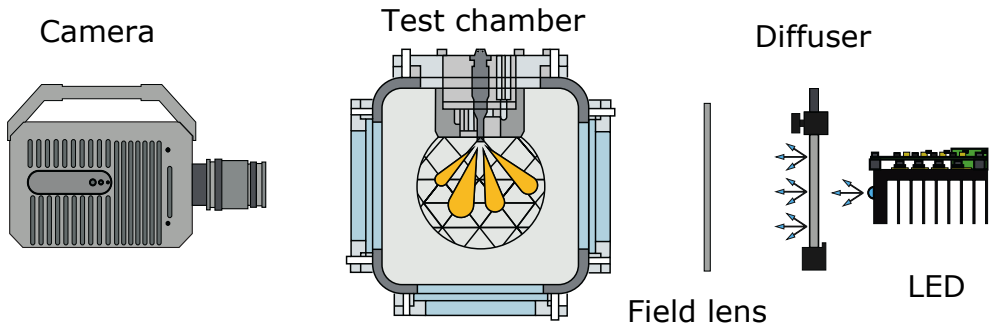

Figure 3.21: Diagram of diffused back-illumination (DBI) setup on the GDI test rig.

3.7.3 Mie scattering

Mie-scattering (MIE) is an optical phenomenon named after Gustav Mie. It refers to the elastic scattering of light from atomic and molecular particles whose diameter is larger than about the wavelength of the incident light. In other words, MIE phenomenon can be used in liquid spray investigation since

the incident light is reflected by the liquid droplets of the spray. The MIE set up used in the experiments is illustrated in Figure 3.22. Two Mercury-Xenon arc lamp light sources are used. The light is transported using optical fiber to a 7mm diameter collimator lens that permit to concentrate the light in the region of interest.

MIE set up is much harder to configure than DBI, since the light-source orientation can greatly influence on the visualized spray. Hamzah et al. [44] compared DBI and MIE optical techniques for measuring the liquid length of severely flashing spray. They conclude that qualitative assessment are similar for both techniques, however, maximum liquid penetration can be very dependent on the set up and image processing method. Their result yielded differences between the two optical approaches up to 20 % in the most severe flashing cases.

Generally, DBI results are more independent from the illumination source and set up than MIE, nevertheless, in some cases there is no other optical accesses for DBI, and only MIE set up is possible to study the spray. Other consideration is when it is required a frontal view of the spray. In that case, unless the injector mount side has an optical access to locate a light source, the only way to visualize the spray is by MIE set up, as depicted in Figure 3.22.

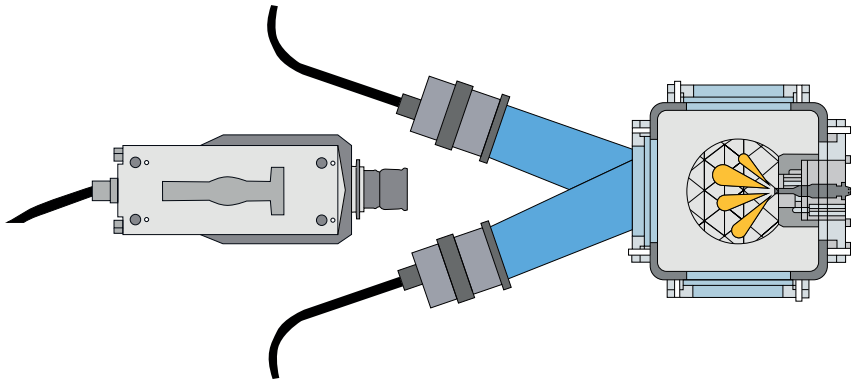

Figure 3.22: Diagram of MIE-scattering (MIE) setup on the GDI test rig.

3.7.4 Single-pass Schlieren technique

Single-pass Schlieren is a widely known optical technique used by researchers to study gasoline and diesel macroscopic parameters such as vapor phase spray angle and spray penetration [2, 21, 32, 45–48]. These parameters are useful, since in addition to revealing behaviors in the phenomena, they are also necessary to validate numerical studies.

The method principle consists in a light rays that travels uniformly through homogeneous media. They bend proportionally to the refractive index of the medium they encounter and go through [3]. Equation 3.21 show the proportional relation that exist between the gas density (ρ) and the reflective index (n) introduced by Gladstone and Dale [49].

$$k_{GD} \cdot \rho = n - 1 \tag{3.21}$$

Where k_{GD} is the Gladstone-Dale coefficient. Then, the deflected ray angle ε in a perpendicular plane X-Y of a light beam traveling to Z direction, is described by [50]:

$$\varepsilon_x = \frac{L}{n_0}\frac{\partial n}{\partial x} \quad , \quad \varepsilon_y = \frac{L}{n_0}\frac{\partial n}{\partial y} \tag{3.22}$$

Where n_0 is the refractive index of the medium and L is the optical path length. The combination of the equations shows the relation between the refractive index and deflected ray angle. This appears visually in Schlieren and shawdography methods. Both methods are related, however, Schlieren set up uses a diaphragm to cut-off the refracted light. In fuel spray application, along the optical path of the light, the rays are bent due to the density gradient between the ambient gas and the fuel spray in the test section. Thus, the boundaries between the two elements can be differentiated and fuel spray vapor can be isolated from the background.

The schileren set ups can be single-pass and double-pass [51]. The first one is the most common solution for test vessels with two opposite optical accesses, where the light goes through the test section one time. It permits to see the lateral vapor phase of the spray. Nevertheless, the double-pass is used to investigate the frontal view of the spray, requiring a special mirror that withstand the camber conditions situated at the injector holder side.

A typical Schlieren single-pass set up like the one employed in this study is illustrated in Figure 3.23. The light, from a 1 KW Mercury-Xenon arc lamp, is transported using a optical fiber up to a 1.2mm opening, which creates a

point illumination. Then, a 150 mm parabolic mirror is used to parallelize the rays at its focal length (450 mm). After passing through the test section, a biconvex lens of 150 mm converges the rays at its focal length (450 mm). Next, an iris diaphragm featuring 4 mm aperture was used to cutoff the deviated rays, thus, resulting in a higher contrast image. The set-up employed is similar to the one used in many previous studies [2, 4, 6].

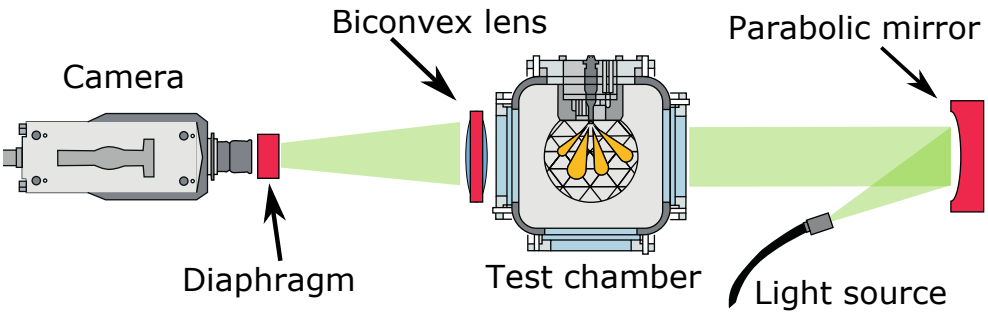

Figure 3.23: Diagram of single-pass Schlieren setup on the GDI test rig.

3.8 Fuel spray image processing methods

Image processing is one of the crucial steps in any visualization data analysis and greatly depends in the parameters of interest that are intended to obtain. Normally, the background is subtracted from the phenomena, in this case the fuel spray. Once the object of interest is differentiated from the background, the contour analysis can provide important parameters like spray penetration, angle, width, etc. The fast-cameras record a video, in which each frame is processed separately as an independent image. There are four principal steps to process each frame: image masking, background subtraction, contour detection, and contour analysis. The algorithms used for image processing were programmed in MATLAB at CMT-Motores Térmicos.

3.8.1 Image masking

Computer software sees an image as a 2D matrix in which each element is the value of that corresponding pixel. The values in a gray scale image can vary from 0 (black) to 1 (white) when normalized. However, the sensitivity or the numbers of values depend on the bit depth of the camera sensor. For example, the bit depth of the cameras used was 12-bit, which permitted to acquire values from 0 to 4095 ($2^{BitDepth}$).

Image masking consist in selecting the region of the image that is going to be useful for processing, such as where the spray is going to develop. The rest of the image can be discarded, such as the windows limit, injector holder or nozzle tip among other. Applying a mask to an image consists in constructing a matrix with the same size of the image, the mask region is filled with zeros whereas the region of interest is filled with ones. It is constructed in polar coordinates, determining the origin in the nozzle tip and providing two radius and an angle. Finally, operation of element-by-element multiplication of both matrix is performed to obtain the masked image as is illustrated in Figure 3.24.

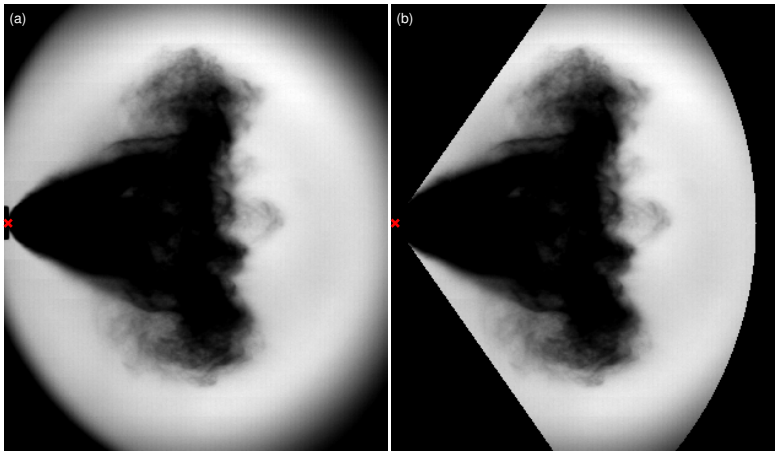

Figure 3.24: Example of image masking over a snapshot of DBI technique. The red cross indicates the nozzle tip. The original and mask images are depicted left and right respectively.

3.8.2 Background subtraction

Once the frame is masked, the following step would be to separate the spray from the background. In the case of DBI or MIE images, it is done by Equation 3.20, where the optical thickness is calculated being I_0 the image of the background before the injection event and I the image containing the spray. An example of the optical thickness of a frame in which the spray is developed is depicted in Figure 3.25.

For the case of Schlieren data the process is similar but extra consideration must be taken. The density gradients in the background would deflect the light rays and could appear on the final images. These gradients are cause by uneven temperature distributions in the test chamber as well as hot convection

from the chamber walls. Therefore, the collection of images from one injection event could end up having many different backgrounds patterns, which might move along the duration of the injection event.

The spray contour is obtained by using the approach described by Payri et al. [51]. Its principle is based in dynamic-background-composition subtraction [8, 21, 51], however, improved with image temporal derivative assessment [6, 23, 51, 52]. The dynamic-background is continuously updating the background information to be subtracted. Thus, it is calculated in two steps, first, everything that was not spray from previous image is set as background, and where the spray was in the previous image is filled by average of the first 8 images (static background).

3.8.3 Contour detection

To detect the contour of the spray in the image, it is necessary to binarized it through thresholding. In other words, each pixel of the image is set to 0 (black) when there is background and 1 (white) when spray. Then, the threshold selection is crucial to determine whether a gray level is considered spray or background. For DBI and MIE, a fix value of optical thickness was used [42, 53]. For schilieren on the contrary, the selected threshold was set as a fixed factor multiplied by the dynamic range of the frame analyzed [51, 53, 54]. Westlye et al. [55] found beam-steering at the tip of the liquid plume in a DBI set up which could led to countour detection uncertainty. As stated before, the value of the threshold has greatly influence in differentiating the spray, thus it is desired images as sharp as possible, with fast intensity decay at the borders of the spray.

Despite background subtraction, some structures could present high levels of intensity that can cause confusion and considered as spray when applying the threshold binarization. Therefore, a filtering process is implemented to enhance the accuracy through erosion strategies, removal of pixel noises and pixel connectivity criteria [51]. Figure 3.26 reproduce the steps of the contour detection procedure for a given Schlieren frame. The steps followed were:

(a)- Original image.

(b)- Image with background subtraction. Using an average of 4 frame before start of injection.

(c)- Image temporal derivative. As fuel dilutes in the chamber, the local density gradients of these areas are similar to their surroundings. Thus,

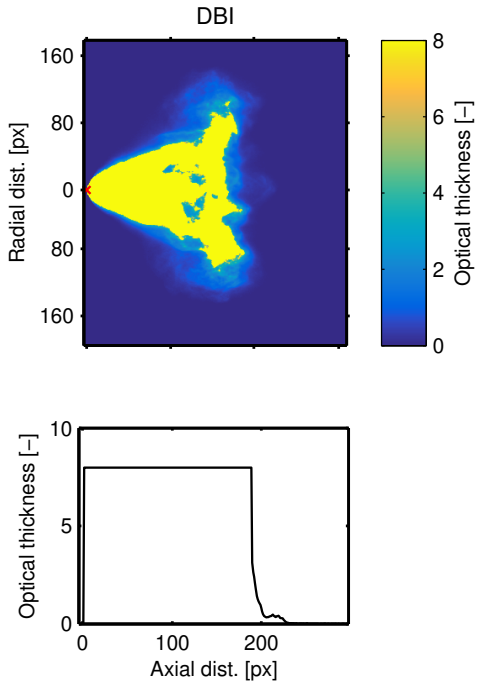

Figure 3.25: Maximum optical thickness and intensity levels along the spray axis of a DBI image.

the deflection angle of the rays is reduced and the contrast between the background and spray is lower. This temporal derivative handles well the spray contour in these dilutes regions.

(d)- Contour detection image. This sharp image is formed by combining (a) and (b), which takes advantage of both approaches.

(e)- Binarization with selected threshold (the approach of this step depends on the optical technique employed).

(f)- Image with erosion filter. For this step it has been applied a two-step erosion filter that removes small pixels areas and background noise.

(g)- Image with dilation filters. This is applied to compensate the erosion filter on the true dimensions of the spray contour.

(h)- Original image with the found contour overlapped.

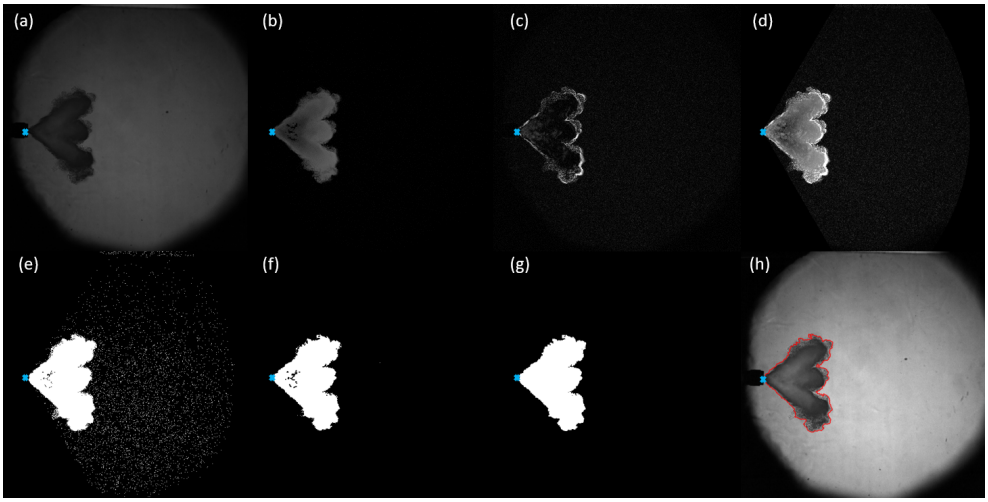

Figure 3.26: Secuential example of the contour detection algorithm.

3.8.4 Contour analysis

After the contour have been obtained, a post-processing algorithm is executed to extract the characteristic and relevant information from the sprays. These macroscopic variables are illustrated in Figure 3.27. Liquid and vapor penetration is contemplated as the furthest point of the spray contour, considering only axial distance from the nozzle (on the spray axis) [8, 21, 38]. The spray angles are more difficult to obtain since its value depends significantly on the criteria followed, and in some cases/conditions such as spray collapse, the spray could not be conical, so the criteria could fail as shown by Vaquerizo [2]. Figure 3.28 depicts two DBI conditions with overlapped contour. The angles have been calculated using the least square fit setting a lower and upper limits from the penetration for the fits. The left picture shows a spray pattern that can be approximated to a triangle. On the right there is a spray collapse due to the high density conditions, which is rounded and more asymmetrical. So a solution to this is perform the angle fit at a much closer distance from the nozzle, which end up being 1% and 50% of the total penetration for this case.

3.8.5 Data averaging and measurement procedure

Ten injection events were recorded for each test condition. Each of them is processed individually, in which each frame is analyzed using the explained

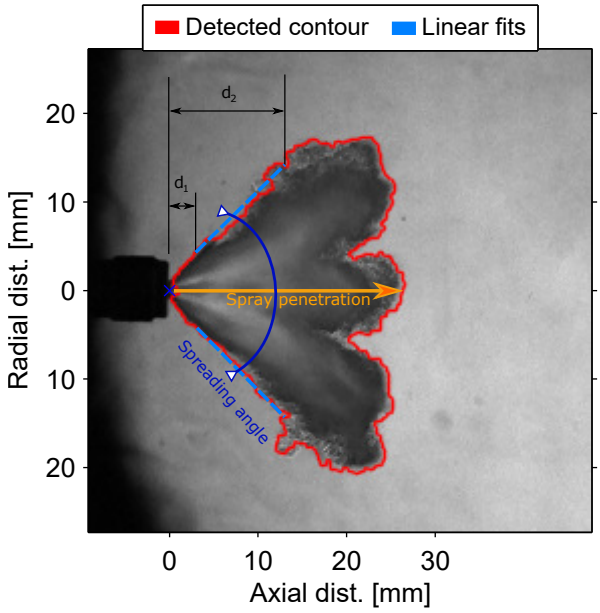

Figure 3.27: Macroscopic spray parameters extracted from the contour analysis.

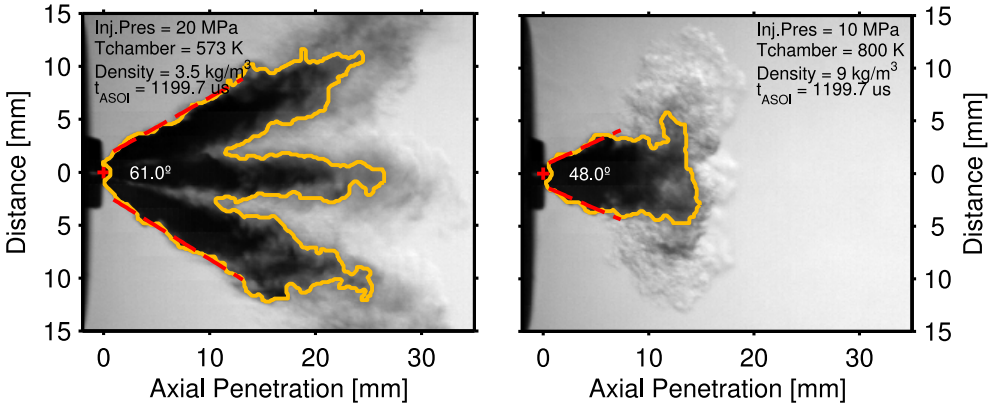

Figure 3.28: DBI images showing two different test conditions and how it could influence the general shape of the spray. Adapted from [2].

algorithm. The contour processing results are averaged within the repetitions using a moving average strategy. The steps followed were:

1. A time window (Δt) is selected, being 9 μs for all experiments.
2. Then, data inside the interval $t_i \pm \Delta t/2$ is extracted for averaging.

3. A linear fit is performed using the data selected and a function $f(t)$ is obtained. The averaged value $\hat{y}$ is achieved by computing $f(t_i)$.

4. The process is repeated along each time step of the test point by moving t_i.

References

[1] "Engine Combustion Network". In: *https://ecn.sandia.gov/gasoline-spray-combustion/* (2020).

[2] Vaquerizo, Daniel. "Study on Advanced Spray-Guided Gasoline Direct Injection Systems". PhD thesis. Universitat Politècnica de València, 2017.

[3] Viera, Alberto. "Effect of multiple injection strategies on the diesel spray formation and combustion using optical diagnostics". PhD thesis. Universitat Politècnica de València, 2019.

[4] Viera, Juan Pablo. "Experimental study of the effect of nozzle geometry on the performance of direct-injection diesel sprays for three different fuels". PhD thesis. 2017.

[5] Payri, Raul, Bracho, Gabriela, Gimeno, Jaime, and Bautista, Abian. "Rate of injection modelling for gasoline direct injectors". In: *Energy Conversion and Management* 166 (2018), pp. 424–432. DOI: 10.1016/j.enconman.2018.04.041.

[6] Bardi, Michele. "Partial needle lift and injection rate shape effect on the formation and combustion of the Diesel spray". PhD thesis. Valencia (Spain): Universitat Politècnica de València, 2014. DOI: 10.4995/Thesis/10251/37374.

[7] Zhao, Hua. *Advanced direct injection combustion engine technologies and development*. Woodhead Publishing Limited, 2010. DOI: 10.1533/9781845697327.

[8] Payri, Raul, Hardy, Gilles, Gimeno, Jaime, and Bautista, Abian. "Analysis of counterbore effect in five diesel common rail injectors". In: *Experimental Thermal and Fluid Science* 107 (2019), pp. 69–78. DOI: 10.1016/j.expthermflusci.2019.05.008.

[9] Payri, Raul, Gimeno, Jaime, Mata, Carmen, and Viera, Alberto. "Rate of injection measurements of a direct-acting piezoelectric injector for different operating temperatures". In: *Energy Conversion and Management* 154.October (2017), pp. 387–393. DOI: 10.1016/j.enconman.2017.11.029.

[10] Payri, Raul, Viera, Juan Pablo, Wang, Hua, and Malbec, Louis-Marie. "Velocity field analysis of the high density, high pressure diesel spray". In: *International Journal of Multiphase Flow* 80.24 (2016), pp. 69–78. DOI: 10.1016/j.ijmultiphaseflow.2015.10.012.

[11] Payri, Raul, Gimeno, Jaime, Martí-Aldaraví, Pedro, and Vaquerizo, Daniel. "Internal flow characterization on an ECN GDi injector". In: *Atomization and Sprays* 26.9 (2016), pp. 889–919. DOI: 10.1615/AtomizSpr.2015013930.

[12] Bosch, Wilhelm. "The Fuel Rate Indicator: A New Measuring Instrument For Display of the Characteristics of Individual Injection". In: *SAE Technical Paper 660749*. 1966. DOI: 10.4271/660749.

[13] Lemmon, Eric W., McLinden, M. O., and Friend, D. G. "Thermophysical Properties of Fluid Systems". In: *NIST Chemistry WebBook, NIST Standard Reference Database Number 69*. Ed. by P. J. Linstrom and W. G. Mallard. 2011.

[14] Payri, R., Salvador, F.J., Gimeno, J., and Bracho, G. "A new methodology for correcting the signal cumulative phenomenon on injection rate measurements". In: *Experimental Techniques* 32.1 (2008), pp. 46–49. DOI: 10.1111/j.1747-1567.2007.00188.x.

[15] Shahangian, Navid et al. "Spray Orientation Assessment and Correction Method for GDI Momentum Flux Measurements". In: October (2019), pp. 231–241.

[16] Strek, Piotr et al. "X-Ray Radiography and CFD Studies of the Spray G Injector". In: *SAE Technical Papers* 2016-April.April (2016). DOI: 10.4271/2016-01-0858.

[17] Payri, Raul, Garcia-Oliver, Jose Maria, Salvador, Francisco Javier, and Gimeno García, Jaime. "Using spray momentum flux measurements to understand the influence of diesel nozzle geometry on spray characteristics". In: *Fuel* 84.5 (2005), pp. 551–561. DOI: 10.1016/j.fuel.2004.10.009.

[18] Gimeno, Jaime. "Desarrollo y aplicación de la medida de flujo de cantidad de movimiento de un chorro Diesel". PhD thesis. E.T.S. Ingenieros Industriales, Universidad Politécnica de Valencia, 2008. DOI: 10.4995/Thesis/10251/8306.

[19] Payri, Raul, Gimeno, Jaime, Marti-Aldaravi, Pedro, and Vaquerizo, Daniel. "Momentum Flux Measurements on an ECN GDi Injector". In: *SAE Technical Paper 2015-01-1893*. 2015. DOI: 10.4271/2015-01-1893.

[20] Moon, Seoksu et al. "Ultrafast X-ray study of multi-hole GDI injector sprays: Effects of nozzle hole length and number on initial spray formation". In: *Experimental Thermal and Fluid Science* 68 (2015), pp. 68–81. DOI: 10.1016/j.expthermflusci.2015.03.027.

[21] Payri, Raul, Salvador, Francisco Javier, Martí-Aldaraví, Pedro, and Vaquerizo, Daniel. "ECN Spray G external spray visualization and spray collapse description through penetration and morphology analysis". In: *Applied Thermal Engineering* 112 (2017), pp. 304–316. DOI: 10.1016/j.applthermaleng.2016.10.023.

[22] Venegas Pereira, Oscar Hernando. "Estudio del fenómeno de la cavitación en la inyección Diesel mediante la visualización del flujo interno en orificios transparentes." PhD thesis. Valencia (Spain): Universitat Politècnica de València, 2014. DOI: 10.4995/Thesis/10251/37375.

[23] Payri, Raul, Viera, Juan Pablo, Gopalakrishnan, Venkatesh, and Szymkowicz, Patrick G. "The effect of nozzle geometry over the evaporative spray formation for three different fuels". In: *Fuel* 188 (2017), pp. 645–660. DOI: 10.1016/j.fuel.2016.06.041.

[24] Payri, Raul, Viera, Juan Pablo, Gopalakrishnan, Venkatesh, and Szymkowicz, Patrick G. "The effect of nozzle geometry over ignition delay and flame lift-off of reacting direct-injection sprays for three different fuels". In: *Fuel* 199 (2017), pp. 76–90. DOI: 10.1016/j.fuel.2017.02.075.

[25] Shost, Mark Anthony. "Evaluation of nozzle geometry on high pressure Gasoline Direct Injection spray atomization". PhD thesis. Wayne State University, 2014, p. 295.

[26] Saha, Kaushik et al. "Numerical Investigation of Two-Phase Flow Evolution of In- and Near-Nozzle Regions of a Gasoline Direct Injection Engine During Needle Transients". In: *SAE International Journal of Engines* 9.2 (2016), pp. 2016–01–0870. DOI: 10.4271/2016-01-0870.

[27] Kostas, J et al. "Effect of nozzle transients and compressibility on the penetration of fuel sprays". In: *Applied Physics Letters* 95.2 (2009), p. 024101. DOI: 10.1063/1.3182821.

[28] Swantek, Andrew et al. "Quantification of Shot-to-Shot Variation in Single Hole Diesel Injectors". In: *SAE International Journal of Fuels and Lubricants* 8.1 (2015), pp. 2015–01–0936. DOI: 10.4271/2015-01-0936.

[29] Duke, Daniel, Swantek, Andrew, Kastengren, Alan, Fezzaa, Kamel, and Powell, Christopher. "Recent Developments in X-ray Diagnostics for Cavitation". In: *SAE International Journal of Fuels and Lubricants* 8.1 (2015), pp. 2015–01–0918. DOI: 10.4271/2015-01-0918.

[30] ANL. "Advance Photron source overview". In: *https://www.aps.anl.gov/About/Overview* (2020).

[31] Shen, Qun et al. "Dedicated full-field X-ray imaging beamline at Advanced Photon Source". In: *Nuclear Instruments and Methods in Physics Research Section A: Accelerators, Spectrometers, Detectors and Associated Equipment* 582.1 (2007), pp. 77–79. DOI: 10.1016/j.nima.2007.08.169.

[32] Viera, Juan Pablo et al. "Linking instantaneous rate of injection to X-ray needle lift measurements for a direct-acting piezoelectric injector". In: *Energy Conversion and Management* 112 (2016), pp. 350–358. DOI: 10.1016/j.enconman.2016.01.038.

[33] Sharma, K. Sen, Seshadri, S., Feser, M., and Wang, G. "Accurate Resolution Measurement for X-Ray Micro-CT Systems". In: *AIP Conference Proceedings*. Vol. 1365. September. 2011, pp. 337–340. DOI: 10.1063/1.3625373.

[34] Lewis, J P. "Fast Template Matching Template". In: *Pattern Recognition* (1995).

[35] Wei, Shou-Der and Lai, Shang-Hong. "Fast Template Matching Based on Normalized Cross Correlation With Adaptive Multilevel Winner Update". In: *IEEE Transactions on Image Processing* 17.11 (2008), pp. 2227–2235. DOI: 10.1109/TIP.2008.2004615.

[36] Sarvaiya, J.N., Patnaik, Suprava, and Bombaywala, Salman. "Image Registration by Template Matching Using Normalized Cross-Correlation". In: *2009 International Conference on Advances in Computing, Control, and Telecommunication Technologies*. IEEE, 2009, pp. 819–822. DOI: 10.1109/ACT.2009.207.

[37] Kastengren, Alan et al. “The 7BM beamline at the APS: a facility for time-resolved fluid dynamics measurements”. In: *Journal of Synchrotron Radiation* 19.4 (2012), pp. 654–657. DOI: 10.1107/S0909049512016883.

[38] Duke, Daniel J. et al. “Internal and near nozzle measurements of Engine Combustion Network ’Spray G’ gasoline direct injectors”. In: *Experimental Thermal and Fluid Science* 88.June (2017), pp. 608–621. DOI: 10.1016/j.expthermflusci.2017.07.015.

[39] Gürsoy, Doga, De Carlo, Francesco, Xiao, Xianghui, and Jacobsen, Chris. “TomoPy: a framework for the analysis of synchrotron tomographic data”. In: *Journal of Synchrotron Radiation* 21.5 (2014), pp. 1188–1193. DOI: 10.1107/S1600577514013939.

[40] Duke, Daniel J. et al. “Time-resolved X-ray Tomography of Gasoline Direct Injection Sprays”. In: *SAE International Journal of Engines* 9.1 (2015), pp. 143–153. DOI: 10.4271/2015-01-1873.

[41] Miles, Richard B. “Optical diagnostics for high-speed flows”. In: *Progress in Aerospace Sciences* 72 (2015), pp. 30–36. DOI: 10.1016/j.paerosci.2014.09.007.

[42] Manin, Julien, Bardi, Michele, and Pickett, Lyle M. “Evaluation of the liquid length via diffused back-illumination imaging in vaporizing diesel sprays”. In: *Comodia*. Fukuoka, 2012.

[43] Ghandhi, J B and Heim, D M. “An optimized optical system for backlit imaging”. In: *Review of Scientific Instruments* 80.5 (2009), p. 056105. DOI: 10.1063/1.3128728.

[44] Hamzah, A et al. “A comparison of diffuse back-illumination (DBI) and Mie-scattering technique for measuring the liquid length of severely flashing spray”. In: *20th Australasian Fluid Mechanics Conference*. December. Perth, Australia, 2016.

[45] Du, Jianguo, Mohan, Balaji, Sim, Jaeheon, Fang, Tiegang, and Roberts, William L. “Experimental and analytical study on liquid and vapor penetration of high-reactivity gasoline using a high-pressure gasoline multi-hole injector”. In: *Applied Thermal Engineering* 163.July (2019), p. 114187. DOI: 10.1016/j.applthermaleng.2019.114187.

[46] Manin, Julien et al. “Experimental Characterization of DI Gasoline Injection Processes”. In: 2015. DOI: 10.4271/2015-01-1894.

[47] Payri, Raul, Gimeno, Jaime, Viera, Juan Pablo, and Plazas, Alejandro Hernan. "Needle lift profile influence on the vapor phase penetration for a prototype diesel direct acting piezoelectric injector". In: *Fuel* 113 (2013), pp. 257–265. DOI: 10.1016/j.fuel.2013.05.057.

[48] Fansler, Todd D. and Parrish, Scott E. "Spray measurement technology: a review". In: *Measurement Science and Technology* 26.1 (2015), p. 012002. DOI: 10.1088/0957-0233/26/1/012002.

[49] Gladstone, J H and Dale, T P. "Researches on the Refraction, Dispersion, and Sensitiveness of Liquids". In: *Philosophical Transactions of the Royal Society of London* 153 (1863), pp. 317–343.

[50] Settles, G. S. *Schlieren and Shadowgraph Techniques*. Berlin, Heidelberg: Springer Berlin Heidelberg, 2001, p. 376. DOI: 10.1007/978-3-642-56640-0.

[51] Payri, Raul, Salvador, F.J., Bracho, Gabriela, and Viera, Alberto. "Differences between single and double-pass schlieren imaging on diesel vapor spray characteristics". In: *Applied Thermal Engineering* 125 (2017), pp. 220–231. DOI: 10.1016/j.applthermaleng.2017.06.140.

[52] Pastor, Jose Vicente, Payri, Raul, Garcia-Oliver, Jose Maria, and Nerva, Jean-Guillaume. "Schlieren Measurements of the ECN-Spray A Penetration under Inert and Reacting Conditions". In: *SAE Technical Paper 2012-01-0456*. 2012. DOI: 10.4271/2012-01-0456.

[53] Payri, R., Gimeno, J., Bracho, G., and Vaquerizo, D. "Study of liquid and vapor phase behavior on Diesel sprays for heavy duty engine nozzles". In: *Applied Thermal Engineering* 107 (2016), pp. 365–378. DOI: 10.1016/j.applthermaleng.2016.06.159.

[54] Siebers, Dennis L. "Liquid-Phase Fuel Penetration in Diesel Sprays". In: *SAE Technical Paper 980809*. 1998, pp. 1–23. DOI: 10.4271/980809.

[55] Westlye, Fredrik R et al. "Diffuse back-illumination setup for high temporally resolved extinction imaging". In: *Applied Optics* 56.17 (2017), p. 5028. DOI: 10.1364/AO.56.005028.

Chapter 4

Developing a new GDI facility

4.1 Introduction

CMT-Motores Térmicos has a strong background in diesel sprays and over the years it has been recognized internationally as one of the top research institutions in combustion engines because of the numerous contributions to the ICE community as well as for being consultant for many companies. During the last decade, CMT-Motores Térmicos has developed and acquired many research equipment for this purpose. Particularly, for the study of diesel sprays commercially injector rate indicators have been purchased as well as high-pressure high-temperature test chamber. On the other hand, new research facilities have been developed and manufactured successfully such as the rate of momentum test rig, cold spray visualization vessel and a higher specs high-pressure high-temperature test chamber. All of them were primarily thought for diesel sprays, however, they can be used for gasoline sprays as well.

On the last lustrum, CMT have made a significant effort into researching gasoline sprays to follow the market and research trend as exposed in section 2.1. To this end, already available facilities were appropriate to convey gasoline spray research, nevertheless, certain gasoline engine conditions could not be reproducible with the present equipment. Flash boiling and spray collapse phenomena are an example of that, which could not be extensively tested. It occurs at specific engine conditions when injecting during the intake stroke so the fuel spray finds sub-atmospheric chamber conditions. Figure 4.1 shows the chamber conditions covered by the already available diesel facilities

at CMT. In section 2.6, it was explained that flash boiling occurs at a sudden drop of pressure such as the one experienced by the fuel spray when injected into the combustion chamber [1–3]. The fuel could change from a 200 bar injection pressure and 90°C to 0.5 bar and 60°C. It is noteworthy mention that flash boiling occurs during a sudden pressure difference and not at a sudden temperature difference, because the time to get temperature equilibrium in the fuel is much higher than the injection event itself.

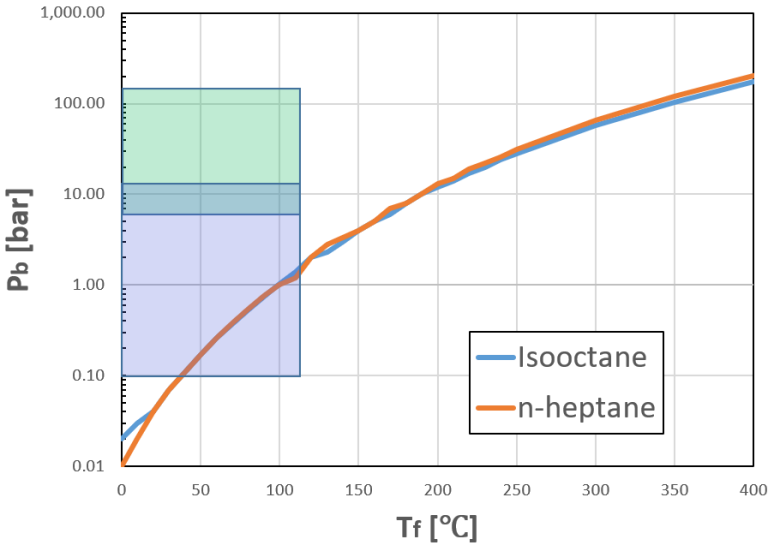

Figure 4.1: Vapor pressure curve of two different mono-component fuels. The green shadow represent the diesel facility range of operation, whereas the blue one is the desired to study gasoline engine conditions.

This chapter presents the design, development and construction of a new test vessel for GDI sprays research. The blue square in Figure 4.1 represents the desired range of conditions for this new facility.

4.2 Design

4.2.1 Test chamber requirements

The test rig's main purpose is to be able to reproduce the engine conditions required for testing. At the same time, it have to meet other requirement such as the following:

1. **Safety**. It has to be able to operate safely along all the range of conditions tested.

2. **Cost**. It needs to be kept under a reasonable budget.

3. **Test condition**. It needs to accommodate all the desired conditions by withstanding required temperatures (ambient to 150°C) and pressures (10 KPa to 1.5 MPa absolute).

4. **Optical accesses**. It needs to be sufficient big to perform imaging measurements as well as to operate with PDA and PIV equipment.

5. **Flow recirculation**. To be able to renovate the gas volume inside the vessel so the excesses of fuel can be removed.

6. **Ground support**. Design of a test rig stand and configure optics tables.

7. **Injector holder**. Access piece to be able to install a variety of injectors.

4.2.2 Materials and structural design

Due to the less expensive cost and availability, a piece of 300 mm of an extruded steel beam was used as the vessel core. It has a square shape with rounded corners, thus, two caps were manufactured to close the volume so it could be pressurized. The adopted solution is illustrated in Figure 4.2. At the horizontal plane, three of the four faces of the cube were perforated to accommodate 180 mm optical accesses. The last face was set to locate the injector holder, leaving space for different specific injector adapters.

For all the mechanized parts as well as for the core structure, the material selected was AISI 1042 Carbon Steel. Nevertheless, a bluing treatment was performed in the pieces to avoid rust. It consists in an electro-chemical coating resulting from an oxidizing chemical reaction with iron on the surface selectively forming magnetite (Fe_3O_4).

The optical accesses were made of fused quart, with a special finish specifically to improve transparency and allow the use of laser optical techniques. Moreover, the size of the window was designed to be able to implement Phase Doppler Anemometry (PDA) measurements, accounting for the angle between the laser and the receiver of 110° going through the region of interest.

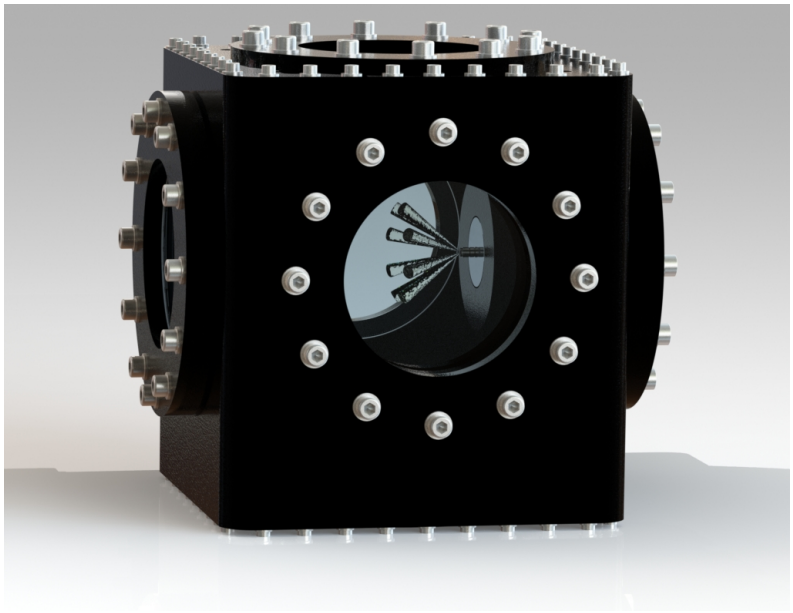

Figure 4.2: Render of the GDI test rig.

4.2.3 Flow heater module

An additional feature incorporated to the vessel is the ability to set a controlled chamber temperature through the installation of a heater module. The temperature range of operation is sought to be similar to those found in gasoline combustion engines that are in the order of ambient temperature to approximately 120°C. Thus, as a target design objective it is desired to achieve a temperature of 150°C in the chamber. The module is composed by a resistor, a case for the resistor and a electronic control box. Figure 4.4 shows a render of the flow heater module, which is installed in the bottom of the test chamber. It can be appreciated the casing and the coil resistor inside.

Casing

The casing is the piece that protects and holds the resistor. The fluid, as it passes through it, increases its temperature and enters the test chamber with the required temperature conditions. Theoretically, it is a heat-exchanger in which the heat yielded to the flow is achieved by the passage of electric current through a resistance immersed in a fluid (N_2 in this case).

The casing is designed to meet the dimensional requirements and to be large enough to accommodate the resistor. The 175 x 311 mm hole at the

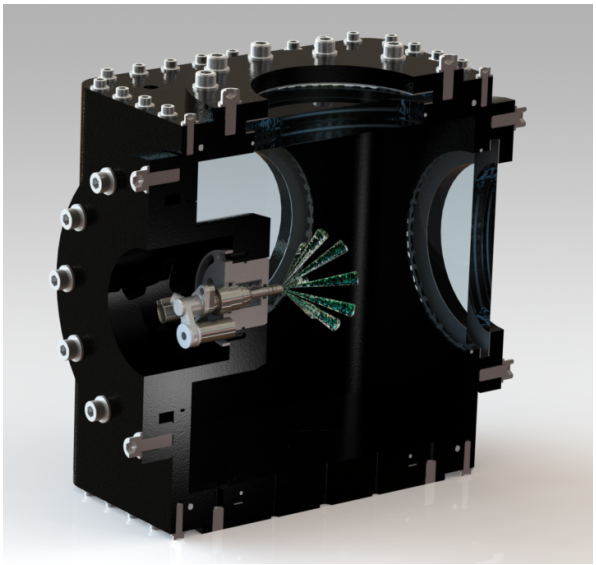

Figure 4.3: Middle section of the GDI test rig render.

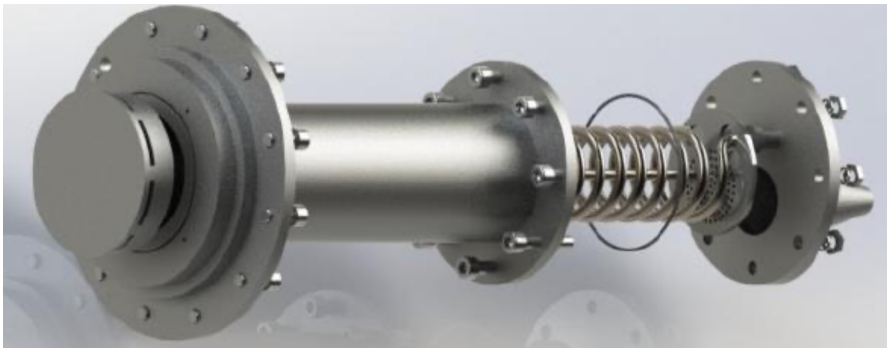

Figure 4.4: Resistor module for the GDI test rig.

bottom of the model with the support table in place must be taken into account, as well as the distance to the floor. There must be enough space both for the fluid inlet and for the different sensors and instruments that are necessary for the experimental test. In addition, it is necessary to place O-rings to guarantee the airtightness of the set. Moreover, a difussor is installed at the inlet to distribute flow around the cylinder and another difussor is employed at the outlet to distribute the hot gas along the test chamber. This last diffusor design can be seen in Figure 4.5.

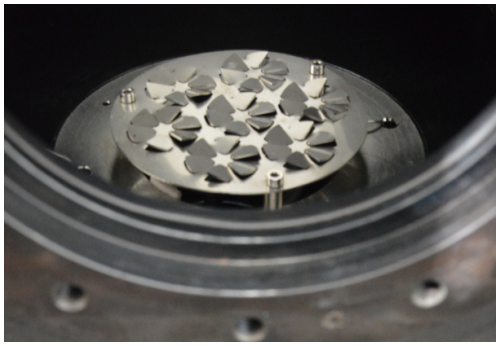

Figure 4.5: Outlet difussor of the resistor module.

Resistor

The Resistor design was a complex process which yielded different designs along the way. Conduction and convection are the two main drivers in transferring the heat to the gas. Both cases are modeled by Equation 4.1, where T_a and T_b represent the hot point and cold point respectively, and A is the contact surface. In the case of conduction, θ is defined as the thermal conductivity/thickness, whereas in the convection case θ is the convection coefficient.

$$\frac{\partial Q}{\partial t} = \theta \cdot A \cdot (T_a - T_b) \tag{4.1}$$

According to the theory of heat transfer, the heat transmitted by conduction through the resistance will depend on both its geometry and the thermal conductivity of the materials that conform it. Conversely, heat transmitted by convection is influenced by the properties and conditions at which a flow passes over a surface, such as its temperature and speed. As per Equation 4.1, increasing the contact area, the temperature difference and the convection and thermal conductivity coefficients improve the heat transfer per unit of time. That is, these values should be as high as possible. The coefficients depend on the type of material used and the maximum temperature of the resistance is determined by the manufacturer, therefore, the main design objective will be the maximization of the contact surface between the resistance and the air.

The resistance wire is made of a Nickel-Chromium alloy (NICROM) with 80/20 percentages, respectively. This alloy is chosen because of its high electrical resistance, its marked tendency to heat by the passage of electricity and its excellent resistance to oxidation and corrosion. An AISI 321 alloy (Fe-Cr18/Ni9/Ti) with a maximum air temperature of 1073 K is used for the shielding.

The resistor was selected to have 2 kW of power to ensure correct functioning of the module and achieve the desired temperature. The passage of an electric current through it produces heat thanks to the Joule's law and this heat is transmitted to the fluid. It is similar to the ones that are typically used in domestic ovens. Two special connections are located the ends so that it can be fixed at the steel piece that support and acts as a cover. The connections allow to insulate the resistor and prevent overheating in the casing. The final design is displayed in Figure 4.6.

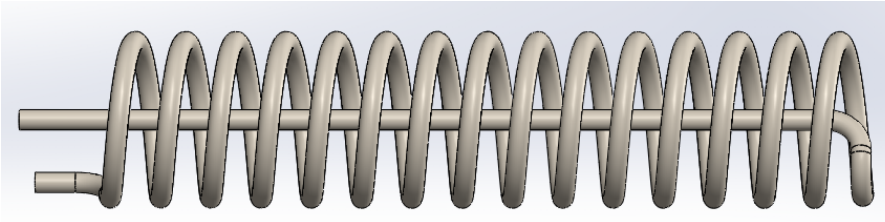

Figure 4.6: Final design of the shielded resistor.

4.2.4 Safe operation

Safety is a crucial aspect in the operation of any facility. In this case, two main solutions were implemented as passive and active safety:

- Pressure safety valve: the vessel is equipped with a pressure safety valve that automatically opens when the pressure inside the vessel is over 17.5 bar. A tension spring is closing the valve, thus it does not depend on electrical power.
- The heater module is operated by a PID control that does not allow to go beyond the maximum resistor operation temperature of 250°C by using a closed loop termocouple sensor at the resistor.

4.2.5 Instrumentation

The facility is equipped with an absolute pressure sensor in the main chamber, Kistler 4262A, with the capacity to measure 0 to 50 bar absolute. Moreover, several thermo-couples of K type are distribute along the vessel to monitor the temperature distribution. The exact locations are at the top and bottom of the chamber, as well as at the top and bottom of the casing of the resistor, so there is a control over the flow temperature evolution through its path.

4.3 Simulations

Although the design of the vessel is matured in a iterative manner, once the design is finished several finite element analysis simulations are executed in order to guarantee the structural integrity and functioning of the test rig. Both mechanical and CFD simulations are performed. The first ones will predict the loads in the vessel walls and windows due to the inside chamber pressure. The latter, will yield results about the flow velocity field and temperature distribution along the chamber. All the work in this section was performed using SolidWorks® Simulation and ANSYS® FLUENT.

4.3.1 Vessel integrity analysis

The materials chosen for the test rig were first selected to withstand the temperatures of operation and the maximum temperature of the resistor surface (400°C). Once the appropriate materials have been selected, the pressure response is studied. According to the design requirements, the vessel pressure may vary from 20 kPa to 1.5 MPa for different test conditions. To check the validity of the design, a static analysis is carried out with those pressure loads.

The first step is to discretize the geometry of the continuous medium into points or nodes in order to apply the equations. This process is known as meshing. An unstructured, curvature-centred mesh is used that is capable of replicating the design details. An example of the mesh used for the resistor casing is depicted in Figure 4.7.

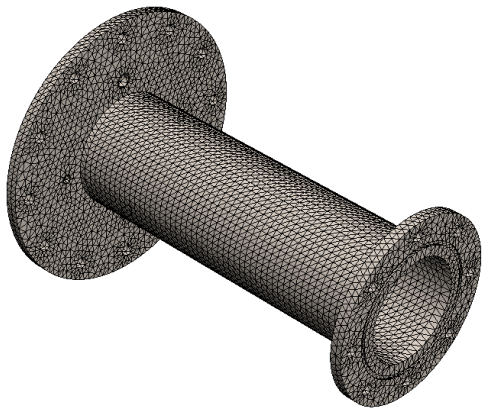

Figure 4.7: Mesh of the casing of the flow heater module.

The calculation process is aimed at obtaining the structural limit of the element, so the Von Mises yield criterion is used to obtain the safety coefficient.

To begin with, the maximum expected stresses in the central piece are found. The Von Mises stress $\sigma_{\mathtt{vm}}$ is defined in Equation 4.2 for principal stresses, where $\sigma_{1,2,3}$ correspond to the principal stresses in the workpiece and are obtained by diagonalizing the stress tensor so that the shear stresses are zero.

$$\sigma_{\mathtt{vm}} = \sqrt{\frac{(\sigma_1 - \sigma_2)^2 + (\sigma_2 - \sigma_3)^2 + (\sigma_3 - \sigma_1)^2}{2}} \tag{4.2}$$

However, in order to make the previously calculated values useful, it is necessary to check that the material can withstand and that the stresses obtained do not exceed the elastic limit of the material, thus producing deformations that could be catastrophic for the design. Therefore, the safety factor is defined as the elastic limit of the material divided by the maximum stress represented in Equation 4.3.

$$n = \frac{\text{Element elastic limit}}{\text{Maximum stress}} = \frac{\sigma_{limit}}{\sigma_{\mathtt{vm}}} \geq 1 \tag{4.3}$$

As is known, there are different safety factors depending on the criterion applied. By applying a very conservative criterion throughout the process to ensure that the objectives are met, the most restrictive model is applied, corresponding to the Tresca criterion (maximum shear stress). Tresca postulates that a structural element fails when the maximum shear stress is greater than half the elastic limit of the material. It is presented in Equation 4.4.

$$\tau_{max} \geq \frac{\sigma_{limit}}{2} \Rightarrow n = \frac{\sigma_{limit}}{2\tau_{max}} \tag{4.4}$$

Test chamber

The test chamber simulation analysis was performed using the assembly model in SolidWorks®. For the simulation, it was excluded the windows and resistor part since it was only tested the viability of the main frame of the vessel. Results depicting the safety factor using the Von Mises criteria is shown in Figure 4.8. It can be appreciated that the weakest points are the corners of the cube, where stresses are concentrated. Moreover, lower SF is found in the screw holes. Noted that the minimum factor of safety value was 1.6, which means that the frame can withstand the desired working pressures.

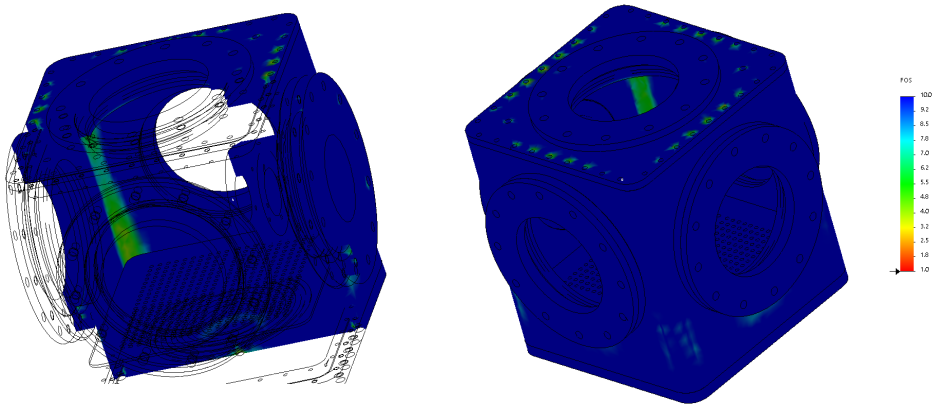

Figure 4.8: Window holder set up (a), and section (b).

Resistor casing

The resistor Casing is analysed for two cases. First, the maximum pressure configuration shown in Figure 4.9, then, the subatmopheric pressure in Figure 4.10.

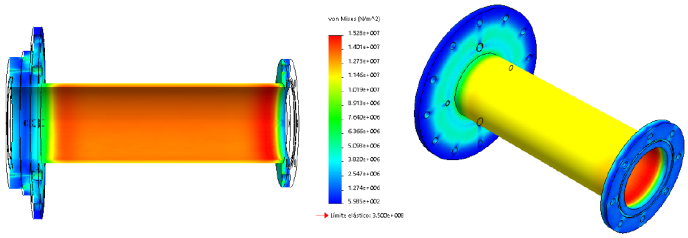

Figure 4.9: Stresses in the body for Von Mises' criteria for 1.5 MPa.

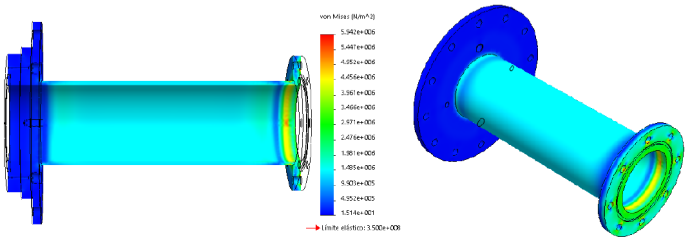

Figure 4.10: Stresses in the body for Von Mises' criteria for 20 kPa.

The Tresca criterium for this cases, gave a segurity factor of 21 for the maximum pressure and 51 for subtamospheric pressure. As expected, the

part behaves worse as external loads increase. The safety factor obtained is of the order of at least 20 times greater than that required to support the design loads. It follows that the choice of a cylindrical geometry is very suitable for supporting the design loads. Likewise, it can be seen that there is a correlation between the stress and the thickness of the same area, producing a greater concentration of stress in the central area of the part due to the smaller thickness of this zone.

4.3.2 Windows integrity analysis

For the windows integrity analysis the geometry is simplified to just the window holder, depicted in figure 4.11. Because of its circular symmetry, the simulation can be reduced to that in the section plane of the center axis.

In this case, the criteria employed is the Mohr Culomb criterium. It applies to materials for which the compressive strength is much higher than the tensile strength, as is the case with ceramic materials. The optical access is built of fuzed quartz, which is a brittle material so its safety factor (SF) is calculated with the Mohr criterium. The calculation of the SF is computed in a similar fashion to the one presented in Equation 4.3. It gave SF of 2.54 as it can be seen in Figure 4.12, when applying a load of 1.5 MPa on the window surface.

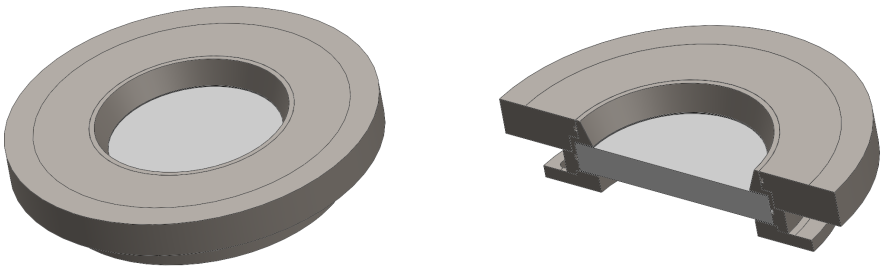

(a) *(b)*

Figure 4.11: Window holder set up (a), and section (b).

4.3.3 Heat module simulation

There were several trials and errors to arrive to the final design. In this section, it is shown the most relevant simulation results that led to the final design of the resistor and its power. The program used for this purpose was ANSYS® FLUENT, which solves RANS (Reynolds Averaged Navier-Stokes) equations with k-ϵ turbulence model. For the simulations, it was set a gas

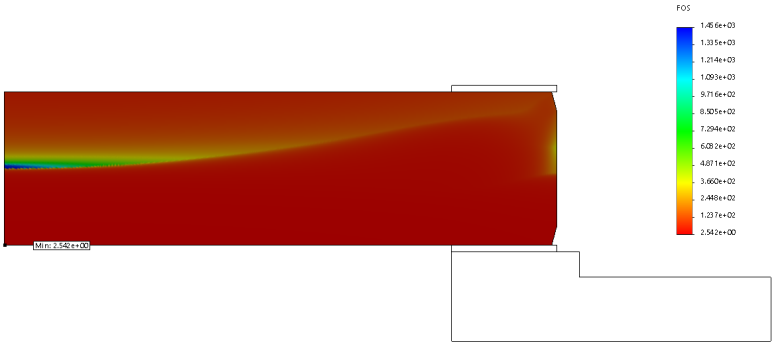

Figure 4.12: Mohr Culomb Safety factor.

inlet velocity of 76 m/s with temperature of 300K. The velocity is selected considering the maximum probable fluid speed as the worst case scenario, since slower velocities would imply higher residence time inside the heater module thus greater temperature increase of the flow. The resistor wall was set with a temperature of 673K. Finally, the outside walls were set at 298K.

Figures 4.13 and 4.14 show the velocity field along a section on the the axis and exit plane of the resistor module. The flow is at maximum speed at the model inlet. After the sudden change of section at the inlet, a flow distributor is set to homogenize the velocity around the cylinder (although the figure only shows some orifices due to the longitudinal section view). Once inside the body, a zone of predominant speed is observed in the central part along the thermal resistance. The marked difference in diameters between the entrance zone and the body produces a notable decrease in speed due to the action of the continuity equation, which favours the appearance of numerous recirculation zones of a marked turbulent character. The recirculation helps the heat exchange process with the flow.

The output section is a representation of what happens inside the body. There is a central zone of greater speed corresponding to the main mass of air passing through the exchanger around the longitudinal resistance cylinder. However, there is also a much smaller portion of air that behaves in a turbulent manner around the spiral zone and the rest of the body, varying the direction and module of its velocity. The average speed in the output plane is approximately 2.2 m/s.

Once the behavior of the air fluid has been understood, its thermal behavior is analyzed. Figure 4.15 and 4.16 show the temperature contours in a longitudinal plane in the exit plane.

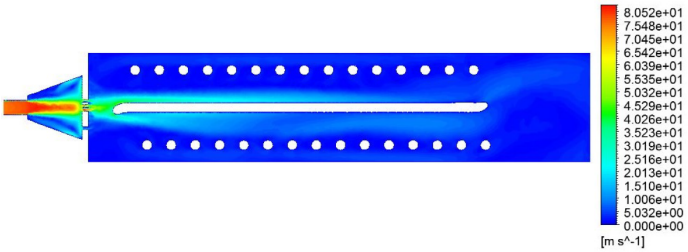

Figure 4.13: Contour Plot of the velocity distribution on the middle section of the resistor module.

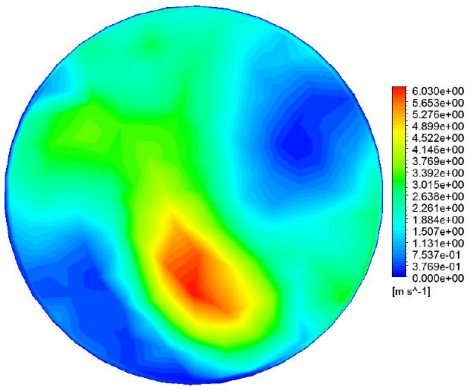

Figure 4.14: Contour Plot of the velocity distribution on the exit plane of the resistor module.

The stationary solution of the problem demonstrates the fulfillment of the design objectives. If the resistance operates at maximum power the fluid is capable of changing its temperature from 298K to 460K. The temperature distribution is directly related to the speed. Thus, in the exit plane there is a higher temperature in the areas with lower speed due to the longer residence time of the gas particles. It should be noted that the stationary solution shows a fairly homogeneous temperature in the control volume. The airflow that does not pass directly (central beam) moves along the entire control volume heating the areas farthest from the exit plane. Finally, the temperature and velocity of the flow is expected to be homogenized even further before reaching the test chamber thanks to the last flow diffusor (shown in Figure 4.5).

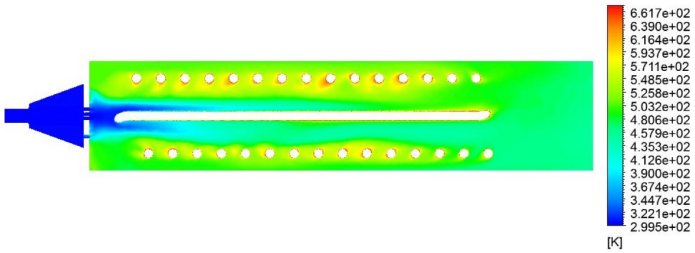

Figure 4.15: Contour Plot of the temperature distribution on the middle section of the resistor module.

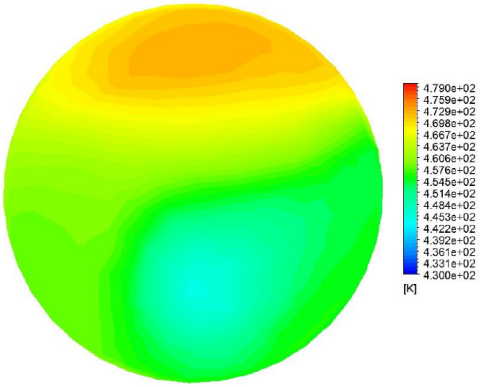

Figure 4.16: Contour Plot of the temperature distribution on the exit plane of the resistor module.

4.4 Tests

Several tests were carried out with the maximum standards of safety. The methodology consisted in slowly increasing a characteristical parameter of the rig such as temperature or pressure and monitoring its proper behavior. Two main tests were executed:

1. First, the pressure and leakage tests were done on the chamber, by increasing slowly the pressure inside and checking for a correct sealing. In this process some parts needed to be welded again because of small cracks that led the gas out. It consisted in numerous trials and errors until the test rig was completely sealed. When maximum pressure was reached, it was monitored successfully that the pressure in the vessel remain unchanged and stabilized.

2. Second, temperature resistance tests were done. To monitor it, several termocouples were installed along the test rig chamber. Two at the top and bottom of the vessel, a third one touching the resistance that closed the control loop with the heater control. Finally, one installed at the air entrance. The power of the resistance was more than enough to provide the required heat to the gas flow. It was observed that it took around 1h to completely homogenize the temperature inside the vessel because the walls and conducts had to be warmed up too.

4.5 Summary

A test rig to study GDI sprays was built successfully. The facility will allow to perform research and experimentation on external fuel sprays at gasoline engine conditions. It is able to simulate stable chamber settings covering early injection strategies which could led to sub-atmospheric conditions. Therefore, it is suitable for the study of flash boiling and spray collapse. In addition, wide optical accesses were arranged to provide a large field of view of the volume of study. The core of the vessel was obtained from an extruded steel beam to reduce cost, which was made, as the rest of the components, of AISI 1042 Carbon Steel. Moreover, a flow heater module was built in order to control the inner chamber temperature, consisting in a resistor, an air diffusor and its casing. It was performed FEA to verify the structural integrity and safe operation of the facility at high pressures as well as the proper heat distribution from the heater module. From the simulations it was concluded that a 2kW resistor was enough to achieve the desired flow temperatures. Finally, several test were executed to ensure that the facility withstand the required conditions safely before any measurements. The final specifications are summarized below:

1. Pressure range between 0.01 to 15 bar absolute.
2. Temperature range between ambient up to 150 °C.
3. Up to 4 optical accesses to perform several measurements simultaneously.
4. Able to perform PDA measurements since it is possible to maintain an angle between 70° and 120°.

Note that final range of operation have been exceeded with respect to the initial ones, which gives place to have a higher working margin. The facility

will remain in the CMT institution to be used by other researchers after the completion of this thesis. Following works will include PDA measurements, close field microscopy and wall impingement studies among others.

References

[1] Guo, Hengjie, Wang, Bo, Li, Yanfei, Xu, Hongming, and Wu, Zhijun. "Characterizing external flashing jet from single-hole GDI injector". In: *International Journal of Heat and Mass Transfer* 121 (2018), pp. 924–932. DOI: 10.1016/j.ijheatmasstransfer.2018.01.042.

[2] Guo, Hengjie, Li, Yanfei, Wang, Bo, Zhang, Huiqiang, and Xu, Hongming. "Numerical investigation on flashing jet behaviors of single-hole GDI injector". In: *International Journal of Heat and Mass Transfer* 130 (2019), pp. 50–59. DOI: 10.1016/j.ijheatmasstransfer.2018.10.088.

[3] Montanaro, Alessandro and Allocca, Luigi. "Flash Boiling Evidences of a Multi-Hole GDI Spray under Engine Conditions by Mie-Scattering Measurements". In: *SAE Technical Paper 2015-01-1945* (2015).

Chapter 5

Characterizing GDI internal and near nozzle flow

5.1 Introduction

This chapter shows the results obtained in internal and near nozzle flow of the injectors employed during this work. Different techniques are applied and combined to acquire a full descriptive behavior of the hardwares. The characterization includes injection rate, rate of momentum, plastic deformation technique and pintle motion. Most of the characterization methods and techniques have been applied first to diesel injectors. As explained in chapter 2, the spray jet in diesel engines is critical for the mixture formation and proper combustion in opposite to gasoline pre-GDI era. For this reason diesel sprays are frequently better understood than gasoline sprays.

The reason of the selected conditions used in the hydraulic characterization is to obtain a representative range of the condition encountered in a running gasoline combustion engine. Nevertheless, they are greatly influenced by the ECN guidelines [1] and variations around its main conditions for the GDI case. The injectors are compared through different tests since they share same technology: both are solenoid activated and have similar specifications as show in table 3.1.

5.2 Rate of injection results

Rate of injection data from the ECN Spray G injector has been analyzed before. First, because it is a research injector which has been produced for different institutions. Thus, it already exists experimental rate of injection data from several researchers [2, 3], although the results could be slightly different from one Spray G to another probably for small manufacture uncertainties (defects). Secondly, because the one available at CMT (injector AV67-026) was studied to evaluate how the typical parameters that are subjected to change in a normal engine operation affect its performance.

On the other hand, the PIU injector has not been analyzed before. Although it has the same injector body technology, the nozzle presents great difference from the ECN injector since it is designed to be side mounted, contrary to the Spray G which is designed to be installed at the top of the cylinder. In addition, the approach of orifices geometry and distribution is completely different.

The ROI results are presented as a comparison between these two injectors, but also, the modeling of the ROI signal of the Spray G through a 0-D approach.

The fuel used for this characterization is isooctane since it is the one used by the ECN and not other fuels were available at that time, contrary to spray visualization. The experimental matrix showing the conditions tested for both injectors is presented in Table 5.1. However, there were extra conditions tested for each injector separately since their experimental campaign were performed in different moments.

Table 5.1: Hydraulic characterization test plan.

Parameter	Value/Type	Units
Fuel	Isooctane	
ET	0.68/1.2	ms
Rail pressure (P_r)	100/200	bar
Back pressure (P_b)	1/3/6/10	bar
Fuel temperature (T_{fuel})	90	°C
Number of repetitions per test	50	

5.2.1 Injectors characterization

Figure 5.1 shows an example of the 50 injections performed for each test condition while measuring ROI. Note that there is little shot to shot deviation,

and that the ensemble average signal of all the measurement represent a ROI signal with high fidelity. This shows good repetitive quality of the injector.

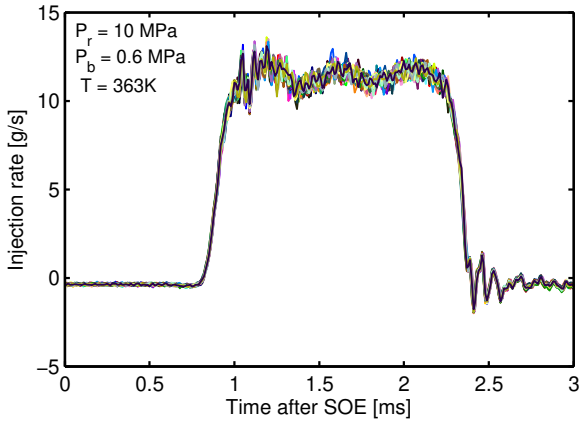

Figure 5.1: Shot to shot variation of Rate Of Injection for PIU injector.

Figure 5.2 depicts the standard condition of the ECN on the PIU and Spray G injectors. It can be noted that both ROI signals have similar level of steady injection rate when the needle if fully lifted. Moreover, the opening slope for the PIU injector is less stepper than the Spray G. This is probably because of the smaller peak current of the commanded electrical signal. On the other hand, closing slopes are similar. The discrepancy in the injection duration is due to different energizing times (ET) for each injector: 1.2ms for Spray G compared to 1.5 ms for PIU.

Figure 5.3 and 5.4 illustrate the effects of typical injection parameters such as rail pressure and discharge/back pressure on ROI. First, the injection pressure effects is well known because of the inheritance of diesel injectors [4]. The theory states that a higher ROI is caused by an increase of the injection pressure mainly because of a rise in flow velocity. From the continuity equation, it can be extracted a proportionality expression that represent the relationship between the two variables, given in Equation 5.1.

$$\dot{m} \propto \sqrt{P_r - P_b} = \sqrt{\Delta P} \tag{5.1}$$

Where P_r and P_b represent the rail pressure and the back pressure respectively. Figure 5.3 depicts the injection rate for several P_r. Note that there is a much broader range of data for the Spray G, however, the effect of P_r is the same. As expected, the increase in injection pressure produces higher

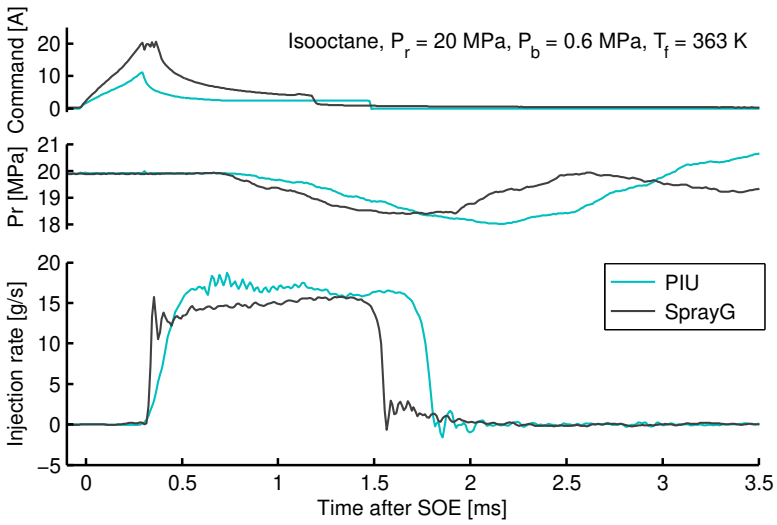

Figure 5.2: Rate of injection comparison for the same conditions except for the Energizing time, being 1.5ms for PIU injector and 1.2 ms for Spray G.

stabilized ROI. Moreover, the start of injection (SOI) does not change with injection pressure, which is not generally the case in diesel injectors [4]. On the contrary, the end of injection (EOI) has a delay depending on the P_r. This is explained by the pressure differences across the nozzle: when the electrical signal stop energizing the coil, the pressure from the rail inside the injector forces the needle to close in addition to the spring used by the needle for this purpose.

Figure 5.4 illustrates the effect of ambient/back pressure in the ROI signal. The effect is not as noticeable since the maximum change in pressure the drop is 0.9 MPa, on the contrary to figure 5.3 where there was higher ΔP. Even though the mass flow lines seemed collapsed, there is some noticeable effects at the opening and closing events. It is observed for higher P_b that the overshoot produced at the end of the opening and closing ramps is damped. This behavior is either cause by needle motion that bounces when arriving to its limits or caused by pressure wave generated by the injection. Measurements of needle lift on the same conditions could provide the answer.

5.2.2 ROI modelling

Modelling rate of injection has been done few times before for a diesel injector, however, it has never been done for GDI injectors. Creating the model

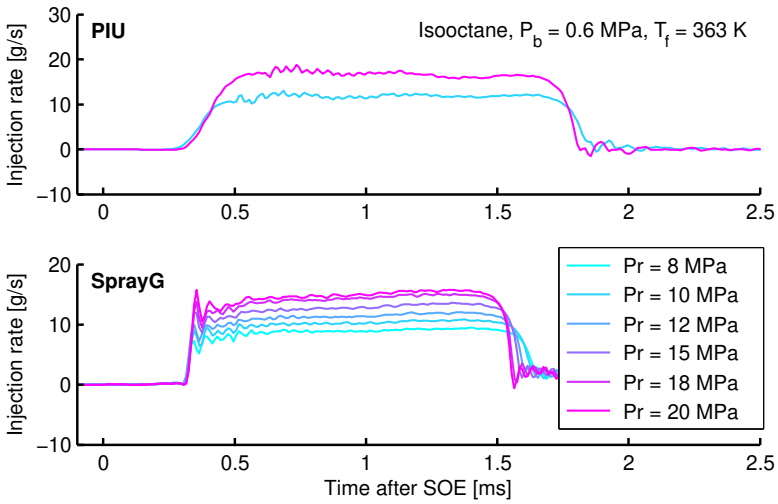

Figure 5.3: Effect of rail pressure on the rate of injection signal. ET employed were 1.2 ms in the Spray G and 1.5 ms in PIU.

allows to go deeply in understanding the parameters influencing the ROI signal. In this section, the Spray G is chosen to be modelled since it is the most widely-used hardware across researchers. The results are presented in order to help engine calibration and modelling for an extensive range of configurations without the need for experimental measurements. The measure of rate of injection (ROI) [5], is achieved from experimental sources with controlled and stabilized boundary conditions. These measurements are of vital importance to validate CFD models, which can provide detailed information of the injection/combustion process as it is reflected in some studies [5–7]. Nonetheless, the number of test points that have to be measured to achieve all the desired engine conditions could be exceptionally large. Other option to get all the desired conditions is through a model of the shape of the injection rate. This will reduce the experimental matrix and supplement with all conditions that have not been measured, providing a full database of the ROI signal.

The 1D modelling includes all the components such as pump, injector and valves, which requires to have detailed information to understand all the process geometries and physical phenomena behind. Conversely, the 0D model is understood as a black box whose outputs are obtained by mathematical expressions without considering detailed knowledge of the systems. Therefore, we will procedure with the 0-D model.

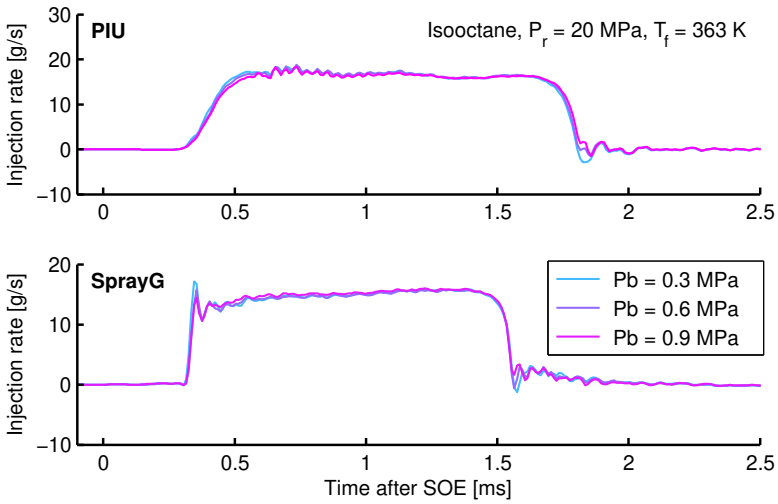

Figure 5.4: Effect of ambient pressure on the rate of injection signal.ET employed were 1.2 ms in the Spray G and 1.5 ms in PIU.

Single injection decomposition

At first, the shape of the ROI signal is analyzed, as explained in the chapter 3. The curve is composed of the average of the 50 measures for each condition. It is easier to start with longer injections since they have the particularity to maintain a similar shape almost independently of the injection condition. Long injections have a trapezoidal shape, whereas short injections have a more triangular-like one. The most accessible manner to address the modelling is by decomposing these forms and relate them with mathematical expressions.

The ROI signal is separated into parametric equations in two parts: the shape function and the logistic function. The shape function is the trapezoidal silhouette which is defined by a compromise of simplest mathematical expression and best accuracy. The functions used to describe it were straight slopes for opening and closing stages and second-order Bezier curves to soften the corners (defined by Cs_x, Cs_y, Ce_x and Ce_y). Lastly, eight parameters that defined the shape are parameterized: start slope, end slope, start of injection (SOI), duration of injection (DOI) and the four control points for the Bezier curves. The Figure 5.5 depicts the eight parameters. For this modelling, the overshoot at the start of the injection is not considered because the added noise to the signal is not good for CFD modelling. Besides, adding this complexity that could be over-amplified by the sensor does not compensate the added complexity in the expressions.

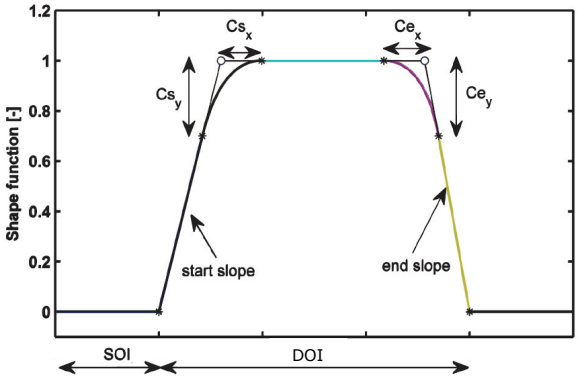

Figure 5.5: Sketch for the shape function decomposition.

As it can be noticed, at the maximum of the signal (full needle lift) there is a slight increment at a certain point of the ROI shape. This is addressed by means of a logistic function. This function represents a step response with smoothed corners. The parameters that define the logistic functions are X0, AX and AY. The first one sets the point where the step starts. Then, AX and AY establish the length and height of the step, as it can be observed in Figure 5.6. The logistic function is depicted in equation (5.2). Then, the equation (5.3) represents the specific logistic function, where $\dot{m}$ is the averaged mass flow rate.

$$L(t) = \frac{AY}{1 + \exp(\frac{-(t-X0)}{AX})} \tag{5.2}$$

$$y = \bar{\dot{m}} \cdot L(t) \tag{5.3}$$

The coefficients of the logistic function are adjusted to the experimental data using linear and non-linear fittings. A non-dimensional curve is obtained for doing further parameterization. The shape function S(t) shown in figure 5.7, is obtained by dividing the real mass flow rate signal by $\dot{m}\cdot$ L(t), resulting in an easier non-dimensional curve for parameterization as it is shown in equation (5.4).

$$S(t) = \frac{\dot{m}(t)}{\bar{\dot{m}} \cdot L(t)} \tag{5.4}$$

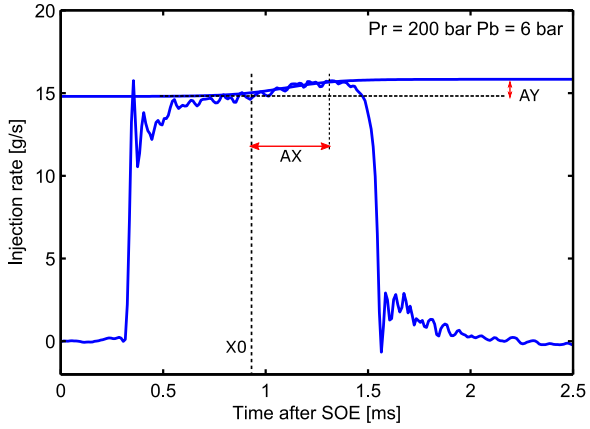

Figure 5.6: Logistic function over the crest of a ROI signal.

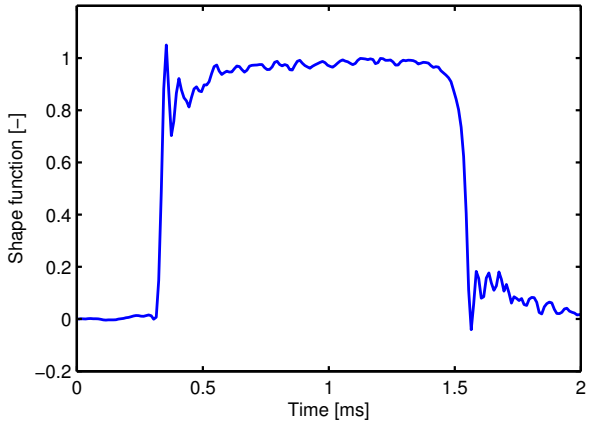

Figure 5.7: Shape function.

Variable dependency construction

All the extracted parameters have to be set as a function of the input parameters, which can be back pressure, rail pressure and energizing time.

First, the stationary mass flow is modelled. The stationary value is reached when the needle is completely lifted, such that the flow velocity is only constrained by the hole geometry. This state is characterized employing Bernoulli and mass conservation equation [8].

Bernoulli's theoretical velocity (u_b) can be represented as a function of the rail pressure (P_r) and back pressure (P_b) shown in equation 5.5. Then, this velocity is included in the expression derived from the mass conservation,

which is the mass flow rate (equation 5.6), where $\dot{m}$ is the mass flow rate, ρ_f is the liquid density, A_0 represents the cross-section area of all orifices and C_d is the discharge coefficient.

$$u_b = \sqrt{\frac{2(Pr - Pb)}{\rho_f}} \tag{5.5}$$

$$\dot{m} = Cd \cdot A_0 \cdot \rho_f \cdot u_b \tag{5.6}$$

Combining these two equations, the mass flow parameterization can be written as a function of the pressure drop, as shown in equation 5.7. A_0, C_d and ρ_f are represented in form of coefficients since they change little or are constant in the range of the injection conditions.

$$\dot{m} = C1 + C2\sqrt{Pr - Pb} \tag{5.7}$$

The coefficients $C1$ and $C2$ are adjusted to the experimental data. This is achieved by linear and non-linear fittings, minimizing the relative error and the statistical number which uses the interval of the normal distribution. The fit of the experimental hydraulic characterization of the nozzle is depicted Figure 5.8. It can be observed that the flow rate, represented in the y-axis, increases linearly with the increase of square root of the pressure drop, represented in the x-axis, which is the expected behaviour of a non-cavitating nozzle.

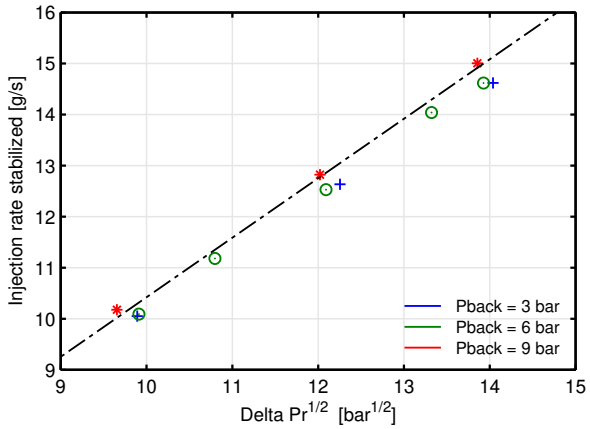

Figure 5.8: Mass flow against square root of pressure drop. Experimental data and fitted curve.

Next, considering the opening and closing slopes, they depend on the velocity of the needle movement. In this case, it has to be noticed that this injector is direct acting type, using a solenoid to create the magnetic field to influence the needle. The movement of the needle is ruled by force equilibrium between the pressure difference, effective area (where the pressure is applied) and magnetic field in one side, and a spring in the other side. Due to the difficulty to measure the magnetic field and spring force (the injector would need to be broken to access those parts), the opening and closing slopes are represented by the pressure difference between rail and back pressures, and the rest of the parameters should be included in the expression by means of fitting coefficients. The acquisition of the equation that represents the slopes is a challenge and, as mentioned before, is achieved by an iterative process of trial and error. Various iterations led to equations (5.8) and (5.9), which were the best polynomial expression that fitted the opening and closing slopes respectively. The comparison of the approximated curves compared to the experimental data can be observed in Figure 5.9 and Figure 5.10. It has to be noticed that in this figures not all the experimental data is presented because it would be hard to visualize. Nevertheless, the equation is adjusted using all the experimental data available. For this two figures, only ET of 1.2 ms and injection pressures of 100 to 200 bar are displayed.

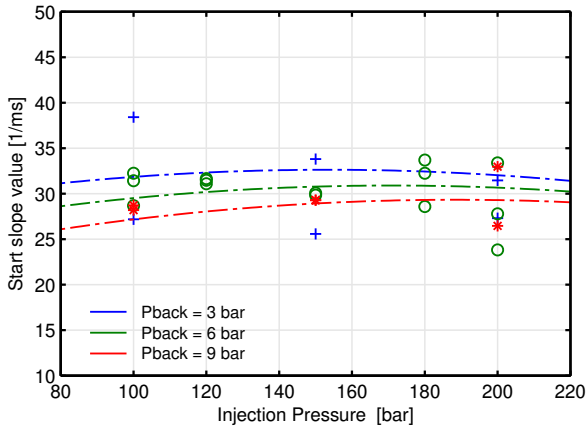

Figure 5.9: Experimental data and curve of opening slopes.

$$O = C_{O_1} + C_{O_2} \cdot Pr + C_{O_3} \cdot \sqrt{Pr} + C_{O_4} \cdot Pb + C_{O_5} \cdot Pr \cdot Pb \tag{5.8}$$

$$C = C_{C_1} + C_{C_2} \cdot Pr + C_{C_3} \cdot \sqrt{Pr} + C_{C_4} \cdot Pb + C_{C_5} \cdot \sqrt{Pb} \tag{5.9}$$

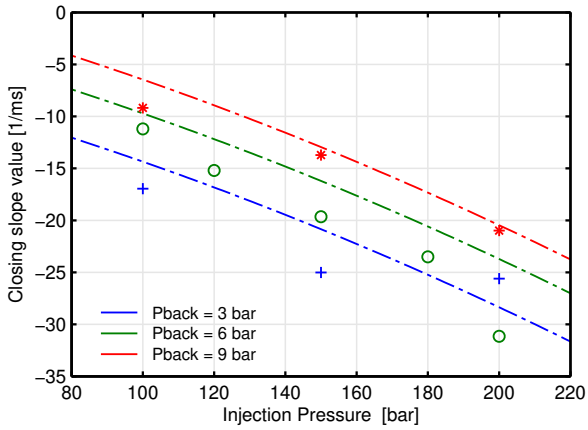

Figure 5.10: Experimental data and curve of closing slopes.

Having set the opening and closing slopes, the next step is to model the Start of Injection (SOI), which is demarcated as the time difference between the commanded signal (electric pulse) and the delay that appears in the injector. The SOI has not effect on the ROI shape, nevertheless, it sets the initial point of the curve, and it is very important for engine testers and combustion modellers. It is necessary for the injection time location in the engine map as well as CFD simulations. The main physical parameters that affects the SOI are the rail pressure and the back pressure whose force components are applied on the needle. It could be considered the flow velocity in the interior of the sac as well. However, this is a function of the pressure, as explained before. Thus, the SOI can be parameterized as it is shown in equation (5.10). Figure 5.11 depicts the correlation for the SOI, in which experimental data using all the ETs and injection pressures of 100 to 200 bar are displayed. Although the tendency is hard to appreciate, it can be observed increased SOI for higher P_b. However, the variation range of SOI value is small.

$$SOI = C_{SOI_1} + C_{SOI_2} \cdot Pr + C_{SOI_3} \cdot Pb \tag{5.10}$$

Finally, the last parameter modelled is the end of injection (EOI). It depends primarily in the electrical pulse, which is the cause for the magnetic field and needle movement. However, it also depends on the inner volume and sac pressure difference and finally on the spring that pushes the needle back when the coil is not energized anymore. Normally, the injection duration is longer than the ET duration because of the inertia of the components.

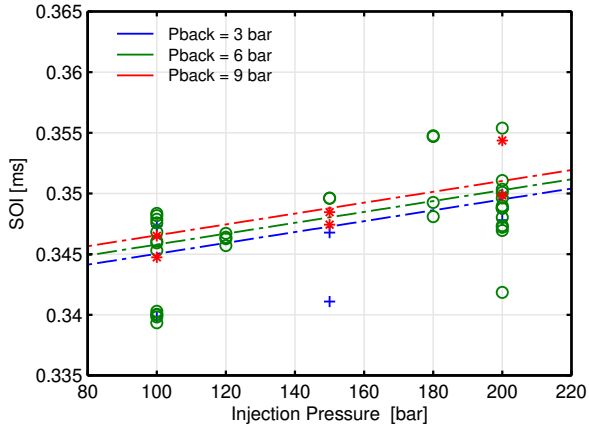

Figure 5.11: Fitted curve and experimental data for the SOI.

To isolate the event, the EOI was modelled establishing the SOI as the origin in time, so the hydraulic delay is not included. The dependent variables were P_b, P_r and End of Energizing (EOE). It can be expected that for small ET, the needle could not be totally lifted so when the electrical pulse ends, the time to return to the closing position is shorter. On the contrary, when the ET is large, the needle reaches its maximum position and when the pulse ends, it will close slower than in the other case. Figure 5.12 depicts this behavior. Internal geometric characteristics impact on the EOI, however they were included in the modelled coefficients in equation 5.11, which is the result of the best fit found.

$$EOI = C_{EOI_1} + C_{EOI_2} \cdot Pb + C_{EOI_3}/Pr + C_{EOI_4} \cdot EOE + C_{EOI_3}/Pr^2 \quad (5.11)$$

All the acquired equations and fittings performed were intended to achieve a coefficient of determination (R^2) close to one. It was obtained at least an R^2 of 0.88, which would confirm that observed data is replicated by the model.

Validation

When the model expressions are acquired with sufficiently low deviation, a final step of validation of the model is performed. Two main comparisons are used as a tool to validate the model. The comparison is made with several experimental measurements including two injection pressure and various ET. The first comparison is shown in both Figure 5.13 and Figure 5.14, in which it

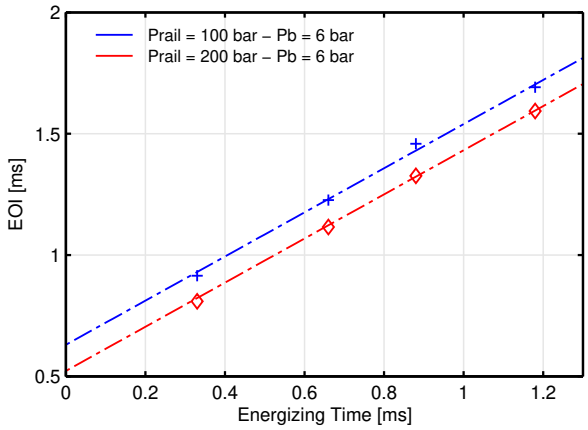

Figure 5.12: Fitted curve and experimental of end of injection.

can be seen both rate of injection signals for the model and the experiments. Injection pressures of 100 bar and 200 bar were selected to be compared since are representative for high and low injection pressures for this kind of injector. It can be observed that the model qualitatively captures the shape of the ROI signal. It can be appreciated that the opening and closing slopes are well reproduced. The SOI is well capture too, however, the EOI is little deviated for P_{rail} of 200 bar and the second shortest ET. Moreover, although there is some deviation in the upper right corner of the trapezoid shape, it does not affect the total mass injected to great extend.

On the other hand, Figure 5.15 depicts the total mass injected (integral of the ROI shape) versus energizing time, both for the model and experimental measurements. It can be seen a good agreement between the model and experimental. The maximum differences found are lower than 8% for reasonable short injections, where the shape of the ROI signal changes and there is not stabilized region (the flow rate is not dominated by the nozzle discharge coefficient [7, 9]).

The measurements performed for a representative range of conditions have resulted in a very well characterized injector. Although the model captures well enough the injector behavior, it has its limitations since the coefficients chosen are not universal. Its implementation outside the measured ranges or injector type should be executed carefully.

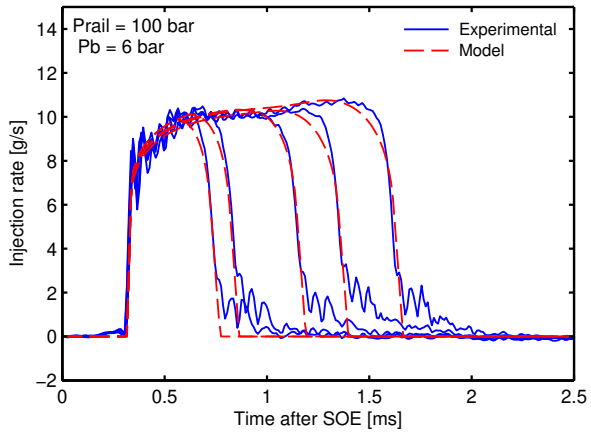

Figure 5.13: Experimental and modelled rate of injection signal for 100 bar.

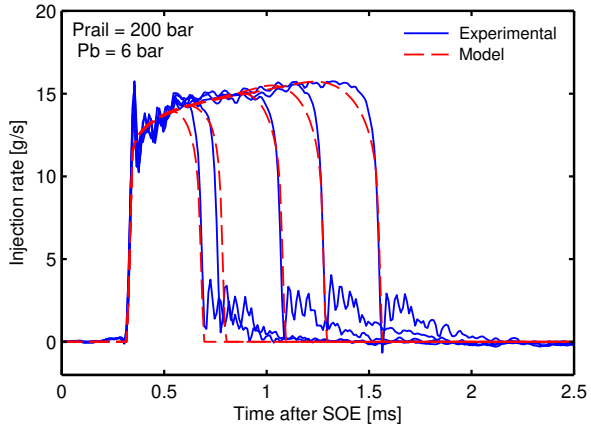

Figure 5.14: Experimental and modelled rate of injection signal for 200 bar.

5.3 Plastic deformation technique results

Introduction

The rate of momentum (ROM) method consists of the spray impinging on a piezoelectric sensor (a technique used before for diesel injectors). However, the spray orientation needs to be known for a correct ROM assessment of the impingement angle of the spray on the sensor. Failure on the impingement angle would result in an incorrect measurement, which could happen for injectors with unconventional spray distributions. Also, in the case that the spray plumes cannot be isolated, all sprays could be measured at once considering

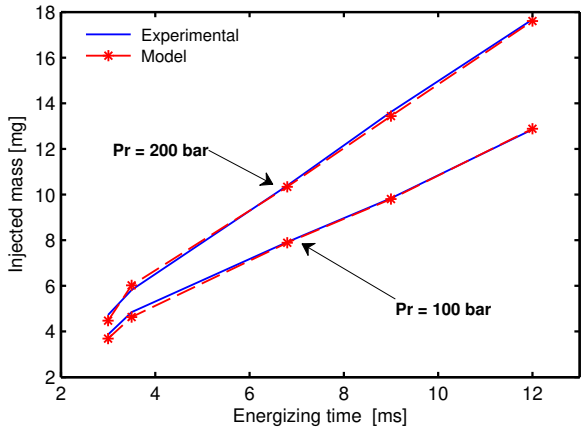

Figure 5.15: Experimental and modelled injected mass for 100 and 200 bar.

a global contribution on the sensor. Therefore, this section presents a new technique developed to obtain spray's jet orientation -which could be different from the manufacturer drill angles- through injections events over a plastic deformation material. Furthermore, a new correction method to compute the theoretical contribution of each plume to the momentum is presented.

As commented in chapter 3, in spray-guided injectors the control of the mixture formation process relies on the spray itself to achieve a correct combustion operation. The technology depends on a suitably designed fuel injector to enable rapid vaporization and mixing of the fuel [10]. There are several phenomena involved such as cavitation, flash boiling, turbulence and, in some cases, complex geometrical designs such as counterbores whose effects compound a difficult spray behavior [8]. Research on gasoline sprays needs to be addressed by combining the development of Computational Fluid Dynamics (CFD) tools (allowing the prediction of the interaction between the airflow field, fuel spray and combustion chamber design), along with experiments that permit to obtain relevant information about the spray characteristics [11, 12]. The measurement of the spray momentum flux is, midst the experimental approaches, the technique that is receiving attention because it permits to quantify a physical value, directly related to the fuel-air mixing potential [13]. The method stands out from others, such as PDA or imaging, since the former is difficult to perform in regions of excessive spray density, whereas the later hardly gives quantitative information about the flow distribution or interactions between the spray plumes. Some researches have performed measurements using X-rays, although it is costly and the access to that equipment is difficult [14]. One problem that arises inheriting the diesel injectors mo-

mentum measurements methodology is that the fuel sprays of GDI injectors are one order of magnitude smaller, which make it difficult for the sensor to achieve such accuracy on the measurements of single sprays. Therefore, Payri et al. [8] compared two configurations for measuring spray momentum, one measuring single sprays and other measuring all together. They reported that only when measuring the whole spray cone they obtained consistent results.

The development of spray-guided systems led to design novel injectors with tilt orifices close together, oriented to the spark plug in the combustion chamber [15]. These injectors regularly have several orifices in order to deliver the right amount of fuel to the system, however this adds complexity to the flow field because of spray interactions. Moreover, this makes it really difficult to study since single jets cannot be isolated. Payri et al. [8] presented a spray momentum methodology to obtain momentum flux for GDI injectors with several orifices and orientations using the well known Spray G injector. Thus, since the Spray G was already characterized, the plastic deformation methodology will be tested using the PIU injector (Denso injector).

Results discussion

The technique was applied to the Denso injector. Measurements from various distances to the deforming material were performed. At the near distance, the global footprint was standing out. However, the footprints of single sprays were too close together to be able to distinguish them. At a farther distance, the sprays' footprint spread out.

Nevertheless, there was not enough momentum of the spray to deform the material. After several attempts, it was concluded that at 14 mm was the optimal length to observe the footprint of the sprays. Five repetitions were performed to ensure replication. The accuracy of the measurements was found to be 2°. Some symmetry was observed in impingement angles for sprays (2, 6) and (3, 5), as illustrated in Figure 5.16. The angles of the spray plumes respect to the axis of the injector calculated by this technique are shown in Table 5.2. They are reasonable values since presents the symmetry observed in the footprint. Finally, the centroid of all sprays was computed, which result in a general tilted angle of 26° from the injector axis.

5.4 Rate of Momentum results

The measurements of the rate of momentum were performed installing the sensor from the bottom of the test rig. Then, the injector was located on the

Table 5.2: Test matrix for the study.

Spray #	Mean Angle (°)	STD
1	9.3	1.5
2	27.1	1.2
3	43.5	0.9
4	29.8	1.3
5	44.9	0.9
6	26.5	0.8
	Tilt angle = 26.7° ± 1°	

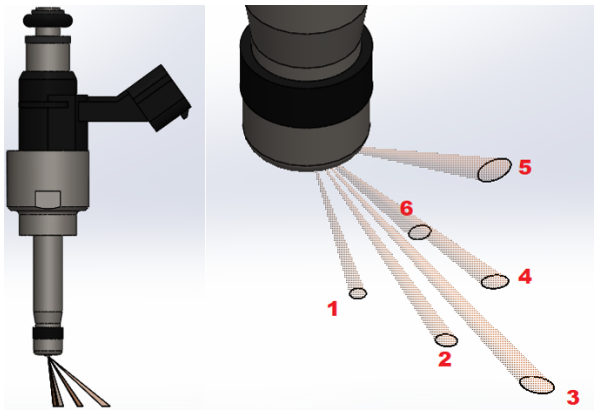

Figure 5.16: Side view of the injector with the spray plumes.

top. For the Spray G injector, the procedure is simpler since the injector axis is aligned with the sensor axis because the centroid of the sprays is the axis of the nozzle [8]. For the PIU injector, the installation is tilted 26°, so the centroid of the sprays is collinear with the axis of the sensor, thus, the individual impingement angles of each spray plume are minimized. As presented in the previous section, it was impossible to isolate one spray because of the wide plume and too close to each other, so they were measured all together. Figure 5.17 shows a render cut plane of the test rig set up for the PIU injector, where it can be noticed the inclination angle of the injector to respect the sensor axis. The injector tip was situated at 4 mm from the target surface, which was a sufficient distance to capture all the spray plumes by the sensor.

It can be observed the difference between the raw momentum measurements and the corrected one in Figure 5.18. Considering the angles of this injector and assuming that all orifices contribute the same amount, the ROM

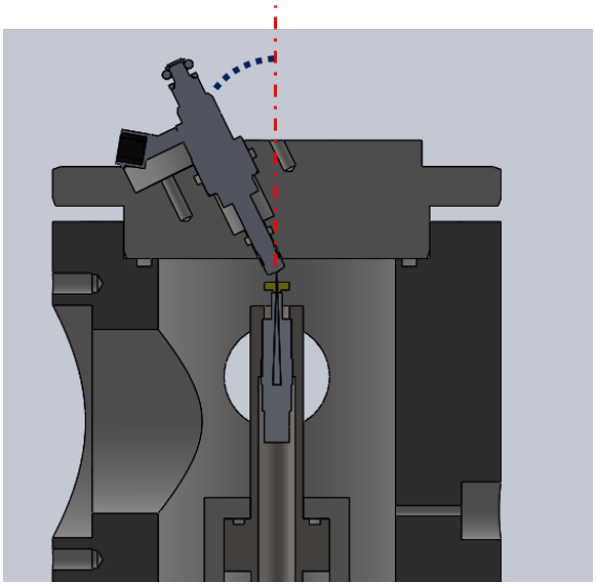

Figure 5.17: Sketch of the relative position of the injector and the sensor inside the ROM test rig.

signal is corrected to an approximately general increase of 3% by applying the Equation 3.18 explained in subsection 3.5.3. The correction is not significant since the angles of impingement are minimized with the inclination of the spray by 26°. The resultant impingement angles are low, being 18° the highest deviation from the axis.

For the Spray G case, the correction equation is applied similarly. However, since the spray cone is centered with the injector axis, the same correction is applied to all plumes. Figures 5.19 and 5.20 report the effect of injection pressure and discharge pressure on the rate of momentum signal. Figure 5.19 depicts the expected tendency. It is shown similar behavior that appeared on rate of injection regarding the opening an closing slopes. However, the overshoot presented in ROI for the Spray G is shown only for the low injector pressures in the ROM signal. Thus, it could be that the overshoot of ROI signal for rail pressures higher than 14 MPa is an artifact made by the sensor. On the other hand, figure 5.20 depicts how the back pressure affects very little the rate of momentum. This effect may be due to the change in density in the discharge volume, which would influence the spray angle and because of some droplets may not be captured by the sensor the momentum decrease very little.

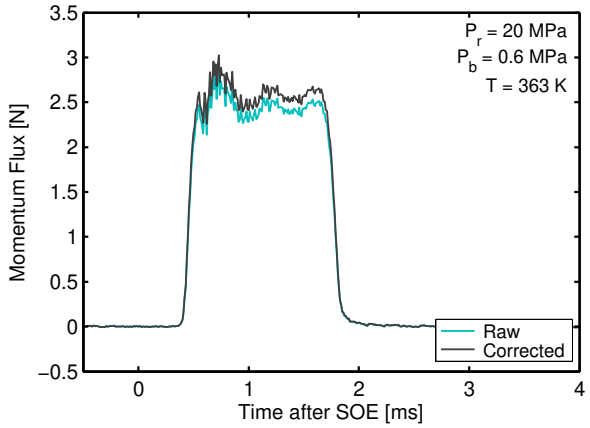

Figure 5.18: Comparison between corrected and non corrected signal. Applying the correction eq. 3.18 on the PIU injector.

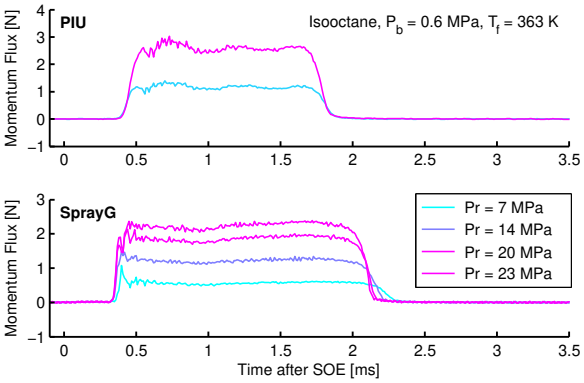

Figure 5.19: Effect of rail pressure on the rate of momentum signal for both injectors.

5.5 Hydraulic Analysis

This section discuss the hydraulic characteristics of both nozzles by means of flow descriptive coefficients. From the previous figures (figures 5.3, 5.19 and 5.20 among others), if time-averages are calculated from the table-top regions of the signal (stationary injection), the complete test matrix could be condensed into a single figure for further analysis.

Figure 5.21 (top) depicts the stabilized mass flow rate as a function of the square root of the pressure difference across the nozzle. Note that the values increase for higher rail pressure, suggesting a linear dependency. Note that for the PIU injector is displayed two injection pressures because of different

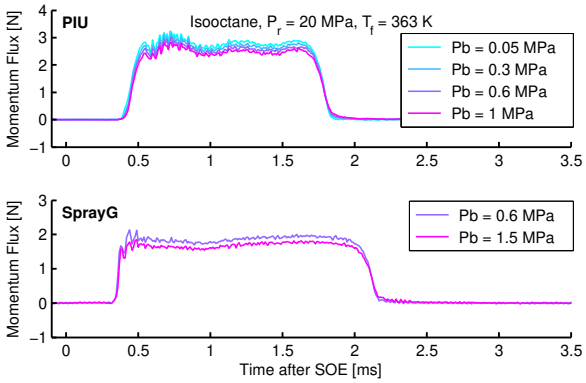

Figure 5.20: Effect of chamber pressure on the rate of momentum signal for both injectors.

experimental campaigns with the Spray G. In each of them, there is a subgroup representing different back pressures which does not affect much on the stabilized value. To make a fair comparison between the two injectors, It is taken into account the orifice diameter difference and number of holes. Using these two parameters a total exit area of both injectors can be calculated, inferring that since the PIU injector has 4.5% higher area it is expected the same increase in stabilized mass flow for the same condition. However, we are not considering internal hole geometries effects that could make the difference even higher. Imagining a line along the spray G points, it could be observed that the PIU injector points lie over that line, which is expected given its higher exit section. Injector characteristics and area calculation are shown in Table 5.3.

Table 5.3: Injectors orifice properties.

	Spray G	PIU	Unit
Orifice diameter	165	195	μm
Orifice area	21382.46	29864.77	μm^2
Orifice #	8	6	-
Total area	171059.72	179188.6	μm^2
Difference	4.53		%

Figure 5.21 (bottom) shows the discharge coefficients. It can be observed that both nozzles have similar C_d values. For the Spray G, the C_d slightly increase with rail pressure, nonetheless, it can be stated that remain fairly constant for the range of pressures studied in both injectors (lot more than

the nominal operational range of the injectors), which indicates the nozzles are in a turbulent regime in the range studied [4].

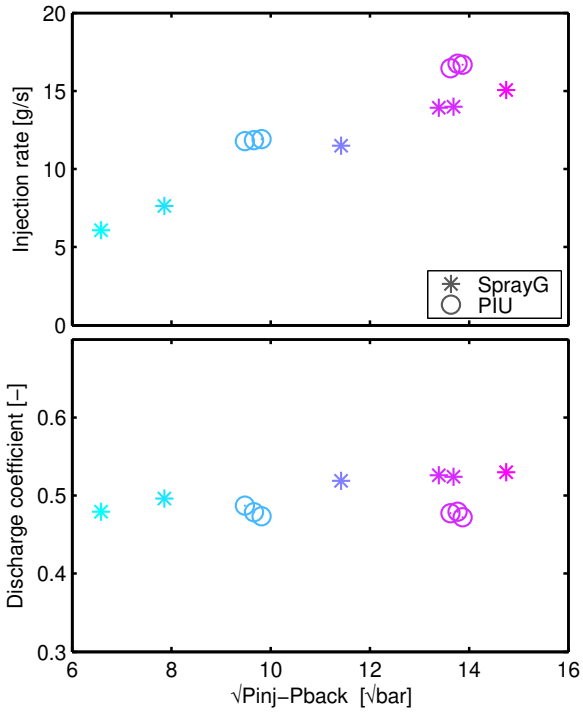

Figure 5.21: Averaged steady rate of injection (top) and discharge coefficient as function of the square root of the pressure difference across the nozzle. Note that different symbols indicate nozzles and colors denote injection pressures.

The spray momentum flux is directly proportional to the pressure drop through the nozzle, as stated in chapter 3. Figure 5.22 represents the steady state momentum flux for different injection and ambient pressures. The data follows approximately a straight line, as expected from the theory for both injectors. Although, each injector line would have a different slope value. The PIU inspector values are slightly higher, as expected.

Then, using both the rate of injection and the rate of momentum measurements, it is possible to compute the effective flow velocity and area coefficient at the outlet orifices of both nozzles [16]. Figure 5.22 (top) depicts the effective velocities (V_e) estimated as a function of the square root of the pressure difference across the nozzle. Note that the V_e increases with the rail pressure. The PIU nozzle has slightly lower V_e, which is probably an effect of higher nozzle orifices. Figure 5.22 (bottom) shows the area coefficients (C_a) where the

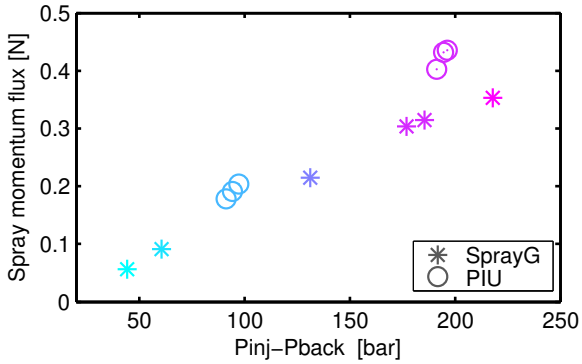

Figure 5.22: Stabilized rate of momentum.

reduction in cross section is probably originated by the great flow detachment in both geometries. The Spray G straight step hole and the PIU conical orifice (growing outwards) generate cavitation or flow detachment to some extent so the effective exit area is reduced. For the PIU injector it can be observed how the C_a increases for higher back pressure. There is not visual trend in the computed range for either of the injectors, however, it can be observed how this reduction is greater for the Spray G.

The observed low values of C_d, V_e and C_a and the unclear tendencies they have with square root of pressure drop contrast with the typical values found for diesel injectors whose tendencies are clearer, and, even with cavitating nozzles, the values are considerably higher [4, 17, 18]. Differences between these injectors and diesel ones are significant. Probably come from different fundamental nozzle geometry designs of state of art GDI injectors as well as from the use of more volatile fuel (isooctane vs diesel), besides using bigger holes and lower operating pressures. The differences have the main objective of increase mixing and turbulence, promote spray break up and improve plume to plume interaction for a convenient flame propagation. The low coefficients reported are probably a result of sharp inner corner of the orifices, low L/D values of the nozzle orifices of the spray G and the diverging-tapered orifices of the PIU nozzle, which causes flow separation and recirculation zones [3, 19–28]. Therefore, the flow phenomena in these GDI injectors are significantly more complicated to understand than in Diesel ones due to intricate geometries of counterbores and inverse conical shapes, external plume interaction, more volatile fuels, etc.

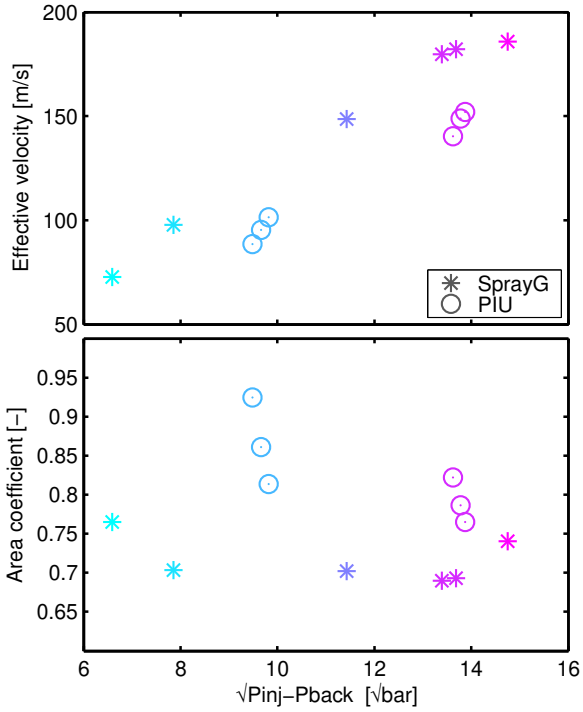

Figure 5.23: Effect of rail pressure on the rate of momentum signal for both injectors.

5.6 Needle lift comparison

The needle lift data was acquired at ANL using phase contrast imaging technique, which was explained in chapter 3. Then, a template matching algorithm was used to track the needle movement while injecting. In order to have the needle wobble, two orientation were tested. Modern GDI injectors are designed with relatively low needle lift to increase turbulence and enhance spray atomization, being around few tenths of micrometers [21, 29, 30].

Figure 5.24 shows the needle lift for both injectors. Note that they have different duration because the ET was 0.68 ms for the Spray G and 1.5 ms for the PIU nozzle. The rail pressure is 200 bar for the spray G, however for the PIU injector it was measured 100, 200 and 280 bar. The color gradient represents different rail pressures, being the darkest color the lowest pressure. It is observed that the lifting slope is steeper for the Spray G, as expected from the ROI results. Regarding the stabilized needle lift, it is observe a value around 70 μm for the PIU injector, whereas the Spray G presents a smaller value of around 50 μm. This values contrast with the nozzle orifice diameters

(approximately 3 times smaller), which may suggest that there is a choked flow by the needle inside the injector [31].

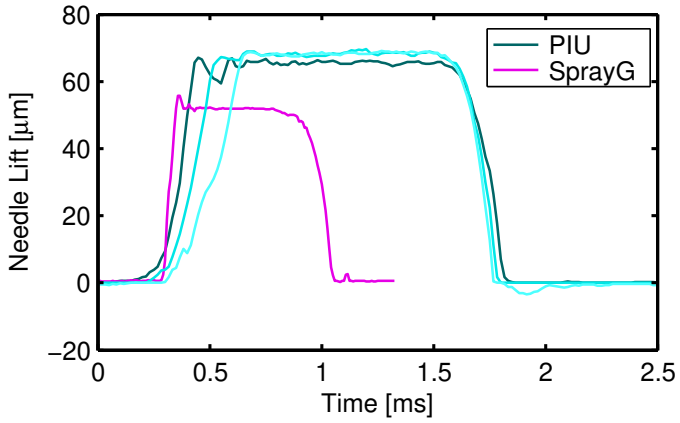

Figure 5.24: Needle lift of both injectors. Note that the ET for Spray G is 0.68 ms while for PIU is 1.5 ms. The figure presents three P_r (100, 200 and 280 bar) for the PIU injector depicted in color degradation being the darkest color for the lowest pressure.

Figure 5.25 depicts the wobble movement at P_r of 200 bar for both injectors. Note that the needle wobble for the PIU injector is almost five times wider than on the Spray G. The reason for this is probably higher needle lift that allows greater flow instabilities and turbulence inside the injector, given that the PIU needle geometry has sharp edges whereas the Spray G one has a rounded head (see Figure 2.16).

5.7 Summary and conclusions

In this chapter, a complete hydraulic characterization has been performed for both of the studied injectors. The characterization of both hardware help understanding its performance along a vast range of conditions that typically appear on gasoline engines. To this end, time-resolved injection rate, momentum flux and needle movement results were analyzed. Along the path, two tools or techniques were matured.

The first one was the development of a simple 0-D model able to predict the rate of injection signal over a GDI engine operation range of the Spray G injector. It was constructed from a set of experimental data measured at CMT, which provided a well characterized injector. The model was built

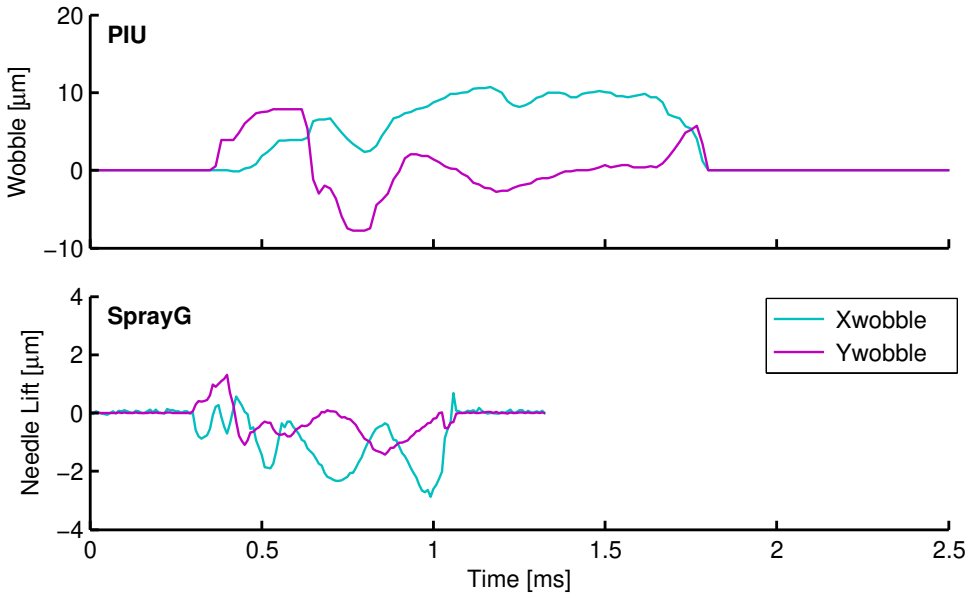

Figure 5.25: Needle wobble in X and Y axis for both injectors. The conditions were P_r of 200 bar, P_b = 3 bar, ET = 1.5 ms for PIU injector, 0.68 for Spray G.

using correlations and complex equations which takes into account ET, mass, duration and rail and chamber pressure as inputs to assemble the final ROI signal. Nevertheless, injection pressure was the parameter that has the most influence in the output signal in terms of total mass and shape. The physical phenomena were considered to help approximating the expressions to what was happening during the injection event. One important limitation of the model is that the simulations outside the measured range should be used carefully, since the empirical coefficients are chosen for the measured range. Another limitation is the use of the model for pilot injections. It was difficult to obtain reliable ROI measurements with low variability, so its modeling was therefore a challenge with a strong non-linear behavior. Finally, the model presented a total mass difference error below 5% in most of the cases, which can be considered good accuracy since is on the range of the natural error of the injector. The 0-D model of the ECN Spray G would be available for spray and combustion simulations, which will streamline the process of understanding the injection phenomena.

The second is a methodology to identify the angle of single sprays in multi-orifices injector nozzles, which is crucial for rate of momentum tests. The technique reported the sprays angles with an error of +-2 degrees, computed

from a spray footprint over a deformable material. The limitations of these techniques are that the distribution of the nozzle orifices must be in a way that is differentiable on the deforming material, and the fuel jets should have enough momentum to deform the body. Other types of sprays should have a deforming material in coherence with the order of magnitude of its momentum.

Thanks to the prior information about the spray angles, it was possible to install the injector for spray momentum at a certain angle, hence the centroid of all the sprays was colinear with the sensor axis. The sprained sprays were very close together one to another, so it was not possible to isolate them for spray momentum measurements; therefore, it was only possible to perform the test measuring all the sprays at once. Then, the measurements were corrected assuming all sprays were contributing the same (which could be supported with CFD) and using each angle to obtain the real spray momentum. The applied correction formula is valid for the previous investigation having the same problem. The difference is that it considers the orientation of individual sprays.

Regarding ROI, needle lift and ROM results, while both nozzles showed expected trends of P_r and P_b in the injection rate, the Spray G injector reported stepper opening slope which is probably due to the difference in operating peak current of the solenoid. This behavior appears on the needle lift and to a lesser extent on the rate of momentum signal. Moreover, is was noted a constant $\approx 5\%$ higher stabilized ROI of the PIU injector respect to the Spray G nozzle. For the stabilized momentum, the difference was not constant and higher stabilized momentum was reported in the PIU nozzle for the highest injection pressures. The main reason is probably the additional 4% in the total outlet area of the PIU injector, besides the small effects that could appear due to different nozzle geometries. From the coefficient analysis, it was reported that both nozzles present similar C_d and V_e values, which are very different from diesel nozzles and conditions. Nevertheless, the C_a is more diverse between the injectors indicating a slightly better use of outlet area for the PIU nozzle. Finally, it can be stated that the differences between the injectors are not so pronounced, having the same technology and similar performance, so they can be compared in the following chapter of external flow.

The results and methodologies presented help to obtain a better comprehension of flow structure in this type of injectors whose needle lift is small and the orifices are relatively big and close together combined with low cone angle. Thus, it could be applied to obtain reliable experimental data and to validate simulations in new similar injectors.

References

[1] "Engine Combustion Network". In: *https://ecn.sandia.gov/gasoline-spray-combustion/* (2020).

[2] Payri, Raul, Viera, Juan Pablo, Wang, Hua, and Malbec, Louis-Marie. "Velocity field analysis of the high density, high pressure diesel spray". In: *International Journal of Multiphase Flow* 80.24 (2016), pp. 69–78. DOI: 10.1016/j.ijmultiphaseflow.2015.10.012.

[3] Du, Jianguo, Mohan, Balaji, Sim, Jaeheon, Fang, Tiegang, and Roberts, William L. "Experimental and analytical study on liquid and vapor penetration of high-reactivity gasoline using a high-pressure gasoline multi-hole injector". In: *Applied Thermal Engineering* 163.July (2019), p. 114187. DOI: 10.1016/j.applthermaleng.2019.114187.

[4] Gimeno, Jaime. "Desarrollo y aplicación de la medida de flujo de cantidad de movimiento de un chorro Diesel". PhD thesis. E.T.S. Ingenieros Industriales, Universidad Politécnica de Valencia, 2008. DOI: 10.4995/Thesis/10251/8306.

[5] Payri, R., Salvador, F.J., Gimeno, J., and Bracho, G. "A new methodology for correcting the signal cumulative phenomenon on injection rate measurements". In: *Experimental Techniques* 32.1 (2008), pp. 46–49. DOI: 10.1111/j.1747-1567.2007.00188.x.

[6] Bosch, Wilhelm. "The Fuel Rate Indicator: A New Measuring Instrument For Display of the Characteristics of Individual Injection". In: *SAE Technical Paper 660749*. 1966. DOI: 10.4271/660749.

[7] Coppo, Marco and Dongiovanni, Claudio. "Experimental Validation of a Common-Rail Injector Model in the Whole Operation Field". In: *Journal of Engineering for Gas Turbines and Power* 129.2 (2007), p. 596. DOI: 10.1115/1.2432889.

[8] Payri, Raul, Gimeno, Jaime, Marti-Aldaravi, Pedro, and Vaquerizo, Daniel. "Momentum Flux Measurements on an ECN GDi Injector". In: *SAE Technical Paper 2015-01-1893*. 2015. DOI: 10.4271/2015-01-1893.

[9] Chung, N. H., Oh, B. G., and Sunwoo, M. H. "Modelling and injection rate estimation of common-rail injectors for direct-injection diesel engines". In: *Proceedings of the Institution of Mechanical Engineers, Part D: Journal of Automobile Engineering* 222.6 (2008), pp. 1089–1101. DOI: 10.1243/09544070JAUTO647.

[10] Sehr, Andreas et al. “Potential of the Spray-guided Combustion System in Combination with Turbocharging”. In: *SAE Technical Paper Series*. 2010. DOI: 10.4271/2008-01-0139.

[11] Cavicchi, Andrea et al. “Numerical and experimental analysis of the spray momentum flux measuring on a GDI injector”. In: *Fuel* 206 (2017), pp. 614–627. DOI: 10.1016/j.fuel.2017.06.054.

[12] Saha, Kaushik et al. “Modeling of Internal and Near-Nozzle Flow for a Gasoline Direct Injection Fuel Injector”. In: *Journal of Energy Resources Technology* 138.5 (2016). DOI: 10.1115/1.4032979.

[13] Payri, Raul, Ruiz, Santiago, Salvador, Francisco Javier, and Gimeno, Jaime. “On the dependence of spray momentum flux in spray penetration: Momentum flux packets penetration model”. In: *Journal of Mechanical Science and Technology* 21.7 (2007), pp. 1100–1111.

[14] Strek, Piotr et al. “X-Ray Radiography and CFD Studies of the Spray G Injector”. In: *SAE Technical Papers* 2016-April.April (2016). DOI: 10.4271/2016-01-0858.

[15] Fansler, Todd D. and Parrish, Scott E. “Spray measurement technology: a review”. In: *Measurement Science and Technology* 26.1 (2015), p. 012002. DOI: 10.1088/0957-0233/26/1/012002.

[16] Payri, Raul, Garcia-Oliver, Jose Maria, Salvador, Francisco Javier, and Gimeno García, Jaime. “Using spray momentum flux measurements to understand the influence of diesel nozzle geometry on spray characteristics”. In: *Fuel* 84.5 (2005), pp. 551–561. DOI: 10.1016/j.fuel.2004.10.009.

[17] Desantes, Jose Maria, Payri, Raul, Salvador, Francisco Javier, and Gimeno, Jaime. “Measurements of Spray Momentum for the Study of Cavitation in Diesel Injection Nozzles”. In: *SAE Technical Paper 2003-01-0703*. Society of Automotive Engineers, Inc., Warrendale, Pennsylvania, USA, 2003. DOI: 10.4271/2003-01-0703.

[18] Viera, Juan Pablo. “Experimental study of the effect of nozzle geometry on the performance of direct-injection diesel sprays for three different fuels”. PhD thesis. 2017.

[19] Shost, Mark A., Lai, Ming-Chia, Befrui, Bizhan, Spiekermann, Peter, and Varble, Daniel L. “GDi Nozzle Parameter Studies Using LES and Spray Imaging Methods”. In: *SAE Technical Papers*. Vol. 1. 2014. DOI: 10.4271/2014-01-1434.

[20] Befrui, Bizhan, Corbinelli, Giovanni, Spiekermann, Peter, Shost, Mark, and Lai, Ming-Chia. "Large Eddy Simulation of GDI Single-Hole Flow and Near-Field Spray". In: *SAE International Journal of Fuels and Lubricants* 5.2 (2012), pp. 2012–01–0392. DOI: 10.4271/2012-01-0392.

[21] Moon, Seoksu et al. "Ultrafast X-ray study of multi-hole GDI injector sprays: Effects of nozzle hole length and number on initial spray formation". In: *Experimental Thermal and Fluid Science* 68 (2015), pp. 68–81. DOI: 10.1016/j.expthermflusci.2015.03.027.

[22] Shahangian, Navid et al. "Spray Orientation Assessment and Correction Method for GDI Momentum Flux Measurements". In: October (2019), pp. 231–241.

[23] Guo, Hengjie, Li, Yanfei, Wang, Bo, Zhang, Huiqiang, and Xu, Hongming. "Numerical investigation on flashing jet behaviors of single-hole GDI injector". In: *International Journal of Heat and Mass Transfer* 130 (2019), pp. 50–59. DOI: 10.1016/j.ijheatmasstransfer.2018.10.088.

[24] Cavicchi, Andrea, Postrioti, Lucio, and Scarponi, Edoardo. "Hydraulic analysis of a GDI injector operation with close multi-injection strategies". In: *Fuel* 235.July 2017 (2019), pp. 1114–1122. DOI: 10.1016/j.fuel.2018.08.089.

[25] Cavicchi, Andrea, Postrioti, Lucio, Berni, Fabio, Fontanesi, Stefano, and Di Gioia, Rita. "Evaluation of hole-specific injection rate based on momentum flux measurement in GDI systems". In: *Fuel* 263.June 2019 (2020). DOI: 10.1016/j.fuel.2019.116657.

[26] Payri, Raul, Hardy, Gilles, Gimeno, Jaime, and Bautista, Abian. "Analysis of counterbore effect in five diesel common rail injectors". In: *Experimental Thermal and Fluid Science* 107 (2019), pp. 69–78. DOI: 10.1016/j.expthermflusci.2019.05.008.

[27] Shahangian, Navid et al. "Transient nozzle flow simulations of gasoline direct fuel injectors". In: *Applied Thermal Engineering* 175.January (2020). DOI: 10.1016/j.applthermaleng.2020.115356.

[28] Moon, Seoksu, Huang, Weidi, and Wang, Jin. "Spray formation mechanism of diverging-tapered-hole GDI injector and its potentials for GDI engine applications". In: *Fuel* 270.March (2020), p. 117519. DOI: 10.1016/j.fuel.2020.117519.

[29] Papoulias, D., Giannadakis, E., Mitroglou, N., Gavaises, M., and Theodorakakos, A. "Cavitation in fuel injection systems for spray-guided direct injection gasoline engines". In: *SAE Technical Papers* 724 (2007), pp. 776–790. DOI: 10.4271/2007-01-1418.

[30] Mitroglou, N., Nouri, J. M., Yan, Y., Gavaises, M., and Arcoumanis, C. "Spray structure generated by multi-hole injectors for gasoline direct-injection engines". In: *SAE Technical Papers* 724 (2007), pp. 776–790. DOI: 10.4271/2007-01-1417.

[31] Vaquerizo, Daniel. "Study on Advanced Spray-Guided Gasoline Direct Injection Systems". PhD thesis. Universitat Politècnica de València, 2017.

Chapter 6

Characterizing GDI external flow

6.1 Introduction

This chapter is divided into two section and covers results related to external flow visualization. The first section consists of an experimental campaign in which visible light optical techniques were used. Four fuels were employed to study the effects of flash boiling and spray collapse during gasoline injection. The fuels chosen were intended to simulate the volatility of gasoline in addition to provide more extreme cases of flash boiling. Moreover, they were chosen to be mono-component to provide an easier starting point for CFD modelers to simulate flashing conditions. The conditions measured were decided from the recommendations of the ECN [1], in addition to playing with the phase diagram in which mild and strong conditions flash boiling points were chosen.

The second section consists of experiments performed at Argonne National Laboratory using tomography x-ray techniques to study gasoline wall impingement for injector spray G. The spray radiography and tomography x-ray techniques have been previously used to study near nozzle flow, however, it has never been employed for near wall spray iteration.

6.2 Spray visualization

6.2.1 Test plan and optical set up

In this section the test plan employed in the experimental campaign is presented. The experiment conditions were selected with the aim to cover different regions of the vapor-liquid phase diagram for the fuels used. However, it was also considered possible chamber conditions the spray could encounter when injecting in gasoline engines operating conditions. The phase diagram of the fuels used as well as the test point studied are depicted in Figure 6.1. The curves of vapor-liquid phase diagram were obtained in NIST website [2] considering the mono-component fuels. The figure presents the vapor pressure curve of the used fuels, as well as the curve for a commercial gasoline fuel RON98 extracted from [3, 4]. The conditions tested are also depicted in Table 6.1.

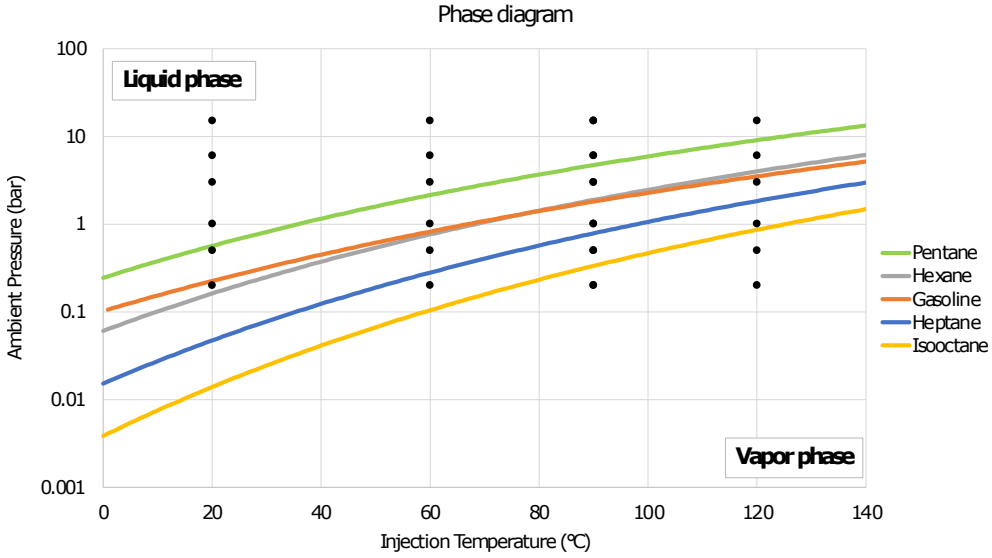

Figure 6.1: Phase Diagram of all the fuels and the experimental conditions represented as points.

Fuels used

Gasoline fuel is composed of many hydrocarbons fuels. The same gasoline composition is often difficult to reproduce in a research environment because of the diverse nature of gasoline fuel. Surrogate fuels are used to study similar

Table 6.1: Test matrix for visualization experiments.

Parameter	Value/Type	Units
Fuels	iso-octane/n-heptane n-hexane/pentane	
ET	0.68/1.2	ms
Rail pressure (P_r)	100/200	bar
Back pressure (P_b)	0.2/0.5/1/3/6/15	bar
Fuel temperature (T_{fuel})	20/60/90/120	°C
Ambient temperature (T_{amb})	20/90	°C
Repetitions per test	10	

behaviors of gasoline while replicating some of the thermo-physical properties. Typical gasoline surrogate has been iso-octane/n-heptane mixtures that aimed to simulate the octane number or, in other words, to control the degree of auto- ignition. However, despite being a good surrogate for combustion, given the ease of controlling the octane rating, it does not represent gasoline volatility conditions. When studying flash boiling, in which the volatility factor is crucial, iso-octane/n-heptane mixtures fail in replicating that behavior.

Mono-component fuels are the easiest fuels to replicate, and in this case, they are carefully chosen to have similar distillation curve of a commercial gasoline. They have been chosen imitate the commercial gasoline fuel volatility and also to provide extreme conditions of fuel volatility. The mono-component surrogates used in this work were isco-octane [5], n-heptane [6], n- hexane [7, 8] n-pentane [8, 9]. The selected fuels were previously used in other GDI studies related to flash-boiling; they maintain similarities with gasoline without complex mixtures that are difficult to replicate. Table 6.2 shows the most relevant properties of each fuel. It was found that the hexane has the closest vapor pressure curve to the commercial gasoline from Huang et al. [3] and Kar et al. [4].

6.2.2 Variations on typical fuel spray parameters

This section presents how the injection conditions affect typical spray descriptors such as penetration and angle. The parameters identify reasonable well the spray performance, however, it is observed that for particular flash boiling conditions when spray collapse occur, these parameters are not capable of describe the spray behavior. The results presented are for iso-octane and the Spray G, whose injection parameters of chamber and nozzle temperature, pressure and densities are selected to represent the general trends, which are

Table 6.2: Fuel properties obtained from the National Institute of Standards and Technology (NIST) [2].

Properties (@300K)	pentane	n-hexane	n-heptane	iso-octane	Units
Liquid density	618.8	652.84	677.81	696.57	kg/m^3
Viscosity	0.214	0.291	0.376	0.456	$mN{\cdot}s/m^2$
Surface tension	15.25	17.73	19.82	20.96	mN/m
Vapor pressure	73.57	22.01	6.72	2.08	kPa
Latent heat	35.1	31.1	36.3	41.4	kJ/mol
Specific heat	2.34	2.26	2.24	2.04	kJ/kg·K

similar for the different fuels. Moreover, similar outcomes were obtained for the PIU injector, although they are not shown.

Fuel Pressure

Figure 6.2a shows the effect of fuel pressure in the spray penetration for iso-octane. It is observed that higher injection pressures is translated into faster penetration, as expected from the literature [10–14]. On the other hand, Figure 6.2b illustrates the effect of P_r on the spray angle. There was not remarkable effect more than a slightly lower angle for the case of 10 MPa.

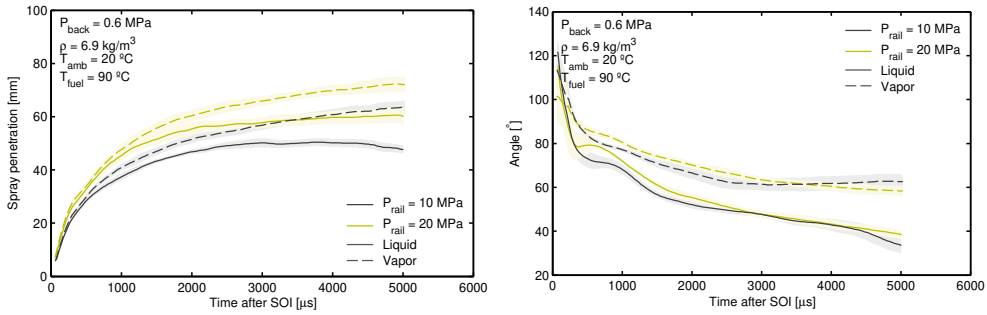

(a) Spray penetration. *(b) Spray angle.*

Figure 6.2: Liquid and vapor penetration and angle of Spray G injector for two injection pressures. Note that the shadow area shows the standard deviation of the measurement.

Chamber density

Various gas-density values are common inside Otto engines, in which the injector needs to supply the right amount and location of fuel for the different

conditions. For diesel injectors the relation between liquid and vapor penetration with density has been thoroughly study and found to be on of the most influential factors on vapor penetration [15, 16]. Figure 6.3 illustrates the effect of ambient density in the spray penetration and angle. It can be observed that higher ambient densities yields a slower penetration because aerodynamic interaction with surrounding gas becomes important. Note that from 1 ms and onward the separation between the liquid and vapor penetration is greater, which coincides approximately with the end of the injection. The effect on the spray angle is depicted in Figure 6.3b. It is observed how for higher densities the angle is increased as expected. It has to be remarked that the difference between liquid and vapor penetration in the angles is slightly higher.

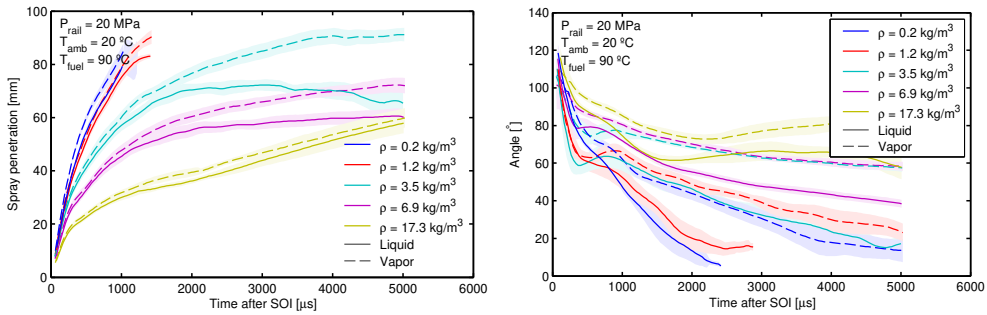

(a) Spray penetration. *(b) Spray angle.*

Figure 6.3: Density effect on liquid and vapor penetration and angle of Spray G injector. Note that the shadow area shows the standard deviation of the measurement.

Fuel and chamber temperature

Figure 6.4 and Figure 6.5 illustrate the effect of fuel and chamber temperature in the penetration and angle. The first one depicts the penetration for two different chamber temperatures. Note that the vapor penetration does not change much, however, the liquid one is affected to a greater extent as seen in Payri et al. [12]. In fact, around t = 3 ms the spray is close to be fully evaporated for the highest chamber temperature. Conversely, the penetration is not affected by the fuel temperature at least in the range presented.

Figure 6.5a and 6.5b depict the angles for two different chamber temperatures. As in the figure 6.4 , the liquid angles are greatly affected by the different discharge temperature. For example, for T_{amb} = 90 °C at t ≈ 1 ms (developed spray) the liquid angles are smaller than the lower temperature

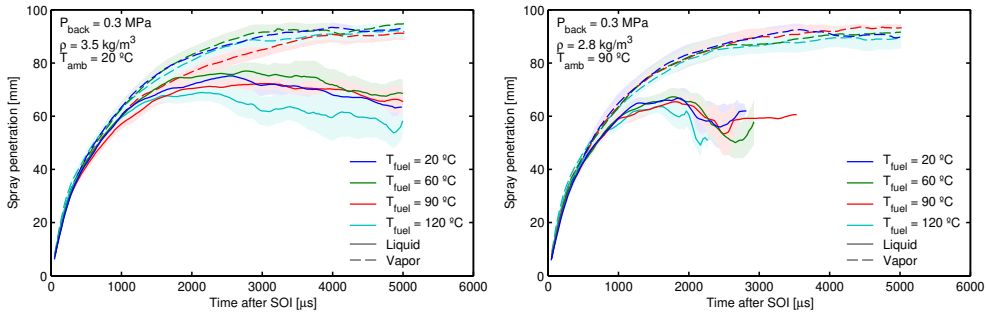

(a) Tamb = 20 ° C. *(b) Tamb = 90 ° C.*

Figure 6.4: Fuel temperature effect on liquid and vapor penetration and angle of Spray G injector. Note that the shadow area shows the standard deviation of the measurement.

case. This result can be attributed to the lower density at higher temperature and increased evaporation rate. As explained before, for lower chamber density the angles are smaller. On the other hand, the vapor angles are not significantly influenced by the chamber temperature. Regarding the fuel temperature, it does not play a major role except for the case of 120°C, which separates from the group because probably the injection condition is close to the vapor pressure line of the fuel, which is translated in a faster evaporation and probably, effects of spray collapse are starting to appear [17–19].

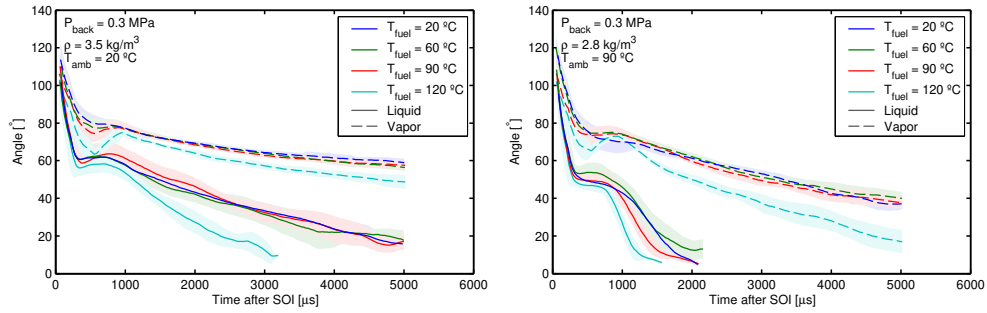

(a) Tamb = 20 ° C. *(b) Tamb = 90 ° C.*

Figure 6.5: Fuel temperature effect on liquid and vapor angle of Spray G injector. Note that the shadow area correspond with the standard deviation of the measurement.

6.2.3 Comparing fuels

This section presents the comparison of the fuels by results of penetration and angles. Figure 6.6 shows the spray penetration for the different fuels employed including two ambient temperatures. Note that in figure 6.6a, all of cases have similar vapor and liquid penetration until t = 2 ms. Upon this point, that the injection has finished, the liquid penetration differs in each fuel due to its density and volatility properties. The pentane and hexane fuels evaporate earlier resulting in a shorter penetration. Similar results are shown in figure 6.6b, however, at this condition, the higher T_f produces even a sooner liquid fuel evaporation. The vapor penetration is slightly lower for the two most volatile fuels, probably due to the smaller momentum transmitted during injection because its lower density.

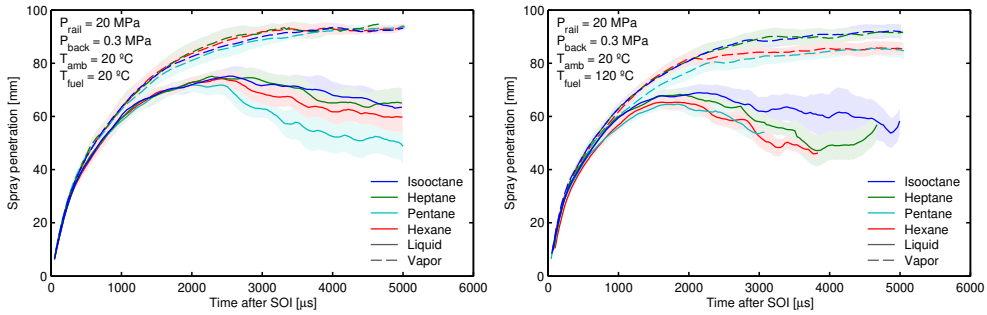

(a) T_f = 20 °C. *(b) T_f = 120 °C.*

Figure 6.6: Liquid and vapor penetration of Spray G injector for different fuels. Note that the shadow area shows the standard deviation of the measurement.

Figure 6.7 reports the spray angles for the different fuels at two representative conditions. On the left it is represented the spray angle for a T_f = 20°C. It can be observed that liquid angles are similar until 1 ms, presenting pentane the lowest angle. On the right, figure 6.7b presents the angles for T_f = 120°C. Between 0.5 and 1 ms, pentane and hexane yield a higher liquid angles. Conversely, the vapor pentane shows a different trend. Thus, the angle may not be representing correctly the spray behavior on these conditions.

6.2.4 Comparing Nozzles

This section presents the differences of the two hardware's used, the Spray G and the PIU injector. Figure 6.8 depicts the penetration of both fuels for two different fuel temperatures. Note that in both figures the Spray G injector has

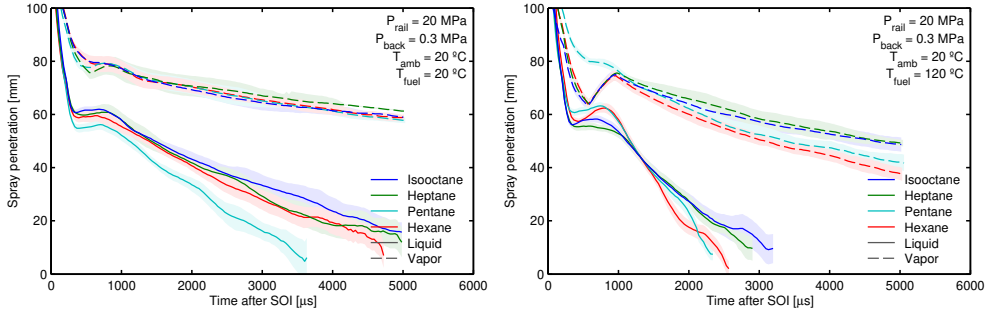

(a) $T_f = 20\,^{\circ}C$. *(b)* $T_f = 120\,^{\circ}C$.

Figure 6.7: Liquid and vapor angle of Spray G injector for different fuels. Note that the shadow area shows the standard deviation of the measurement.

a faster penetration compared to the PIU injector. This is due mostly to the slower needle opening, also shown in the flatter opening slope presented in ROI curves, as seen in chapter 5. Therefore, the full fuel stream takes more time to reach the outside, which is translated into a slower penetration. However, once the injection event has finished (t > 2 ms) the liquid penetration decreases for the Spray G. This is probably due to the difference in distribution and number of holes of the injectors. The Spray G has 8 equally distributed orifices with a wider cone angle, which provides a better solution for air-fuel mixing and evaporation than the PIU injector using 6 orifices (with higher diameter) and a narrower cone angle (see Table 3.1).

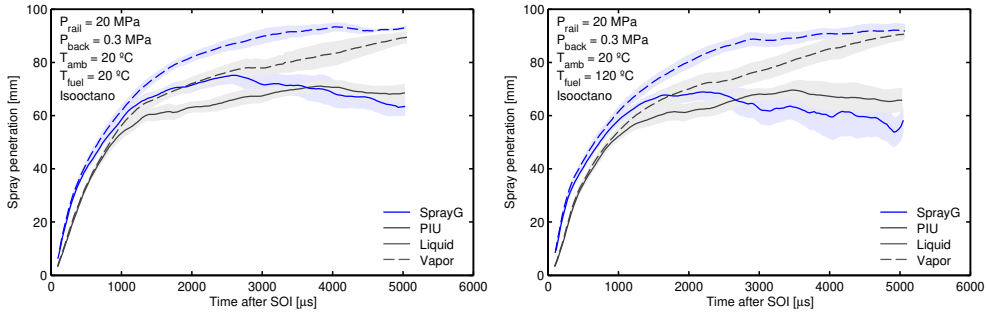

(a) $T_f = 20\,^{\circ}C$. *(b)* $T_f = 120\,^{\circ}C$.

Figure 6.8: Liquid and vapor penetration of Spray G and PIU injector. Note that the shadow area shows the standard deviation of the measurement.

Figure 6.9 illustrates spray angle results for the two nozzles. The PIU injector yield lower spray angles as expected given its narrower geometrical

spray cone. The angle evolution over time is smoother for the PIU injector than for the Spray G injector. This is probably due to higher flow vortices that appear at the spray tip mostly at higher fuel temperatures, which make the spray contour and angle calculation noisier. This phenomena is probably related to the fact that the spray cone is wider on the Spray G injector.

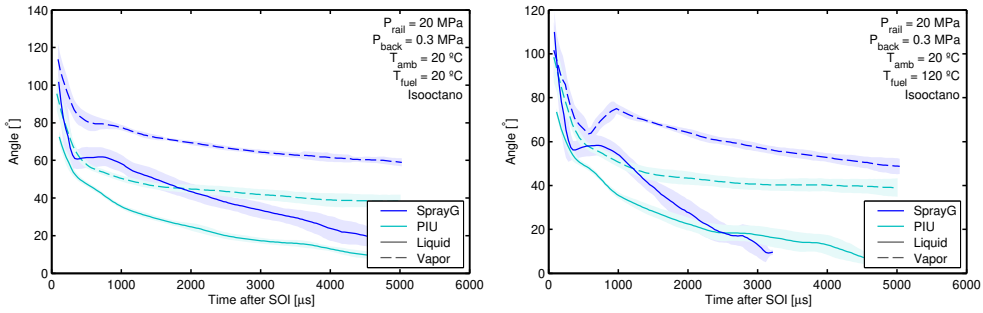

(a) T_f *= 20 °C.* *(b)* T_f *= 120 °C.*

Figure 6.9: Liquid and vapor spray angle of Spray G and PIU injector. Note that the shadow area shows the standard deviation of the measurement.

6.2.5 Jet structure/ spray morphology

Spray cone morphology versus T_f and P_{amb}

The previous analysis of the fuel spray through penetration and angle may have not fully described the flow morphology. At flashing conditions, the spray structure suffers several changes that are difficult to describe only with parameters of penetration and angle, so a deeper analysis of the contour is needed.

Figures 6.10 to 6.13 aim to illustrate a snapshot (at t = 0.5 ms ASOI) to describe qualitatively the spray cone development for different experimental condition. The first two figures correspond to the Spray G and the following ones for the PIU injector. Each sub-figure depicts the spray state at the same given time step. Note that it is embedded in the image the R_p number for each conditions. A R_p>1 indicates that the spray under flash boiling conditions. Note that for some of the highest R_p there is collapse of the sprays. At first glance, it can be observed for the PIU that the spray collapse appears in less extreme conditions than for the Spray G, this is a remarkable difference due mostly to the distribution of the nozzle holes and cone angle. Remember that the PIU injector has a cone angle of $\approx 37°$ in the visualization position and the G spray has a cone angle of $\approx 80°$. The difference in cone size affects the

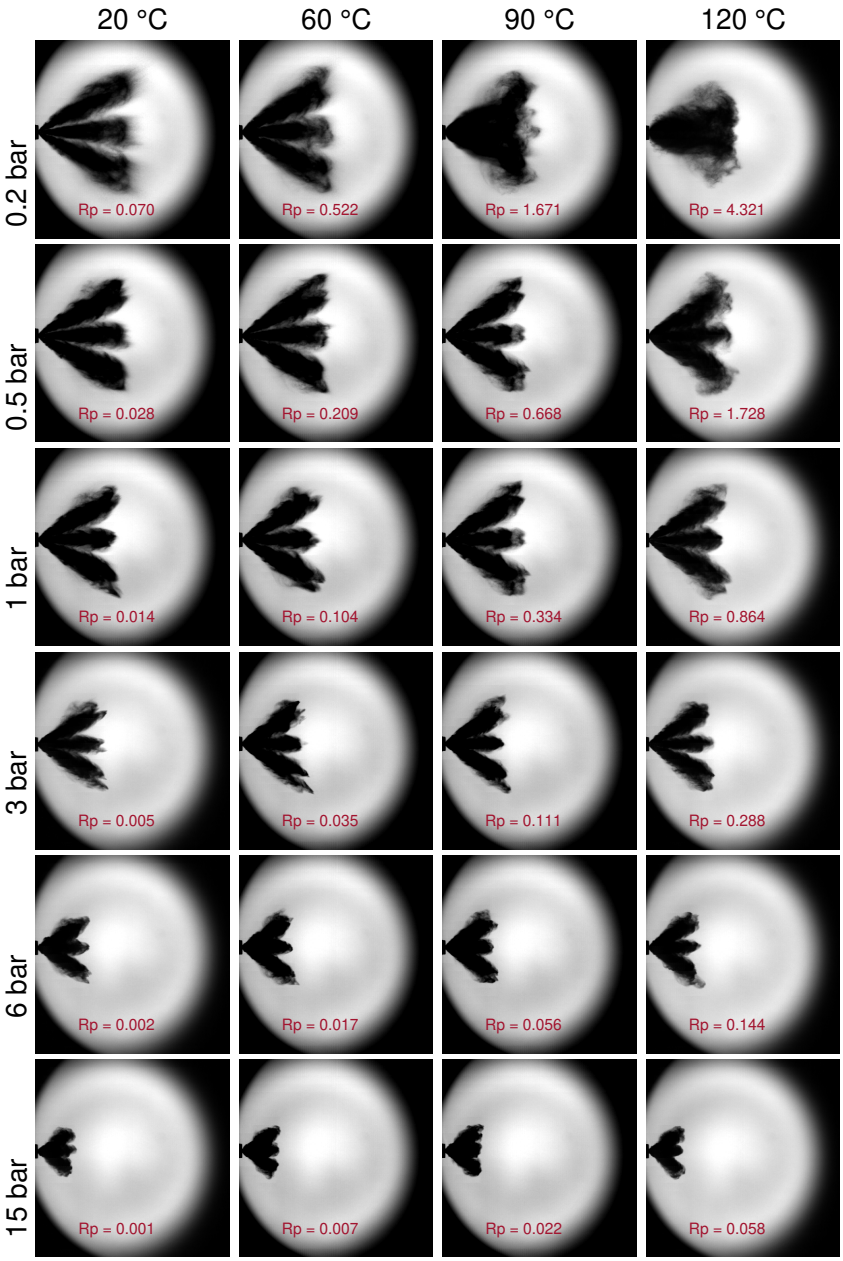

Figure 6.10: Spray cone morphology for iso-octane in Spray G injector at $t = 0.5$ ms ASOI.

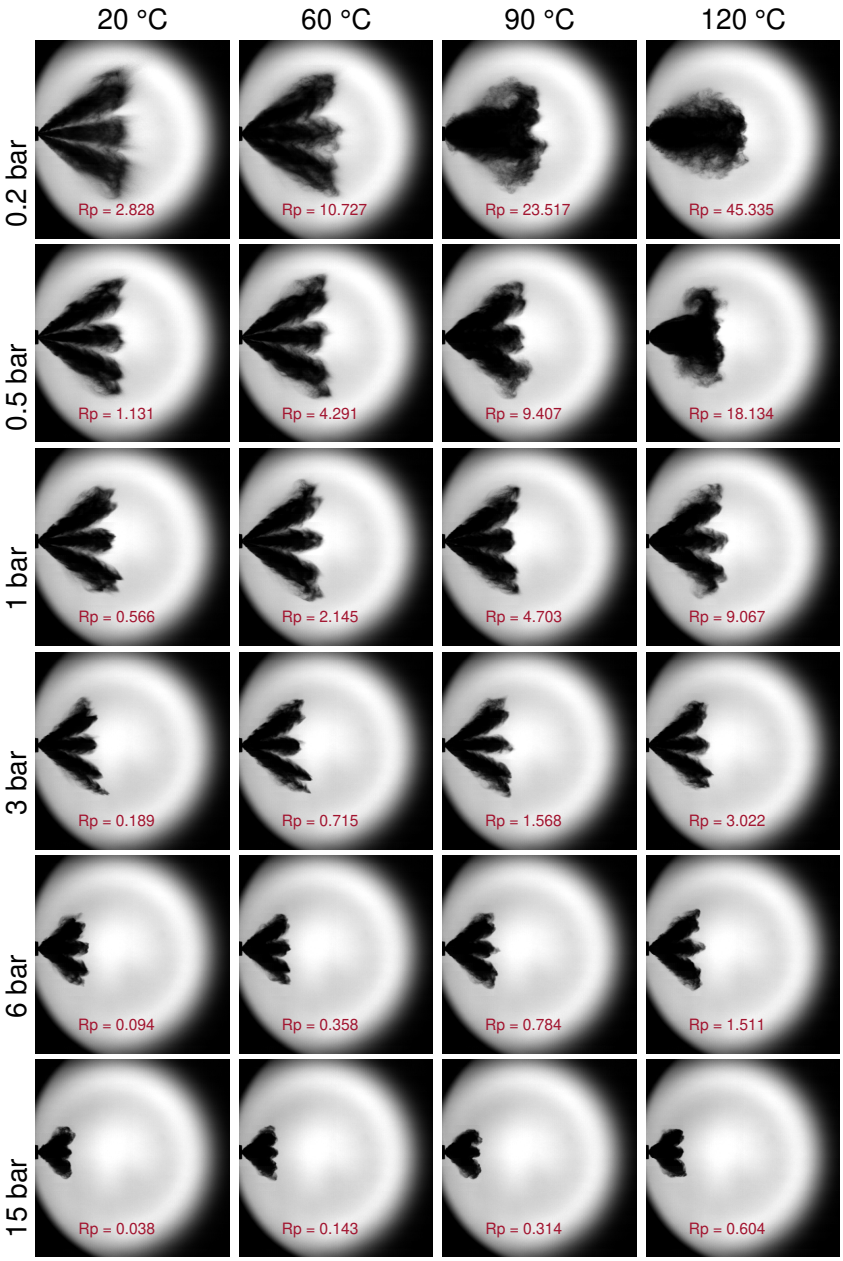

Figure 6.11: Spray cone morphology for pentane in Spray G injector at t = 0.5 ms ASOI.

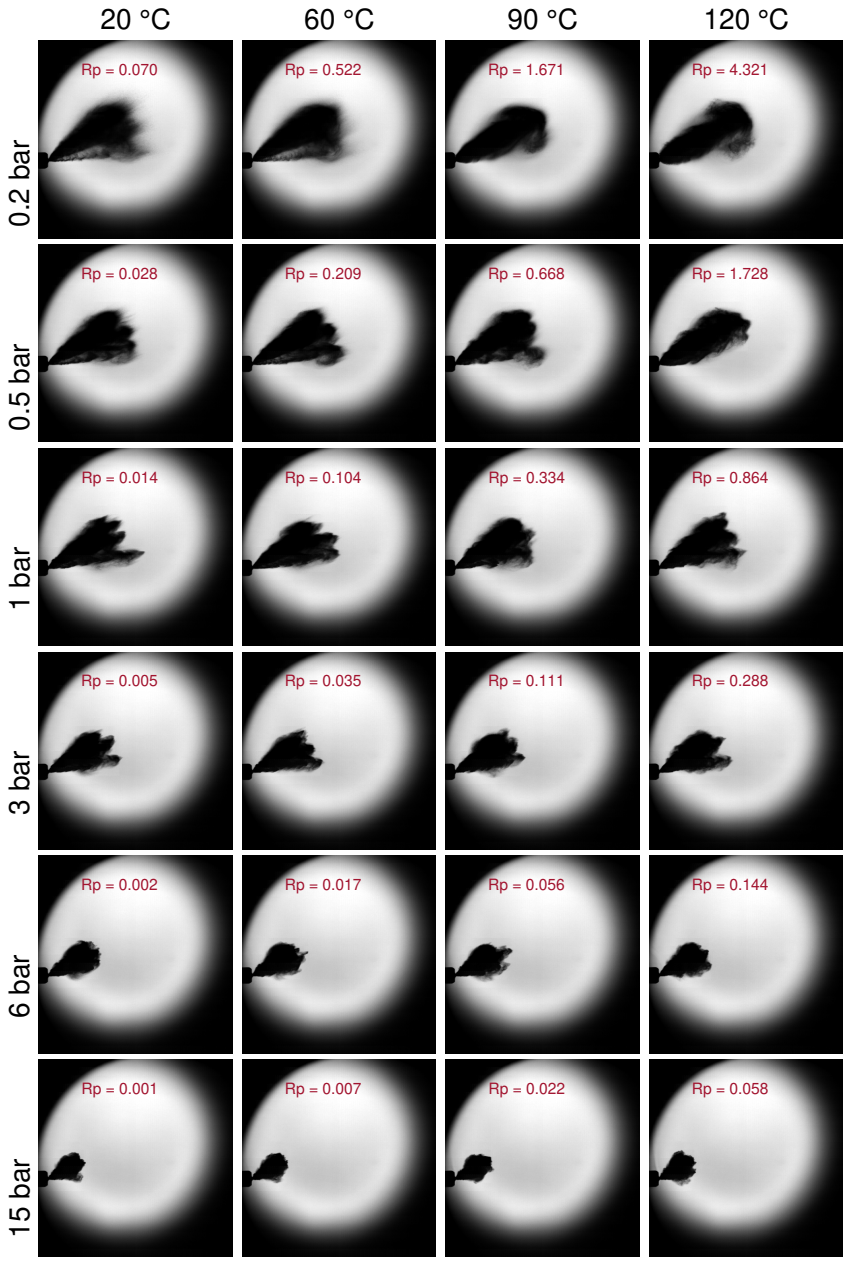

Figure 6.12: Spray cone morphology for iso-octane in PIU injector at t = 0.5 ms ASOI.

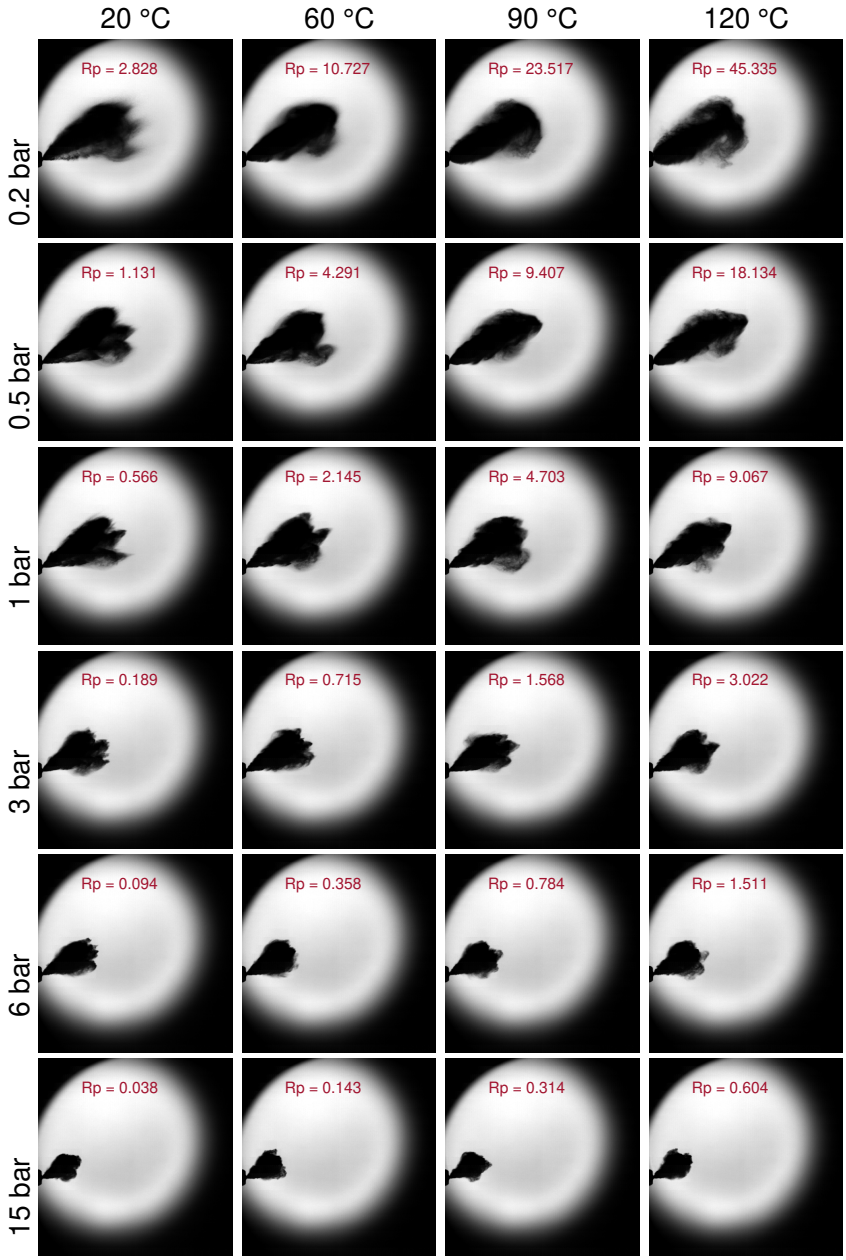

Figure 6.13: Spray cone morphology for pentane in PIU injector at t = 0.5 ms ASOI.

conditions at which the spray collapse occurs. Figures for the remaining fuels are shown in appendix A.1.

Previous works have been trying to characterize the level of flash boiling at each particular injection condition through the R_p number, however, it has been observed that not always describe the spray morphology [20, 21]. Therefore, R_p is an indicative of flash boiling but not spray morphology, e.g. indicate the collapse of the sprays. For example, in Figure 6.10 it is observed that for similar R_p (0.6 and 0.58), the spray morphology is different. This seems to suggest that only R_p can not be considered an indicative of spray structure. Other examples can be found for the other fuels and injector.

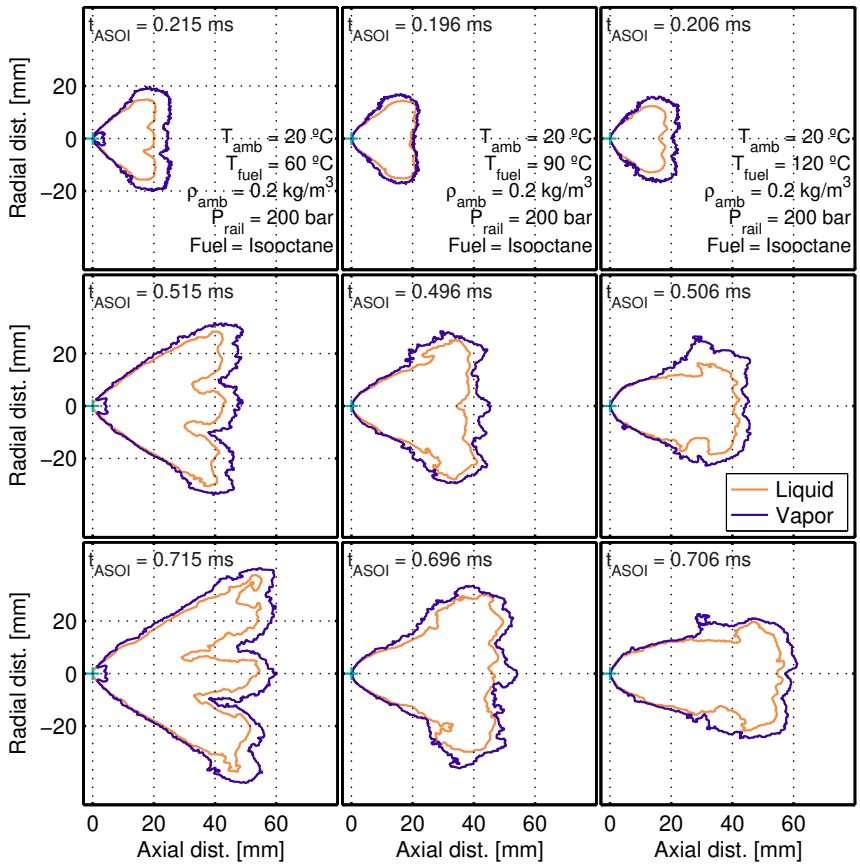

Figure 6.14: Liquid and vapor spray contour of Spray G injector for three fuel temperatures. From left to right the R_p is 0.52, 1.67, 4.32.

An example of different jet structures illustrating the vapor and liquid contour is shown in figure 6.14. It is illustrated the spray contour development

at three different time steps for the most extreme discharge pressure condition (0.2 bar). The fuel temperature varies from 60°C (first column) to 120°C (last column). These three examples illustrated the different structures of spray collapse, in which the first column correspond to non-collapse behavior, the center column shows a transitional collapse. Lastly the third column depicts a fully collapse structure. Note that the difference between liquid and vapor contour are modest since it is not a vaporizing conditions. The last row shows the contour in a rather developed spray, in which the differences in fuel distribution are evident. The collapse and transitional collapse conditions have fuel concentration in the center axis whereas in the non-collapse case the fuel expands in radially. Moreover, while the differences between vapor and liquid in the collapse conditions are small, for the non-collapse it is observed greater differences indicating better evaporation and diffusion of the fuel. Thus, it is clear that the spray collapse is not a desirable phenomena to have.

Spray width

The spray width is a good approach to describe the spray morphology. For a given time step, it captures the instantaneous spray shape for that condition. It is substantially more detailed than providing just a value of angle for the jet, nevertheless, it is more complicated parameter to predict or analyze given that there is a width value for each axial distance.

Figure 6.15 reports the vapor and liquid width of the sprays for different discharge densities for iso-octane. Note that the spray width is decreased notably for the case of 0.2 kg/m^3, which indicates a collapse of the sprays into a single big jet. Moreover, it is observed the different penetration levels at that instant, which was already reported the penetration figures. As seen before, it is observed that for lower density the difference between liquid and vapor are more noticeable, which is an indicative of how the ambient density affects on the evaporation of the fuel.

Figure 6.16 shows the effect of the fuel temperature on the spray width. It can be observed at least three different spray patterns. The first one correspond to the highest fuel temperature (120 °C). At this condition, the R_p is 4.32, so there is a strong flashing conditions that shows clearly a collapse of the sprays. The second patter is found for $T_f = 90$ °C at an R_p of 1.67, which depicts a mild collapse of the sprays. Note that the profile of first axial 20 mm matches the case of 120°C. From that point onward the width increases because of big vortices that appear due to the resistance to the advance of the spray, since the spray cone has not fully collapse [22, 23].

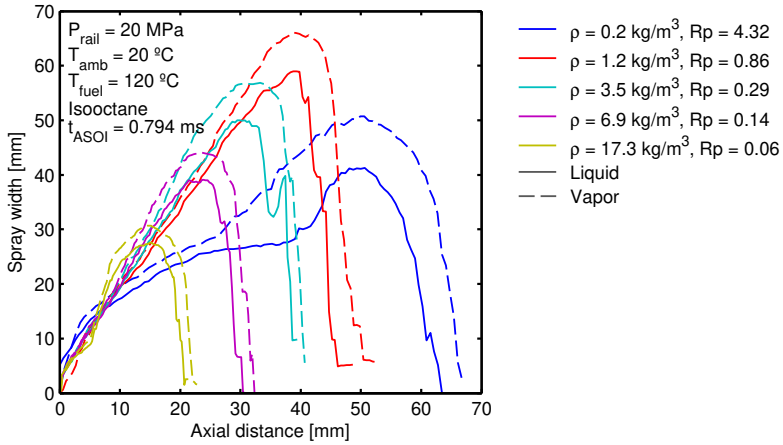

Figure 6.15: Liquid and vapor spray width of Spray G injector for different ambient densities.

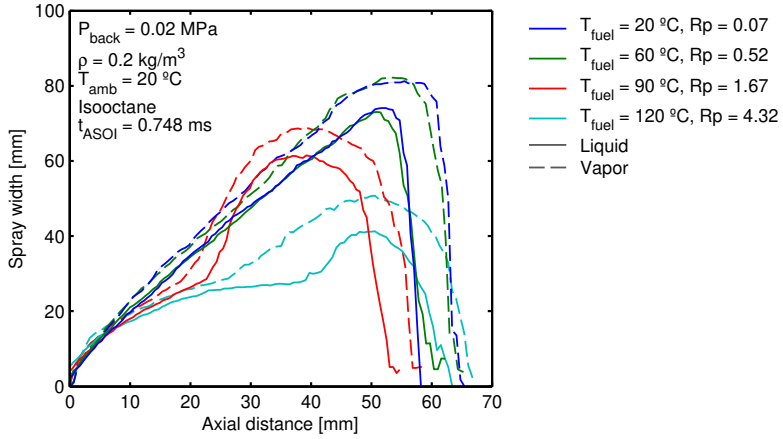

Figure 6.16: Liquid and vapor spray width of Spray G injector for different fuel temperatures.

Figure 6.17 demonstrates the spray width curves for the collapse and non-collapse spray in the first 15mm of spray penetration. From the very first millimeters from the nozzle it can be determined that the flashing condition yields different width curves. Moreover, it is noted that the curves nature is different at flashing condition which could be approximated to a log eq. for the first millimeters whereas for the non-flash boiling is likely to fit on a linear curve.

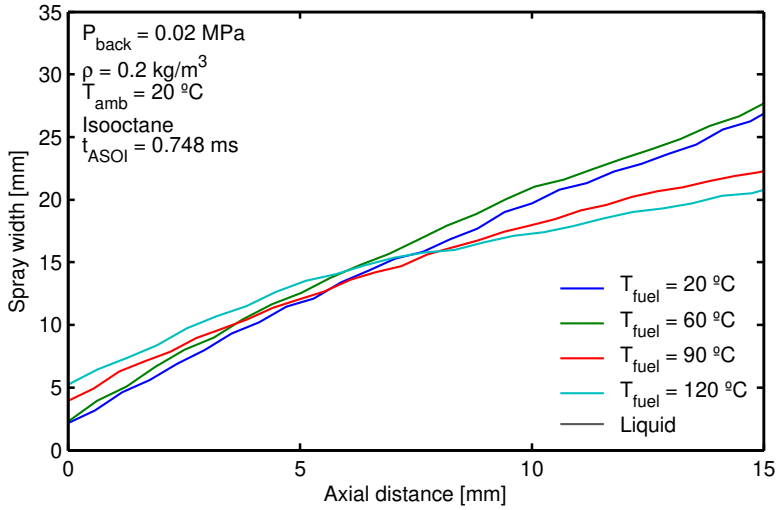

Figure 6.17: Liquid and vapor spray width of Spray G injector for different fuel temperatures.

Figure 6.18 reports the time resolved fixed spray width at 30 mm from the nozzle. It can be noted the differences with T_f, which were explained in the previous figure 6.16. For temperatures of 120 and 90°C the width reports a peak around 400 us which captures the fuel front of the jet, following by a decrease in the case of 90°C or steady level at a much lower value for the case of 120°C. This figure supports the argument of the existence of three spray structures.

Finally, when comparing fuels, it is noted that for a given test condition each fuel would provide different R_p values. Therefore, it could be obtained a more severe flashing conditions for the most volatile fuels. Figure 6.19 depicts a condition in which because of different fuel properties the spray structure changes. In this case, it can be found three assorted spray structures: the iso-octane and n-heptane curves depict non collapse spray structures, however, the hexane and pentane depicts two different spray structures with some level of collapse.

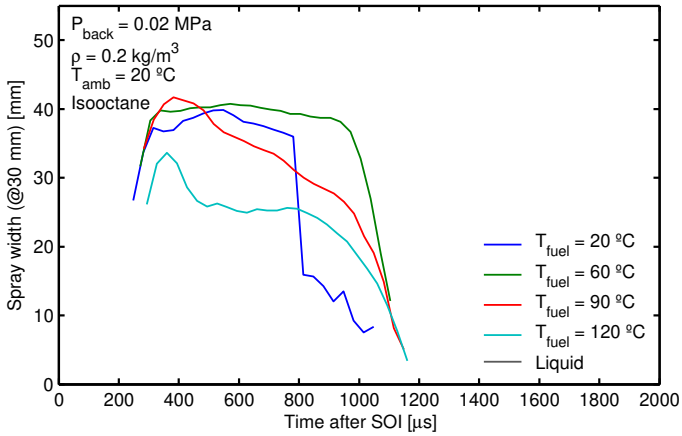

Figure 6.18: Evolution in time of liquid spray width at 30mm of Spray G injector for different fuel temperatures.

6.2.6 Radial expansion of the spray

When the injection takes place close to flashing conditions, it was observed that the width curve close to the injector changed its nature. This section aims to analyze the radial expansion of the spray plumes. Previous studies have analyzed the evolution of the width using R_p [5–7, 9, 20, 21], however, at more extreme flashing regimes there could be different jet width at similar R_p. Therefore this part aims to evaluate not only the R_p, but also search physical parameters to relate each injection condition to the spray cone width. The parameters considered should include dependency to test conditions such as fuel properties, pressures and temperatures.

Figure 6.20 shows the relation between R_p and width, at two axial distances from the nozzle tip based in the orifice diameter (width for 5d and 20d) for the Spray G. It can be observed how the width increases with Rp in general, especially at flashing conditions ($R_p > 1$). The increment is more noticeable for the most volatile fuels, which are hexane and pentane. Note that at highly flashing sprays ($R_p > 4$) the trend is not as clear as for lower R_p. Probably at those high R_p , the mechanism that produce spray collapse are starting to affect the spray width. In one hand the flashing sprays produces a radial expansion of the jets, however, in the other hand, the choke of the air entrainment due to the jet expansion (spray interaction) creates the inner low pressure zone that attracts the sprays [19, 22]. Thus, there are effects that could counteract each other to some extend.

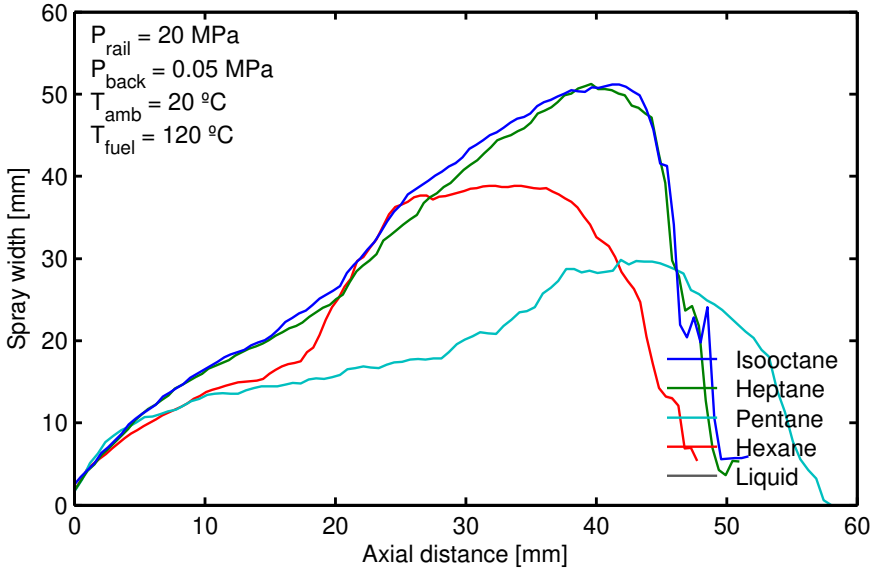

Figure 6.19: Liquid width for the different fuels used.

Other approach that appear in the literature to correlate the jet width with the flashing phenomena is by introducing the nucleation rate. The radial expansion of the spray jet is caused by the mixing of the vapor phase in the two phase flow and limited by the ambient gas. Thus, parameters influencing the vaporization rate and discharge ambient resistance are relevant. As explained in chapter 2, the nucleation rate can be expressed as :

$$J \propto \sqrt{\frac{2\sigma}{\pi m}} exp\left(-\frac{\Delta G^*}{k_B T_{fuel}}\right) \tag{6.1}$$

where m is the molecular weight, ΔG^* is the free energy barrier, σ the surface tension and finally k_B is the Boltzmann constant. Since the start of the vaporization is caused by homogeneous nucleation in the internal flash boiling jet [24], the free energy barrier for homogeneous nucleation could be represented by Eq 6.2 [25].

$$\Delta G^* = \frac{16\pi v_l^2 \sigma^3}{3k_B^2 T_f^2 \ln^2(R_p)} \tag{6.2}$$

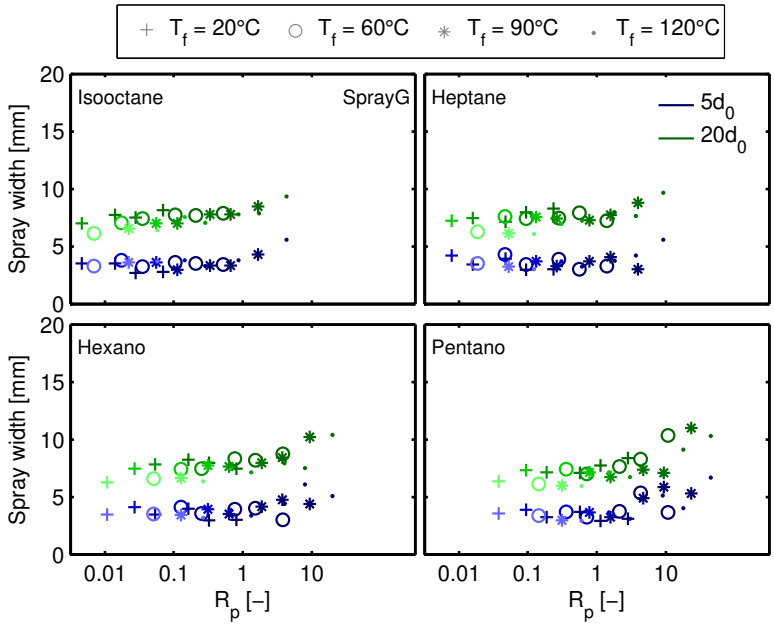

Figure 6.20: Width vs Rp, for all the fuels tested on SprayG injector at t = 0.5 ms ASOI.

where v_l is the specific volume of liquid, which is defined as:

$$v_l = \frac{m}{\rho_l N_A} \tag{6.3}$$

In this work, the range of experimental conditions is mostly influenced by the exponential term of Equation 6.1. Consequently, the exponent, called from now on X presented in Equation 6.4 , is used as an indicator of the nucleation rate.

$$X = \frac{\Delta G^*}{k_B T_{fuel}} \tag{6.4}$$

Figure 6.21 reports the relation between the X parameter and the cone width of the Spray G injector. For a better display, the cone width is plotted against $X^{-0.5}$. Moreover, to account for the drag effects of the discharge density [26, 27], the $X^{-0.5}$ is multiplied by $P_b^{-0.5}$ (chamber pressure). It is observed that there is a general weak relation between the two parameters, at least much weaker than with R_p. Thus, there is not clear relation of the

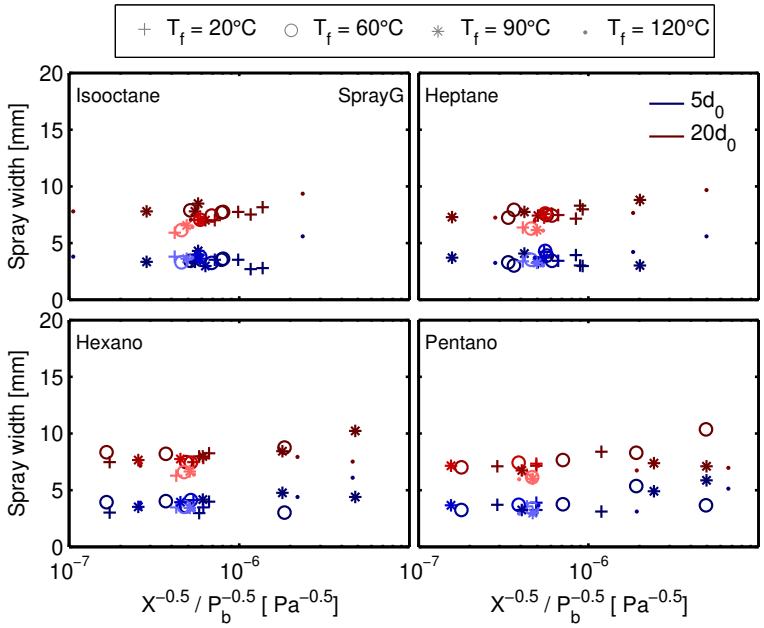

Figure 6.21: Width vs X, for all the fuels tested on SprayG injector at t = 0.5 ms ASOI.

width with the nucleation rate, despite the isooctane which it can be observed certain trend for $20d_0$. However, for the other fuels or diameters the relations are not clear. A possible cause is that the spray expansion is reliant on the flow state at nozzle exit. According to Chang et al. [22] and Park and Lee [28], at the internal flashing regime, there is already a two phase flow developed inside the nozzle. The nucleation processes occurs at the start of the phase transition, therefore, in this case, the nucleation is not as important as the rate of vaporization, which could be the driving phenomena during the observable jet expansion. Moreover, the particular nozzle geometries employed promote air entertainment, which favors the occurrence of two phase flow at the nozzle exit.

Finally, a relation of the rate of vaporization with the spray cone width is presented. It can be done through the phase change chemical potential (Equation 6.5), which is denoted as $\Delta\mu$ as explained in [29].

$$\Delta\mu = \mu_{liquid} - \mu_{gas} \tag{6.5}$$

Assuming that the flash boiling injection event is an iso-thermal process

[30], the Maxwell relation to represent the chemical potential is shown in Equation 6.6.

$$\left(\frac{\delta\mu}{\delta p}\right)_{T,n} = \left(\frac{\delta V}{\delta n}\right)_{T,p} = v \tag{6.6}$$

being v the specific volume. v is defined for ideal gas and liquid phases as shown in Eqs 6.7 and 6.3.

$$v_g = \frac{RT}{P} \tag{6.7}$$

Being R the ideal gas constant and Na the Avogadro number. Then, combining equations it could be obtained an expression for the chemical potential difference, depicted in Equation 6.8.

$$\Delta\mu = RT_{fuel}\ln\left(R_p\right) - \frac{M}{\rho_l}(P_{sat} - P_{amb}) \tag{6.8}$$

Figure 6.22 reports the relation between the chemical potential, $\Delta\mu$, and the width of the spray. The parameter is multiplied by $T_f^{-0.5}$, which it was seem to provide a better visualization and relates to the spray cone width values. It can be observed that in general all fuels follow a similar trend to the one showed with the R_p plots, however, for $\Delta\mu$>1, which is indeed at flashing conditions, it is shown an increment of cone width for all distances except to $60d_0$. According to Vetrano et al. [31], the flash boiling phenomena last at least $20d_0$, thus, for further distances the width may not be complete related to the jet flashing nature, which in the presented case is from $40d_0$. It is likely that from that distance onward other causes like aerodynamics forces due to gas-fuel interaction as well as the onset of spray collapse could play a major role on the spray cone width.

6.2.7 Approaching the spray collapse

Spray collapse by lateral cone angle

The most intuitive way to separate one collapsing conditions to a non-collapsing one is the change in spray morphology, but more specifically the spray con angle. Previous works have study the spray collapse, trying to characterize its spray cone angle [22, 32, 33].

In addition to explain the expansion of the sprays and the jet interaction, that has been probed to be the main collapse trigger mechanisms [19, 22],

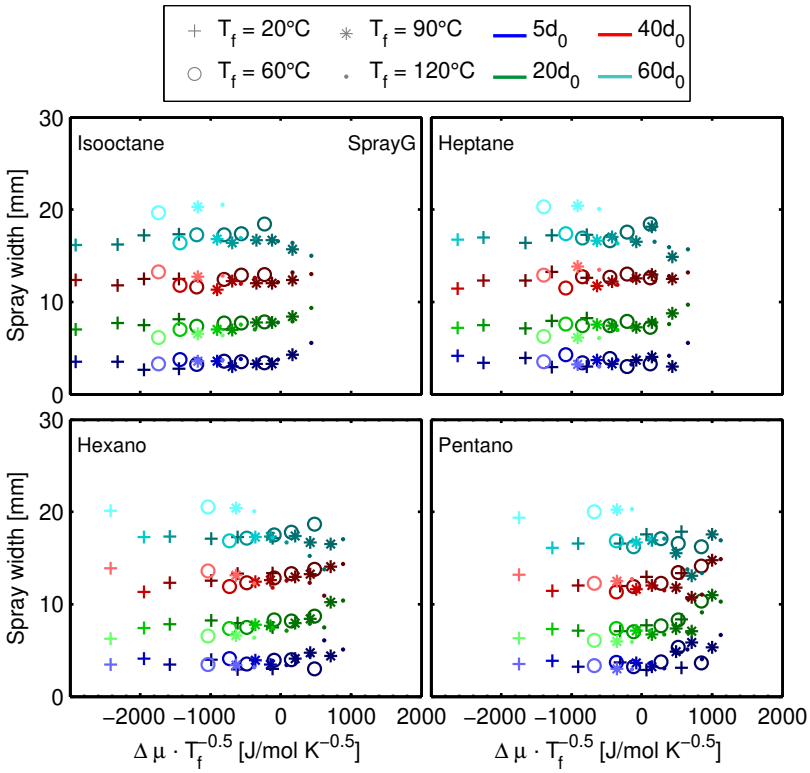

Figure 6.22: Width vs $\Delta\mu$, for all the fuels tested on SprayG injector. For distances relatively close to the nozzle at t = 0.5 ms ASOI.

additional injector geometrical features of the nozzle such as number of orifices or their distribution along the nozzle tip affect greatly to the spray interaction and thus, the conditions at which the spray cone collapses.

In this study two injectors with different cone angle are employed, the Spray G which has a geometrical cone angle of 80° and the PIU injector whose cone angle is 37 °. To be able to compare the injector angles, the spray cone is divided by the geometrical cone angles resulting in a adimensionalized or normalized values. Therefore, as a first step towards the study of the collapse, the angles of each injector over on the developed spray are analyzed. The normalized angles are obtained by averaging the angle values between 0.7 and 1 ms which is when the spray is already developed.

Figure 6.23 reports the normalized angles of each injector against the fuel temperature for each tested fuel. The symbol type indicates the nozzle, and a lighter color represent lower P_b. Note that in general the PIU nozzles presented

higher normalized angle values. The reason is that the change between collapse and non-collapse is less noticeable for this injector than on the Spray G nozzle since its angle is already small. Moreover, the PIU injector shows a higher dispersion in angles as the temperature increase. At the highest temperature tested, it is observed the highest and lowest normalized angle values. This is because at those high fuel temperatures there are extreme flash boiling conditions that induce spray collapse by decreasing the normalized angle as well as flash boiling conditions where the cone angle is increased. For this injector, the spray collapses at around 0.6 Norm.Angle. For the Spray G the behavior is similar, nevertheless the spray is considered to be collapsed at a value of around 0.4 Norm.Angle. It was noted when observing different fuels that the strongest parameter in determining the lowest norm angle is by having the lowest back pressure of 0.2 bar (light color).

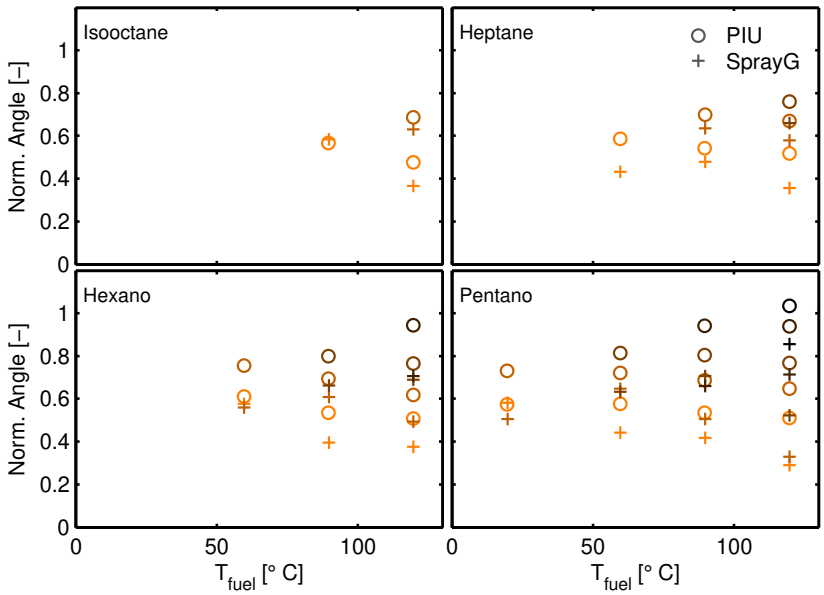

Figure 6.23: Normalized Angles at different fuel temperatures. The symbol indicate the nozzle.Color indicates different P_b (lightest color refers to lowest P_b). Only flashing conditions are plotted (R_p>1).

Figure 6.24 shows the normalized angles of each injector against R_p for each tested fuel. The symbol type indicates the nozzle, and a lighter color represent lower P_b. It is observed that for all fuels there is a trend of decreasing Norm. Angle with R_p. In all fuels but pentane, the tendency is stable for both nozzles. As stated before, it is considered that the sprays are collapsed with

a Norm. Angle of 0.6 for the PIU injector and 0.4 for the Spray G nozzle. It was observed that the collapse took place approximately for R_p>3.5 for the Spray G and R_p>1.5 for the PIU nozzle. This result is coherent with the geometrical characteristic of each injector. The narrower spray cone in the PIU injector produces higher jet interaction which is translated in a collapse with smaller R_p. On the contrary, the Spray G nozzle has its orifices more separated resulting in a retarded spray collapse with R_p.

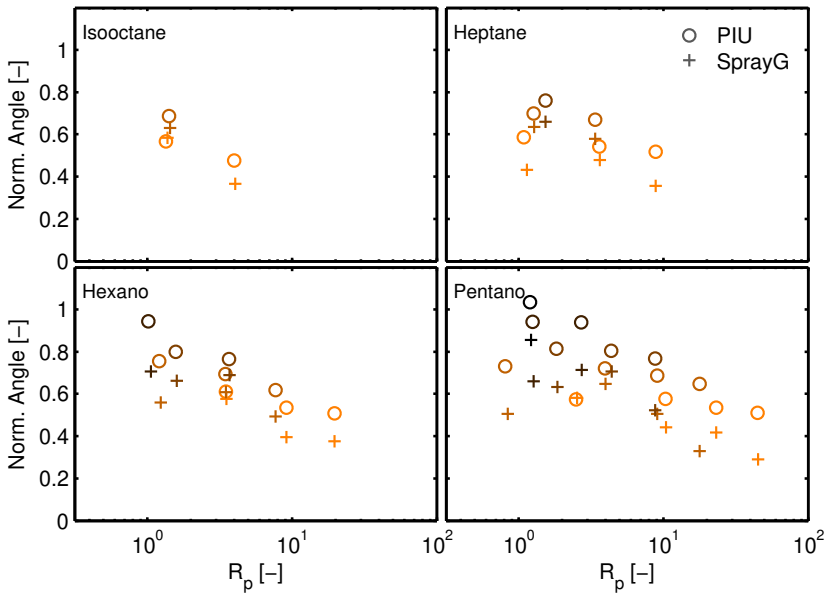

Figure 6.24: Normalized Angles at different R_p. Color indicates different P_b (lightest color refers to lowest P_b).Only flashing conditions are plotted (R_p>1).

MIE analysis, frontal view

One of the visualization experiments carried out was the frontal view through MIE technique of the Spray G injector. This allows to obtain a frontal perspective, identifying individual jets, and it allows to visualize the moment in which the individual jets collapse.

The MIE images have been processed similarly to the DBI method. The method provides information about the liquid phase of the spray, however a careful optical set up has to be made to illuminate homogeneously the whole spray. Because of the tilted spray cone of the PIU injector, and due to the impossibility of the facility to mount the injector at a certain angle, so the

spray cone axis was on on the same line as the camera sensor, the PIU injector was excluded from this analysis. Thus, only the Spray G, whose injector axis match to the spray cone axis, was possible to analyze using this view.

MIE Surface analysis

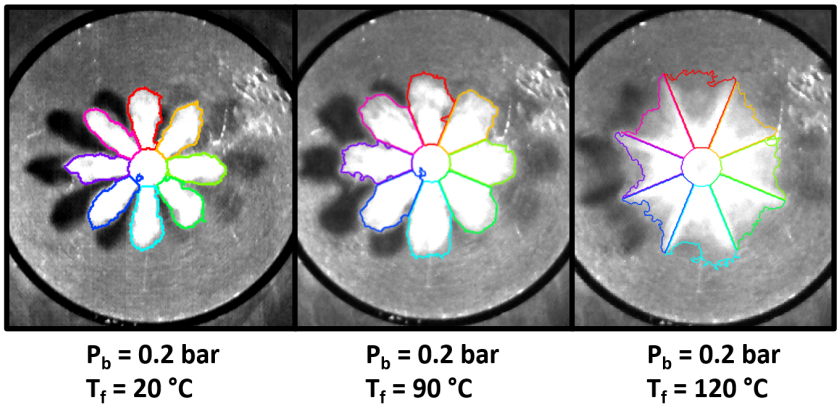

Figure 6.25: MIE images for iso-octane, at a given time step (15), with superposed contour of each spray. Each captures represent diverse sprays structures due to flash boiling. From left to right, it can that at $T_f = 20\,^\circ C$ there is not flash boiling. The center image represent a mild flash boiling at $T_f = 90\,^\circ C$ and the last image depicts strong flash boiling at $T_f = 120\,^\circ C$.

The first analysis performed for this frontal view is the study of the evolution of spray surfaces over time. It is though to be a reveling data for spray collapse diagnostic. The treated frame is sliced into 8 pieces, one for each jet, in which the spray contour is analyzed. The algorithm does not count the nozzle tip, so the contour detection starts from a distance to the center or nozzle axis. Figure 6.25 shows three different test conditions for iso-octane for the same time step. The $P_b = 0.2$ bar, however, as the fuel temperature changes it is shown different flashing conditions. For $T_f = 20$ (left image), the R_p is 0.07 so were are not under flashing conditions. For $T_f = 90$ and 120 (center and right images), the spray is under flashing conditions ($R_p =$ 1.67 and 4.32 respectively) and it is observed how the spray morphology and surface detected changes.

One interesting phenomena that occur during the most extreme flash boiling cases is that the spray cone structure is switched. Due to the great expansion and interaction of the spray plumes, the final fuel distribution is concentrated in the boundaries between two jets. Therefore, the fuel is concentrated in just the areas that for a regular injection there would not be spray. This occurrence appears in the right image of Figure 6.25.

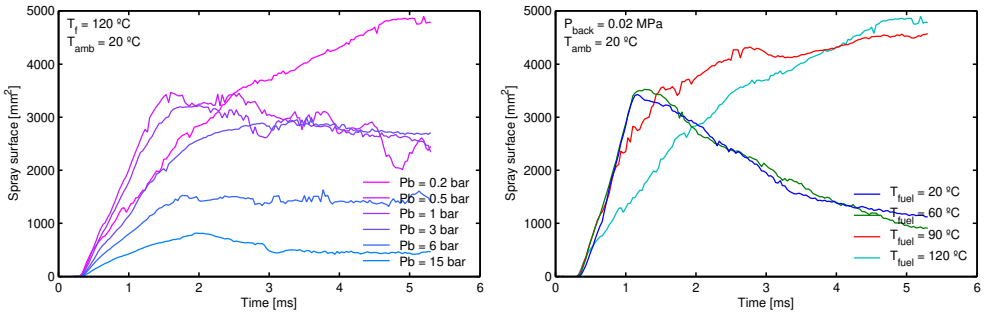

(a) Spray surface for different P_b. *(b) Spray surface for different T_f.*

Figure 6.26: Spray surface against time for iso-octane.

If all the individual jet surfaces are added together for each frame, it could be obtained the evolution of the frontal projection surface over time. The growth or decrease of the surface detected is related to the amount of fuel liquid phase projected on the frontal view. It could also indicate to some extend the amount of fuel that could be evaporated or the advancement of the liquid phase. Figure 6.26 shows the spray surface evolution over time. The left image (6.26a) depicts the surface for various back pressures. Note that as the discharge pressure decreases, the spray surface growth with a greater rate, because it allows for a faster expansion of the sprays. However, when it reaches a point of pb = 0.2 bar, the the tendency changes since it is under flash boiling conditions. The growth rate is different because of fuel evaporation, but also due to spray collapse that concentrate the spray in the injector axis, whereas in the other conditions the fuel is pushed outside the field of view of the camera.

In the other hand, the right image (6.26b) reports the surface for different fuel temperatures at a discharge pressure of 0.2 bar. it is observed two major trend, the non-flash boiling cases, (T_f = 20 and 60) have a steep rise until the EOI at around 1.1 ms. From that point onward the fuel moves out of the image and evaporates so the surface detected decreases. Contrary, for the flashing cases, there are two spray structures. One in which spray collapse occurs from a very beginning (T_f = 120°C),because the concentration of the fuel in the injector axis. The other has a similar spray surface slope to the non-flashing cases however at some point diverges. In this cases, the concentration of the fuel in the injector axis causes that even after injection fuel does not spread and remains in the center axis.

Considering the injection duration, it is selected the surface values in which the spray is under the most stable conditions for the injection duration tested,

which is just before the EOI. Figure 6.27 represents an average surface value calculated between 0.7 and 1.1 ms, so it can be condensed all the test points. The surface values are reported against the R_p for each investigated fuel. A symbol color is assigned for each fuel temperature and each shape represents different P_b. Lower P_b reported higher surface values, which is related to the density and faster penetration of the spray [34]. It can be observed that there is a linear relation of spray surface with R_p for each temperature in all the fuels, however, at extreme flashing conditions $R_p > 3.5$, the surfaces stagnated or decrease. At these R_p values is where the spray collapses and changes morphology. Regarding the effect of the fuel, it is noted that the most volatile fuels have higher R_p values for the same test conditions, shifting the test points to the right [21].

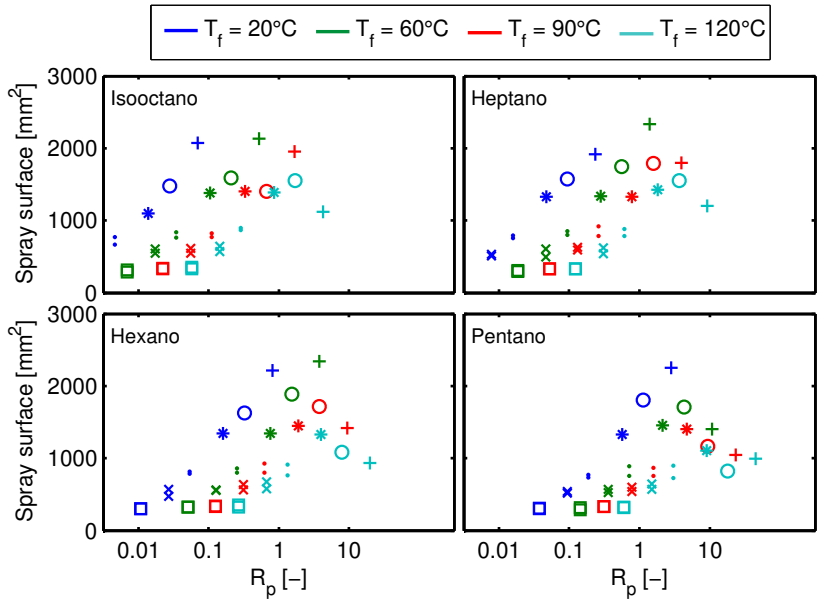

Figure 6.27: Averaged spray surfaces at different R_p for each fuel tested. The symbols indicate different P_b. Color indicates different T_f.

MIE analysis Collapse through intensity monitoring

The collapse of the sprays into a single liquid jet due to flash boiling has been analyzed as a state of the developed spray, however, there is some transitory mechanism that induce the spray collapse described by Li et al. [19] and Guo et al. [23], thus, it could also be seen as a transitory phenomena until is fully developed. The approach of this part, aims to detect the moment of

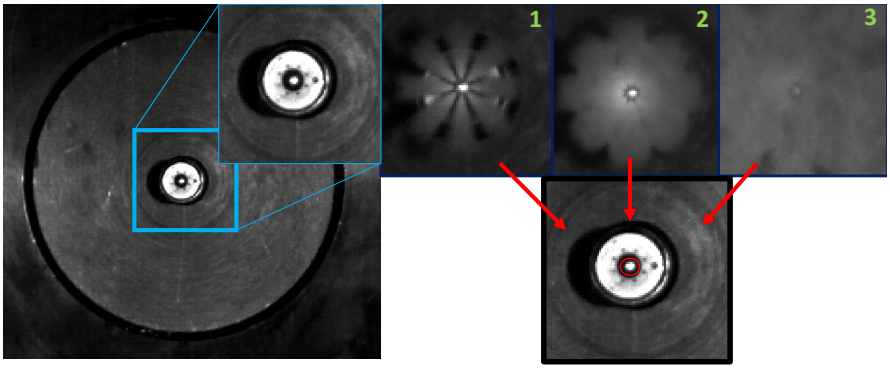

Figure 6.28: Diagram of the nozzle tip intensity monitoring.

collapse of the spray cone. For this purpose a precise monitoring of the central area of the spray is performed over the injection event.

Figure 6.28 aim to show the steps that led to the decision of nozzle intensity monitoring. It was noticed that the nozzle tip reflect was seen through all the injection event, and only clouded by the fuel when the collapse occurred. Therefore special attention was paid to the nozzle tip of zone A. The nozzle image before injection, is save a the background, to later be subtracted to the frames with spray.

On the right side, there is three images of different injection conditions. Image #1 depicts a developed spray which is not under flash boiling conditions. In this case the the white spot of reflection of the nozzle tip is visible through the whole injection. Image #2 shows a flash boiling test condition. despite having an $R_p > 1$, this condition has not collapsed yet and it is possible to visualize the nozzle tip. For Image #3, the spray is just about to collapse since the intensity levels for the nozzle tip are very low. Therefore, by monitoring the intensity levels of the pixels composing the nozzle tip, it can be analyzed the time at which the spray collapses.

Figure 6.29 depicts the time-resolved nozzle area pixels intensities. Note that all the intensity values start with 0 since the background has been already subtracted. This figure depicts the conditions of $P_b = 0.2$ bar and $T_{amb} = 20$ °C. As seen before (figure 6.19), the fuel properties affect greatly on the spray behavior. It is observed that for hexane three of the four temperatures are collapsing, whereas on the other fuels it can be noted only two. The iso-octane, for example, has two collapsing conditions at 90 and 120 °C. The nozzle pixel intensity values suffer a sudden increment at the star of the injection due to light reflection on the spray plumes that are starting to develop, but then, the

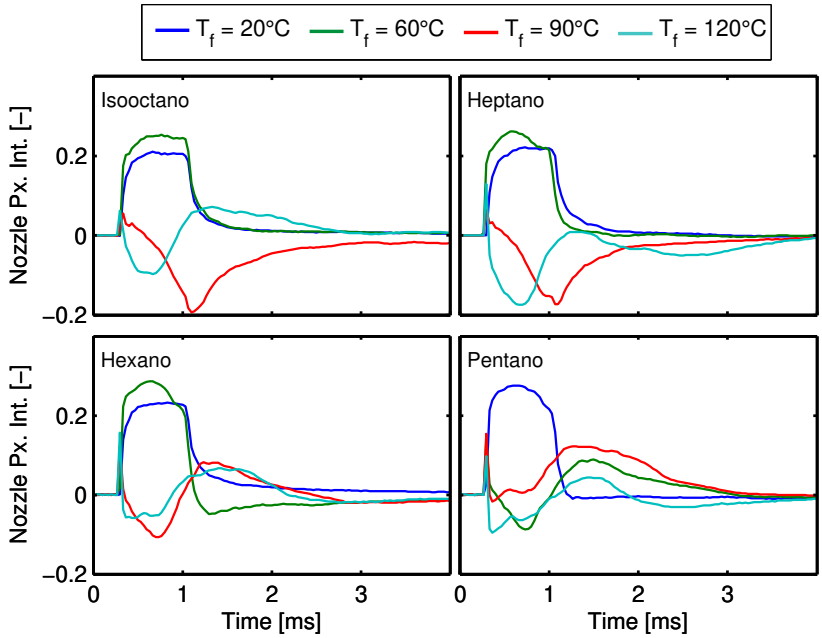

Figure 6.29: Normalized nozzle area pixels intensity vs. time for the four fuels tested. Each color represent a fuel temperature. Test points shown are taken at $P_b = 0.2$ bar and $T_{amb} = 20\,^{\circ}C$.

wide sprays and rapid collapse decrease rapidly the intensity, going to values under 0. After being darkened for some time, the pixels of the nozzle start to rise its intensity due to the formation of the liquid core and its illumination by the MIE light beams. For other collapse cases, the time to reach the maximum intensity is longer before drops to zero and negatives values, so the fuel takes longer to cloud the nozzle sight. In those cases when the pixels intensities average are 0 again is when the spray is considered to be collapsed. These intensity curves over time help us gain an different insight of the transients of the collapse mechanism that appear on GDI injectors.

If all the collapse moments are recorded, as explained before, using the nozzle pixel intensity monitoring, a new figure can be created condensing all the test conditions. Figure 6.30 shows the collapse times against R_p for all fuels and test conditions, noted that it is only shown R_p>1 since we are studying only collapse through flash boiling cases. Inside the figure, it is marked the SOI and the EOI times, which are of important at explaining the different collapsing behaviors. It reports that there are three different zones depending of the collapse time. The first zone is situated close to the SOI line. Here, there

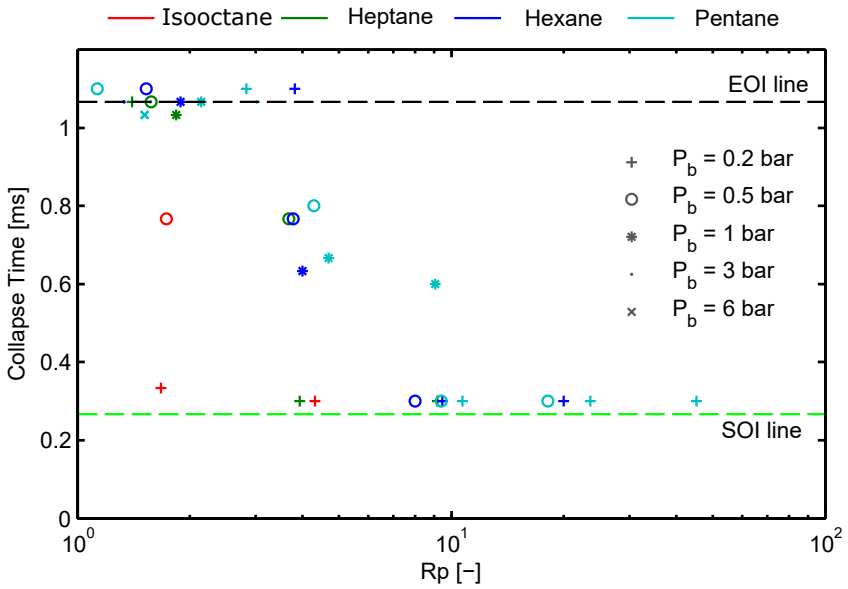

Figure 6.30: Collapse time interpreted as the moment when the nozzle is clouded by the fuel versus R_p. Horizontal lines represent SOI and EOI.

is the most extreme collapsing cases, which indicate that the spray plumes are collapsed from the very injection start. This zone is dominated by the lowest discharge pressure tested, and the resulted flashing conditions led to wider sprays, provoking high interaction between the spray plumes. Resulting in a almost instantaneous collapse. At this conditions, it can be observed a high concentration of fuel in the boundaries between two spray plumes as depicted in Figure 6.25. The next zone, is located between the SOI and EOI. There is collapse for this conditions, however, the interaction between plumes is not sufficient for a strong collapse, so as the spray is developing, the jets get wider and the full interaction and collapse happens further downstream. The last location is referred to the conditions whose "collapse" occurs close to the EOI line. The "collapse" in this last zone does not appear on a stationary spray. Nevertheless, as the injector needle closes, the last liquid fuel coming out of the orifices is attracted to the nozzle axis, probably because there is a slightly low pressure zone in that area due to the weak interaction between plumes, which was not sufficient to collapse the sprays but allows that some "collapse" or fuel concentration appears at th nozzle axis, appearing as a collapse from the point of view of the nozzle pixel intensity diagnostic.

All the graphs used to show the collapse due to flash boiling illustrate the difficulty of developing empirical correlations given the non- progressive

trends and behavior with the parameters employed. The study of GDI sprays behavior and parameters that led to spray collapse is crucial for understanding the evaporation and mixing to allow for predictive fuel concentration maps in the engines and avoidance of wall wetting, with the ultimate goal of decrease consumption and pollutants.

6.3 Preliminary work on X-ray Spray G wall impingement

6.3.1 Introduction

In internal combustion engines (ICEs), the phenomenon of spray-wall interaction (SWI) can be advantageous for engine efficiency as it facilitates better fuel-air mixing with particular piston designs. Nevertheless, the accumulation of liquid fuel on the walls of the cylinder can lead to undesirable phenomena, such as pool fire and pollutant generation,for example unburned hydrocarbons and soot. A detailed understanding of SWI physics in ICEs will allow strategies to monitor and prevent wall-wetting, resulting in lower emissions and improved engine efficiency. Optical methods such as DBI, Mie scattering, and Schlieren are used from an experimental perspective to examine the structure of the impinging jet and gain insights into the spray's global evolution. The study of local spray behavior while impingement is usually done through single or train of droplet experiments. Although informative, these experiments are distinguished by an order and symmetry that are seldom seen in real SWI engines. The advantages of X-rays techniques is that can access optically thick regions to extract quantitative and qualitative time-resolved data at the impact location.

In this work, a preliminary x-ray approach to SWI is analyzed. The ECN Spray G injector is used along with pure iso-octane as fuel. The data was taken during the international stay at Argonne National Laboratory. Note that ANL is one of the few places in the world able to run this kind of experiments in which x-rays are used to measure fuel flow in a particular region of interest of the domain. Typical fuel spray parameters of penetration and angle among others were calculated to evaluate it before and after the impact. In addition, free spray was measured and compared with wall impingement cases. Moreover, two wall inclinations were used to investigate how the impact angle affects the fuel spread and accumulation in the wall. X-rays techniques have been successfully applied and validated before, for example Duke et al. [11] compared the spray penetration of Spray G x-ray radiography at ANL

against MIE and DBI penetration data from Sandia National Laboratory for the same injector. They could only compare first 15mm of penetration due to the reduced domain of the facility, however, it was conclude that the methodology provided good results. Thus, radiography is a validated tool to perform spray diagnostics as other visible optical techniques.

As in previous experiments, the fuel is delivered to the injector by a common-rail system, in which the fuel is accumulated and supplied by a high-pressure fuel pump. The piece that holds the injector is designed to provide liquid cooling to control its temperature. For this experimental campaign, It was set fuel temperature (T_f) of 20 °C and discharge pressure (P_b) of 1 bar, except in the case of flash-boiling which is set at 90 °C and 0.5 bar. The conditions used for the experimental tests are shown in Table 6.3.

Table 6.3: Experimental matrix for radiography research.

Point	**Type**	**P_b [bar]**	**P_r [bar]**	**T_f [°C]**	**Wall configuration**
1	Radio.	1	50	20	P. wall y=12.295
2	Radio.	1	100	20	P. wall y=12.295
3	Radio.	1	200	20	P. wall y=12.295
4	Radio.	1	200	20	No wall
5	Radio.	1	200	20	L. wall (x=12)
6	Radio.	1	200	20	L. wall (x=7.33)
7	Radio.	0.5	200	90	L. wall (x=7.33)
8	Tomo.	1	100	20	(P. wall y=12.295)
9	Tomo.	1	200	20	(P. wall y=12.295)
10	Tomo.	1	200	20	No wall

Note that in Table 6.3 exist two types of radiological tests, X-ray radiography and tomography. Thus, the data obtained will be analyzed according to each techniques. Moreover, two different wall configurations will be used, in addition to the configuration without wall, which will be very useful for comparing results.

6.3.2 Spray Radiography results

2D maps reconstruction

In this section it is presented the images created when reconstructing the spray on a 2D map. The different cases will be exposed and, in a qualitative basis, the first conclusions will be drawn.

First, the no-wall configuration for 200 bar injection pressure is shown in Figure 6.31 which will coincide with Figure 6.32 (Perpendicular configuration) until the moment the spray hits the wall. By observing both images, the impact of the spray against the wall can be clearly differentiated, causing the fuel to spread over the wall surface.

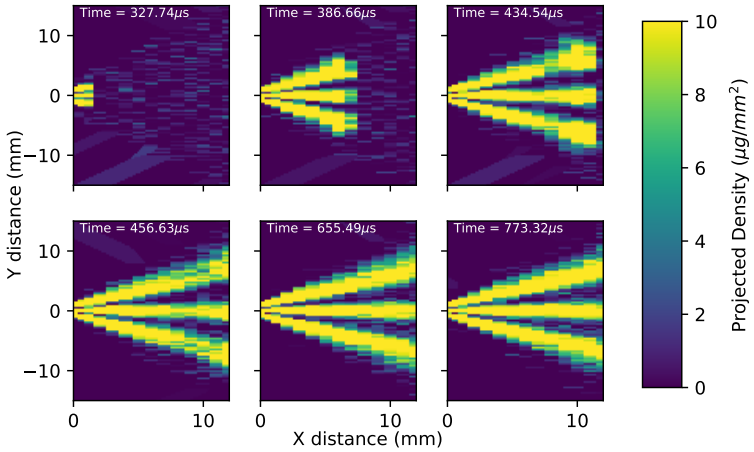

Figure 6.31: 2DMaps for six different time steps (No-Wall).

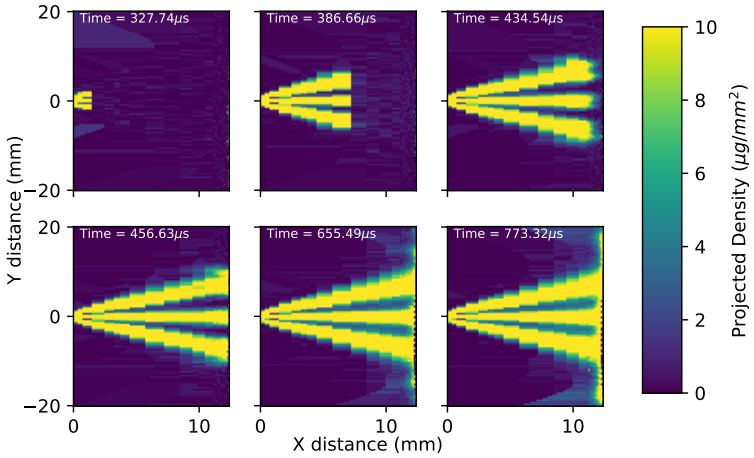

Figure 6.32: 2DMaps for six different time steps (perpendicular wall).

Finally, the lateral wall configuration is shown in Figures 6.33 and 6.34 in the conditions of $P_b = 1$ bar and $T = 20°C$ (ambient condition) and $P_b = 0.5$ bar and $T = 90°C$ (flash-boiling condition for iso-octane). By comparing both images, some conclusions can be drawn about the effects of the flash-boiling phenomenon . It can be seen an increase in the evaporation of the spray that leads to a reduction in the amount of fuel that comes into contact with the wall, this leads to a smaller amount of fuel deposited on the wall and a greater amount of fuel droplets dispersed through the chamber that probably favors the process of mixing with air. From the point of view of reducing the amount of fuel on the wall surface the flash-boiling condition is clearly favourable in this case.

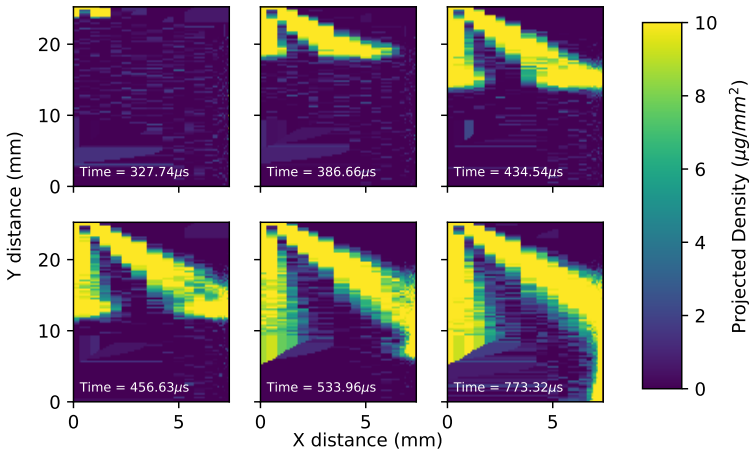

Figure 6.33: 2DMaps for six different time steps (lateral wall).

Transversal scans

As mentioned above, spray/wall impact analysis is an inherently transient phenomenon that can be analyzed as a stabilized spray hitting the wall (differences between conditions) or a transient analysis can be performed to see the differences between different moments of the process for the same condition.

Therefore, the results for the same situation at different moments in the process are shown first, where the evolution of the process can be observed from the individual cross-sectional scans. Figure 6.35 shows the results of the

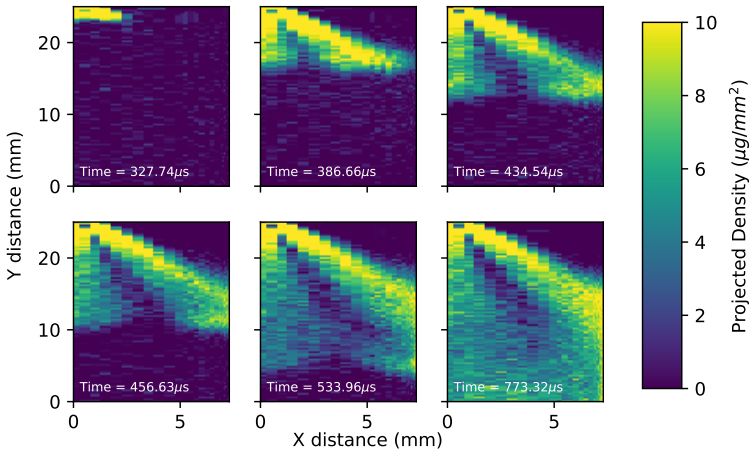

Figure 6.34: 2DMaps for six different time steps (lateral wall), with a fuel temperature of 90 °C and discharge pressure of 0.5 bar.

perpendicular wall configuration for an injection pressure of 100 bar. The first image corresponds to a t = 0.460 ms and the following images are taken every 0.1841 ms which corresponds to an increment of 50 temporary jumps. It can be seen that in the first image the fuel spray has not yet reached the scanner located 12mm from the injector, thus, the spray has not yet impacted the wall located 12.30 mm. In the following image it can be observed how the spray has already reached 12 mm so there will be impact against the wall, since some small peaks begin to appear in the image in addition to the three clearly differentiated peaks that correspond to the three jets of fuel. As time passes from that moment on, these small peaks can be seen more clearly in the image, which indicate that the fuel has begun to spread over the surface of the wall. In addition, it can be seen how these peaks move axially away from the position of the jets, another proof that the fuel is propagating through the wall. Finally, if the last image is analyzed, it can be seen how the distribution of the fuel is not homogeneous, in this case the fuel jet located at -5mm from the transversal position has propagated more causing a greater distribution of the fuel that leads to a smaller quantity of fuel in the impact zone of the jet, on the other hand, the jet located on the opposite side has propagated less causing a greater accumulation of fuel in the impact zone of the jet.

It can be observed how the projected fuel density in the impact zone at a distance of +-12mm ends up in values between 20-35 $\mu g/mm^2$, which is higher than in the propagation zone which is around 10-15 $\mu g/mm^2$.

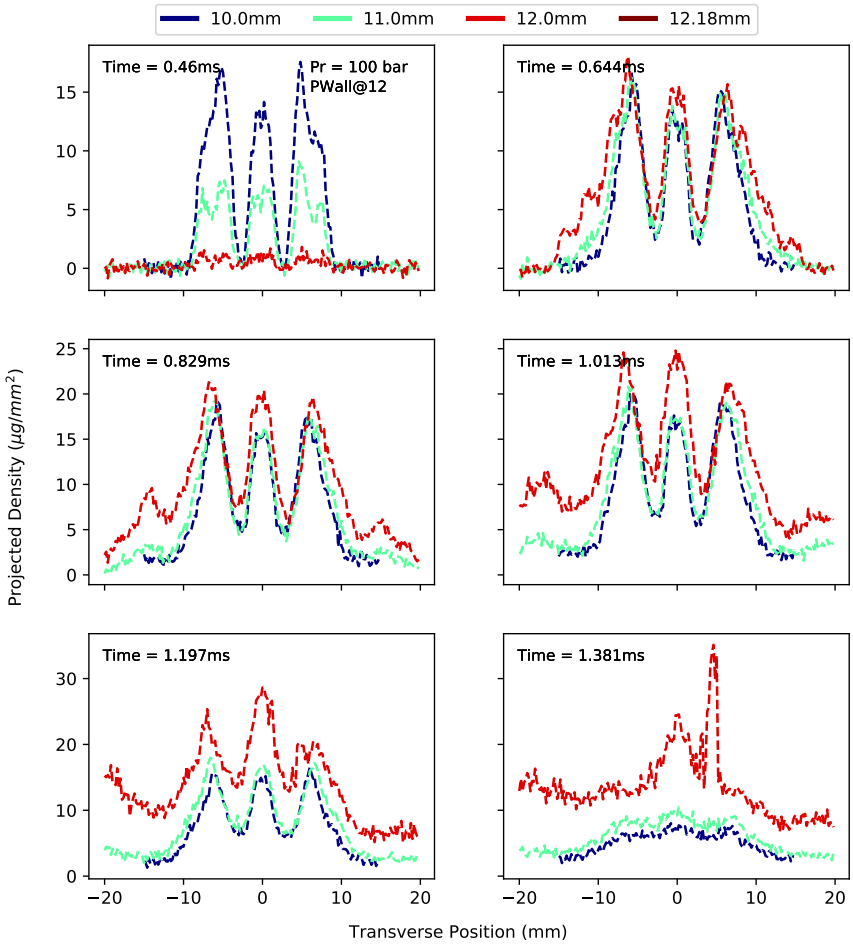

Figure 6.35: Transversal scans from t = 0.46ms increasing 50 time steps for each figure. Conditions of P_r= 100 bar, T_f= 20 °C (P. wall).

If the same analysis is performed in the same moments of time for a P_r = 200 bar, the images of Figure 6.36 are obtained, where the data have also been included at a distance of 12.18 mm, a distance even closer to the wall. First, it can be seen as in the first image the fuel spray for this case if it has reached the scanner located 12 mm from the injector and even the 12.18mm, ie, has already impacted the spray against the wall. In the following images there are again some small peaks in the image in addition to the three clearly differentiated peaks that indicate that the fuel has begun to propagate through the wall surface. Finally, from the analysis of the last image it can be noted

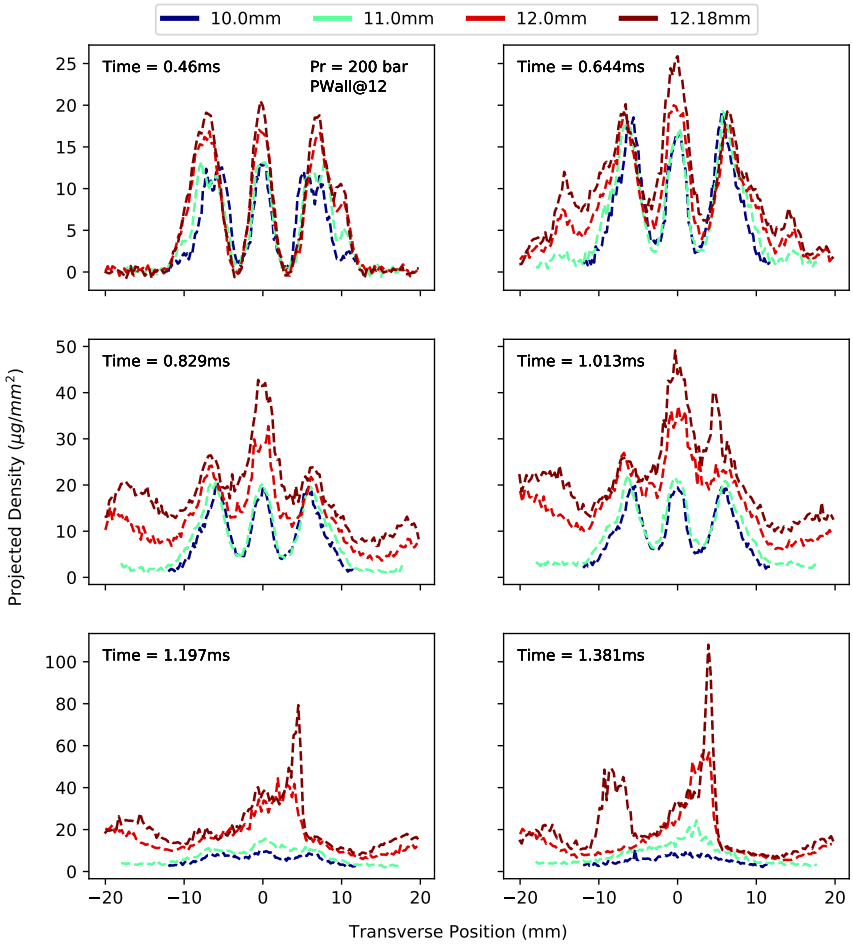

Figure 6.36: Transversal scans from t = 0.46ms increasing 50 time steps for each figure. Conditions of P_r= 200 bar, T_f= 20 °C (P. wall).

how the projected density of fuel in the impact zone again at a distance of +-12 mm in this case reaches values between 30-60 μg/mm^2 and in the area of propagation of about 10-20 μg/mm^2. If the results at 12.18 mm are taken into account, the projected density values would be much higher as they are closer to the wall, again very large point values can be seen in the impact zone.

Figure 6.37 below shows the results of the side wall configuration in ambient conditions T = 20 °C and P_b = 1 bar. The first image corresponds to a t = 0.383 ms and the following images are taken every 0.0368 ms corresponding to

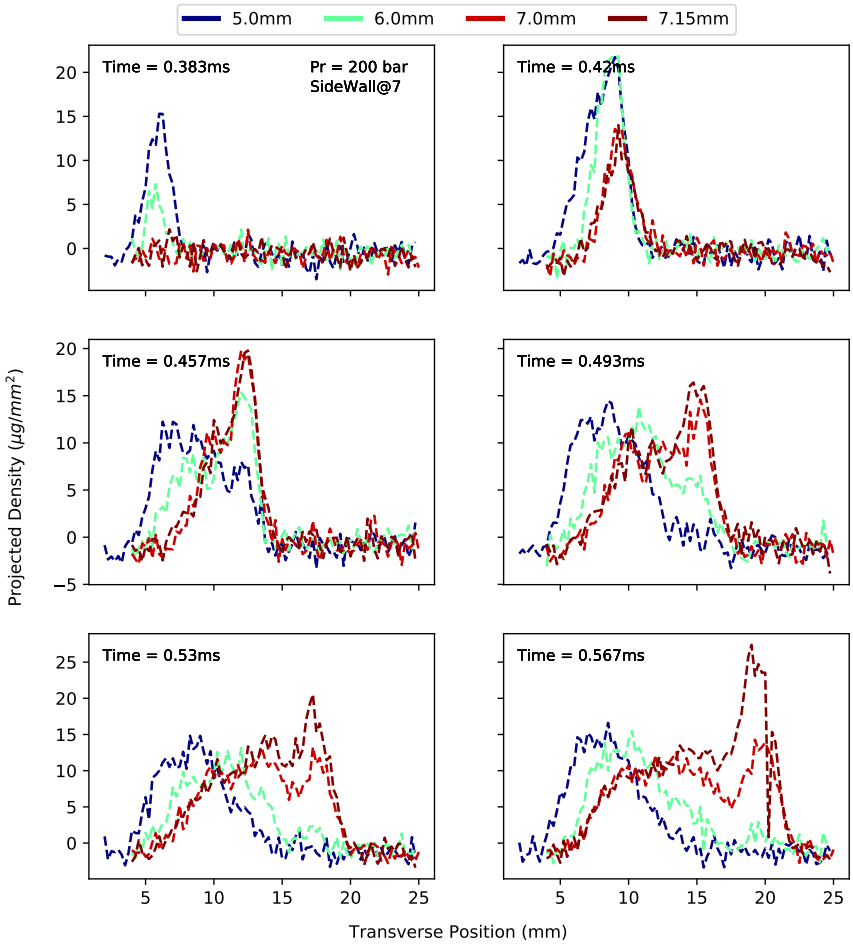

Figure 6.37: Transversal scans from t = 0.383 ms increasing 10 time steps for each figure. Conditions of P_r = 200 bar, P_b = 1 bar, T_f = 20 °C (L. wall).

the step of 10 temporary jumps. Following the same reasoning as for the case of a perpendicular wall, it can be seen that in the first image the fuel spray has not yet reached the scanner located at 7.15 mm from the injector, that is, the spray has not yet impacted the wall located at 7.33 mm. In the following image it is noted how the spray already reaches 7.15 mm. As time passes from that moment, it is clearly appreciated how the peak corresponding to the only jet that in this case hits the wall laterally begins to move indicating that the fuel has begun to spread over the surface of the wall. Finally, if the last images are analyzed, it is possible to see the projected density of fuel oil that remains

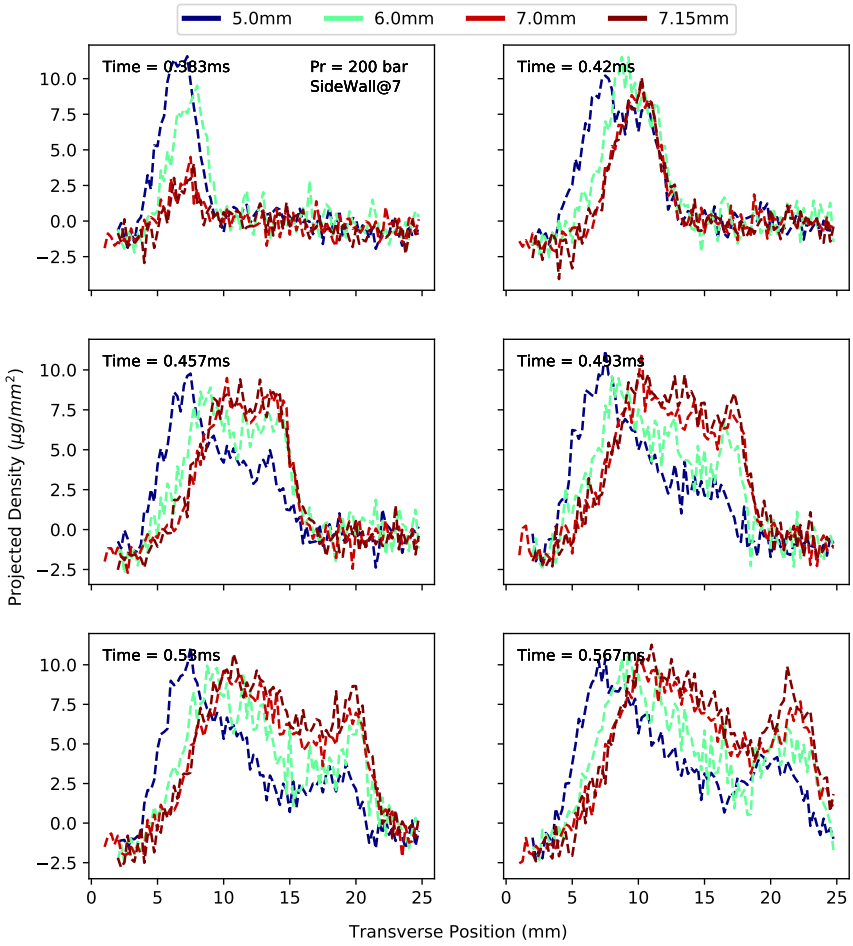

Figure 6.38: Transversal scans from t = 0.383 ms increasing 10 time steps for each figure. Conditions of P_r= 200 bar, P_b= 0.5 bar, T_f= 90 °C (L. wall).

at a distance of 7.15mm, that is, very close to the wall as the jet advances, values between 10-15 μg/mm^2 are observed in the last areas where the jet has reached and, contrary to what happened in the perpendicular configuration, now in the impact zone there are minimum values of between 0-5 μg/mm^2.

If the same analysis is performed in the same moments of time, but in flash-boiling conditions T = 90 °C and P_b = 0.5 bar, the images of Figure 6.38 are obtained. Firstly, it can be seen as in the first image that the fuel spray for this case has reached already the scanner located 7.15 mm from the injector, although it has not reached very high values, so it can be deduced that it is

about to hit the wall, although it has not yet done so either. However, it can be seen how in these conditions it will impact earlier than in the previous case. In the following images it can be noted how the peak corresponding to the jet of fuel is no longer so clearly visible, but the advance of the fuel through the wall is still visible, although this time in a more dispersed way. Taking into account the images in Figure 6.34 these results can be explained because in this condition of flash-boiling is observed a large amount of fuel scattered in the area near the wall in addition to the fuel for the advance of the jet through the wall. Finally, analyzing the last image it can be observed that the projected density of fuel at a distance of 7.15 mm reaches values between 4-10 $\mu g/mm^2$ in the last areas where the jet has reached and in the impact zone have minimum values of between 0-5 $\mu g/mm^2$.

On the other hand, in order to perform the analysis as a stabilized spray that hits the wall, a combination of cross-sectional scans of the same instant is performed, but under different conditions so in this way the differences between them can be analyzed. Combined transversal scans are depicted in Figures 6.39 and 6.40.

In the comparison between the perpendicular wall-non-wall configuration of Figure 6.39, it can be seen how in addition to increasing the mass of fuel in the surrounding areas due to fuel spread, the mass of fuel in the impact zone also increases. The impact therefore causes an increase in the mass of fuel both in the impact zone due to the accumulation of fuel and in the surroundings due to the propagation on the wall surface. In the impact zone, the projected density doubles from 12-17 $\mu g/mm^2$ without wall to 25-35 $\mu g/mm^2$ in perpendicular wall configuration.

Figure 6.40 shows the comparison between the free spray without wall interaction and the spray that impacts the sidewall configuration. The comparison is not trivial since the scans for the side wall are parallel to the wall and the injector while in the wall-to-wall configuration they are perpendicular to the injector. A tolerance of 1mm is used between scans to make it comparable. However, the number of comparable points is much lower than in the perpendicular wall configuration because here too the scans are made parallel to the wall which will now be perpendicular to the injector as in the non-wall configuration.

Finally, a comparison between the side wall and the free spray shows that the mass of fuel increases in the entire area of propagation due to the advance of the jet on the wall surface, although in this case the fuel does not accumulate in the impact area and, unlike in the previous case, the mass of fuel in the impact area is now reduced compared to the configuration without a wall. In

the impact zone, the projected density is almost halved from 15-20 μg/mm^2 without a wall to 0-10 μg/mm^2 in a sidewall configuration.

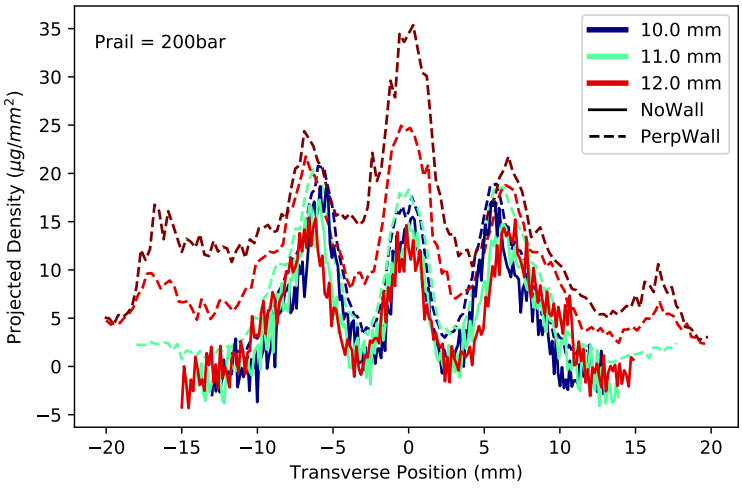

Figure 6.39: Transverse scans comparisons at t = 0.736 ms.

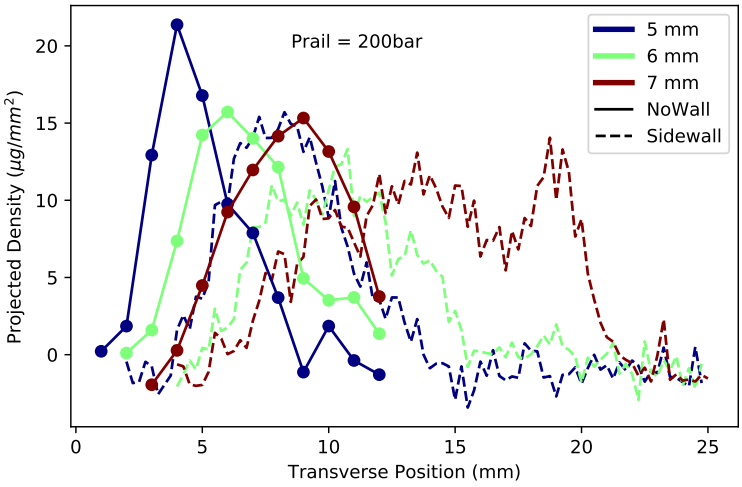

Figure 6.40: Transverse scans comparisons at t = 0.552 ms.

Transverse integrated mass (TIM)

The projected mass from the X-ray can be integrated in space to obtain the transverse integrated mass (TIM) of the spray at some axial location. This is an interesting parameter since a key feature of these GDi injectors in relation to diesel injectors is the rapid decrease of the projected mass with distance due to the rapid mixing with the environment [35]. It can be interpreted as the amount of fuel mass that crosses a given section (or axial position).

As can be seen in Figure 6.41 under normal conditions without a wall, the TIM is reduced at any axial location. In contrast, the perpendicular wall configuration it can be seen that the TIM parameter increases as it approaches the wall position. This result confirms what was previously stated: because of the impact in the perpendicular wall configuration, the fuel mass increased considerably in the area close to the wall due to fuel accumulation in the impact zone and fuel spread over the wall surface. Note that just before the TIM reaches to a stabilized value, there is a peak on the signal observed in all axial distances. This peak is translated to an accumulation of mass at the leading edge of the spray, which exhibits a higher liquid mass density than any other location in the spray. It has been observed in previous studies [36, 37].

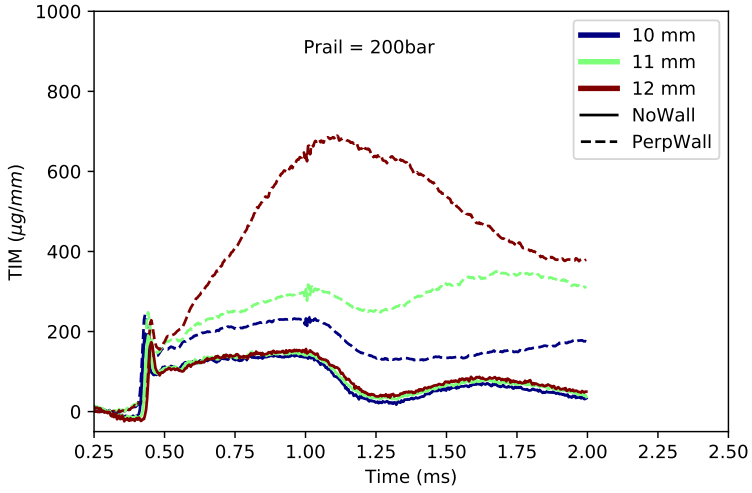

Figure 6.41: Transverse integrated mass (TIM) comparison between perpendicular wall and the free spray.

Figure 6.42 shows the comparison between the side wall and the free jet, where it can be seen how the TIM parameter increases also in the area near

the wall, although in this case it does so in a lesser extend. For the P-wall case the TIM reached values around 700 μg/mm near the wall while in the L-wall case reaches values around 200 μg/mm. This is explained by what was exposed before, in the P-wall configuration the fuel mass increases in the entire area near the wall, whereas in the L-wall configuration the fuel mass decreases in the impact area and increases in the surroundings due to the propagation of the fuel, this causes the total fuel mass near the wall to increase, although to a much lesser extent than in the P-wall configuration.

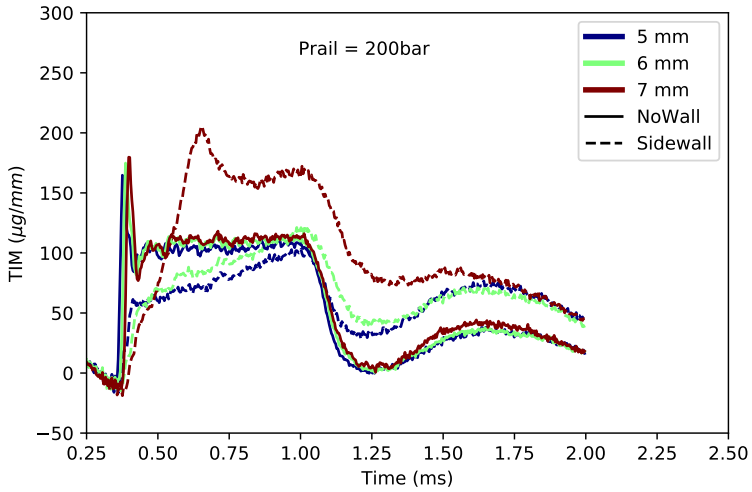

Figure 6.42: Transverse integrated mass (TIM) comparison between lateral wall and the free spray.

6.3.3 Spray Tomography results

As explained in section 3.6, the data in spray tomography data is acquired in a similar fashion as spray radiography, however, in this case all the data is obtained at a certain distance. Then, the injector is rotated by angle steps to complete 0 to 180 ° to finally be able to reconstruct the tomography.

2D map reconstruction

The 2D map reconstructions of the spray tomography are depicted in this section in a similar fashion to the previous method.

Figures 6.43 and 6.44 show the 2D maps for the perpendicular wall configuration for 100 bar and 200 bar injection pressures respectively. Observing

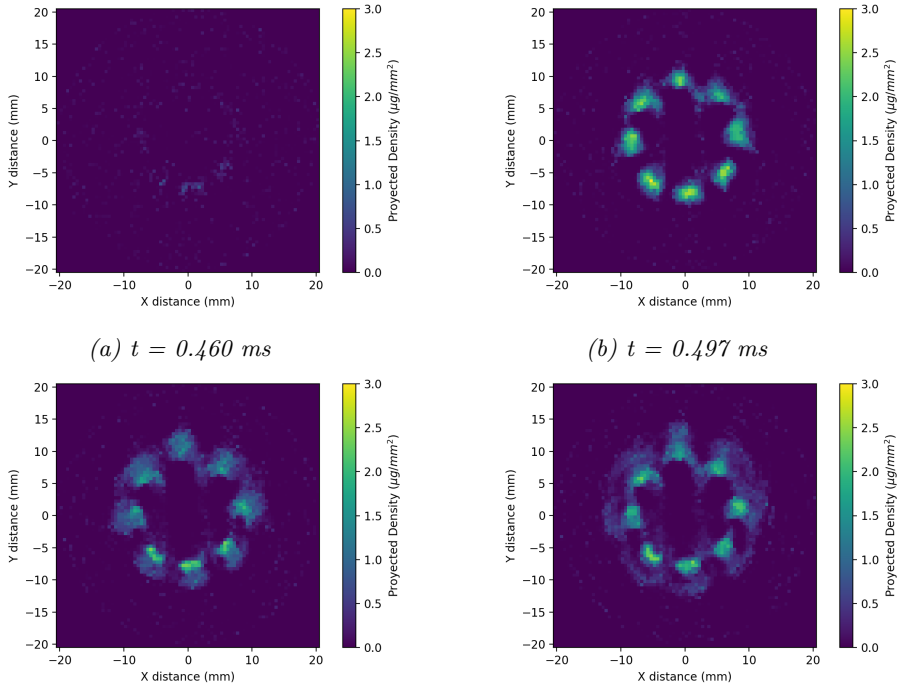

(a) t = 0.460 ms *(b) t = 0.497 ms*

(c) t = 0.533 ms *(d) t = 0.570 ms*

Figure 6.43: 2D tomography reconstruction for P_r = 100 bar. Figures evolution in time are presented each 10 time steps (Δt = 0.0368 ms). (P. wall).

both figures, the propagation front formed due to the impact of the spray against the wall can be clearly seen. In addition, it can be noted how by increasing the P_r this phenomenon occurs earlier, since the spray propagation is faster. Finally, Figure 6.45 shows the case without impact against the wall for P_r = 200 bar , it can be seen as a major difference that now the propagation front that was observed in the previous figures no longer appears.

Fuel surface over time

One approach to analyze the spray impingement effect from the tomography data is by monitoring the surface that is occupied by the fuel at that scan distance. Following the steps outlined in the section of image processing, the fuel surface evolution over time is depicted in Figure 6.46. It reports how higher P_r is translated to an earlier appearance of the spray at that distance. In addition, the high P_r case present greater fuel accumulation at the end of the propagation. Again, the hump shown in the free spray is explained by

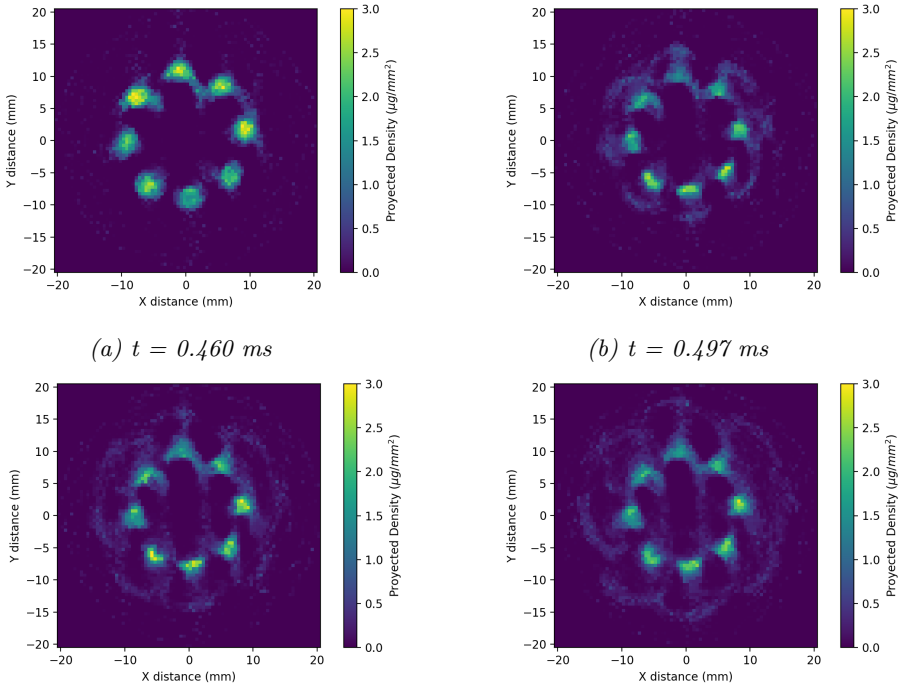

(a) t = 0.460 ms *(b) t = 0.497 ms*

(c) t = 0.533 ms *(d) t = 0.570 ms*

Figure 6.44: 2D tomography reconstruction for P_r = 200 bar. Figures evolution in time are presented each 10 time steps (Δt = 0.0368 ms). (P. wall).

spray tip fuel accumulation as seen in TIM figures. Finally, if the fuel surface is compared with the no-wall configuration it can be estimated an increase of approximately 270% in the surface of fuel at the end of the propagation, from 101 mm^2 without wall to 372 mm^2 with perpendicular wall.

6.3.4 Analysis of spray penetrations and velocities

The last analysis performed on the tomography and radiography data is related to spray penetrations and velocities before and after wall impingement.

Firstly, penetrations and velocities of the free spray and the jet before wall impingement can be obtained for the perpendicular wall configuration. On the other hand, from the tomography images the same parameters are obtained by this time is considered spray propagation after impact with the wall (P.wall) . Finally, in the case of the lateral wall, a joint analysis of both moments (spray before and after impingement) is performed based on the images obtained by radiography of the spray.

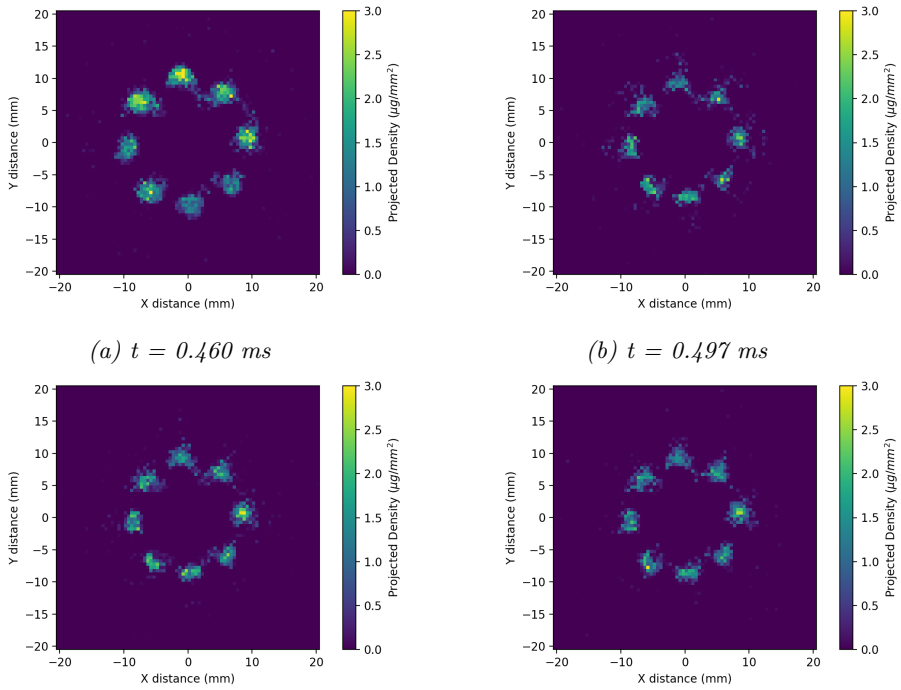

(a) t = 0.460 ms *(b) t = 0.497 ms*

(c) t = 0.533 ms *(d) t = 0.570 ms*

Figure 6.45: 2D tomography reconstruction for P_r = 200 bar. Figures evolution in time are presented each 10 time steps (Δt = 0.0368 ms). (Free spray).

Perpendicular wall

Figure 6.47a presents the penetration of the spray radiography, in which the spray cone is visualized from a side. The two observable jets are analyzed whose penetrations are quite similar supporting the idea of equal nozzle orifices. The distance of the central jet is lower and coincides with the axial distance to the wall with the other jets, however, its lower penetration is due to the fact that this jet would have a component perpendicular to the plane that cannot be seen in the image. The figure reports similar results to those obtained by other optical techniques such as lateral DBI or MIE [11]. On the right side (Figure 6.47b), is depicted the instantaneous velocities at each distance. it can be observed an average velocity of approximately 109 m/s for both jets, which coincides with the hydraulic results from chapter 5.

Following this, in Figure 6.48 it is shown the spray spread after impact employing the same parameters: penetration and velocity. Both are extracted this time from the x-ray tomography reconstruction. Figure 6.48a depicts

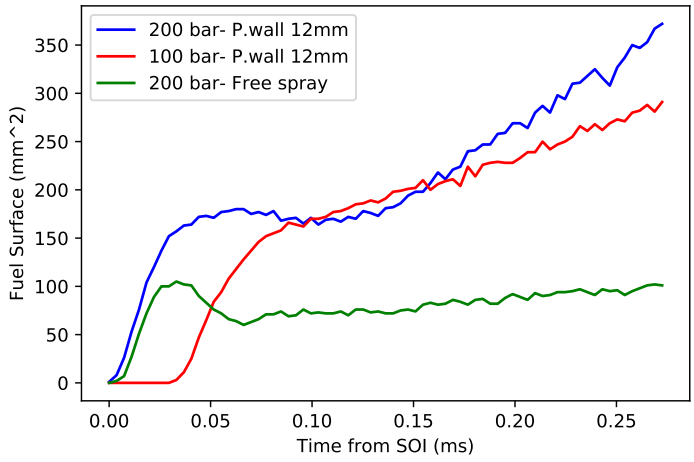

Figure 6.46: Fuel surface comparison between free spray and after wall impingement accumulation.

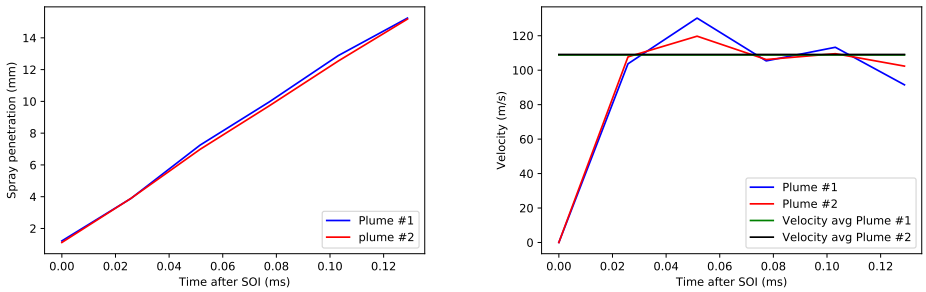

(a) Spray penetration. *(b) Spray velocity.*

Figure 6.47: Spray parameters before wall impingement analyzing the radiography data.

the spray spread for the two rail pressures tested. It can be seen that the higher the P_r, the greater spread distance. This can be explained taking into account that the greater the P_r, the higher the velocity of injection, so, as can be seen in Figure 6.48b, when impacting at a greater speed, the velocity of propagation is also higher for a given instant.

If it is compared the averaged velocity results for the case of $P_r = 200$ bar before and after the spray impingement it can be noted the effect of the impact on the spray velocity. The jet before impingement has an averaged

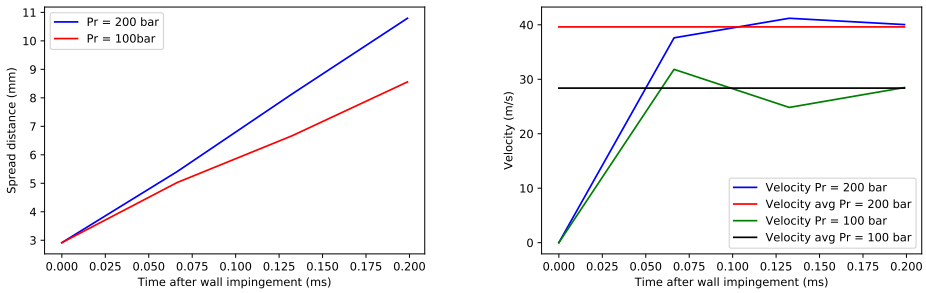

(a) Spray penetration. *(b) Spray velocity.*

Figure 6.48: Spray parameters after wall impingement analyzing the tomography data (P.wall).

velocity of 109 m/s, while the fuel spread after impact has 39.6 m/s. The velocity difference is of ≈ 70 m/s, which led to a avg. velocity decrease of 64 %.

Lateral wall

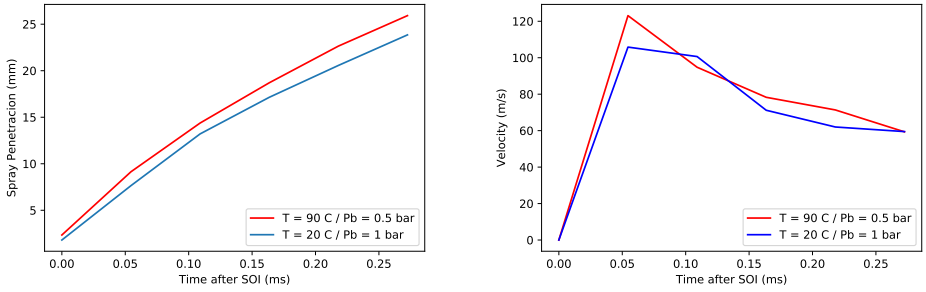

(a) Spray penetration. *(b) Spray velocity.*

Figure 6.49: Spray parameters after wall impingement analyzing the tomography data (L.wall).

Finally, the fuel penetration/spread and velocity on the lateral wall is presented in Figure 6.49. In the figure is shown two different cases both with rail pressure of 200 bar, however, one is tested at T_f of 90 °C and P_b of 0.5 bar which is a flash boiling case. The other is at ambient fuel temperature and pressure (T_f = 20 °C and P_b of 1 bar). Figure 6.49a reports that at flash-boiling conditions, as the temperature increases and the ambient

pressure decreases, jet penetration is faster. This effect can be explained by two factors. On the one hand, the reduced ambient pressure is translated in lower discharge density, thus, less drag and advance resistance to the jet. In addition, increasing the temperature causes a reduction in viscosity and this favors the propagation through the wall surface. This results can be observed in Figure 6.33 and 6.34.

Lastly, regarding the spray speed values depicted in Figure 6.49b, it can be seen that in the first section the speed is around 105 m/s for the ambient conditions case, which are values close to those previously obtained for the injection speed at $P_r = 200$ bar. However, now the final speed is around 60 m/s while in the perpendicular configuration were obtained propagation speeds of 40 m/s. As expected, the lateral impact (at much smaller angle) slows down the spray to a less extent, assuming a loss of speed of 43%. If the results are compared with the flash-boiling condition, it can be seen how the spraying velocities increase considerably reaching values around 120m/s, but in this case the impact with the wall means a greater reduction in velocity so that practically the same velocities are reached at the end of the propagation. The speed loss in flash-boiling conditions is 50%. The fact that the loss of speed in this case is greater is possibly because, as previously demonstrated, the amount of fuel that impacts against the wall in these conditions is lower than that which impacts at ambient conditions. Thus, the remaining momentum of the spray for a less condensed liquid core, is much lower. And due to the greater diffusion of this conditions same air drag is affecting less fuel leading to a decrease of spread velocity after impact, causing a greater reduction in the velocity of propagation through the wall.

6.4 Summary and conclusions

In this chapter, several external flow results have been exposed and discussed. The first part of optical techniques provided an insight of the effects of different levels of flash boiling in the fuel sprays. In the second part, a preliminary study on spray wall impingement using x-rays techniques is exposed. The principal conclusions are summarized below:

- The first section showed the spray visualization results. It was employed three different optical techniques to analyze the fuel spray development on two different injector nozzles. Four surrogate mono-component fuels were tested with different molecular weight and volatile properties, in order to investigate more extreme flashing conditions. Also, to imitate

gasoline volatile properties in a simpler way. From the fuels investigated, the hexane was found to have the most similar volatile properties to gasoline. Isooctane, which has been typically used as gasoline surrogate imitating the auto-ignition avoidance properties must not be employed to research and imitate the flash boiling phenomena. Hexane should be used instead. The main conclusions can be summarized as follows:

- It was studied the effect of different test conditions using typical spray parameters such as penetration and spray angle through the lateral DBI and Schlieren techniques. At non flash boiling conditions, higher fuel pressure showed faster penetrations as expected. The chamber density affect the penetration by decreasing the penetration speed but also increasing the spray cone angle. The fuel temperature showed little effect in terms of penetration nor angle. However, the chamber temperature yield different evaporation distances for the liquid spray. Moreover, it was observed that the less volatile fuels showed faster penetration and smaller angles in general. Regarding the nozzle comparison, it was noted that the PIU injector penetrated faster due to internal geometry design and its needle lift velocity. The spray cone angles were more stable for the PIU nozzle along the observed time window, which is consistent with its smaller cone angle.
- The spray morphology was analyzed through the whole test matrix in order to find pattern to characterized the flashing behavior. It was observed for the most extreme flashing conditions a vortex appears on the spray tip. From the spray width it was observed that at flashing conditions, two collapse structures could appear: transitional collapse and severe collapse. The transitional collapse showed the greatest vortex in the spray front. Also, it was observed a greater spray expansion at the first mm from the nozzle. Regarding the fuel tested, it was shown that for the same test conditions the most volatile fuels yielded more extreme flashing conditions leading to an early collapse.
- Following, a study of spray expansion was performed. For this section it was used nucleation theory and phase change potential to relate the spray expansion at different flashing and non-flashing conditions. The spray width at different distances from the nozzle exit were observed to have good agreement with R_p smaller than 3.5. The parameter X from the nucleation theory was also related

to the width however it did not show a relation as clear as with the chemical potential, that indicated that was the main expansion mechanism for internal flashing sprays. The relations were reasonable for close distances to the nozzle, until 20d-40d. Further distances did not appropriately correlate the spray with so it was probably dominated by other mechanisms such as aerodynamic forces and droplets diffusion into air.

– Finally, a study to approach and get further understanding on the spray collapse mechanisms regarding fuel properties and nozzle geometry was performed. First, the two injectors with different cone angle were compared adimensionalizing the angles and plotted against fuel temperature and R_p. It could be understandable that for lower cone angles the collapse of the spray appears at lower R_p because of earlier interaction between sprays, however, the flashing effect that produced jet expansion yielded on the PIU injector similar cone angles across the conditions tested. Therefore, the final angle when collapsing was very similar to the non collapsing one for the PIU injector. However, for the Spray G injector the difference between collapsing and non-collapsing was more noticeable. For the second part, it was used a MIE frontal visualization to study spray surface evolution and the collapsing time by monitoring the clouding of the nozzle tip by the fuel. The surface results yielded that a strong correlation between spray surface and R_p at each T_F when the spray was stabilized. However, this correlation was non longer valid at high R_p when the spray collapsed, which happened at similar R_p independently of the fuel tested. Regarding the collapse times, it was observed three main collapse moments:

  1. First, the typical collapse structure, in which the sprays collide into the center almost at the same instant that the injection starts.
  2. Secondly, the mild collapse conditions. In this case it was found that the collapsed occurred after the spray had developed to some extend.
  3. Finally, it was observed that for flashing conditions the nozzle was also clouded at the end of the injection. This result proposed that the inner low pressure zone induced by plume interaction was present, and although not sufficient for the collapse, suctioned to the spray axis the last flow exiting the nozzle.

- In the second part, the process of gasoline wall impingement was study through the use of x-rays techniques. It was observed how the injection variables affects the spray and therefore its behavior after impingement. The impact angles with the wall were 60° for the perpendicular configuration, and 40° for the lateral configuration. Each impact angle yield very different fuel accumulation and spread results.

  - The x-rays radiography technique provided information about the fuel accumulation after the impact. In the P-wall case, the projected density doubled in the impacted zone from 12-17 to 25-35 $\mu g/mm^2$ with respect to the free jet. For the L.wall case the fuel did not accumulate on the impact surface but move through the wall. Therefore, on the contrary to the P.wall, in the L.wall case the projected density on the impact zone is decreased with respect to the free jet at that point. Also, it was observed that the Pr affected the level of fuel accumulation near the wall, it was found an increase of 270 % of the projected mass for the case of 200 bar and an increase of 190% for the 100 bar case. The fuel surface at the end of the spread in perpendicular wall configuration increases by ∼28% by doubling the injection pressure from 100 to 200 bar.
  - With regard to the transverse integrated mass (TIM), the impact with the perpendicular wall caused an increase in the maximum values reached with respect to the lateral wall configuration. Values around 700 $\mu g/mm$ are reached near the wall in perpendicular configuration while in the case of the side wall it reaches values around 200 $\mu g/mm$. This can be explained by the fact that in the perpendicular wall configuration the fuel mass increases in the entire area near the wall, whereas in the side wall configuration the fuel mass decreases in the impact area and increases in the surroundings due to the fuel propagation. This results in an increase in the total fuel mass near the wall, although to a much lesser extent than in the perpendicular wall configuration. The greater fuel mass accumulation in the perpendicular case set the bases for potential pool fires and pollutant source during engine operation, therefore, it can be concluded that the perpendicular impact is the less favorable case.
  - Finally, it was analyzed the penetration and velocity results, observing the following effects: The fuel velocity is reduced after impact as expected. The velocity is decreased ∼64% after the impact in the P-wall case, and ∼43% in the L-wall case. Moreover, the

velocity of propagation after impact increases ∼40% by doubling the injection pressure from 100 to 200 bar.

For the flash boiling conditions case tested in the L-wall, it was found that the amount of fuel that hits the wall under these conditions is less than the amount that hits the wall under ambient conditions. In addition, it involves an increase in the speed of spray penetration and an increase in the loss of speed from impact against the wall. The loss of velocity increases in flash-boiling conditions with respect to ambient conditions varying from ∼43% to ∼50%.

References

[1] "Engine Combustion Network". In: *https://ecn.sandia.gov/gasoline-spray-combustion/* (2020).

[2] Lemmon, Eric W., McLinden, M. O., and Friend, D. G. "Thermophysical Properties of Fluid Systems". In: *NIST Chemistry WebBook, NIST Standard Reference Database Number 69*. Ed. by P. J. Linstrom and W. G. Mallard. 2011.

[3] Huang, Yuhan, Hong, Guang, and Huang, Ronghua. "Numerical investigation to the dual-fuel spray combustion process in an ethanol direct injection plus gasoline port injection (EDI + GPI) engine". In: *Energy Conversion and Management* 92 (2015), pp. 275–286. DOI: 10.1016/j.enconman.2014.12.064.

[4] Kar, Kenneth, Last, Tristan, Haywood, Clare, and Raine, Robert. "Measurement of vapor pressures and enthalpies of vaporization of gasoline and ethanol blends and their effects on mixture preparation in an SI engine". In: *SAE International Journal of Fuels and Lubricants* 1.1 (2009), pp. 132–144. DOI: 10.4271/2008-01-0317.

[5] Moulai, Maryam, Grover, Ronald, Parrish, Scott, and Schmidt, David. "Internal and Near-Nozzle Flow in a Multi-Hole Gasoline Injector Under Flashing and Non-Flashing Conditions". In: *SAE Technical Papers*. Vol. 2015-April. April. 2015. DOI: 10.4271/2015-01-0944.

[6] Weber, Daniel, Leick, Philippe, Gmbh, Robert Bosch, and Systems, Gasoline. "Structure and Velocity Field of Individual Plumes of Flashing Gasoline Direct Injection Sprays". In: *ILASS Europe, 26th Annual Conference on Liquid Atomization and Spray Systems* September 2014 (2014), pp. 8–10. DOI: 10.13140/RG.2.1.1227.2724.

[7] Wu, Shengqi, Xu, Min, Hung, David L.S., Li, Tianyun, and Pan, Hujie. "Near-nozzle spray and spray collapse characteristics of spark-ignition direct-injection fuel injectors under sub-cooled and superheated conditions". In: *Fuel* 183 (2016), pp. 322–334. DOI: 10.1016/j.fuel.2016.06.080.

[8] Yin, Peng, Yang, Shangze, Li, Xuesong, and Xu, Min. "Numerical simulation of in-nozzle flow characteristics under flash boiling conditions". In: *International Journal of Multiphase Flow* 127 (2020). DOI: 10.1016/j.ijmultiphaseflow.2020.103275.

[9] Aleiferis, P. G. and Van Romunde, Z. R. "An analysis of spray development with iso-octane, n-pentane, gasoline, ethanol and n-butanol from a multi-hole injector under hot fuel conditions". In: *Fuel* 105 (2013), pp. 143–168. DOI: 10.1016/j.fuel.2012.07.044.

[10] Vaquerizo, Daniel. "Study on Advanced Spray-Guided Gasoline Direct Injection Systems". PhD thesis. Universitat Politècnica de València, 2017.

[11] Duke, Daniel J. et al. "Internal and near nozzle measurements of Engine Combustion Network 'Spray G' gasoline direct injectors". In: *Experimental Thermal and Fluid Science* 88.June (2017), pp. 608–621. DOI: 10.1016/j.expthermflusci.2017.07.015.

[12] Payri, Raul, Salvador, Francisco Javier, Martí-Aldaraví, Pedro, and Vaquerizo, Daniel. "ECN Spray G external spray visualization and spray collapse description through penetration and morphology analysis". In: *Applied Thermal Engineering* 112 (2017), pp. 304–316. DOI: 10.1016/j.applthermaleng.2016.10.023.

[13] Moon, Seoksu, Huang, Weidi, and Wang, Jin. "Spray formation mechanism of diverging-tapered-hole GDI injector and its potentials for GDI engine applications". In: *Fuel* 270.March (2020), p. 117519. DOI: 10.1016/j.fuel.2020.117519.

[14] Du, Jianguo, Mohan, Balaji, Sim, Jaeheon, Fang, Tiegang, and Roberts, William L. "Experimental and analytical study on liquid and vapor penetration of high-reactivity gasoline using a high-pressure gasoline multi-hole injector". In: *Applied Thermal Engineering* 163.July (2019), p. 114187. DOI: 10.1016/j.applthermaleng.2019.114187.

[15] Siebers, Dennis L. "Liquid-Phase Fuel Penetration in Diesel Sprays". In: *SAE Technical Paper 980809*. 1998, pp. 1–23. DOI: 10.4271/980809.

[16] Payri, Raul, Gimeno, Jaime, Viera, Juan Pablo, and Plazas, Alejandro Hernan. "Needle lift profile influence on the vapor phase penetration for a prototype diesel direct acting piezoelectric injector". In: *Fuel* 113 (2013), pp. 257–265. DOI: 10.1016/j.fuel.2013.05.057.

[17] Zeng, Wei, Xu, Min, Zhang, Gaoming, Zhang, Yuyin, and Cleary, David J. "Atomization and vaporization for flash-boiling multi-hole sprays with alcohol fuels". In: *Fuel* 95 (2012), pp. 287–297. DOI: 10.1016/j.fuel.2011.08.048.

[18] Parrish, Scott E and Zink, R. J. "Development and Application of Imaging System To Evaluate Liquid and Vapor Envelopes of Multi-Hole Gasoline Fuel Injector Sprays Under Engine-Like Conditions". In: *Atomization and Sprays* 22.8 (2012), pp. 647–661. DOI: 10.1615/AtomizSpr.2012006215.

[19] Li, Yanfei et al. "An exploration on collapse mechanism of multi-jet flash-boiling sprays". In: *Applied Thermal Engineering* 134.May 2017 (2018), pp. 20–28. DOI: 10.1016/j.applthermaleng.2018.01.102.

[20] Guo, Hengjie, Wang, Bo, Li, Yanfei, Xu, Hongming, and Wu, Zhijun. "Characterizing external flashing jet from single-hole GDI injector". In: *International Journal of Heat and Mass Transfer* 121 (2018), pp. 924–932. DOI: 10.1016/j.ijheatmasstransfer.2018.01.042.

[21] Li, Yanfei et al. "Spray morphology transformation of propane, n-hexane and iso-octane under flash-boiling conditions". In: *Fuel* 236.August 2018 (2019), pp. 677–685. DOI: 10.1016/j.fuel.2018.08.160.

[22] Chang, Mengzhao, Lee, Ziyoung, Park, Sungwook, and Park, Suhan. "Characteristics of flash boiling and its effects on spray behavior in gasoline direct injection injectors: A review". In: *Fuel* 271.December 2019 (2020), p. 117600. DOI: 10.1016/j.fuel.2020.117600.

[23] Guo, Hengjie et al. "Comparison of spray collapses at elevated ambient pressure and flash boiling conditions using multi-hole gasoline direct injector". In: *Fuel* 199 (2017), pp. 125–134. DOI: 10.1016/j.fuel.2017.02.071.

[24] Oza, Rajshekhar D. and Sinnamon, James F. "An Experimental and Analytical Study of Flash-Boiling Fuel Injection". In: *SAE Technical Papers*. 1983. DOI: 10.4271/830590.

[25] Girshick, Steven L. and Chiu, Chia Pin. "Kinetic nucleation theory: A new expression for the rate of homogeneous nucleation from an ideal supersaturated vapor". In: *The Journal of Chemical Physics* 93.2 (1990), pp. 1273–1277. DOI: 10.1063/1.459191.

[26] Naber, Jeffrey D and Siebers, Dennis L. "Effects of Gas Density and Vaporization on Penetration and Dispersion of Diesel Sprays". In: *SAE Paper 960034*. Vol. 105. 412. Society of Automotive Engineers, Inc., Warrendale, Pennsylvania, USA, 1996, pp. 82–111. DOI: 10.4271/960034.

[27] Guo, Hengjie et al. "Radial expansion of flash boiling jet and its relationship with spray collapse in gasoline direct injection engine". In: *Applied Thermal Engineering* 146.October 2018 (2019), pp. 515–525. DOI: 10.1016/j.applthermaleng.2018.10.031.

[28] Park, Byung Suh and Lee, Sang Yong. "An experimental investigation of the flash atomization mechanism". In: *Atomization and Sprays* (1994). DOI: 10.1615/atomizspr.v4.i2.30.

[29] Job, G. and Herrmann, F. "Chemical potential - A quantity in search of recognition". In: *European Journal of Physics* 27.2 (2006), pp. 353–371. DOI: 10.1088/0143-0807/27/2/018.

[30] Sher, Eran, Bar-Kohany, Tali, and Rashkovan, Alexander. "Flash-boiling atomization". In: *Progress in Energy and Combustion Science* 34.4 (2008), pp. 417–439. DOI: 10.1016/j.pecs.2007.05.001.

[31] Vetrano, M. R., Simonini, A., Steelant, J., and Rambaud, P. "Thermal characterization of a flashing jet by planar laser-induced fluorescence this article is part of the topical collection on application of laser techniques to fluid mechanics 2012". In: *Experiments in Fluids* 54.7 (2013). DOI: 10.1007/s00348-013-1573-8.

[32] Lamanna, Grazia, Kamoun, Hend, Weigand, Bernhard, and Steelant, Johan. "Towards a unified treatment of fully flashing sprays". In: *International Journal of Multiphase Flow* 58 (2014), pp. 168–184. DOI: 10.1016/j.ijmultiphaseflow.2013.08.010.

[33] Chang, Mengzhao and Park, Suhan. "Spray characteristics of direct injection injectors with different nozzle configurations under flash-boiling conditions". In: *International Journal of Heat and Mass Transfer* 159 (2020). DOI: 10.1016/j.ijheatmasstransfer.2020.120104.

[34] Sphicas, Panos, Pickett, Lyle M., Skeen, Scott A., and Frank, Jonathan H. "Inter-plume aerodynamics for gasoline spray collapse". In: *International Journal of Engine Research* (2018). DOI: 10.1177/1468087417740306.

[35] Wang, Zihan et al. "LES of Diesel and Gasoline Sprays with Validation against X-Ray Radiography Data". In: *SAE International Journal of Fuels and Lubricants* 8.1 (2015), pp. 147–159. DOI: 10.4271/2015-01-0931.

[36] Tanner, F. X. and Boulouchos, K. "A Computational Investigation of the Spray-Induced Flow and its Influence on the Fuel Distribution for Continuous and Intermittent DI-Diesel Sprays". In: *SAE Technical Paper Series* 1.412 (1996). DOI: 10.4271/960631.

[37] Tanner, F.X. et al. "Analysis of X-Ray-Based Computer Simulations of Diesel Fuel Sprays". In: *Proceedings of the Institution of Mechanical Engineers, Part D: Journal of Automobile Engineering* May (2004). DOI: 10.1243/09544070JAUTO392.

Chapter 7

Conclusions and future works

The purpose of this chapter is to draw the key conclusions with regard to the work carried out alongside this study. The key objectives accomplished in this research are addressed in relation to the findings obtained in the various stages of the investigation and placing them in a broader sense.

A list of the potential developments of the present work is provided in the last section of this chapter, suggesting directions for new research and future improvements to the nature of the findings presented in this thesis.

7.1 Summary

This thesis aimed to contribute to the understanding of flash boiling and spray collapse on multi-hole solenoid injectors through an experimental approach. To this end, several tests were performed in the two injectors employed in this research. Moreover, a new test facility was designed, built and tested, to be dedicated to the study of flashing sprays which could heat and withstand sub-atmospheric pressures. Thus, a tremendous effort was made to design a state-of-art facilities, develop and implement imaging processing algorithms in order to asses vast databases systematically.

The results of this study were divided into three different chapters and reported base on each category, which together provided an overview of the requirements in the development of a new test facility as well as the flash boiling and spray collapse injection event. Using the facilities, equipment and

technology available at CMT, in addition to the new test rig developed, the experimental campaigns performed were:

- Rate of injection.
- Plastic deformation technique.
- Rate of momentum.
- Spray visualization, considering both liquid and vapor phases.

The experiment were carried out for the two nozzles, Spray G and PIU injector. However, the experimental test covering the hydraulic characterization were not performed in the same moment. Therefore, conditions of the tests were different to some extend, although they coincide in sufficient points to characterize similarly the injectors. The visualization part was done once the built of the test rig was completed and tested. To study the flash boiling event, four different fuels with various volatility were used to reach more extreme conditions as well as try to mimic the vapor pressure curve of a commercial gasoline whose curve turn out to be much more volatile than the typically used fuel for gasoline research (iso-octane).

The dedicated test rig was built due to the necessity to have a facility that could cover the ambient conditions needed to study the flash boiling phenomena. There was not a facility in the CMT able to go to sub-atmospheric pressures and heat the ambient temperature. The vessel, which is intended to be dedicated to GDI research, had to meet other requirements for future studies, such as wide optical accesses to perform PDA measurements, able to install the injector and windows from different positions or versatility in the mounting of different instrumentation such as pressure sensors or termocouples. For its design, finite element analysis were performed in each part of the vessel to ensure the safety and the integrity of the facility, able to operate in the pressure range of 10 kPa to 1.5 MPa, although the lowest sub-atmospheric pressure is limited to the power of the vacuum pump available. It was differentiated the main vessel and the resistor casing, in which Von Misses criterium was used to determined the safety factor greater than 2. The resistance of the quartz windows was evaluated through the Morh Coulumb criterion which was the appropriate one for brittle material, which resulted in a SF of 1.9 in the most demanding situation of 1.5 MPa. In addition, CFD simulations were executed in order to calculate the necessary power of the resistor to elevate the ambient temperature up to 150 °C, which resulted to be sufficient 2kW.

The hydraulic characterization of the injectors provided an insight of its performance. One particular featured that differentiated the nozzles besides the number and diameter of orifices, was the total outlet area, which was 4% higher for the PIU injector. This was reflected in $\approx 5\%$ increase in stabilized injection rate and even higher difference in the stabilized momentum. It was observed that the opening and to less extend the closing slopes were different which was probably due to different peak current in the command signal. The needle lift measurements illustrated a higher maximun for the PIU injector which support the results of higher ROI and ROM. The hydraulic coefficient showed that both nozzles were in a turbulent regime, since C_d was constant over the range of P_r studied. Although having different internal geometry (step hole vs divergent orifice), the nozzle performed similarly. Finally, a 0-D model of the rate of injection was developed for the Spray G, since it is the most studied injector [1]. The rate of injection signal was decomposed into more elemental parts and modeled through simple equations. The mathematical expression were built based on physical equations when possible, however, the phenomena that were not captured were included in the model as constants when fitting the data.

The visualization of the spray reported noticeable differences in spray behavior considering the four fuels and the two nozzles tested. The surrogate mono-component fuels aim to study various levels of volatility properties and to imitate that property of a commercial gasoline. Hexane was found to be the most similar in terms of volatility to the gasoline. It was used DBI and Schlieren visualization techniques to observe the lateral spray and MIE scattering to perform a frontal visualization. At non-flashing conditions, typical spray parameters such as penetration and angle showed expected tendencies from literature considering chamber density effect, chamber temperature or fuel temperature effect among others. It was also observed the differences between the two nozzles. The PIU injector yielded smaller angle which was produced because of narrower hole distribution. The faster penetration of the nozzle was probably due to the already quicker needle lift. For studying the flash boiling phenomena in both injectors, it was study the spray morphology through qualitative spray images as well as spray width for the developed spray, and at given distances from the nozzle tip. It was realized that there were transitional collapse and collapse spray structures, which depended in the level of flash boiling or R_p. The appearance of flash boiling was link to the fuel properties and collapse was influenced by the nozzle hole distribution. The PIU nozzle with narrower cone angle showed collapsed for early R_p than the Spray G, which has a much wider cone angle. The study of the spray surface using frontal MIE scattering visualization on Spray G reported

strong correlation between spray surface and R_p, however this correlation was not valid at high R_p when the spray collapsed, which happened at similar R_p independently of the fuel tested. Lastly, a study of the collapse time was performed by monitoring the fuel clouding of the nozzle tip. Three different collapse moment were differentiated. The first moment was almost at the SOI, in which the spray collide just from the start, which was the case of the complete collapse. Then, at transitional or mild collapse conditions, it was observed that the spray interaction took some time to develop and produce collapse. At last, it was observed that at flashing condition the end of injection the nozzle tip was also clouded. This outcome suggested that the inner low pressure zone caused by plume interaction was present and, while not enough for the collapse, the last flow leaving the nozzle was suctioned to the spray axis.

Finally, an initial exploration was perform in studying the feasibility of X-rays measurements in spray wall impingement, thanks to the research stay at ANL. It was study spray impact angles of 60° and 40° for the perpendicular and lateral wall configuration respectively. The x-rays radiography technique reported remarkable fuel accumulation in the impact zone with respect to the free spray. In the lateral wall and due to smaller impingement angle, the accumulation decreased respect to the frontal configuration. It was also observed that the rail pressure affected the fuel accumulation increasing ∼28% for the higher P_r, which was probably due to higher injected mass. TIM analysis yielded that on the perpendicular configuration at the end of the injection the fuel accumulation occurs in the entire area near the wall, whereas in the L-wall case the fuel decreases in the impact area but accumulates in the surroundings due to the lower impact angles. In the perpendicular case, the greater fuel mass deposition paved the way for future pool fires and the source of contaminants during engine operation, so it can be inferred that the less favorable case is the perpendicular case. In addition, analysis of penetration and velocity on spray radiography and tomography were performed. It was observe that the spray velocity was decreased after impact. The velocity is decreased ∼64% after the impact in the P-wall case, and ∼43% in the L-wall case. Moreover, the velocity of propagation after impact increases ∼40% by doubling the injection pressure from 100 to 200 bar. Regarding the flash boiling condition case using x-rays, it was detected that less fuel concentration was hitting the wall due to higher atomization and diffusion. Also, it was noticed a faster penetration, however, after impact, the spray spreading velocity decreased 50%.

7.2 Future works

The gasoline direct injection is a complicated process because of the transitory nature of the event and the many physical mechanisms involved. Among the injection conditions, flash boiling is a particular operating conditions that greatly influences the spray behavior, and although this work has gathered vast amount of data, the developed analysis is by no means sufficient to obtain a comprehensive understanding of the dynamic phenomenon involving flash boiling and spray collapse.

There are several path that can continue and contribute to the work already done, considering the relevant of this subject to engine research. Below, it is presented a list of potential works that can be done in future developments:

- Rate of injection, momentum, and needle lift measurements with the fuels used for spray visualization. A further insight of the effect of different volatility fuels could be study in the injector performance. There are probably not strong differences among them when looking at internal hydraulic behavior. For instance, the same text matrix used for visualization in chapter 6 could be performed in ROM and ROI measurements if the range of operations of the test rigs allow it.

- Rate of injection meter for flash boiling conditions. The rate meter available at CMT is a commercial installation that uses the Bosch method to obtain ROI, which can not be used in sub-atmospheric pressures. It would be necessarily the design and implementation of an upstream rate of injection meter, that could measure ROI from the rail.

- Deeper understanding in spray-wall interaction during flash boiling conditions is still needed. Therefore, taking advantage of the new GDI facility available at CMT, new parts can be manufactured to study the fuel jet impingement using lateral and frontal visualization through a transparent wall made of optical quartz. A render of the future set up is shown in Figure 7.1. In addition to this path, in order to obtain a further insight of the heat transfer phenomena, an instrumented wall can be implemented. It could reveal how the fuel heat is transferred to the wall, however, an additional tempered wall, could provide information about how the wall temperature affects spray impingement and development after impact. A render of the design of the test rig modification allowing an instrumented wall is illustrated in Figure 7.2.

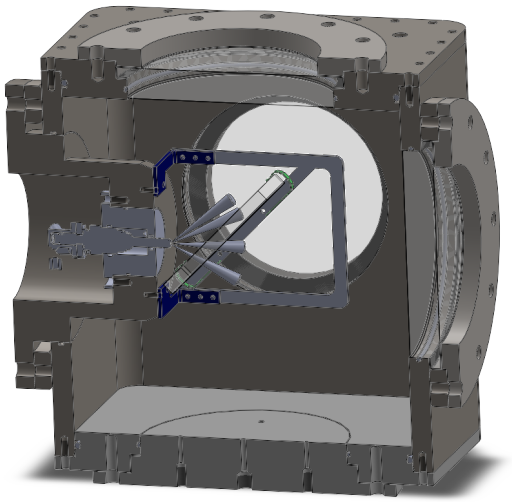

Figure 7.1: Render of the future set up used for spray-wall interaction visualization, using a optical quartz plate, which is able to be installed at different angles.

- Planar MIE measurements. One interesting test would be to obtain the near nozzle spray through frontal MIE scattering using planar illumination. It could be study various spray sections at several distances from the nozzle tip. The results could be comparable to the ones obtained in the spray x-rays tomography, and it will allow to study further the plume interaction which is of great importance in the spray collapse.

- A potential revealing experiment that could enormously contribute to the conclusion of this work is the droplet and velocity analysis through Phase Doppler Anemometry (PDA) measurements. The PDA equipment, which was not available during the development of this work, could provide crucial data about the distribution of droplets. It could indicate the level of fuel-air mixing and how the flash boiling affects its size and distribution. Moreover, the particles velocities could clarify the mechanism of spray collapse, and how fuels and nozzle geometries affect it.

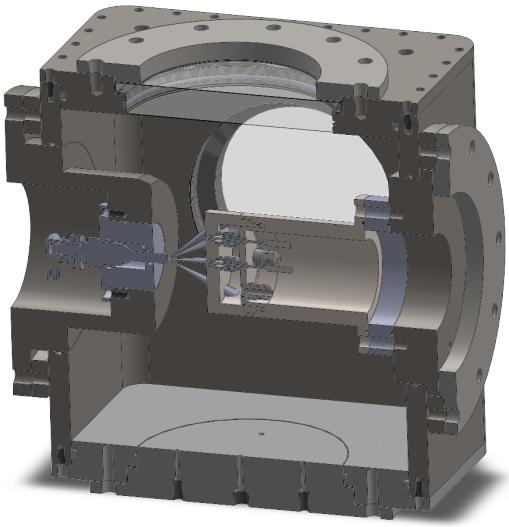

Figure 7.2: Render of the future set up used for spray-wall interaction, composed by an instrumented metal wall with fast response termocouples.

Global Bibliography

Aleiferis, P. G. and Van Romunde, Z. R. "An analysis of spray development with iso-octane, n-pentane, gasoline, ethanol and n-butanol from a multi-hole injector under hot fuel conditions". In: *Fuel* 105 (2013), pp. 143–168. DOI: 10.1016/j.fuel.2012.07.044.

ANL. "Advance Photron source overview". In: *https://www.aps.anl.gov/About/Overview* (2020).

Arcoumanis, C., Flora, H., Gavaises, M., and Badami, M. "Cavitation in Real-Size Multi-Hole Diesel Injector Nozzles". In: *SAE Technical Papers*. 724. 2000. DOI: 10.4271/2000-01-1249.

Bahattin, Mustafa and Ozdaly, Bulent. "Gasoline Direct Injection". In: *Fuel Injection*. Sciyo, 2010. DOI: 10.5772/9693.

Baldwin, E.T. et al. "String flash-boiling in gasoline direct injection simulations with transient needle motion". In: *International Journal of Multiphase Flow* 87 (2016), pp. 90–101. DOI: 10.1016/j.ijmultiphaseflow.2016.09.004.

Banerjee, R. and Kumar, Santhosh. "Numerical investigation of stratified air/fuel preparation in a GDI engine". In: *Applied Thermal Engineering* 104 (2016), pp. 414–428. DOI: 10.1016/j.applthermaleng.2016.05.050.

Bardi, Michele. "Partial needle lift and injection rate shape effect on the formation and combustion of the Diesel spray". PhD thesis. Valencia (Spain): Universitat Politècnica de València, 2014. DOI: 10.4995/Thesis/10251/37374.

Befrui, B., Corbinelli, G., Hoffmann, G., Andrews, R. J., and Sankhalpara, S. R. "Cavitation and Hydraulic Flip in the Outward-Opening GDi Injector Valve-Group". In: *SAE Technical Papers*. 2009. DOI: 10.4271/2009-01-1483.

Befrui, Bizhan, Corbinelli, Giovanni, Spiekermann, Peter, Shost, Mark, and Lai, Ming-Chia. "Large Eddy Simulation of GDI Single-Hole Flow and Near-Field Spray". In: *SAE International Journal of Fuels and Lubricants* 5.2 (2012), pp. 2012–01–0392. DOI: 10.4271/2012-01-0392.

Befrui, Bizhan, Hoffmann, Guy, Kirwan, John, Piock, Walter, and Schilling, Sebastian. "Analytical Optimization of Delphi GDi Fuel Injection Systems". In: *15th Conference "The Working Process of the Internal Combustion Engine"* September 2015 (2015).

Befrui, Bizhan et al. "ECN GDi Spray G : Coupled LES Jet Primary Breakup - Lagrangian Spray Simulation and Comparison with Data". In: *ILASS Americas 28th* June (2016).

Benz, Carlz. *No. 382,585*. 1888.

Bergwerk, W. "Flow Pattern in Diesel Nozzle Spray Holes". In: *Proceedings of the Institution of Mechanical Engineers* 173.1 (1959), pp. 655–660. DOI: 10.1243/PIME_PROC_1959_173_054_02.

Berni, Fabio, Breda, Sebastiano, Lugli, Mattia, and Cantore, Giuseppe. "A numerical investigation on the potentials of water injection to increase knock resistance and reduce fuel consumption in highly downsized GDI engines". In: *Energy Procedia* 81 (2015), pp. 826–835. DOI: 10.1016/j.egypro.2015.12.091.

Bode, J et al. "Fuel spray in Diesel engines. Part I: Spray formation". In: *ATA 92A065* (1992).

Bosch, Wilhelm. "The Fuel Rate Indicator: A New Measuring Instrument For Display of the Characteristics of Individual Injection". In: *SAE Technical Paper 660749*. 1966. DOI: 10.4271/660749.

Cavicchi, Andrea and Postrioti, Lucio. "Simultaneous needle lift and injection rate measurement for GDI fuel injectors by laser Doppler vibrometry and Zeuch method". In: *Fuel* 285.August 2020 (2021), p. 119021. DOI: 10.1016/j.fuel.2020.119021.

Cavicchi, Andrea, Postrioti, Lucio, Berni, Fabio, Fontanesi, Stefano, and Di Gioia, Rita. "Evaluation of hole-specific injection rate based on momentum flux measurement in GDI systems". In: *Fuel* 263.June 2019 (2020). DOI: 10.1016/j.fuel.2019.116657.

Cavicchi, Andrea, Postrioti, Lucio, and Scarponi, Edoardo. "Hydraulic analysis of a GDI injector operation with close multi-injection strategies". In: *Fuel* 235.July 2017 (2019), pp. 1114–1122. DOI: 10.1016/j.fuel.2018.08.089.

Cavicchi, Andrea et al. "Numerical and experimental analysis of the spray momentum flux measuring on a GDI injector". In: *Fuel* 206 (2017), pp. 614–627. DOI: 10.1016/j.fuel.2017.06.054.

Chan, Qing N., Bao, Yongming, and Kook, Sanghoon. "Effects of injection pressure on the structural transformation of flash-boiling sprays of gasoline and ethanol in a spark-ignition direct-injection (SIDI) engine". In: *Fuel* 130 (2014), pp. 228–240. DOI: 10.1016/j.fuel.2014.04.015.

Chang, Mengzhao, Lee, Ziyoung, Park, Sungwook, and Park, Suhan. "Characteristics of flash boiling and its effects on spray behavior in gasoline direct injection injectors: A review". In: *Fuel* 271.December 2019 (2020), p. 117600. DOI: 10.1016/j.fuel.2020.117600.

Chang, Mengzhao and Park, Suhan. "Spray characteristics of direct injection injectors with different nozzle configurations under flash-boiling conditions". In: *International Journal of Heat and Mass Transfer* 159 (2020). DOI: 10.1016/j.ijheatmasstransfer.2020.120104.

Chehroudi, Bruce. "Laser Ignition For Combustion Engines". In: *Engineering* October (2004), pp. 1–5. DOI: 10.13140/2.1.1845.1206.

Chen, Longfei, Liang, Zhirong, Zhang, Xin, and Shuai, Shijin. "Characterizing particulate matter emissions from GDI and PFI vehicles under transient and cold start conditions". In: *Fuel* 189 (2017), pp. 131–140. DOI: 10.1016/j.fuel.2016.10.055.

Chincholkar, S.P. and Suryawanshi, J.G. "Gasoline Direct Injection: An Efficient Technology". In: *Energy Procedia* 90.December 2015 (2016), pp. 666–672. DOI: 10.1016/j.egypro.2016.11.235.

Cho, Jaeho, Kim, Kangjin, Baek, Sungha, Myung, Cha Lee, and Park, Simsoo. "Abatement potential analysis on CO2 and size-resolved particle emissions from a downsized LPG direct injection engine for passenger car". In: *Atmospheric Pollution Research* 10.6 (2019), pp. 1711–1722. DOI: 10.1016/j.apr.2019.07.002.

Cho, Jungkeun and Song, Soonho. "Prediction of hydrogen-added combustion process in T-GDI engine using artificial neural network". In: *Applied Thermal Engineering* 181.May (2020), p. 115974. DOI: 10.1016/j.applthermaleng.2020.115974.

Chung, N. H., Oh, B. G., and Sunwoo, M. H. "Modelling and injection rate estimation of common-rail injectors for direct-injection diesel engines". In: *Proceedings of the Institution of Mechanical Engineers, Part D: Journal of Automobile Engineering* 222.6 (2008), pp. 1089–1101. DOI: 10.1243/09544070JAUTO647.

Cleary, Vincent, Bowen, Phil, and Witlox, Henk. "Flashing liquid jets and two-phase droplet dispersion. I. Experiments for derivation of droplet atomisation correlations". In: *Journal of Hazardous Materials* 142.3 (2007), pp. 786–796. DOI: 10.1016/j.jhazmat.2006.06.125.

Coppo, Marco and Dongiovanni, Claudio. "Experimental Validation of a Common-Rail Injector Model in the Whole Operation Field". In: *Journal of Engineering for Gas Turbines and Power* 129.2 (2007), p. 596. DOI: 10.1115/1.2432889.

Costa, M., Catapano, F., Sementa, P., Sorge, U., and Vaglieco, B. M. "Mixture preparation and combustion in a GDI engine under stoichiometric or lean charge: an experimental and numerical study on an optically accessible engine". In: *Applied Energy* 180 (2016), pp. 86–103. DOI: 10.1016/j.apenergy.2016.07.089.

Costa, M. et al. "Split injection in a homogeneous stratified gasoline direct injection engine for high combustion efficiency and low pollutants emission". In: *Energy* 117.2016 (2016), pp. 405–415. DOI: 10.1016/j.energy.2016.03.065.

Dahlander, Petter, Iemmolo, Daniele, and Tong, Yifei. "Measurements of Time-Resolved Mass Injection Rates for a Multi-Hole and an Outward Opening Piezo GDI Injector". In: *SAE Technical Papers*. Vol. 2015-April. April. 2015. DOI: 10.4271/2015-01-0929.

Delphi Technologies. "New 500+ bar GDi system cuts particulates by up to 50% without engine changes". In: *News release* (2019).

Desantes, Jose Maria, Payri, Raul, Salvador, Francisco Javier, and Gimeno, Jaime. "Measurements of Spray Momentum for the Study of Cavitation in Diesel Injection Nozzles". In: *SAE Technical Paper 2003-01-0703*. Society of Automotive Engineers, Inc., Warrendale, Pennsylvania, USA, 2003. DOI: 10.4271/2003-01-0703.

Desantes, Jose Maria, Payri, Raul, Salvador, Francisco Javier, and Morena., J. de la. "Cavitation effects on spray characteristics in the near-nozzle field". In: *SAE Technical Paper 09ICE-0151*. 2009. DOI: 10.4271/2009-24-0037.

Du, Jianguo, Mohan, Balaji, Sim, Jaeheon, Fang, Tiegang, and Roberts, William L. "Experimental and analytical study on liquid and vapor penetration of high-reactivity gasoline using a high-pressure gasoline multi-hole injector". In: *Applied Thermal Engineering* 163.July (2019), p. 114187. DOI: 10.1016/j.applthermaleng.2019.114187.

Duan, Xiongbo et al. "Quantitative investigation the influences of the injection timing under single and double injection strategies on performance, combustion and emissions characteristics of a GDI SI engine fueled with gasoline/ethanol blend". In: *Fuel* 260.August 2019 (2020), p. 116363. DOI: 10.1016/j.fuel.2019.116363.

Duke, Daniel J. et al. "Time-resolved X-ray Tomography of Gasoline Direct Injection Sprays". In: *SAE International Journal of Engines* 9.1 (2015), pp. 143–153. DOI: 10.4271/2015-01-1873.

Duke, Daniel J. et al. "Internal and near nozzle measurements of Engine Combustion Network 'Spray G' gasoline direct injectors". In: *Experimental Thermal and Fluid Science* 88.June (2017), pp. 608–621. DOI: 10.1016/j.expthermflusci.2017.07.015.

Duke, Daniel, Swantek, Andrew, Kastengren, Alan, Fezzaa, Kamel, and Powell, Christopher. "Recent Developments in X-ray Diagnostics for Cavitation". In: *SAE International Journal of Fuels and Lubricants* 8.1 (2015), pp. 2015–01–0918. DOI: 10.4271/2015-01-0918.

"Engine Combustion Network". In: *https://ecn.sandia.gov/gasoline-spray-combustion/* (2020).

EPA. "Light-Duty Automotive Technology, Carbon Dioxide Emissions, and Fuel Economy Trends: 1975 Through 2016 - Executive Summary (EPA-420-S-16-001, November 2016)". In: November (2016), pp. 1–11.

Erjavec, Jack. *Automotive Technology : A systems approach*. 5th. Cengage Learning, Inc, 2009, p. 1665.

Fansler, Todd D. and Parrish, Scott E. "Spray measurement technology: a review". In: *Measurement Science and Technology* 26.1 (2015), p. 012002. DOI: 10.1088/0957-0233/26/1/012002.

Feng, Shuang et al. "Influence of stratified charge organized by double injection strategy on combustion and emissions on an EGR diluted GDI engine". In: *Applied Thermal Engineering* 158.May (2019), p. 113803. DOI: 10.1016/j.applthermaleng.2019.113803.

Fontanesi, Stefano, D'Adamo, Alessandro, and Rutland, Christopher J. "Large-Eddy simulation analysis of spark configuration effect on cycle-to-cycle variability of combustion and knock". In: *International Journal of Engine Research* (2015). DOI: 10.1177/1468087414566253.

Ghandhi, J B and Heim, D M. "An optimized optical system for backlit imaging". In: *Review of Scientific Instruments* 80.5 (2009), p. 056105. DOI: 10.1063/1.3128728.

Gilles-Birth, Isabell, Bernhardt, Sören, Spicher, Ulrich, and Rechs, Manfred. "A Study of the In-Nozzle Flow Characteristic of Valve Covered Orifice Nozzles for Gasoline Direct Injection". In: *SAE Technical Papers*. 724. 2005. DOI: 10.4271/2005-01-3684.

Gimeno, Jaime. "Desarrollo y aplicación de la medida de flujo de cantidad de movimiento de un chorro Diesel". PhD thesis. E.T.S. Ingenieros Industriales, Universidad Politécnica de Valencia, 2008. DOI: 10.4995/Thesis/10251/8306.

Girshick, Steven L. and Chiu, Chia Pin. "Kinetic nucleation theory: A new expression for the rate of homogeneous nucleation from an ideal supersaturated vapor". In: *The Journal of Chemical Physics* 93.2 (1990), pp. 1273–1277. DOI: 10.1063/1.459191.

Gladstone, J H and Dale, T P. "Researches on the Refraction, Dispersion, and Sensitiveness of Liquids". In: *Philosophical Transactions of the Royal Society of London* 153 (1863), pp. 317–343.

Gomot, Dipl Baudouin and Hülser, Holger. "Delphi Technologies Next Generation GDi-System, improved Emissions and Efficiency with higher Pressure". In: *Internationales Wiener Motorensymposium* (2019), pp. 1–21.

Gong, Changming, Yi, Lin, Zhang, Zilei, Sun, Jingzhen, and Liu, Fenghua. "Assessment of ultra-lean burn characteristics for a stratified-charge direct-injection spark-ignition methanol engine under different high compression ratios". In: *Applied Energy* 261.January (2020), p. 114478. DOI: 10.1016/j.apenergy.2019.114478.

Granqvist, Peter. "High efficient SI-engine with ultra high injection pressure [Research @ Chalmers University]". In: October. Gothenburg, Sweden: Energirelaterad forskning 2017, 2017.

Guo, Hengjie, Li, Yanfei, Wang, Bo, Zhang, Huiqiang, and Xu, Hongming. "Numerical investigation on flashing jet behaviors of single-hole GDI injector". In: *International Journal of Heat and Mass Transfer* 130 (2019), pp. 50–59. DOI: 10.1016/j.ijheatmasstransfer.2018.10.088.

Guo, Hengjie, Li, Yanfei, Xu, Hongming, Shuai, Shijin, and Zhang, Huiqiang. "Interaction between under-expanded flashing jets: A numerical study". In: *International Journal of Heat and Mass Transfer* 137 (2019), pp. 990–1000. DOI: 10.1016/j.ijheatmasstransfer.2019.04.010.

Guo, Hengjie, Wang, Bo, Li, Yanfei, Xu, Hongming, and Wu, Zhijun. "Characterizing external flashing jet from single-hole GDI injector". In: *International Journal of Heat and Mass Transfer* 121 (2018), pp. 924–932. DOI: 10.1016/j.ijheatmasstransfer.2018.01.042.

Guo, Hengjie et al. "Comparison of spray collapses at elevated ambient pressure and flash boiling conditions using multi-hole gasoline direct injector". In: *Fuel* 199 (2017), pp. 125–134. DOI: 10.1016/j.fuel.2017.02.071.

Guo, Hengjie et al. "Effect of flash boiling on microscopic and macroscopic spray characteristics in optical GDI engine". In: *Fuel* 190 (2017), pp. 79–89. DOI: 10.1016/j.fuel.2016.11.043.

Guo, Hengjie et al. "Radial expansion of flash boiling jet and its relationship with spray collapse in gasoline direct injection engine". In: *Applied Thermal Engineering* 146.October 2018 (2019), pp. 515–525. DOI: 10.1016/j.applthermaleng.2018.10.031.

Gürsoy, Doga, De Carlo, Francesco, Xiao, Xianghui, and Jacobsen, Chris. "TomoPy: a framework for the analysis of synchrotron tomographic data". In: *Journal of Synchrotron Radiation* 21.5 (2014), pp. 1188–1193. DOI: 10.1107/S1600577514013939.

Halderman, James D. *Automotive Fuel and Emissions control systems*. 2012.

Hamzah, A et al. "A comparison of diffuse back-illumination (DBI) and Mie-scattering technique for measuring the liquid length of severely flashing spray". In: *20th Australasian Fluid Mechanics Conference*. December. Perth, Australia, 2016.

Harada, Jun, Tomita, Tsutomu, Mizuno, Hiroyuki, Mashiki, Zenichiro, and Ito, Yasushi. "Development of direct injection gasoline engine". In: *SAE Technical Papers* 412 (1997). DOI: 10.4271/970540.

He, Lv, Jingyuan, Li, Xiumin, Yu, Mengliang, Li, and Tian, Yang. "Numerical study on combustion and emission characteristics of a PFI gasoline engine with hydrogen direct-injection". In: *Energy Procedia* 158 (2019), pp. 1449–1454. DOI: 10.1016/j.egypro.2019.01.348.

Hentschel, W. et al. "Optical Diagnostics and CFD-Simulations to Support the Combustion Process Development of the Volkswagen FSI® Direct-Injection Gasoline Engine". In: *SAE Technical Papers*. 724. 2001. DOI: 10.4271/2001-01-3648.

Hentschel, Werner. “Optical Diagnostics Combustion Process Development DI Gasoline Engines”. In: 28 (2000), pp. 1119–1135.

Hoffmann, Guy, Befrui, Bizhan, Berndorfer, Axel, Piock, Walter F., and Varble, Daniel L. “Fuel System Pressure Increase for Enhanced Performance of GDi Multi-Hole Injection Systems”. In: *SAE International Journal of Engines* 7.1 (2014), pp. 2014–01–1209. DOI: 10.4271/2014-01-1209.

Huang, Yuhan, Hong, Guang, and Huang, Ronghua. “Numerical investigation to the dual-fuel spray combustion process in an ethanol direct injection plus gasoline port injection (EDI + GPI) engine”. In: *Energy Conversion and Management* 92 (2015), pp. 275–286. DOI: 10.1016/j.enconman.2014.12.064.

Husted, Harry, Spegar, Timothy D., and Spakowski, Joseph. “The Effects of GDi Fuel Pressure on Fuel Economy”. In: *SAE Technical Papers*. Vol. 1. 2014. DOI: 10.4271/2014-01-1438.

IEA. *A technology roadmap: Electric and plug-in hybrid electric vehicles*. Tech. rep. June. International Energy Agency, 2011, pp. 3471–3473.

IEA. “Global Energy Review 2020”. In: *Global Energy Review 2020* (2020). DOI: 10.1787/a60abbf2-en.

Ingraham, Joseph C. *Automobiles: Races; Everybody Manages to Win Something At the Daytona Beach Contests*. 1957.

Iwamoto, Y., Noma, K., Nakayama, O., Yamauchi, T., and Ando, H. “Development of Gasoline Direct Injection Engine”. In: *SAE Technical Papers*. 412. 1997. DOI: 10.4271/970541.

Jeon, J., Bock, N., and Northrop, W. F. “In-cylinder flame luminosity measured from a stratified lean gasoline direct injection engine”. In: *Results in Engineering* 1.January (2019), p. 100005. DOI: 10.1016/j.rineng.2019.100005.

Jeon, Joonho. “Spatiotemporal flame propagations, combustion and solid particle emissions from lean and stoichiometric gasoline direct injection engine operation”. In: *Energy* 210 (2020), p. 118652. DOI: 10.1016/j.energy.2020.118652.

Job, G. and Herrmann, F. “Chemical potential - A quantity in search of recognition”. In: *European Journal of Physics* 27.2 (2006), pp. 353–371. DOI: 10.1088/0143-0807/27/2/018.

Johansson, Anders N., Hemdal, Stina, and Dahlander, Petter. "Reduction of Soot Formation in an Optical Single-Cylinder Gasoline Direct-Injected Engine Operated in Stratified Mode Using 350 Bar Fuel Injection Pressure, Dual-Coil and High-Frequency Ignition Systems". In: *SAE International Journal of Engines* 10.3 (2017), pp. 2017–01–9278. DOI: 10.4271/2017-01-9278.

Johnson, Timothy. "Vehicular Emissions in Review". In: *SAE International Journal of Engines* 7.3 (2014), pp. 2014–01–1491. DOI: 10.4271/2014-01-1491.

Kanda, Mutsumi et al. "Application of a New Combustion Concept to Direct Injection Gasoline Engine". In: *SAE Technical Papers*. Vol. 2000. 724. 2000. DOI: 10.4271/2000-01-0531.

Kar, Kenneth, Last, Tristan, Haywood, Clare, and Raine, Robert. "Measurement of vapor pressures and enthalpies of vaporization of gasoline and ethanol blends and their effects on mixture preparation in an SI engine". In: *SAE International Journal of Fuels and Lubricants* 1.1 (2009), pp. 132–144. DOI: 10.4271/2008-01-0317.

Kastengren, Alan et al. "The 7BM beamline at the APS: a facility for time-resolved fluid dynamics measurements". In: *Journal of Synchrotron Radiation* 19.4 (2012), pp. 654–657. DOI: 10.1107/S0909049512016883.

Kostas, J et al. "Effect of nozzle transients and compressibility on the penetration of fuel sprays". In: *Applied Physics Letters* 95.2 (2009), p. 024101. DOI: 10.1063/1.3182821.

Kuo, Kenneth K. and Zarchan, Paul. *Recent Advances in Spray Combustion: Spray Atomization and Drop Burning Phenomena*. 1996. DOI: 10.2514/4.866418.

Kwak, H.C. et al. "The New V6 3.5L Turbo GDI Engine from Hyundai-Kia". In: *27th Aachen Colloquium Automobile and Engine Technology*. Aachen, 2018.

Lamanna, Grazia, Kamoun, Hend, Weigand, Bernhard, and Steelant, Johan. "Towards a unified treatment of fully flashing sprays". In: *International Journal of Multiphase Flow* 58 (2014), pp. 168–184. DOI: 10.1016/j.ijmultiphaseflow.2013.08.010.

Lee, Ziyoung, Kim, Taehoon, Park, Sungwook, and Park, Suhan. "Review on spray, combustion, and emission characteristics of recent developed direct-injection spark ignition (DISI) engine system with multi-hole type injector". In: *Fuel* 259.July 2019 (2020), p. 116209. DOI: 10.1016/j.fuel.2019.116209.

Lemmon, Eric W., McLinden, M. O., and Friend, D. G. "Thermophysical Properties of Fluid Systems". In: *NIST Chemistry WebBook, NIST Standard Reference Database Number 69*. Ed. by P. J. Linstrom and W. G. Mallard. 2011.

Lewis, J P. "Fast Template Matching Template". In: *Pattern Recognition* (1995).

Li, Yanfei et al. "An exploration on collapse mechanism of multi-jet flash-boiling sprays". In: *Applied Thermal Engineering* 134.May 2017 (2018), pp. 20–28. DOI: 10.1016/j.applthermaleng.2018.01.102.

Li, Yanfei et al. "Spray morphology transformation of propane, n-hexane and iso-octane under flash-boiling conditions". In: *Fuel* 236.August 2018 (2019), pp. 677–685. DOI: 10.1016/j.fuel.2018.08.160.

Li, Yaoting et al. "A comprehensive experimental investigation on the PFI spray impingement: Effect of impingement geometry, cross-flow and wall temperature". In: *Applied Thermal Engineering* 159.May (2019), p. 113848. DOI: 10.1016/j.applthermaleng.2019.113848.

Lin, Tien Chu, Shen, Yi Jun, and Wang, Muh Rong. "Effects of superheat on characteristics of flashing spray and snow particles produced by expanding liquid carbon dioxide". In: *Journal of Aerosol Science* 61 (2013), pp. 27–35. DOI: 10.1016/j.jaerosci.2013.03.005.

Ma, Dong Shuo and Sun, Z. Y. "Progress on the studies about NOx emission in PFI-H2ICE". In: *International Journal of Hydrogen Energy* 45.17 (2020), pp. 10580–10591. DOI: 10.1016/j.ijhydene.2019.11.065.

Macian, Vicente, Bermudez, V., Payri, Raul, and Gimeno, Jaime. "New technique for determination of internal geometry of a diesel nozzle with the use of silicone methodology". In: *Experimental Techniques* 27.2 (2003), pp. 39–43. DOI: 10.1111/j.1747-1567.2003.tb00107.x.

Magneti Marelli. "Gasoline Direct Injection Technology advancements". In: *2015 SAE-China Congress & Exhibition*. Shanghai, China: Society of Automotive Engineers, 2015.

Manin, Julien, Bardi, Michele, and Pickett, Lyle M. "Evaluation of the liquid length via diffused back-illumination imaging in vaporizing diesel sprays". In: *Comodia*. Fukuoka, 2012.

Manin, Julien et al. "Experimental Characterization of DI Gasoline Injection Processes". In: 2015. DOI: 10.4271/2015-01-1894.

Marchi, A., Nouri, J., Yan, Y., and Arcoumanis, C. "Spray stability of outwards opening pintle injectors for stratified direct injection spark ignition engine operation". In: *International Journal of Engine Research* 11.6 (2010). Ed. by Dinos Arcoumanis, pp. 413–437. DOI: 10.1243/14680874JER605.

Matusik, Katarzyna E, Duke, Daniel J, Swantek, Andrew B, Powell, Christopher F, and Kastengren, Alan L. "High Resolution X-Ray Tomography of Injection Nozzles". In: *ILASS Americas 28th Annual Conference on Liquid Atomization and Spray Systems, Dearborn, MI, May 2016*. May. 2016.

Matusik, Katarzyna E et al. "A study on the relationship between internal nozzle geometry and injected mass distribution of eight ECN Spray G nozzles." In: *Proceedings ILASS,ÄìEurope 2017. 28th Conference on Liquid Atomization and Spray Systems*. September. Valencia: Universitat Politècnica València, 2017, pp. 6–8. DOI: 10.4995/ILASS2017.2017.4766.

McCaffery, Cavan, Durbin, Thomas D., Johnson, Kent C., and Karavalakis, Georgios. "The effect of ethanol and iso-butanol blends on polycyclic aromatic hydrocarbon (PAH) emissions from PFI and GDI vehicles". In: *Atmospheric Pollution Research* August (2020), pp. 0–1. DOI: 10.1016/j.apr.2020.08.024.

Miles, Richard B. "Optical diagnostics for high-speed flows". In: *Progress in Aerospace Sciences* 72 (2015), pp. 30–36. DOI: 10.1016/j.paerosci.2014.09.007.

Mitroglou, N., Nouri, J. M., Yan, Y., Gavaises, M., and Arcoumanis, C. "Spray structure generated by multi-hole injectors for gasoline direct-injection engines". In: *SAE Technical Papers* 724 (2007), pp. 776–790. DOI: 10.4271/2007-01-1417.

Montanaro, Alessandro and Allocca, Luigi. "Flash Boiling Evidences of a Multi-Hole GDI Spray under Engine Conditions by Mie-Scattering Measurements". In: *SAE Technical Paper 2015-01-1945* (2015).

Moon, Seoksu, Huang, Weidi, and Wang, Jin. "Spray formation mechanism of diverging-tapered-hole GDI injector and its potentials for GDI engine applications". In: *Fuel* 270.March (2020), p. 117519. DOI: 10.1016/j.fuel.2020.117519.

Moon, Seoksu et al. "Ultrafast X-ray study of multi-hole GDI injector sprays: Effects of nozzle hole length and number on initial spray formation". In: *Experimental Thermal and Fluid Science* 68 (2015), pp. 68–81. DOI: 10.1016/j.expthermflusci.2015.03.027.

Moulai, Maryam, Grover, Ronald, Parrish, Scott, and Schmidt, David. "Internal and Near-Nozzle Flow in a Multi-Hole Gasoline Injector Under Flashing and Non-Flashing Conditions". In: *SAE Technical Papers*. Vol. 2015-April. April. 2015. DOI: 10.4271/2015-01-0944.

Naber, Jeffrey D and Siebers, Dennis L. "Effects of Gas Density and Vaporization on Penetration and Dispersion of Diesel Sprays". In: *SAE Paper 960034*. Vol. 105. 412. Society of Automotive Engineers, Inc., Warrendale, Pennsylvania, USA, 1996, pp. 82–111. DOI: 10.4271/960034.

Okahara, Akio. "Problems of Plasma Ignition System". In: 1 (2016), pp. 64–72.

Olusegun, Atanda et al. "We are IntechOpen , the world ' s leading publisher of Open Access books Built by scientists , for scientists TOP 1 %". In: *Intech* i.tourism (2012), p. 38. DOI: 10.1016/j.colsurfa.2011.12.014.

Oza, Rajshekhar D. and Sinnamon, James F. "An Experimental and Analytical Study of Flash-Boiling Fuel Injection". In: *SAE Technical Papers*. 1983. DOI: 10.4271/830590.

Papoulias, D., Giannadakis, E., Mitroglou, N., Gavaises, M., and Theodorakakos, A. "Cavitation in fuel injection systems for spray-guided direct injection gasoline engines". In: *SAE Technical Papers* 724 (2007), pp. 776–790. DOI: 10.4271/2007-01-1418.

Park, Byung Suh and Lee, Sang Yong. "An experimental investigation of the flash atomization mechanism". In: *Atomization and Sprays* (1994). DOI: 10.1615/atomizspr.v4.i2.30.

Parotto, Marco, Sgatti, Stefano, and Sensi, Fabio. "Advanced GDI Injector Control with Extended Dynamic Range". In: *SAE Technical Papers*. Vol. 2. 2013. DOI: 10.4271/2013-01-0258.

Parrish, Scott E and Zink, R. J. "Development and Application of Imaging System To Evaluate Liquid and Vapor Envelopes of Multi-Hole Gasoline Fuel Injector Sprays Under Engine-Like Conditions". In: *Atomization and Sprays* 22.8 (2012), pp. 647–661. DOI: 10.1615/AtomizSpr.2012006215.

Pastor, Jose Vicente, Payri, Raul, Garcia-Oliver, Jose Maria, and Nerva, Jean-Guillaume. "Schlieren Measurements of the ECN-Spray A Penetration under Inert and Reacting Conditions". In: *SAE Technical Paper 2012-01-0456*. 2012. DOI: 10.4271/2012-01-0456.

Pauer, Thomas, Yilmaz, Hakan, Zumbrägel, Joachim, and Schünemann, Erik. "New Generation Bosch Gasoline Direct-injection Systems". In: *MTZ worldwide* 78.7-8 (2017), pp. 16–23. DOI: 10.1007/s38313-017-0053-6.

Pavel, Nicolaie et al. “Laser ignition - Spark plug development and application in reciprocating engines”. In: *Progress in Quantum Electronics* 58.April (2018), pp. 1–32. DOI: 10.1016/j.pquantelec.2018.04.001.

Payri, F., Payri, Raul, Salvador, F.J., and Martínez-López, Jorge. “A contribution to the understanding of cavitation effects in Diesel injector nozzles through a combined experimental and computational investigation”. In: *Computers & Fluids* 58 (2012), pp. 88–101. DOI: 10.1016/j.compfluid.2012.01.005.

Payri, Francisco, Arrègle, Jean, Lopez, Jose Javier, and Hermens, Sjoerd. “Effect of Cavitation on the Nozzle Outlet Flow, Spray and Flame Formation in a Diesel Engine.” In: *SAE Paper 2006-01-1391* (2006).

Payri, Francisco and Desantes, Jose Maria. *Motores de combustion interna alternativos*. Editorial Universitat Politecnica de Valencia, 2011.

Payri, R., Gimeno, J., Bracho, G., and Vaquerizo, D. “Study of liquid and vapor phase behavior on Diesel sprays for heavy duty engine nozzles”. In: *Applied Thermal Engineering* 107 (2016), pp. 365–378. DOI: 10.1016/j.applthermaleng.2016.06.159.

Payri, R., Salvador, F.J., Gimeno, J., and Bracho, G. “A new methodology for correcting the signal cumulative phenomenon on injection rate measurements”. In: *Experimental Techniques* 32.1 (2008), pp. 46–49. DOI: 10.1111/j.1747-1567.2007.00188.x.

Payri, Raul, Bracho, Gabriela, Gimeno, Jaime, and Bautista, Abian. “Rate of injection modelling for gasoline direct injectors”. In: *Energy Conversion and Management* 166 (2018), pp. 424–432. DOI: 10.1016/j.enconman.2018.04.041.

Payri, Raul, Garcia-Oliver, Jose Maria, Salvador, Francisco Javier, and Gimeno García, Jaime. “Using spray momentum flux measurements to understand the influence of diesel nozzle geometry on spray characteristics”. In: *Fuel* 84.5 (2005), pp. 551–561. DOI: 10.1016/j.fuel.2004.10.009.

Payri, Raul, Gimeno, Jaime, Marti-Aldaravi, Pedro, and Vaquerizo, Daniel. “Momentum Flux Measurements on an ECN GDi Injector”. In: *SAE Technical Paper 2015-01-1893*. 2015. DOI: 10.4271/2015-01-1893.

Payri, Raul, Gimeno, Jaime, Martí-Aldaraví, Pedro, and Vaquerizo, Daniel. “Internal flow characterization on an ECN GDi injector”. In: *Atomization and Sprays* 26.9 (2016), pp. 889–919. DOI: 10.1615/AtomizSpr.2015013930.

Payri, Raul, Gimeno, Jaime, Mata, Carmen, and Viera, Alberto. "Rate of injection measurements of a direct-acting piezoelectric injector for different operating temperatures". In: *Energy Conversion and Management* 154.October (2017), pp. 387–393. DOI: 10.1016/j.enconman.2017.11.029.

Payri, Raul, Gimeno, Jaime, Viera, Juan Pablo, and Plazas, Alejandro Hernan. "Needle lift profile influence on the vapor phase penetration for a prototype diesel direct acting piezoelectric injector". In: *Fuel* 113 (2013), pp. 257–265. DOI: 10.1016/j.fuel.2013.05.057.

Payri, Raul, Hardy, Gilles, Gimeno, Jaime, and Bautista, Abian. "Analysis of counterbore effect in five diesel common rail injectors". In: *Experimental Thermal and Fluid Science* 107 (2019), pp. 69–78. DOI: 10.1016/j.expthermflusci.2019.05.008.

Payri, Raul, Ruiz, Santiago, Salvador, Francisco Javier, and Gimeno, Jaime. "On the dependence of spray momentum flux in spray penetration: Momentum flux packets penetration model". In: *Journal of Mechanical Science and Technology* 21.7 (2007), pp. 1100–1111.

Payri, Raul, Salvador, F.J., Bracho, Gabriela, and Viera, Alberto. "Differences between single and double-pass schlieren imaging on diesel vapor spray characteristics". In: *Applied Thermal Engineering* 125 (2017), pp. 220–231. DOI: 10.1016/j.applthermaleng.2017.06.140.

Payri, Raul, Salvador, Francisco Javier, Martí-Aldaraví, Pedro, and Vaquerizo, Daniel. "ECN Spray G external spray visualization and spray collapse description through penetration and morphology analysis". In: *Applied Thermal Engineering* 112 (2017), pp. 304–316. DOI: 10.1016/j.applthermaleng.2016.10.023.

Payri, Raul, Viera, Juan Pablo, Gopalakrishnan, Venkatesh, and Szymkowicz, Patrick G. "The effect of nozzle geometry over ignition delay and flame lift-off of reacting direct-injection sprays for three different fuels". In: *Fuel* 199 (2017), pp. 76–90. DOI: 10.1016/j.fuel.2017.02.075.

Payri, Raul, Viera, Juan Pablo, Gopalakrishnan, Venkatesh, and Szymkowicz, Patrick G. "The effect of nozzle geometry over the evaporative spray formation for three different fuels". In: *Fuel* 188 (2017), pp. 645–660. DOI: 10.1016/j.fuel.2016.06.041.

Payri, Raul, Viera, Juan Pablo, Wang, Hua, and Malbec, Louis-Marie. "Velocity field analysis of the high density, high pressure diesel spray". In: *International Journal of Multiphase Flow* 80.24 (2016), pp. 69–78. DOI: 10.1016/j.ijmultiphaseflow.2015.10.012.

Pham, P.X., Vo, D.Q., and Jazar, R.N. "Development of fuel metering techniques for spark ignition engines". In: *Fuel* 206 (2017), pp. 701–715. DOI: 10.1016/j.fuel.2017.06.043.

Postrioti, Lucio et al. "Momentum Flux Measurement on Single-Hole GDI Injector under Flash-Boiling Condition". In: *SAE Technical Papers*. Vol. 24. 2480. 2015. DOI: 10.4271/2015-24-2480.

Poursadegh, Farzad. "An experimental and theoretical investigation of direct fuel injection". PhD thesis. The University Of Melbourne, 2017, p. 205.

Konrad Reif, ed. *Gasoline Engine Management*. Wiesbaden: Springer Fachmedien Wiesbaden, 2015. DOI: 10.1007/978-3-658-03964-6.

Rivera, Edwin A., Mastro, Noreen, Zizelman, James, Kirwan, John, and Ooyama, Robert. "Development of Injector for the Direct Injection Homogeneous Market using Design for Six Sigma". In: *SAE Technical Papers*. 2010. DOI: 10.4271/2010-01-0594.

Saha, Kaushik et al. "Modeling of Internal and Near-Nozzle Flow for a Gasoline Direct Injection Fuel Injector". In: *Journal of Energy Resources Technology* 138.5 (2016). DOI: 10.1115/1.4032979.

Saha, Kaushik et al. "Numerical Investigation of Two-Phase Flow Evolution of In- and Near-Nozzle Regions of a Gasoline Direct Injection Engine During Needle Transients". In: *SAE International Journal of Engines* 9.2 (2016), pp. 2016–01–0870. DOI: 10.4271/2016-01-0870.

Saliba, Georges et al. "Comparison of Gasoline Direct-Injection (GDI) and Port Fuel Injection (PFI) Vehicle Emissions: Emission Certification Standards, Cold-Start, Secondary Organic Aerosol Formation Potential, and Potential Climate Impacts". In: *Environmental Science and Technology* (2017). DOI: 10.1021/acs.est.6b06509.

Sarvaiya, J.N., Patnaik, Suprava, and Bombaywala, Salman. "Image Registration by Template Matching Using Normalized Cross-Correlation". In: *2009 International Conference on Advances in Computing, Control, and Telecommunication Technologies*. IEEE, 2009, pp. 819–822. DOI: 10.1109/ACT.2009.207.

Sehr, Andreas et al. "Potential of the Spray-guided Combustion System in Combination with Turbocharging". In: *SAE Technical Paper Series*. 2010. DOI: 10.4271/2008-01-0139.

Serras-Pereira, J et al. "Cavitation, primary break-up and flash boiling of gasoline, iso-octane and n-pentane with a real-size optical direct-injection nozzle". In: *Fuel* (2010). DOI: 10.1016/j.fuel.2010.03.030.

Settles, G. S. *Schlieren and Shadowgraph Techniques*. Berlin, Heidelberg: Springer Berlin Heidelberg, 2001, p. 376. DOI: 10.1007/978-3-642-56640-0.

Shahangian, Navid et al. "Spray Orientation Assessment and Correction Method for GDI Momentum Flux Measurements". In: October (2019), pp. 231–241.

Shahangian, Navid et al. "Transient nozzle flow simulations of gasoline direct fuel injectors". In: *Applied Thermal Engineering* 175.January (2020). DOI: 10.1016/j.applthermaleng.2020.115356.

Sharma, K. Sen, Seshadri, S., Feser, M., and Wang, G. "Accurate Resolution Measurement for X-Ray Micro-CT Systems". In: *AIP Conference Proceedings*. Vol. 1365. September. 2011, pp. 337–340. DOI: 10.1063/1.3625373.

Shen, Qun et al. "Dedicated full-field X-ray imaging beamline at Advanced Photon Source". In: *Nuclear Instruments and Methods in Physics Research Section A: Accelerators, Spectrometers, Detectors and Associated Equipment* 582.1 (2007), pp. 77–79. DOI: 10.1016/j.nima.2007.08.169.

Sher, Eran, Bar-Kohany, Tali, and Rashkovan, Alexander. "Flash-boiling atomization". In: *Progress in Energy and Combustion Science* 34.4 (2008), pp. 417–439. DOI: 10.1016/j.pecs.2007.05.001.

Shost, Mark A., Lai, Ming-Chia, Befrui, Bizhan, Spiekermann, Peter, and Varble, Daniel L. "GDi Nozzle Parameter Studies Using LES and Spray Imaging Methods". In: *SAE Technical Papers*. Vol. 1. 2014. DOI: 10.4271/2014-01-1434.

Shost, Mark Anthony. "Evaluation of nozzle geometry on high pressure Gasoline Direct Injection spray atomization". PhD thesis. Wayne State University, 2014, p. 295.

Shuai, Shijin, Ma, Xiao, Li, Yanfei, Qi, Yunliang, and Xu, Hongming. "Recent Progress in Automotive Gasoline Direct Injection Engine Technology". In: *Automotive Innovation* 1.2 (2018), pp. 95–113. DOI: 10.1007/s42154-018-0020-1.

Siebers, Dennis L. "Liquid-Phase Fuel Penetration in Diesel Sprays". In: *SAE Technical Paper 980809*. 1998, pp. 1–23. DOI: 10.4271/980809.

Smith, James, Szekely Jr, Gerald, Solomon, Arun, and Parrish, Scott. "A Comparison of Spray-Guided Stratified-Charge Combustion Performance with Outwardly-Opening Piezo and Multi-Hole Solenoid Injectors". In: *SAE International Journal of Engines* 4.1 (2011), pp. 2011–01–1217. DOI: 10.4271/2011-01-1217.

Sphicas, Panos, Pickett, Lyle M., Skeen, Scott A., and Frank, Jonathan H. "Inter-plume aerodynamics for gasoline spray collapse". In: *International Journal of Engine Research* (2018). DOI: 10.1177/1468087417740306.

Spicher, U., Reissing, J., Kech, J. M., and Gindele, J. "Gasoline Direct Injection (GDI) Engines - Development Potentialities". In: *SAE Technical Papers*. 724. 1999. DOI: 10.4271/1999-01-2938.

Starikovskiy, Andrey and Aleksandrov, Nickolay. "Plasma-assisted ignition and combustion". In: *Progress in Energy and Combustion Science* 39.1 (2013), pp. 61–110. DOI: 10.1016/j.pecs.2012.05.003.

Strek, Piotr et al. "X-Ray Radiography and CFD Studies of the Spray G Injector". In: *SAE Technical Papers* 2016-April.April (2016). DOI: 10.4271/2016-01-0858.

Su, Yu Hsuan and Kuo, Ting Fu. "CFD-assisted analysis of the characteristics of stratified-charge combustion inside a wall-guided gasoline direct injection engine". In: *Energy* 175.x (2019), pp. 151–164. DOI: 10.1016/j.energy.2019.03.031.

Swantek, Andrew et al. "Quantification of Shot-to-Shot Variation in Single Hole Diesel Injectors". In: *SAE International Journal of Fuels and Lubricants* 8.1 (2015), pp. 2015–01–0936. DOI: 10.4271/2015-01-0936.

Tanner, F. X. and Boulouchos, K. "A Computational Investigation of the Spray-Induced Flow and its Influence on the Fuel Distribution for Continuous and Intermittent DI-Diesel Sprays". In: *SAE Technical Paper Series* 1.412 (1996). DOI: 10.4271/960631.

Tanner, F.X. et al. "Analysis of X-Ray-Based Computer Simulations of Diesel Fuel Sprays". In: *Proceedings of the Institution of Mechanical Engineers, Part D: Journal of Automobile Engineering* May (2004). DOI: 10.1243/09544070JAUTO392.

Tu, Po-Wen et al. "Numerical Investigation of GDI Injector Nozzle Geometry on Spray Characteristics". In: *SAE Technical Papers*. Vol. 2015-Septe. September. 2015. DOI: 10.4271/2015-01-1906.

Van Basshuysen, Richard and Spicher, Ulrich. *Gasoline engine with direct injection : processes, systems, development, potential*. eng. Ed. by Richard Van Basshuysen and Ulrich Spicher. Wiesbaden, 2009.

Vaquerizo, Daniel. "Study on Advanced Spray-Guided Gasoline Direct Injection Systems". PhD thesis. Universitat Politècnica de València, 2017.

Venegas Pereira, Oscar Hernando. “Estudio del fenómeno de la cavitación en la inyección Diesel mediante la visualización del flujo interno en orificios transparentes.” PhD thesis. Valencia (Spain): Universitat Politècnica de València, 2014. DOI: 10.4995/Thesis/10251/37375.

Vent, Guido and Enderle, Christian. “The new 2.0 l turbo engine from the Mercedes-Benz 4-cylinder engine family”. In: *2nd Aachen Colloquium China* (2012).

Vetrano, M. R., Simonini, A., Steelant, J., and Rambaud, P. “Thermal characterization of a flashing jet by planar laser-induced fluorescence this article is part of the topical collection on application of laser techniques to fluid mechanics 2012”. In: *Experiments in Fluids* 54.7 (2013). DOI: 10.1007/s00348-013-1573-8.

Viera, Alberto. “Effect of multiple injection strategies on the diesel spray formation and combustion using optical diagnostics”. PhD thesis. Universitat Politècnica de València, 2019.

Viera, Juan Pablo. “Experimental study of the effect of nozzle geometry on the performance of direct-injection diesel sprays for three different fuels”. PhD thesis. 2017.

Viera, Juan Pablo et al. “Linking instantaneous rate of injection to X-ray needle lift measurements for a direct-acting piezoelectric injector”. In: *Energy Conversion and Management* 112 (2016), pp. 350–358. DOI: 10.1016/j.enconman.2016.01.038.

Wang, Zhongli et al. “Experimental Study of Influence on Microwave Plasma Ignition Combustion Performance of Pulse Microwave Signals”. In: *IEEE Access* 7 (2019), pp. 23951–23958. DOI: 10.1109/ACCESS.2019.2899911.

Wang, Zihan et al. “LES of Diesel and Gasoline Sprays with Validation against X-Ray Radiography Data”. In: *SAE International Journal of Fuels and Lubricants* 8.1 (2015), pp. 147–159. DOI: 10.4271/2015-01-0931.

Weber, Daniel, Leick, Philippe, Gmbh, Robert Bosch, and Systems, Gasoline. “Structure and Velocity Field of Individual Plumes of Flashing Gasoline Direct Injection Sprays”. In: *ILASS Europe, 26th Annual Conference on Liquid Atomization and Spray Systems* September 2014 (2014), pp. 8–10. DOI: 10.13140/RG.2.1.1227.2724.

Wei, Shou-Der and Lai, Shang-Hong. “Fast Template Matching Based on Normalized Cross Correlation With Adaptive Multilevel Winner Update”. In: *IEEE Transactions on Image Processing* 17.11 (2008), pp. 2227–2235. DOI: 10.1109/TIP.2008.2004615.

Westlye, Fredrik R et al. "Diffuse back-illumination setup for high temporally resolved extinction imaging". In: *Applied Optics* 56.17 (2017), p. 5028. DOI: 10.1364/AO.56.005028.

Wigley, G., Pitcher, G., Nuglisch, H., Helie, J., and Ladommatos, N. "Fuel Spray Formation and Gasoline Direct Injection". In: *8th AVL international symposium on combustion diagnostics*. 2008.

Wood, Andrew. "Optical investigations of the sprays generated by gasoline multi-hole injectors under novel operating conditions". PhD thesis. Loughborough University, 2014.

Wu, Shengqi, Xu, Min, Hung, David L.S., Li, Tianyun, and Pan, Hujie. "Near-nozzle spray and spray collapse characteristics of spark-ignition direct-injection fuel injectors under sub-cooled and superheated conditions". In: *Fuel* 183 (2016), pp. 322–334. DOI: 10.1016/j.fuel.2016.06.080.

Wu, Zengyang, Wang, Libing, Badra, Jihad A., Roberts, William L., and Fang, Tiegang. "GDI fuel sprays of light naphtha, PRF95 and gasoline using a piezoelectric injector under different ambient pressures". In: *Fuel* 223.December 2017 (2018), pp. 294–311. DOI: 10.1016/j.fuel.2018.03.009.

Yang, Zhengjun et al. "Real driving particle number (PN) emissions from China-6 compliant PFI and GDI hybrid electrical vehicles". In: *Atmospheric Environment* 199.September 2018 (2019), pp. 70–79. DOI: 10.1016/j.atmosenv.2018.11.037.

Yi, Jianwen et al. "Development and Optimization of the Ford 3.5L V6 EcoBoost Combustion System". In: *SAE International Journal of Engines* 2.1 (2009), pp. 2009–01–1494. DOI: 10.4271/2009-01-1494.

Yin, Peng, Yang, Shangze, Li, Xuesong, and Xu, Min. "Numerical simulation of in-nozzle flow characteristics under flash boiling conditions". In: *International Journal of Multiphase Flow* 127 (2020). DOI: 10.1016/j.ijmultiphaseflow.2020.103275.

Yu, Xiumin et al. "Investigation of combustion and emissions of an SI engine with ethanol port injection and gasoline direct injection under lean burn conditions". In: *Energy* 189 (2019), p. 116231. DOI: 10.1016/j.energy.2019.116231.

Zeng, Wei and Sjöberg, Magnus. "Utilizing boost and double injections for enhanced stratified-charge direct-injection spark-ignition engine operation with gasoline and E30 fuels". In: *International Journal of Engine Research* 18.1-2 (2017), pp. 131–142. DOI: 10.1177/1468087416685512.

Zeng, Wei, Sjöberg, Magnus, Reuss, David L., and Hu, Zongjie. "The role of spray-enhanced swirl flow for combustion stabilization in a stratified-charge DISI engine". In: *Combustion and Flame* 168.x (2016), pp. 166–185. DOI: 10.1016/j.combustflame.2016.03.015.

Zeng, Wei, Xu, Min, Zhang, Gaoming, Zhang, Yuyin, and Cleary, David J. "Atomization and vaporization for flash-boiling multi-hole sprays with alcohol fuels". In: *Fuel* 95 (2012), pp. 287–297. DOI: 10.1016/j.fuel.2011.08.048.

Zhao, F., Lai, M.-C, and Harrington, D.L. "Automotive spark-ignited direct-injection gasoline engines". In: *Progress in Energy and Combustion Science* 25.5 (1999), pp. 437–562. DOI: 10.1016/S0360-1285(99)00004-0.

Zhao, Hua. *Advanced direct injection combustion engine technologies and development*. Woodhead Publishing Limited, 2010. DOI: 10.1533/9781845697327.

Zheng, Zhaolei, Tian, Xuefeng, and Zhang, Xiaoyu. "Effects of split injection proportion and the second injection time on the mixture formation in a GDI engine under catalyst heating mode using stratified charge strategy". In: *Applied Thermal Engineering* 84 (2015), pp. 237–245. DOI: 10.1016/j.applthermaleng.2015.03.041.

Zhou, Jianwei et al. "Characteristics of near-nozzle spray development from a fouled GDI injector". In: *Fuel* 219.92 (2018), pp. 17–29. DOI: 10.1016/j.fuel.2018.01.070.

Zhu, Rencheng et al. "Tailpipe emissions from gasoline direct injection (GDI) and port fuel injection (PFI) vehicles at both low and high ambient temperatures". In: *Environmental Pollution* 216 (2016), pp. 223–234. DOI: 10.1016/j.envpol.2016.05.066.

Zhuang, Yuan et al. "Investigation of water injection benefits on downsized boosted direct injection spark ignition engine". In: *Fuel* 264.October 2019 (2020). DOI: 10.1016/j.fuel.2019.116765.

Zigan, L., Schmitz, I., Flügel, A., Wensing, M., and Leipertz, A. "Structure of evaporating single- and multicomponent fuel sprays for 2nd generation gasoline direct injection". In: *Fuel* 90.1 (2011), pp. 348–363. DOI: 10.1016/j.fuel.2010.08.001.

Zimmerman, Naomi, Wang, Jonathan M, Jeong, Cheol Heon, Wallace, James S, and Evans, Greg J. "Assessing the Climate Trade-Offs of Gasoline Direct Injection Engines". In: *Environmental Science and Technology* (2016). DOI: 10.1021/acs.est.6b01800.

Appendices

Appendix A

Graph Appendix

A.1 Spray morphology

This section have the remaining spray morphology figures for all cases.

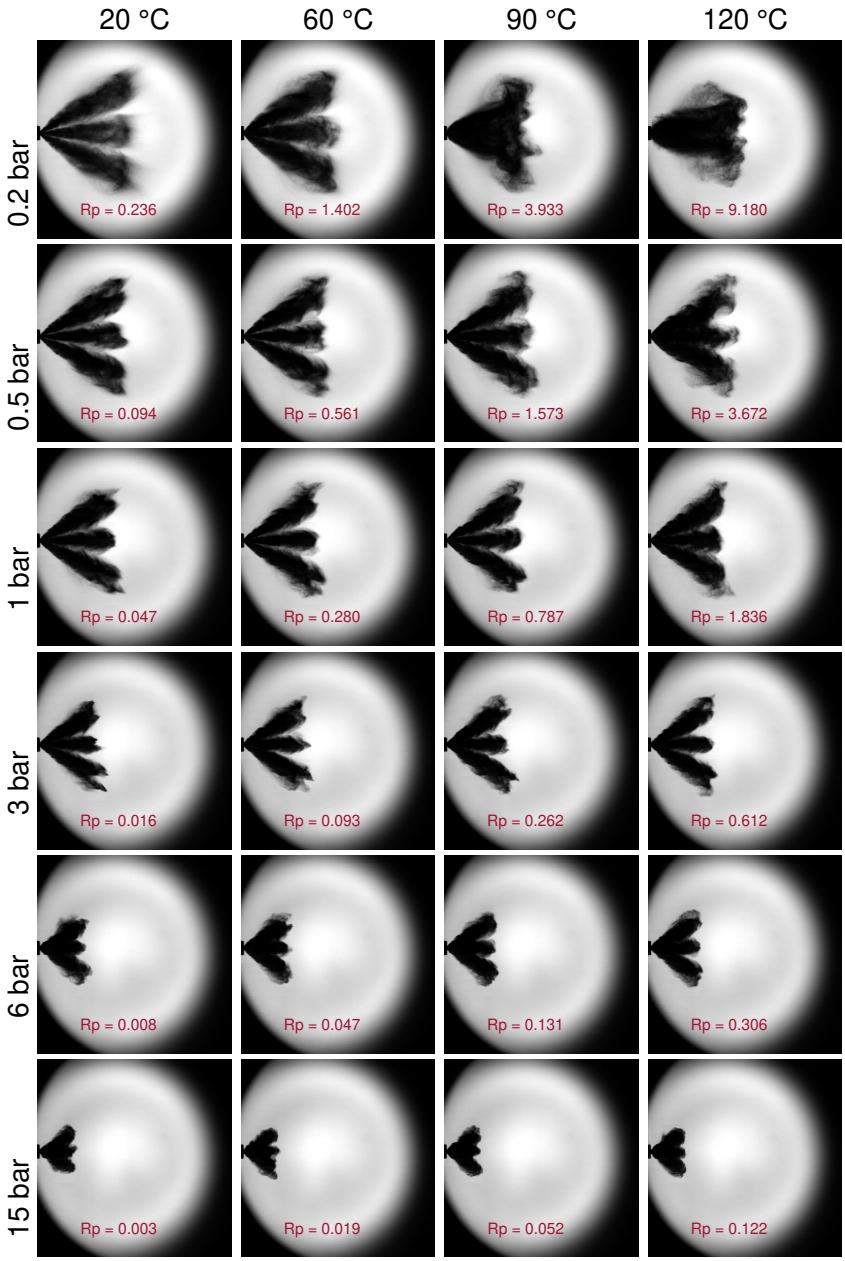

Figure A.1: Spray cone morphology for Heptane in Spray G injector at t = 0.5 ms ASOI.

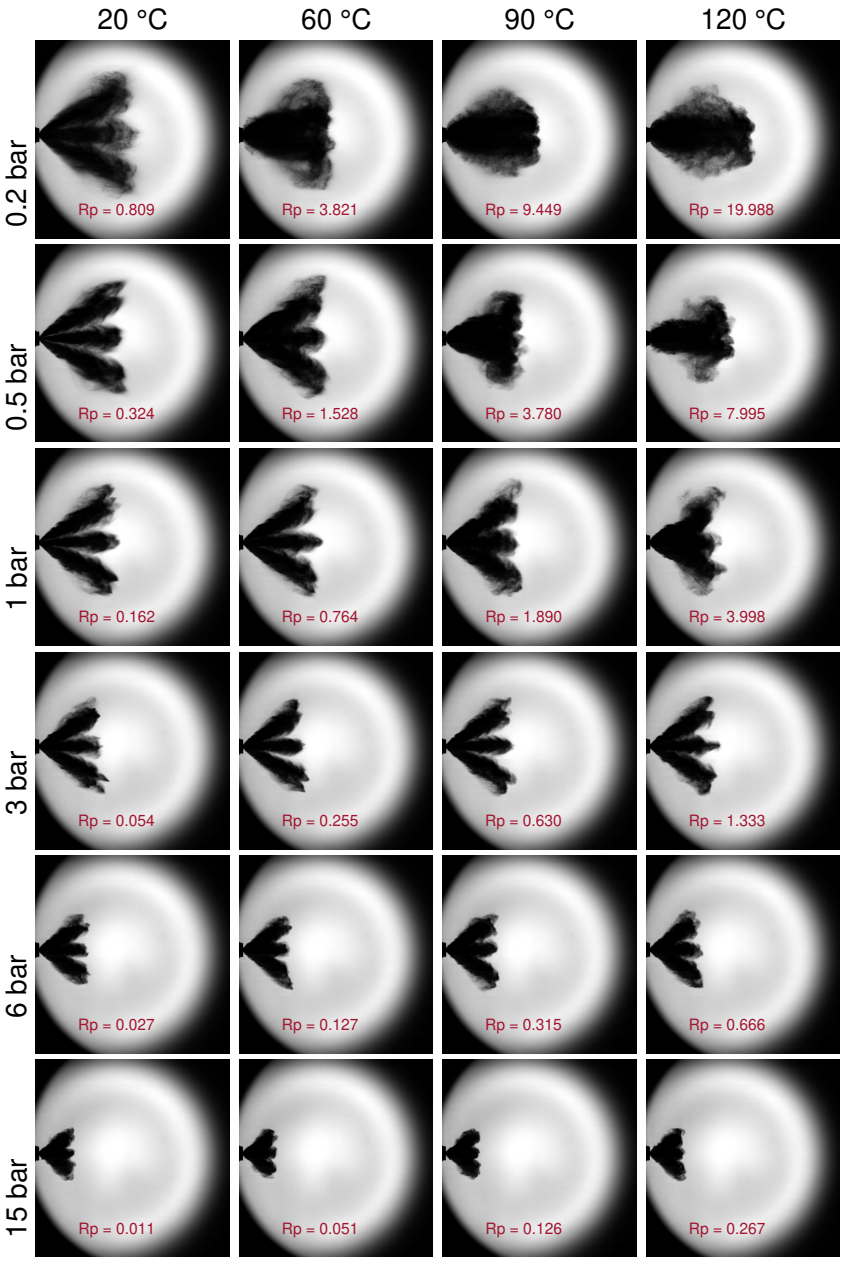

Figure A.2: Spray cone morphology for Hexane in Spray G injector at $t = 0.5$ ms ASOI.

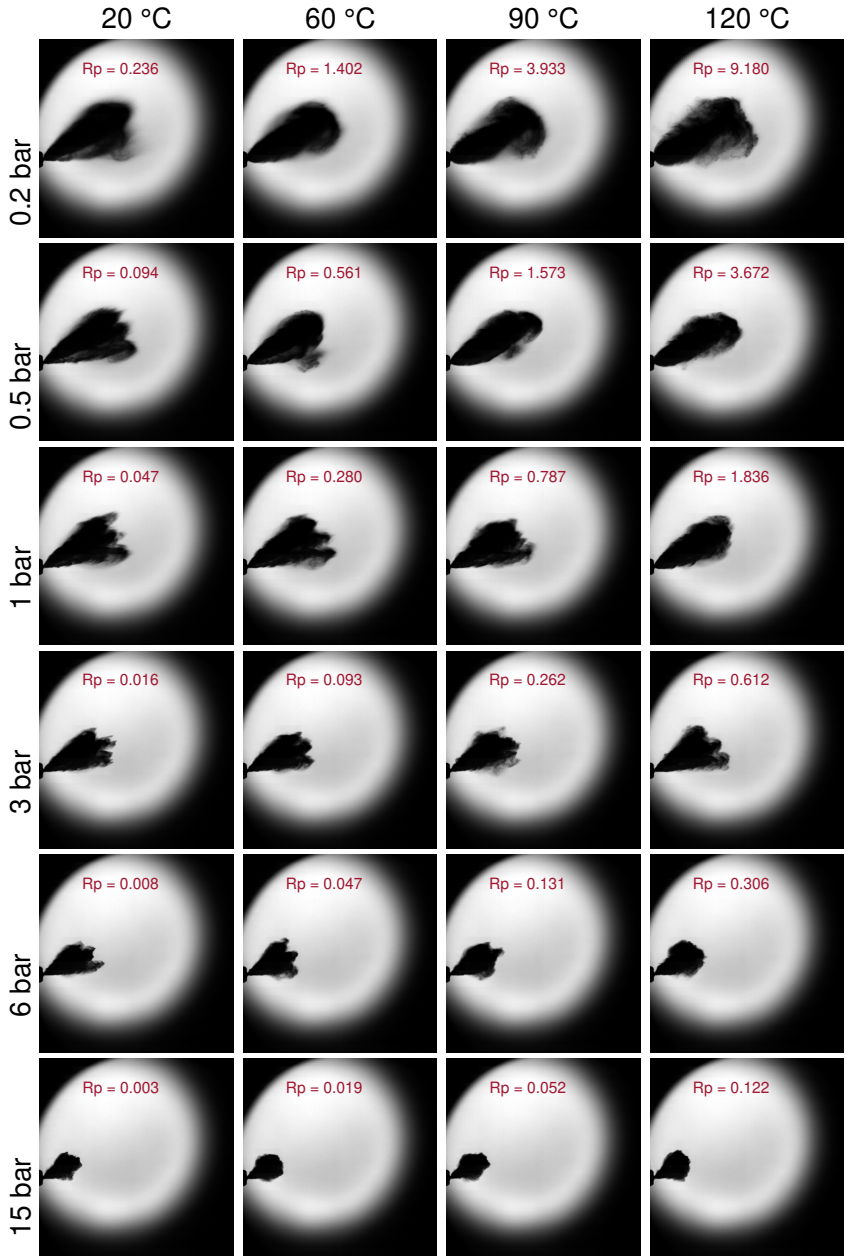

Figure A.3: Spray cone morphology for Heptane in PIU injector at t = 0.5 ms ASOI.

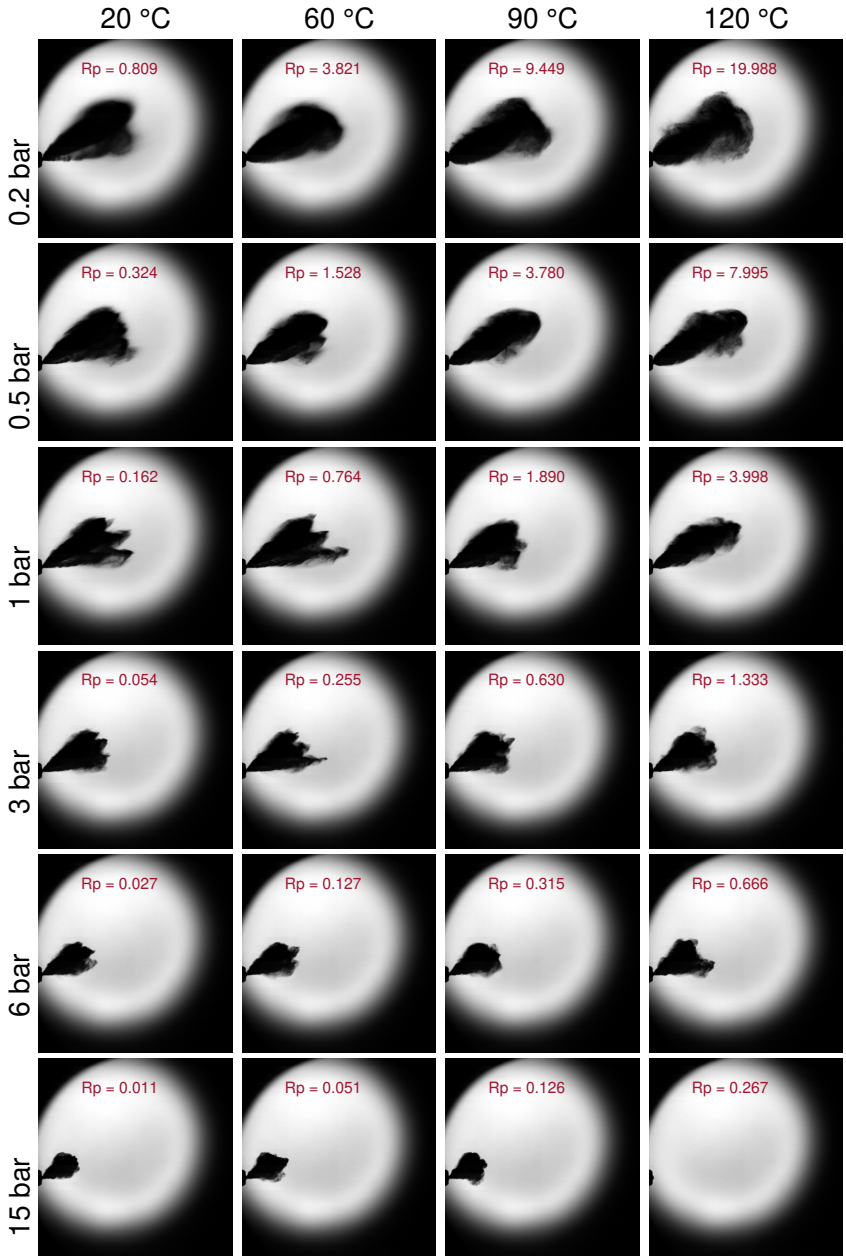

Figure A.4: Spray cone morphology for Hexane in PIU injector at t = 0.5 ms ASOI.